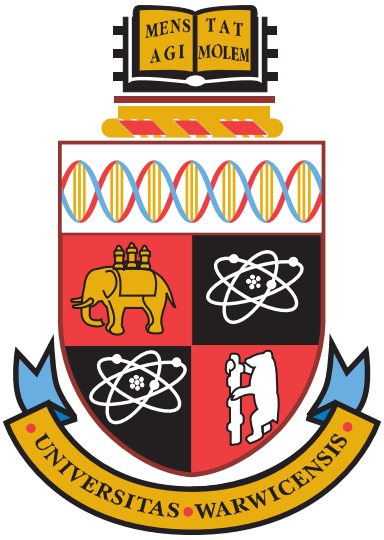

Modelling immunoglobulin metabolism and its effect on prognostic utility in multiple myeloma

by

Felicity Kendrick

Thesis

Submitted to the University of Warwick

for the degree of

Doctor of Philosophy

School of Engineering

January 2018

Contents

List of Tables

List of Figures

Acknowledgements

Firstly I would like to thank my supervisors at the University of Warwick, Prof Mike Chappell and Dr Neil Evans, for all of their support and for inspiring me to work on this problem. I am extremely grateful to my industrial supervisor at The Binding Site, Dr Stephen Harding, who conceived the project and who has taught me so much about the clinical application of our collaboration. I also wish to thank Oscar Berlanga, for many helpful discussions and assistance in interpreting the clinical trial data.

I would like to thank members of the Warwick Engineering in Biomedicine group, past and present. I have made too many good friends among them to list here. I would like to especially thank Yan, whose advice, conversations and encouragement have made me more capable of completing this work. I am also grateful for all the help I have received from the administrative staff in the School of Engineering.

I would like to thank the Midlands Integrative Biosciences Training Partnership (MIBTP) for giving me this opportunity and the Biotechnology and Biological Sciences Research Council (BBSRC) for financially supporting the work. Thank you to the MIBTP directors and administrators, past and present.

I would also like to thank my non-lab friends for all of their support. Finally, the biggest thank you goes to John, Julia, Matthew, Maureen, Rebekah and Theresa, who have always supported me and continue to support me tremendously, in everything I do.

Declaration and published work

I declare that the work presented in this thesis is my own except where stated otherwise, and was carried out entirely at the University of Warwick, during the period of October 2013 to January 2018, under the supervision of Prof Michael Chappell and Dr Neil Evans. The research reported here has not been submitted, either wholly or in part, in this or any other academic institution for admission to a higher degree.

Some parts of the work reported in this thesis have been published, as listed below.

Published papers

1. F. Kendrick, N. D. Evans, B. Arnulf, H. Avet-Loiseau, O. Decaux, T. Dejoie, G. Fouquet, S. Guidez, S. Harel, B. Hebraud, V. Javaugue, V. Richez, S. Schraen, C. Touzeau, P. Moreau, X. Leleu, S. Harding, M. J. Chappell, *Frontiers in Physiology* **8** (2017)

2. F. Kendrick, S. Harding, M. J. Chappell, N. D. Evans, *IFAC-PapersOnLine* **48**, 106–111 (2015)

Conference presentations

1. Poster presentation: F. Kendrick, S. Harding, N. D. Evans, M. J. Chappell, 'Immunoglobulin G (IgG) and neonatal Fc-receptor (FcRn) dynamics in IgG multiple myeloma', *9th IFAC Symposium on Biological and Medical Systems*, Berlin, August 2015

2. Poster presentation: F. Kendrick, S. Harding, N. D. Evans, M. J. Chappell, 'Modelling immunoglobulin G and FcRn dynamics', *8th IEEE EMBS UK & Republic of Ireland Postgraduate Conference on Biomedical Engineering and Medical Physics*, University of Warwick, July 2014

3. Oral and poster presentations: F. Kendrick, S. Harding, N. D. Evans, M. J. Chappell, 'Modelling immunoglobulin G and FcRn dynamics', $[id]^2_{Ox}$ *inter-disciplinary inter-DTC Student Conference*, University of Oxford, June 2014

4. Poster presentation: F. Kendrick, S. Harding, N. D. Evans, M. J. Chappell, 'Modelling immunoglobulin G and FcRn dynamics', *Simplifying Assumptions in Models of Complex Systems: Break, Make, Justify*, University of Birmingham, May 2014

Abstract

Multiple myeloma is a cancer of plasma cells. In multiple myeloma, a clone of plasma cells in the bone marrow secretes a unique, monoclonal immunoglobulin (Ig), whose biological properties depend on its type and structure. The monoclonal Ig offers a convenient opportunity for clinicians to monitor the response of the tumour to therapy via the secreted protein, which is readily quantified in a blood sample. Responses to treatment are assigned based on the percentage reduction in monoclonal Ig; however, response criteria do not take into account the different metabolic half-lives of the proteins.

70% of multiple myeloma patients have either monoclonal IgA- or monoclonal IgG-producing clones. IgA and IgG have metabolic half-lives of 6 days and 23 days, at normal concentrations, respectively. The large difference in their metabolic half-lives suggests that they would respond at different rates during therapy. The elimination rate of IgG is concentration-dependent due to saturable recycling by a receptor. This could further impact upon its response during therapy, with the possibility that IgG is eliminated from the body at different rates at the beginning of therapy, when its concentration is high, and at the end of therapy, when its concentration has decreased.

In this thesis compartmental models of IgG metabolism from the literature are analysed and parameter values are estimated from available data. A model of IgA metabolism is sourced in the literature. These models are used to predict the responses of monoclonal IgA and IgG during therapy. The simulations are able to replicate typical monoclonal IgA and IgG responses seen in a clinical trial of patients with relapsed and refractory multiple myeloma.

Importantly, the plasma cell clone is not directly accessible to measurement and therefore not available to validate model-based predictions. However, monoclonal Ig responses are not evaluated by their ability to predict the tumour burden, but by the strength of their association with patient survival. In this thesis, a prediction is made of how the different metabolic properties of IgA and IgG may influence their association with survival outcomes. Evidence for this effect is then evaluated in data from a clinical trial using the methods of survival analysis.

Abbreviations

AIC	Akaike information criterion
ASCT	autologous stem cell transplantation
BMPC%	bone marrow plasma cells %
CR	complete response
CV	coefficient of variation
Fc	fragment crystallisable
FCR	fractional catabolic rate
FCR_E	fractional catabolic rate of endogenous immunoglobulin
FcRn	neonatal Fc receptor
FCR_T	fractional catabolic rate of tracer
FLC	free light chain
GSF	generalised sensitivity function
HLC	heavy/light chain assay
IFM	Intergroupe Francophone du Myélome
Ig	immunoglobulin
IgA	immunoglobulin A
IgD	immunoglobulin D
IgE	immunoglobulin E
IgG	immunoglobulin G
IgM	immunoglobulin M

IIMM	intact immunoglobulin multiple myeloma
IMWG	International Myeloma Working Group
mAb	monoclonal antibody
mHLC	monoclonal HLC
ML	maximum likelihood
OS	overall survival
PD	progressive disease
PFS	progression-free survival
PR	partial response
QSS	quasi-steady state
RMSE	root-mean-square error
RVD	lenalidomide, bortezomib and dexamethasone
SAEM	stochastic approximation expectation maximisation
sCR	stringent complete response
SD	stable disease
SPEP	serum protein electrophoresis
$T_{1/2}$	half-life
TSF	traditional sensitivity function
VGPR	very good partial response

1

Introduction

Multiple myeloma is a cancer of plasma cells located in the bone marrow. It is characterised as a disease of the elderly, with symptoms including bone pain, fractures, anaemia and frequent infections. Multiple myeloma is considered incurable, with less than half of patients surviving beyond five years from diagnosis; however, treatment extends life expectancy and maintains quality of life. In recent years the introduction of novel agents has substantially improved responses to treatment and survival rates and as such greater emphasis is now being placed on markers of response [1; 2].

Plasma cells normally produce antibodies as part of a healthy, functioning immune system. Antibodies are also known as immunoglobulins, with the two terms often considered synonymous; however, there is a subtle difference in their meanings. 'Antibody', directly translated from the German *Antikörper*, is defined by the Oxford English Dictionary as 'a blood protein produced in response to and counteracting a specific antigen'. The meaning of 'antibody' thus incorporates its function, whereas 'immunoglobulin' refers purely to the protein itself, as a γ-globulin of the immune system. In multiple myeloma, clonal plasma cells usually secrete a unique, monoclonal immunoglobulin into the blood. The monoclonal immunoglobulin serves no immune function and is therefore only referred to as an immunoglobulin, or Ig, and not an antibody throughout this thesis.

There are five classes of Ig – IgA, IgD, IgE, IgG and IgM – which have different biological properties depending on their role in the normal immune response. In myeloma, clonal cells produce a unique monoclonal Ig of a single type. This thesis is only concerned with

patients producing monoclonal IgA and IgG; such patients are said to have IgA or IgG myeloma and comprise 70% of all multiple myeloma patients [3]. For the remainder of this chapter discussion will be restricted to IgA and IgG myeloma.

The monoclonal Ig produced in multiple myeloma serves no useful purpose; however, it does offer a convenient opportunity for physicians to monitor changes in the size of the plasma cell clone via the secreted protein, which can be readily quantified in a blood sample. The cancer itself is only accessible by bone marrow biopsy or aspirate, both of which are unpleasant, invasive procedures. The concentration of monoclonal Ig in the blood is the preferred measure by which the cancer is monitored; patient monitoring in clinical trials and the non-trial setting alike is heavily reliant on measurements of monoclonal Ig concentration in the blood [4; 5].

During therapy, it is important for the physician to know how well the cancer is responding to the treatment, and at the end of therapy, they would also like to make an assessment of the overall success of the treatment in order to give the patient an accurate prognosis. Ideally, the physician would like to know what proportion of the cancer has been eradicated by the therapy; however, rather than accessing the cancer directly, the physician evaluates the percentage reduction in the monoclonal Ig present in the blood. The percentage reduction in the monoclonal Ig is thus a marker for the response of the cancer, and throughout this thesis will be referred to as the monoclonal Ig response.

According to international guidelines for response assignment, a 50% reduction in monoclonal Ig is a criterion that must be met in order for partial response (PR) to be assigned at a particular time during or after treatment; likewise a 90% reduction is a criterion for very good partial response (VGPR) assignment [5; 6]. However, a 50%, say, monoclonal Ig response does not necessarily mean that 50% of the cancer cells have been eradicated: the concentration of monoclonal Ig in the blood at any time depends both on the rate of production, which is assumed proportional to the tumour burden, and also the rate at which it is eliminated. Herein lies the motivation for the work presented in this thesis.

IgA and IgG are known to have metabolic half-lives of 6 days and 23 days, at normal concentrations, respectively. This suggests that, for the same tumour response, monoclonal IgG may respond more slowly compared to IgA. Interestingly, the elimination rate of IgG is concentration-dependent due to saturable recycling by the neonatal Fc

receptor (FcRn). This could complexify its relationship with the tumour response, with the possibility that IgG is eliminated from the body at a faster rate at the beginning of therapy, when its concentration is high, and at a slower rate at the end of therapy, when its concentration has decreased [7; 8].

Presently it is not clear how the different elimination mechanisms of IgA and IgG affect their responses in multiple myeloma. In particular, we would like to ask, for an IgA patient and an IgG patient whose tumours respond at the same rate, whether monoclonal IgG responds more slowly than monoclonal IgA. We would also like to ascertain whether the elimination mechanisms of IgA and IgG influence their final responses at the end of therapy, when a maximal proportion of the tumour has been killed. At the end of therapy, is monoclonal IgG remaining in the system because the therapy has failed to eradicate the cancer, or are the IgG molecules simply being recirculated by the FcRn receptor? These questions could have implications for how monoclonal Ig measurements are interpreted in patients and possibly for response assignment criteria.

To answer these questions, mathematical models of IgA and IgG metabolism are required, describing the elimination of IgA and IgG from the body. Mathematical models of the myeloma cell population during therapy are also required; assuming that the production rate of the monoclonal protein is proportional to the tumour burden, these models will dictate the production rates of monoclonal IgA and IgG. Together, parameterised models of the tumour response and IgA and IgG metabolism will allow for predictions of how monoclonal IgA and IgG respond during therapy.

Due to the systemic distribution of malignant plasma cells in multiple myeloma and the invasiveness of bone marrow examination, physicians are unable to routinely assess the size of the plasma cell clone. Therefore the myeloma cell population is unavailable for validation of model-based predictions of responses. However, the motivation for this research is to consider the possible effects of the metabolic properties of Igs on their prognostic utility. Response markers are evaluated by the strength of their association with patient survival; therefore the aim of this thesis is to qualitatively predict how the different metabolic properties of IgA and IgG may influence their association with survival outcomes. Evidence for these effects can then be assessed in available survival data.

As multiple myeloma is an incurable disease, maintaining and prolonging quality of life is

a primary goal of patient care. It is hugely important that physicians can meaningfully assess response to therapy so that they can provide patients with accurate information about their prognosis and also offer the best care. This thesis aims to improve our understanding of the importance of marker metabolism; it is hoped that further developments in this area will aid physicians in their work.

1.1 Thesis aims

- Select from the literature mathematical models of IgA and IgG metabolism in humans that can be used to simulate IgA and IgG responses in multiple myeloma. Estimate from experimental data, or source in the literature, parameter values for the models.
- Simulate responses to therapy of the myeloma cell population and corresponding monoclonal IgA and IgG responses. Investigate assumptions and hypotheses relating to IgA and IgG responses in multiple myeloma.
- Consider how the respective modes of metabolism of IgA and IgG may impact upon their utility as markers for survival and assess the evidence for any such impact in a dataset of newly diagnosed multiple myeloma patients.

1.2 Thesis outline

- Chapter 2 reviews the relevant literature. The biology of Ig metabolism and how Igs are currently used to monitor patients are discussed in this chapter.
- In chapter 3 the methods used to mathematically model the metabolism of Igs are described. These include compartmental modelling, parameter estimation and structural identifiability analysis.
- The survival analysis methods used to evaluate the prognostic ability of Igs in multiple myeloma are introduced in chapter 4. The Kaplan-Meier survival estimator, the proportional hazards class of survival models and methods for comparing survival models are described.

- In chapter 5 a two-compartment model of IgG metabolism is analysed. Parameter values for humans are estimated from limited experimental data available in the literature.
- In chapter 6 a four-compartment model of IgG metabolism is analysed and parameter values estimated, again using the data available in the literature.
- In chapter 7 the two-compartment and four-compartment models of IgG metabolism are compared.
- In chapter 8 the two-compartment model of IgG metabolism and a two-compartment model of IgA metabolism are used to predict blood monoclonal Ig responses during therapy.
- In chapter 9, the final results chapter, the impact of the different metabolic properties of IgA and IgG upon their association with patient survival is considered; the evidence for this effect is then evaluated in a dataset from a clinical trial.
- Chapter 10 summarises the conclusions that can be drawn from the work presented in this thesis and recommendations for future work are made.

References

1. Cancer Research UK, *Myeloma statistics*, 2016, (2016; http://www.cancerresearchuk.org/health-professional/cancer-statistics/statistics-by-cancer-type/myeloma).
2. M. Mohty, J.-L. Harousseau, Eds., *Handbook of Multiple Myeloma* (ADIS (Springer), Cham, ed. 1, 2015), ISBN: 9783319182186.
3. K. Anderson, *Mayo Clinic Proceedings* **78**, 15–17 (2003).
4. C. A. Hutchison et al., *Clinical Journal of the American Society of Nephrology* **4**, 745–754 (2009).
5. B. G. M. Durie et al., *Leukemia* **20**, 1467–1473 (2006).
6. S. Kumar et al., *The Lancet Oncology* **17**, 328–346 (2016).
7. T. A. Waldmann, W. Strober, *Progress in Allergy* **13**, 1–110 (1969).
8. D. C. Roopenian, S. Akilesh, *Nature Reviews Immunology* **7**, 715–725 (2007).

2

Background

This chapter provides the background to the work and a brief summary of previous research that this work builds upon. It is divided into four sections. The first section deals with metabolism of immunoglobulins, in particular immunoglobulin G. The second section introduces the disease multiple myeloma. The third section discusses how multiple myeloma is monitored using blood monoclonal immunoglobulins, and how the prognostic utility of response markers is assessed using survival analysis. Finally these elements are brought together to formulate the problem that is the subject of this thesis.

2.1 Metabolism of immunoglobulins

2.1.1 Immunoglobulins

Immunoglobulins (Igs), or antibodies, are proteins of the immune system whose role is to identify and neutralise foreign objects, or antigens. Antibodies work by binding to antigens and generating an attack from other parts of the immune system. They are produced by white blood cells called plasma cells. They exist in two forms, membrane-bound as cell-surface receptors and secreted in the blood plasma and other body fluids.

The monomeric Ig consists of two identical heavy chains and two identical light chains connected by disulphide bonds to form a Y-shaped molecule (see figure 2-1). At the ends of the arms of the Y-shape are two identical antigen binding sites; hence this part of the

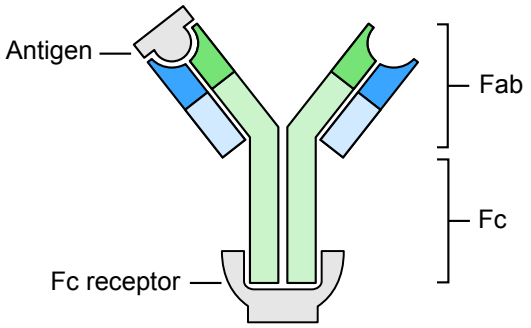

Figure 2-1 Immunoglobulin monomer. Heavy chains are shown in green, with the constant regions in light green and the variable regions in dark green. Light chains are shown in blue, with the constant regions in light blue and the variable regions in dark blue. The Fab region is shown to be binding an antigen and the Fc region is bound by an Fc receptor.

molecule is called the fragment antigen-binding (Fab) region. The base of the Y, known as the fragment crystallisable (Fc) region, is responsible for eliciting an appropriate response from other parts of the immune system, for example by binding to cell-surface receptors on phagocytic or cytotoxic white blood cells, inciting them to destroy the invading pathogen. Receptors which bind the Fc region of Igs are known as Fc receptors.

Humans (and most mammals) have five Ig isotypes – IgA, IgD, IgE, IgG and IgM – each having α, δ, ϵ, γ or μ heavy chains, respectively. There are two classes of light chain, κ and λ. An Ig has a pair of identical heavy chains and a pair of identical light chains; thus an individual molecule belongs to one heavy chain class and one light chain class only. An Ig with γ heavy chains and κ light chains for example is referred to as IgGκ. Each heavy chain has a constant region, identical within each isotype, and a variable region. Light chains also have a constant region, identical within their light chain class, and a variable region. Both heavy and light chains contribute to the variable region situated in the Fab portion of the Ig that enables an individual to produce an enormous range of Igs, specific to a wide variety of different antigens [1].

The five Ig isotypes all share the basic function of identifying and neutralising pathogens, but their roles differ in terms of their location in the body and the types of antigens against which they protect, mediated by the Fc region. The antibody isotypes also have slightly different structures and can form complexes: secreted IgA forms a dimer and IgM forms a pentamer. The Fc region of an Ig consists only of the constant region of two identical heavy chains; thus the immune response generated by the antibody is

Table 2-1 Antibody isotypes [1]

Name	Role	% of total Ig in serum	Half-life (days)
IgA	Protects against pathogens in mucosal locations including gastronintestinal tract and respiratory tract	5–15	6
IgD	Mostly exists as a B-cell receptor with barely detectable amounts in plasma	<1	2–3
IgE	Protects against parasitic worms and involved in allergy	<1	2–3
IgG	Found in plasma and extracellular spaces; responsible for most antibody-based immunity	75–85	23
IgM	Exists as a B-cell receptor and secreted in plasma; operates in the first instance of infection	5–10	5

determined by its isotype. The roles of the isotypes and their respective percentages of total Ig in adult serum are summarised in table 2-1 [1].

In this thesis interest lies primarily with IgA and IgG as they are most frequently implicated in multiple myeloma and we are concerned with their use as biomarkers for this disease. IgG is of particular interest as its concentration-dependent metabolic half-life in large part motivates this work. IgA and IgG both have subclasses: IgA1 and IgA2, and IgG1, IgG2, IgG3 and IgG4. The subclasses have small differences in the structure of their heavy chains that affect their properties. IgG is also special in that it is the only Ig isotype to be transferred across the placenta, offering protection to the newborn before its own immune system has developed [1].

2.1.2 Metabolism of immunoglobulin G

IgG is the most abundant Ig isotype in the circulation, having a plasma concentration of 10–16 $\mathrm{g\,l^{-1}}$ [2]. Its high concentration is enabled by its unusually long metabolic half-life (see table 2-1). Interestingly the half-life of IgG is not constant, but varies with its plasma concentration, as depicted in figure 2-2A. Figure 2-2B shows the fractional catabolic rate (FCR), that is the proportion of the IgG in plasma that is catabolised per day. The relationship between the concentration and half-life of IgG can be explained by its route of catabolism, mediated by the neonatal Fc receptor (FcRn). The receptor derives its name from its role in transporting IgG across the placenta from mother to foetus.

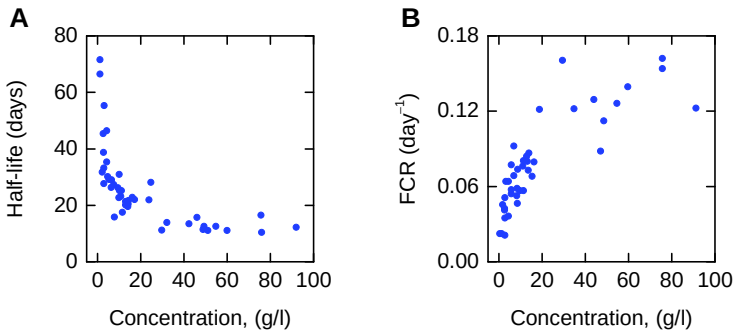

Figure 2-2 Plasma concentration-dependence of (A) metabolic half-life and (B) fractional catabolic rate of IgG; data from Waldmann et al. [3].

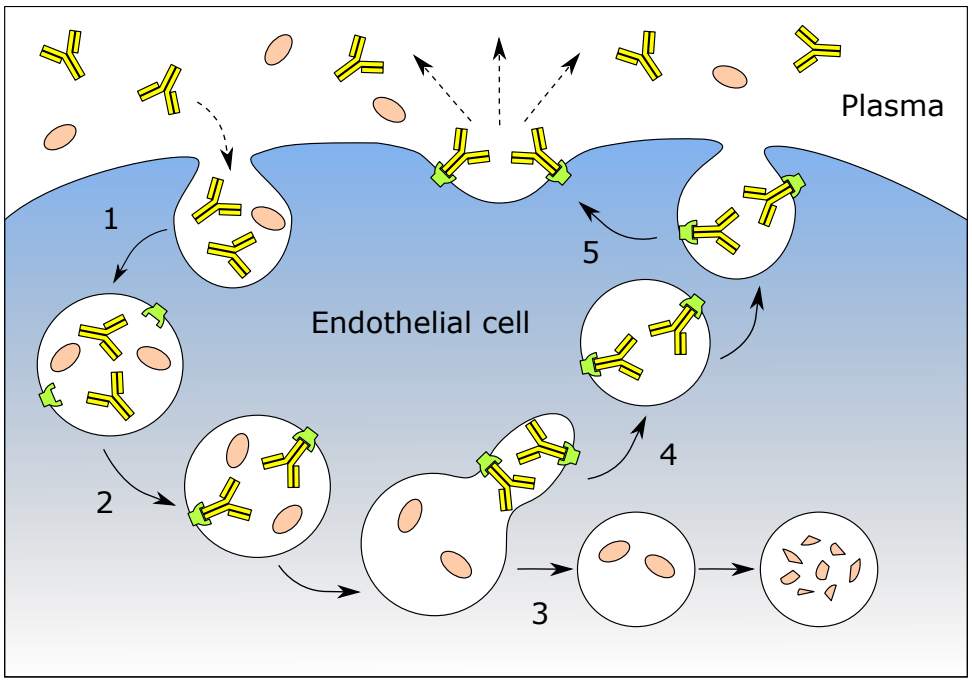

Figure 2-3 FcRn-mediated recycling of IgG. (1) IgG molecules are internalised into endosomes by nonspecific pinocytosis. (2) Endosomes acidify allowing FcRn to bind IgG. Bound and unbound proteins are sorted, with (3) unbound proteins degraded in lysosomes and (4) bound IgG trafficked to the cell surface. (5) Bound IgG is exocytosed back into the circulation.

IgG is catabolised by endocytosis, whereby molecules are internalised into cells in vesicles called endosomes in order to be degraded. FcRn expressed within these cells binds IgG inside the acidic environment of endosomes with a pH-dependent affinity. FcRn then sequesters the bound IgG away from the degradation pathway and back to the cell membrane, releasing it once again into the circulation. Those IgG molecules that are not bound to FcRn continue to follow the pathway to be degraded in lysosomes [4]. The scenario is illustrated in figure 2-3.

In this way, FcRn protects IgG from degradation in a recycling process. The variable half-life can be explained by the saturability of the recycling receptors. At increasing plasma concentrations of IgG the receptors become increasingly saturated and a greater proportion of IgG is degraded. Conversely at very low IgG concentrations a greater proportion is recycled and the half-life is increased. In the absence of FcRn the half-life of IgG is only three days, as has been observed in patients with a condition where FcRn is not expressed. At normal concentrations the half-life is approximately 23 days. The recycling system enables healthy humans to maintain high plasma concentrations of IgG [5; 6].

The relationship between production and concentration of IgG is therefore not entirely straightforward. Many mathematical models of IgG metabolism have been published in the literature (more than 20 at the time of writing), usually with the aim of describing the pharmacokinetics of therapeutic monoclonal antibodies (mAbs) that are similarly regulated by FcRn [7]. Many of the models are therefore pharmacokinetic in nature: their parameter values are obtained from animal experiments and they may be physiologically based, with up to around ten organs explicitly represented in the model [7–17]. Physiologically based pharmacokinetic models typically include the lymphatic system as well as the circulation [7; 9–12; 17]. Models describing mAb disposition may not be suitable for describing endogenous IgG dynamics, as whilst mAbs also benefit from FcRn-mediated recycling, they may be treated differently by the body in other ways, for example due to binding of the mAb to its target. In addition, mAb disposition may be adequately described by linear models in many cases, where the plasma concentration of therapeutic mAb is substantially smaller than the plasma concentration of endogenous IgG and the latter is constant [17].

For investigating the role of IgG as a cancer marker, physiologically based models may be more complex than necessary. Where models are more complex than the data they seek to represent, more sophisticated assumptions are required. Whilst it may be possible to reconcile the outputs of more complex models with human data, this does not imply that the model parameters or model assumptions are accurate, due to the inherent flexibility of such models [13]. In this thesis two comparatively simple models [3; 18; 19] are used. Both models are compartmental (lumped-parameter) models wherein the quantities or concentrations of IgG in discrete compartments are described by ordinary differential equations. The models are based upon the underlying biology of IgG and FcRn, which has been well characterised, and mass-balance principles.

2.1.3 Metabolism of immunoglobulin A

IgA is considered primarily as the antibody of the mucosal surfaces, such as within the gut and respiratory tract, and external secretions, including breast milk, saliva and tears. In mucosal areas, IgA primarily exists as a dimer with an additional secretory component, and is thus known as secretory IgA. IgA in the circulation is predominately monomeric and is known as systemic or serum IgA. Secretory and systemic IgA are synthesised in different physiological spaces. Secretory IgA is synthesised locally in large quantities in the mucosal tissues [20].

Plasma cells located in the bone marrow synthesise mainly monomeric IgA into the circulation [20]. In multiple myeloma monoclonal Igs are synthesised by clonal plasma cells located in the bone marrow and secreted into the plasma [21]; therefore it is the metabolism of systemic IgA that is important to this thesis and that needs to be represented by a mathematical model.

Unlike IgG, the rate at which systemic IgA is catabolised is independent of its plasma concentration, with a constant half-life of 6 days [3]. For this reason, and because most therapeutic monoclonal antibodies are rather based on IgG [22], there are not many mathematical models of systemic IgA metabolism in the literature. Fortunately, the experimental data on IgA metabolism indicate that a simple, linear, two-compartment model will suffice [3].

2.2 Multiple myeloma

Multiple myeloma accounts for 1% of all new cancer diagnoses in the UK. It is the 17th most common cancer in the UK and affects men more than women with 55% of UK diagnoses in men. The incidence rate increases with age, with 70% of cases occurring in people over 65. 77%, 47% and 33% of patients survive more than one, five and ten years with the disease, respectively [23].

Multiple myeloma is the cancer of Ig-producing, long-lived plasma cells. In healthy humans, long-lived plasma cells survive in the bone marrow for months or years following infection or vaccination, continuing to produce Igs against the original antigen in order to maintain serological memory. Multiple myeloma occurs when one of these cells becomes malignant [24]. Malignant plasma cells accumulate in the bone marrow, causing bone disease and hypercalcaemia and interfering with the bone marrow microenvironment, such that other blood cells are not produced in normal quantities. Thus patients develop anaemia and low counts of other white blood cells, rendering them more susceptible to infection.

The preferred treatment course for young (up to 65–70 years), fit patients consists of induction therapy based around novel agents, high dose chemotherapy, autologous stem cell transplantation (ASCT), consolidation therapy and maintenance therapy. The goal of induction therapy is to decrease the tumour burden in order to improve the overall response, and to improve the quality of bone marrow that is harvested before high dose chemotherapy and transplanted afterwards. Induction regimens based around novel agents, particularly proteasome inhibitors, such as bortezomib, and immunomodulatory agents, such as thalidomide and its derivatives, have contributed to the significant improvement in patient outcomes that have been seen in the last decade [21; 25]. Consolidation therapy is optional and short-term. Maintenance therapy is a long-term, 'gentler' therapy, intended to maintain the response achieved by induction therapy and ASCT. Those patients for whom stem cell transplantation is not possible are treated with combinations of chemotherapy, steroids and biological therapies [21; 26].

Malignant plasma cells usually produce a large quantity of a monoclonal Ig and/or Ig light chain (with the exception of oligosecretory and nonsecretory multiple myeloma). As

they are derived from a single clone, myeloma cells produce monoclonal Igs. Thus Igs of a single heavy chain isotype (α, δ, ϵ, γ or μ) and a single light chain isotype (κ or λ) are produced in an individual patient, for example IgGκ (γ heavy chain and κ light chain) [27]. IgG multiple myeloma is the most common form (50%), followed by IgA (20%), whilst IgD, IgE and IgM myelomas are rare [28]. Patients producing a monoclonal Ig are said to have intact Ig multiple myeloma (IIMM). Monoclonal Igs do not fulfil any useful function. In addition, patients' normal, polyclonal, functioning antibodies are usually suppressed [29].

Around 20% of patients do not produce an intact monoclonal Ig, but produce a monoclonal Ig free light chain (κ or λ). These patients are said to have light chain multiple myeloma. Free light chains (FLC) are cleared by the kidneys, which in large quantities can lead to renal failure [30]. Around 3% of patients produce little (oligosecretory myeloma) or no monoclonal protein at all (nonsecretory myeloma) [23].

The initial investigation of a patient with suspected multiple myeloma involves a range of laboratory tests along with physical examination and examination of medical and family history. Symptomatic multiple myeloma is diagnosed by confirmation of all three of the following criteria [31]:

- clonal bone marrow plasma cells $\geq$10%, measured by bone marrow aspirate/biopsy;
- presence of serum and/or urinary monoclonal protein, identified by electrophoresis and immunofixation (except in nonsecretory multiple myeloma);
- evidence of end-organ damage, that is hypercalcaemia, renal insufficiency, anemia and/or bone lesions.

2.2.1 International uniform response and disease progression criteria

During therapy, both serum protein electrophoresis and nephelometric quantification of Igs (see section 2.4) are recommended for the assessment of tumour response. For light chain multiple myeloma patients FLC should be measured in urine. Serum FLC should also be monitored in all patients, particularly in those with nonsecretory or oligosecretory

Table 2-2 IMWG international uniform response criteria. See Kumar et al. [33] for the full version.

Response	Criteria
sCR	CR with normal FLC ratio and absence of clonal cells in bone marrow
CR	Negative immunofixation on serum and urine, disappearance of soft tissue plasmacytomas and $\leq$5% plasma cells in bone marrow
VGPR	Monoclonal protein detectable by immunofixation but not on electrophoresis or $\geq$90% reduction in serum monoclonal protein and urine monoclonal protein <100 mg per 24 h
PR	$\geq$50% reduction in serum monoclonal protein and $\geq$90% reduction in 24 h urinary monoclonal protein or to <200 mg per 24 h
SD	Not meeting criteria for CR, VGPR, PR or PD

multiple myeloma. A multitude of other tests are used in the investigation, diagnosis and monitoring of multiple myeloma, however they are not studied in this thesis [31; 32].

Observations of decreasing blood monoclonal Ig concentration can be used to assess the response to treatment. In order that responses can be assigned that have universal meaning, the International Myeloma Working Group (IMWG) has developed international uniform response criteria. The IMWG responses are stringent complete response (sCR), complete response (CR), very good partial response (VGPR), partial response (PR) and stable disease (SD), as summarised in table 2-2. The criteria have been somewhat simplified; for the full version see Kumar et al. [33].

The involvement of malignant plasma cells in the bone marrow is assessed by the bone marrow plasma cell percentage (BMPC%) in order to confirm diagnosis. The BMPC% is estimated on the bone marrow aspirate and biopsy. These procedures are invasive and unpleasant for the patient and are in practice restricted to diagnosis (more than 10% BMPC required) and when a complete response is suspected (less than 5% BMPC required for CR). Notably physicians do not consider the response in the BMPC% in terms of its proportional decrease during therapy. For response assessment, specifically the assignment of CR, only the absolute value of BMPC% is used. This is in contrast to serum monoclonal protein concentration, which is always considered in terms of its proportional decrease (see table 2-2) [33; 34].

Relapse can be assigned as either progressive disease (PD), clinical relapse or relapse from complete response. PD criteria are important because the assignment of PD is used for

the calculation of progression-free survival (PFS). PD assignment requires an increase of 25% from the lowest value in at least one of the following [33]:

- serum monoclonal protein (absolute increase $\geq$0.5 g/dl) *or* $\geq$1 g dl^{-1}, if the lowest value was $\geq$5 g dl^{-1};
- urine monoclonal protein (absolute increase $\geq$200 mg/24 h);
- the difference between involved and uninvolved FLC (absolute increase $\geq$10 mg dl^{-1});
- bone marrow plasma cell percentage (absolute value $\geq$10%);
- New bone lesions or increase in size of those pre-existing;
- $\geq$50% increase in circulating plasma cells (minimum of 200 cells per µl).

2.3 Early studies linking tumour burden with monoclonal protein

Response assessment and patient monitoring using blood monoclonal proteins are based upon the fundamental assumption that a growing tumour burden causes an increase in blood monoclonal protein and that a shrinking tumour burden causes a decrease. Thus from increases and decreases in monoclonal protein concentrations, clinicians can infer tumour growth or regression, respectively. The earliest studies linking myeloma cell number with monoclonal protein were performed in mice using transplantable mouse plasmacytomas – discrete plasma cell tumours which closely resemble multiple myeloma in human [35; 36]. Plasmacytomas in mice are convenient for study because the animal can be sacrificed and the tumour excised and weighed. Multiple myeloma on the other hand presents with a systemic infiltration of cells in the marrow rather than a discrete mass; estimation of the extent of the infiltration is therefore not as simple. Sacrifice of the animal prior to tumour mass assessment has meant that the author has had difficulty finding studies with serial measurements of tumour size in mouse.

Nathans et al. [35] authored one of the earliest papers to provide conclusive evidence that the monoclonal Ig often present in multiple myeloma is produced by the cancerous cells themselves and not by another tissue in response to the tumour. Nathans et al.

[35] studied mice bearing transplanted plasmacytomas, sacrificing individuals at intervals in order to obtain measurements from the tumours. Using biosynthetic labelling with amino acid (glycine), they showed that monoclonal Igs in the tumour tissue are the immediate precursors of circulating plasma monoclonal Igs, leading to the conclusion that monoclonal IgG is synthesised by the plasma cells of the tumour. They also correlated the mass of excised tumours against the total quantity of plasma monoclonal Ig, finding a strong positive relationship.

Humphrey et al. [36] also studied mice with transplanted IgG-producing plasmacytomas. They injected radiolabelled monoclonal IgG and normal (polyclonal) IgG into mice with plasmacytomas and found that the proportional rate of catabolism of either protein was positively associated with both the tumour burden and the quantity of serum monoclonal IgG. In normal mice, monoclonal and polyclonal IgG had the same half-life; in the mice with IgG-producing plasmacytomas the half-life was the same for both proteins, but dramatically shortened. In general, mice with the highest blood concentrations of monoclonal IgG demonstrated the fastest catabolism of both monoclonal and polyclonal administered IgG. It is now known that this is due to saturation of FcRn receptors; however Brambell et al. [37] first postulated a saturable recycling receptor for IgG three years later and the receptor itself was not discovered until the 1990s. Humphrey et al. [36] excised the plasmacytomas from the recipient mice at the end of the experiment and weighed the tumours; however little analysis was performed on these data, possibly due to the relatively small number of individuals studied. Similarly to Nathans et al. [35], no serial assessment of tumour size was made.

Solomon et al. [38] extended the work of Humphrey et al. [36] to the human case. For a range of human subjects, including IgG- and IgA-myeloma patients, the investigators performed a study of the metabolism of radiolabelled normal IgG. They correlated the half-life of normal IgG against the serum IgG concentration, finding a strong relationship, with those subjects having an elevated IgG concentration having a shorter half-life and vice versa. They concluded that the presence of IgA- or FLC-producing myeloma cells does not accelerate IgG catabolism – nor does the presence of the proteins produced by these cells – therefore the class of the monoclonal protein is important in determining the cause of increased IgG catabolism. Of course it is now known that it is the presence of a

large quantity of IgG that causes FcRn receptor saturation [4].

Salmon et al. [39] provide an early study linking tumour burden with plasma monoclonal Ig in humans. Salmon et al. [39] performed an in vivo turnover study of radiolabelled IgG and calculated the FCR for each patient from the radioactivity data. Using the calculated FCR, along with measurements of serum monoclonal IgG concentration and plasma volume, they calculated the absolute rate of IgG catabolism, assuming steady state conditions. They also measured the in vitro rate of IgG synthesis per myeloma cell. The total number of myeloma cells was estimated from the in vivo monoclonal IgG production rate divided by the in vitro synthesis rate per cell. The authors found that measurements of cellular IgG synthesis varied between patients, but within patients were reproducible; in one patient the cellular IgG synthesis rate was consistent over eight months, both before and after chemotherapy. Receiving chemotherapy prior to the study did not seem to have an effect on the cellular IgG synthesis rate. Estimates of the total myeloma cell population correlated with the extent of skeletal disease; however neither the total IgG synthesis rate nor the cellular IgG synthesis rate correlated with skeletal damage independently. The variability in cellular Ig synthesis rates could contribute to the unreliability of absolute values of plasma monoclonal Ig for prognosis: only percentage changes and not absolute values are used in response criteria (see section 2.2.1).

The study by Sullivan et al. [40] is conceptually similar to that of Salmon et al. [39]; however now serial assessments of serum monoclonal IgG were made, from which growth and regression curves of the myeloma cell population were predicted. Hiramoto et al. [41] performed a similar study but in mice. IgM-producing plasmacytomas were transplanted in mice which were treated with chemotherapy. The actual tumour size was not assessed; however the tumour cell number was calculated based on measurements of plasma IgM, the metabolic half-life of IgM and a model for tumour growth and tumour kill. Hiramoto et al. [41] observed the total quantity of monoclonal IgM per mouse increase between injection of the tumour cells and administration of cyclophosphamide (chemotherapy), and subsequently decrease following the treatment.

2.4 The role of serum monoclonal immunoglobulin in response assessment

Serum monoclonal Ig plays an important part in monitoring and response assessment in multiple myeloma. Firstly it should be clarified that Igs are assayed in patient serum, which simply refers to a blood sample that has been removed of blood cells and clotting factors. They can also be measured in urine, however in this thesis we are only interested in serum monoclonal Ig. Here the laboratory tests used to measure monoclonal Ig in a serum sample are briefly introduced.

2.4.1 Laboratory tests

Serum protein electrophoresis

Serum protein electrophoresis (SPEP) is a gel-based technique in which proteins are separated by their electrophoretic mobility (dependent on size, charge, shape, etc.) on a gel. Staining the proteins with a dye then results in distinct bands representing different proteins in the sample. One such band represents the γ-globulins. A myeloma patient will typically have a dense band in this region, known as an M-spike. The gel is then analysed by densitometry, whereby the stained gel is scanned to produce a line drawing, or 'electrophoretogram', representing the density of stain along the gel, with peaks representing the proteins in different regions. The monoclonal protein typically appears as a large, sharp peak in the γ-globulin region, hence the term 'M-spike'. By quantifying the total protein concentration by an alternative assay and determining the area under the M-spike relative to the area under the whole curve, the analyst can quantify the concentration of monoclonal Ig in the sample [42; 43].

After separation on a gel it is possible to identify the heavy and light chain types of the M-spike by immunofixation. In this technique antibodies are applied to the gel that are specific to IgG, IgA, IgM, κ light chains and λ light chains, respectively. Now the monoclonal band will appear only in one heavy chain lane and one light chain lane, enabling the clinician to identify the monoclonal Ig as, for example, IgAκ.

Nephelometric quantification of immunoglobulins

Nephelometric quantification of Igs uses antibodies specific to the Ig under study, for example IgA. IgA in the serum sample reacts with anti-IgA antibodies to form large complexes. The analyst then measures the light scatter from the sample and compares this with reference curves to obtain the concentration of IgA in the sample. Nephelometric assays are particularly useful for patients with very small amounts of monoclonal Ig in the blood that may not be detected by SPEP [31].

Heavy/light chain assay

More recently it has become possible to measure different light chain types of intact Igs by targeting an epitope between the heavy and light chain, with the heavy/light chain (HLC) assay [44]. It is thus now possible to separately quantify IgAκ, IgAλ, IgGκ, IgGλ, IgMκ and IgMλ in patient sera. The HLC assay also relies on nephelometry; however throughout this thesis HLC is used to refer to the quantification of Igs by both heavy and light chain type, and nephelometry is used to refer to the quantification of Igs by heavy chain type only. In an IgGκ patient, for example, the HLC measurement of IgGκ can be considered to represent the monoclonal Ig. We refer to the IgGκ measurement in an IgGκ patient as the involved HLC.

2.4.2 Limitations of techniques for serum monoclonal immunoglobulin quantification

It is of course not possible to ascertain the 'true' monoclonal Ig concentration as all measurements taken from patients are subject to error. More significantly, it is also difficult to separate the monoclonal Ig from polyclonal Ig in the sample. SPEP can in some sense be considered as quantifying only the monoclonal Ig because it typically presents as a prominent spike on the electrophoretogram. The polyclonal γ-globulin fraction is diffuse and therefore an M-spike present in the γ region is believed to pertain mainly to the monoclonal Ig. Generally SPEP is the preferred technique for M-spike quantification for this reason [45]. There is of course polyclonal Ig present in the background between

the limits of the M-spike and there is also the issue that these limits are set by the interpreter, usually as vertical lines, which can be seen as subjective [43].

Another limitation of SPEP is that monoclonal Igs, particularly IgA, of relatively low concentration migrate in the β-region and are obscured by other proteins in this region, such as transferrin and C3. The aforementioned issues represent a more significant problem when the concentration of monoclonal Ig is comparatively small. Indeed at small concentrations, less than 10 $\mathrm{g\,l^{-1}}$, SPEP is acknowledged to be unreliable. At large concentrations there is the possibility of dye saturation leading to an underestimation of the monoclonal Ig concentration [43; 46; 47].

The HLC assay does not suffer from issues associated with gel-based techniques. The assay is also more sensitive than SPEP and can quantify concentrations less than 1 $\mathrm{g\,l^{-1}}$, presenting a significant advantage over SPEP. One limitation of HLC is that the assay measures both monoclonal and polyclonal Ig of the same heavy- and light-chain type as the monoclonal Ig. This presents a similar problem to background polyclonal Ig in the same region of the gel as the M-spike, and similarly becomes significant when the HLC is in the normal reference range. Fortunately the HLC assay provides the concentration of the polyclonal Ig of the same heavy chain type but alternative light chain type as the paraprotein, e.g. IgAκ in an IgAλ patient. Therefore HLC measurements are often considered as Ig'κ/Ig'λ ratios.

2.4.3 Interpretation of serum monoclonal immunoglobulins in practice

In patient monitoring, monoclonal Igs have two roles as markers: response assessment and follow-up. In this thesis we are primarily interested in monoclonal Igs as response markers. Response assessment is particularly important because it is believed that the better the response to therapy, the better the prognosis of the patient.

In multiple myeloma, the fall in serum monoclonal Ig concentration in the months following initiation of therapy is used as an indication that the tumour is responding. An example of how the monoclonal Ig (in this case involved HLC) for an individual patient changes during the course of therapy is shown in figure 2-4. The data in figure 2-4 is

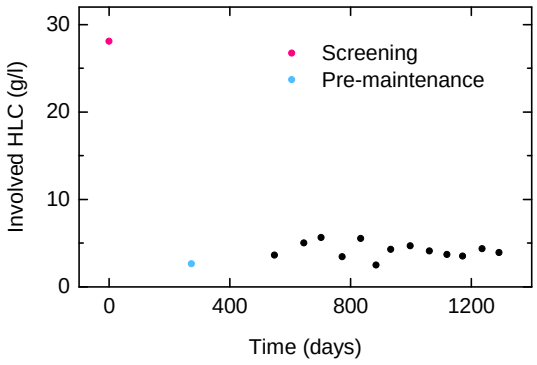

Figure 2-4 Plot of involved HLC concentration during treatment for a patient with IgGλ myeloma. The data is taken from the IFM 2009/01 clinical trial, which is analysed in chapter 9.

from the IFM (Intergroupe Francophone du Myélome) 2009/01 clinical trial [48; 49]. At screening, highlighted in pink, the patient presents with an elevated concentration of the involved HLC. Following induction therapy, the concentration has decreased from 28.09 $\mathrm{g\,l^{-1}}$ at screening to 2.63 $\mathrm{g\,l^{-1}}$ at pre-maintenance (highlighted in light blue), a decrease of 90.6%. At this point the physician can use the proportional decrease in the involved HLC concentration to assess the quality of the response to treatment. Responses are assigned using the decrease in serum monoclonal Ig concentration as a proportion of its baseline value, along with other clinical indicators. A decrease of 90.6% in the monoclonal protein corresponds to VGPR (see table 2-2).

Patient responses are often discussed in terms of their quality or depth. The proportional or percentage decrease in the monoclonal Ig concentration is often referred to as the 'depth' of response, with larger decreases representing deeper, or higher quality, responses. When referring to the IMWG responses given in table 2-2, sCR represents a deeper response than CR, CR represents a deeper response than VGPR, and so on.

At pre-maintenance, the patient shown in figure 2-4 begins a year-long course of maintenance therapy. By this stage, the serum monoclonal Ig has reached a plateau phase. After maintenance therapy, the involved HLC is monitored approximately every two months for 22 months of follow-up. During this time serum monoclonal Ig is monitored for any increase that may indicate regrowth of the tumour [32].

2.4.4 Evaluation of response markers in multiple myeloma

The prognostic ability of response markers is evaluated by the strength of their association with long-term outcomes, specifically event time outcomes. The most widely used event time outcomes in multiple myeloma are overall survival (OS) and progression-free survival (PFS) [50]. These outcomes are used to assess the efficacy of treatment regimens in clinical trials. OS is given by the date of death. PFS is calculated as the time when the criteria for PD are met (see section 2.2.1), or the time of death, when death occurs first. PFS is ultimately decided by the physician and so is somewhat susceptible to investigator bias. OS is less ambiguous, however its use is limited by several factors, outlined by Durie et al. [50]. In chapter 9, the association between monoclonal Ig response during therapy and PFS is analysed.

The multiple myeloma literature has focused on the association between depth of response, as defined by the criteria in table 2-2, and PFS or OS. In order to analyse this association, patients are grouped according to the response achieved at a clinically significant time point, and the subsequent survival times compared between the groups. The survival times, such as PFS, can be compared using the log-rank test or proportional hazards regression [51–54].

The prognostic utility of the currently recommended response criteria, given in table 2-2, has been debated [55; 56]. The strength of the association between response to treatment and survival outcomes depends on the particular therapy administered, at what time the response is evaluated, and the survival endpoint used. In recent years, with the introduction of novel agents, more and more patients have been achieving CR and the importance of accurate response markers has been emphasized [51; 57].

2.5 The research problem

The ultimate goal of therapy is cure; however, given that multiple myeloma is currently considered incurable, preserving and prolonging quality of life is a primary goal of patient care. The means to achieving improved OS and PFS is to eradicate as large a proportion of the tumour burden as possible [57].

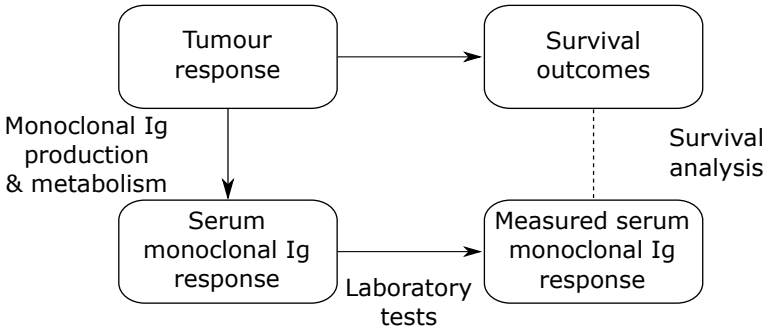

Figure 2-5 Illustration of how different aspects of the research problem are connected to one another. Arrows represent causal relationships. See section 2.5 for details.

Rather than assess the proportion of the tumour that has been eradicated, physicians instead monitor the proportional decrease in the serum monoclonal Ig, as described in section 2.4. Throughout this thesis, the term 'tumour response' is used to refer to either the proportion of the tumour burden eradicated, or the proportion of the tumour burden still remaining, at a certain time during treatment. Similarly, 'monoclonal Ig response' is used to refer to the decrease in serum monoclonal Ig concentration as a proportion of its baseline value, at any time during treatment, or alternatively the proportion remaining. Of course, a monoclonal Ig response of, say, 90% does not necessarily mean that 90% of the tumour cells have been eradicated: the concentration of monoclonal Ig in the blood at any time depends both on its rate of production, which is assumed proportional to the tumour burden, and also the rate at which the Ig is eliminated.

As described in section 2.1, IgA and IgG are known to have metabolic half-lives of 6 days and 23 days, at normal concentrations, respectively, while the elimination rate of IgG is concentration-dependent due to saturable recycling by FcRn. The purpose of this thesis is to investigate possible differences between monoclonal IgA and monoclonal IgG responses, in terms of their relationship with tumour response. Monoclonal Ig responses of 90% in an IgA patient and in an IgG patient do not necessarily correspond to the same tumour response. The long metabolic half-life of IgG suggests that monoclonal IgG would respond more slowly than monoclonal IgA, for the same tumour response. In addition, the concentration-dependent half-life of IgG implies that, at the beginning of treatment, IgG is eliminated at a faster than normal rate, due to saturation of recycling receptors.

Figure 2-5 depicts the different elements of the research problem and how they are related.

The arrows represent links between two elements where one is seen to be driving the other. The dashed line connecting survival outcomes with measured serum monoclonal Ig response represents the associative link between these two measurable outcomes. This association is studied using the methods of survival analysis, which are introduced in chapter 4. The aim of this project is to consider the left hand side of the diagram – the metabolic processes that link tumour response and serum monoclonal Ig response – and how this might impact upon the association between measured monoclonal Ig responses and survival endpoints. Throughout this thesis, and as indicated in figure 2-5, it is assumed that the quality of the tumour response ultimately drives survival outcomes.

2.5.1 Previous contributions to the research problem

The effect of the metabolism of Igs on their application as biomarkers in multiple myeloma has been little studied, perhaps because the importance of accurate response markers has been highlighted only in recent years with the adoption of novel agents and ASCT. Salmon et al. [39] and Sullivan et al. [40] first directed attention to the issue of IgG metabolism in multiple myeloma in the early 1970s. Salmon et al. [39] stated: 'Because of metabolic considerations, serial paraprotein measurements in IgG myeloma may not reflect total paraprotein synthesis or tumor cell mass in a linear fashion. Despite this limitation, determinations of paraprotein concentrations remain the most valuable parameter for objective follow-up of such patients. In IgA myeloma, because of the relatively fixed IgA catabolic rate, changes in the serum concentration would be anticipated to reflect the changes in cell mass more directly'. Sullivan et al. [40] recognised that 'changes in IgG metabolism, which occur as a concentration-dependent phenomenon, could lead to significant underestimation of the degree of change in total body M-component synthesis (and tumor mass)', noting that this would particularly affect patients presenting with low concentrations of IgG and could adversely influence the management of such patients.

A more recent contribution to the problem of IgG metabolism in multiple myeloma has been made by Hattersley [19]. Hattersley derived a reduced model of IgG metabolism and estimated parameter values using HLC data from an IgG myeloma patient, assuming a delayed logistic form for the production rate of monoclonal IgG. Hattersley then evaluated the use of different response markers using mathematical analysis, concluding that the

ratio of monoclonal to polyclonal IgG may be the best response marker.

In spite of the relatively little research in this area, potential issues arising from IgG metabolism are acknowledged in the multiple myeloma community. Bradwell et al. [58] and Koulieris et al. [59] cite the concentration-dependent metabolism of IgG as a possible explanation for why monoclonal IgG can be seen as unreliable and its utility as a biomarker still debated in the literature. Durie et al. [50] also advise that metabolic properties of Igs are a potential problem. Bradwell [60] discusses in detail several aspects of the problem, stating that, due to the concentration-dependent metabolism of IgG, serum IgG concentrations 'do not accurately relate to tumour production rates'.

2.5.2 Contributions of this thesis

In this thesis the effects of IgG metabolism on monoclonal Ig responses in IgG myeloma are investigated, with a focus on the potential differences between monoclonal Ig responses in IgA and IgG myeloma patients, respectively. The different metabolisms of IgA and IgG could have a real impact in patient monitoring and response assessment, which is also investigated in this thesis using survival data from a recent clinical trial.

In this thesis two compartmental models of IgG metabolism, which have previously been published by Waldmann et al. [3], Kim et al. [18] and Hattersley et al. [61], are analysed with respect to parameter identification. In chapters 5 and 6 model parameter values are estimated using data available in the literature from tracer experiments, specifically designed to demonstrate the steady state metabolic behaviour of Igs. The two models of IgG metabolism are compared using simulations in chapter 7. The behaviour of monoclonal Ig responses in IgA and IgG patients is predicted using simulations that qualitatively agree with patient data. The implications of IgA and IgG metabolism for the association between the monoclonal Ig response and survival outcomes is analysed in a dataset from a recent clinical trial.

It is important that physicians can meaningfully assess tumour responses during therapy. With the introduction of novel agents and ASCT, patients are achieving deeper responses to treatment, and, in particular, the achievement of CR is treated as an important therapeutic goal [21; 57]. Therefore assigned responses must be strongly correlated with

long-term outcomes. Whilst the outlook for patients has improved over the last 20 years, still the majority of patients will go on to relapse or develop refractory disease [62]. For this reason it is all the more important to be able to provide patients, who will likely live with the disease until death, with as much information as possible about their response to treatment and prognosis.

References

1. K. S. Rosenthal, M. J. Tan, *Rapid Review Microbiology and Immunology* (Mosby (Elsevier), Philadelphia, ed. 3, 2010), ISBN: 9780323240239.
2. A. Hall, C. Yates, Eds., *Immunology* (Oxford University Press, Oxford, ed. 1, 2010), ISBN: 0199534969.
3. T. A. Waldmann, W. Strober, *Progress in Allergy* **13**, 1–110 (1969).
4. R. P. Junghans, C. L. Anderson, *Proceedings of the National Academy of Sciences of the United States of America* **93**, 5512–5516 (1996).
5. T. A. Waldmann, W. D. Terry, *The Journal of Clinical Investigation* **86**, 2093–2098 (1990).
6. D. C. Roopenian, S. Akilesh, *Nature Reviews Immunology* **7**, 715–725 (2007).
7. Y. Chen, J. P. Balthasar, *The AAPS Journal* **14**, 850–859 (2012).
8. R. J. Hansen, J. P. Balthasar, *Journal of Pharmaceutical Sciences* **92**, 1206–1215 (2003).
9. G. Z. Ferl, A. M. Wu, J. J. DiStefano, *Annals of Biomedical Engineering* **33**, 1640–1652 (2005).
10. A. Garg, J. P. Balthasar, *Journal of Pharmacokinetics and Pharmacodynamics* **34**, 687–709 (2007).
11. L. Fang, D. Sun, *Drug Metabolism and Disposition* **36**, 1153–1165 (2008).
12. S. Urva, V. Yang, J. Balthasar, *Journal of Pharmaceutical Sciences* **99**, 1582–1600 (2010).
13. J. J. Xiao, *Journal of Biomedicine and Biotechnology* **2012** (2012).
14. R. Deng et al., *mAbs* **4**, 101–109 (2012).
15. X. Yan, Y. Chen, W. Krzyzanski, *Journal of Pharmacokinetics and Pharmacodynamics* **39**, 543–560 (2012).
16. C. M. Ng et al., *European Journal of Pharmaceutical Sciences* **51**, 51–58 (2014).
17. L. Fronton, S. Pilari, W. Huisinga, *Journal of Pharmacokinetics and Pharmacodynamics* **41**, 87–107 (2014).
18. J. Kim, W. L. Hayton, J. M. Robinson, C. L. Anderson, *Clinical Immunology* **122**, 146–155 (2007).
19. J. G. Hattersley, PhD thesis, University of Warwick, 2009.

20. J. M. Woof, J. Mestecky, in *Mucosal Immunology*, ed. by J. Mestecky et al. (Academic Press (Elsevier), Amsterdam, ed. 4, 2015), chap. 17, ISBN: 9780124159754.
21. M. Mohty, J.-L. Harousseau, Eds., *Handbook of Multiple Myeloma* (ADIS (Springer), Cham, ed. 1, 2015), ISBN: 9783319182186.
22. A. L. Nelson, E. Dhimolea, J. M. Reichert, *Nature Reviews Drug Discovery* **9**, 767–774 (2010).
23. Cancer Research UK, *Myeloma statistics*, 2016, (2016; http://www.cancerresearchuk.org/health-professional/cancer-statistics/statistics-by-cancer-type/myeloma).
24. G. Bianchi, N. C. Munshi, *Blood* **125**, 3049–3058 (2015).
25. L. Naymagon, M. Abdul-Hay, *Journal of Hematology & Oncology* **9** (2016).
26. H. Ludwig et al., *The Oncologist* **15**, 6–25 (2010).
27. M. S. Raab et al., *Lancet* **374**, 324–339 (2009).
28. K. Anderson, *Mayo Clinic Proceedings* **78**, 15–17 (2003).
29. E. Kastritis et al., *Leukemia* **28**, 2075–2079 (2014).
30. C. A. Hutchison et al., *Clinical Journal of the American Society of Nephrology* **4**, 745–754 (2009).
31. M. Dimopoulos et al., *Blood* **117**, 4701–4705 (2011).
32. H. Ludwig et al., *Leukemia* **28**, 981–992 (2014).
33. S. Kumar et al., *The Lancet Oncology* **17**, 328–346 (2016).
34. S. V. Rajkumar et al., *American Journal of Hematology* **68**, 269–275 (2001).
35. D. Nathans, J. L. Fahey, M. Potter, *Journal of Experimental Medicine* **108**, 121–130 (1958).
36. J. H. Humphrey, J. L. Fahey, *Journal of Clinical Investigation* **40**, 1696–1705 (1961).
37. F. W. R. Brambell, W. A. Hemmings, I. G. Morris, *Nature* **203**, 1352–1355 (1964).
38. A. Solomon, T. Waldmann, J. Fahey, *The Journal of Laboratory and Clinical Medicine* **62**, 1–17 (1963).
39. S. E. Salmon, B. A. Smith, *Journal of Clinical Investigation* **49**, 1114–1121 (1970).
40. P. W. Sullivan, S. E. Salmon, *The Journal of Clinical Investigation* **51**, 1697–1708 (1972).
41. R. N. Hiramoto, V. K. Ghanta, *Cancer Research* **34**, 1738–1742 (1974).

42. B. Kurien, R. Scofield, Eds., *Protein Electrophoresis: Methods and Protocols* (Humana Press (Springer), New York, 2012), ISBN: 9781617798214.
43. D. F. Keren, *Protein Electrophoresis in Clinical Diagnosis* (Arnold, London, ed. 1, 2003), ISBN: 0340812133.
44. A. R. Bradwell et al., *Clinical Chemistry* **55**, 1646–1655 (2009).
45. D. L. Murray, E. Ryu, M. R. Snyder, J. A. Katzmann, *Clinical Chemistry* **55**, 1523–1529 (2009).
46. A. R. Bradwell, *Serum Free Light Chain Analysis* (The Binding Site Ltd., Birmingham, ed. 6, 2010), ISBN: 9780704427969.
47. J. A. Katzmann et al., *Clinical Chemistry* **57**, 1687–1692 (2011).
48. U.S. National Library of Medicine, *Study comparing conventional dose combination RVD to high-dose treatment with ASCT in the initial myeloma up to 65 years (IFM/DFCI2009)*, 2010, (2018; https://clinicaltrials.gov/ct2/show/study/NCT01191060).
49. M. Attal et al., *New England Journal of Medicine* **376**, 1311–1320 (2017).
50. B. G. M. Durie et al., *Leukemia* **20**, 1467–1473 (2006).
51. J.-L. Harousseau, M. Attal, H. Avet-Loiseau, *Blood* **114**, 3139–3146 (2009).
52. J.-L. Harousseau et al., *Journal of Clinical Oncology* **27**, 5720–5726 (2009).
53. R. Niesvizky et al., *British Journal of Haematology* **143**, 46–53 (2008).
54. J. Bladé et al., *Bone Marrow Transplantation* **26**, 845–849 (2000).
55. B. G. M. Durie, J. Jacobson, B. Barlogie, J. Crowley, *Journal of Clinical Oncology* **22**, 1857–1863 (2004).
56. A. Berenson et al., *Blood* **124**, 5771 (2014).
57. A. A. Chanan-Khan, S. Giralt, *Journal of Clinical Oncology* **28**, 2612–2624 (2010).
58. A. Bradwell et al., *Leukemia* **27**, 202–207 (2013).
59. E. Koulieris et al., *Experimental Hematology and Oncology* **1** (2012).
60. A. Bradwell, *Hematology Reports* **2**, 16–18 (2010).
61. J. G. Hattersley et al., *Computer Methods and Programs in Biomedicine* **109**, 126–133 (2013).
62. M. Attal et al., *Blood* **108**, 3289–3294 (2006).

3

Compartmental modelling of physiological systems

The theory and methods of compartmental modelling are used in chapters 5–8. The aim of the thesis is to investigate the impact of immunoglobulin (Ig) metabolism on the association between plasma monoclonal Ig responses and survival, in multiple myeloma. Achieving this aim requires predictions to be generated from compartmental models.

In this chapter compartmental models and their use in pharmacokinetic and physiological applications are introduced. The methods of parameter estimation, structural identifiability analysis and simulation are briefly discussed, along with the computational tools for their application.

3.1 Compartmental modelling

A compartmental model is a mathematical model consisting of a finite number of discrete 'compartments', each representing a homogeneous, well-mixed amount of substance (or other physical quantity). Compartments are connected to one another and the environment by flows of material, which is assumed to mix uniformly and instantaneously on entering a compartment. Given a physical system which can be reasonably approximated by a collection of compartments, the modeller applies the principle of conservation of mass to obtain a mathematical model described by ordinary differential equations. For a

comprehensive overview of compartmental modelling theory see Jacquez [1] and Godfrey [2].

Compartmental models are used widely, particularly in the field of pharmacokinetics. Often the concentration of a drug (or protein, or metabolite) in plasma is homogeneous and can be assumed to behave as a compartment. Pharmacokinetic compartmental models commonly consist of a central compartment (also called the plasma or vascular compartment) and a peripheral compartment (also called the extravascular compartment), representing those tissues which are less rapidly perfused by the drug. Other compartments specific to the drug administration or elimination mechanism may be incorporated, such as the gastrointestinal tract and urine. Similarly, compartmental models can be used to describe the kinetics of substances endogenous to the subject such as proteins and metabolites. Application of the principle of conservation of mass yields a mathematical description of the model, usually in the form of coupled ordinary differential equations with a number of unknown parameters [1–3].

The general conceptual form of a compartmental model is illustrated in figure 3-1. The general compartmental model is described mathematically by

$$\frac{\mathrm{d}x_i}{\mathrm{d}t} = f_{i0} + \sum_{\substack{j=1 \\ j\neq i}}^{p} f_{ij} - \sum_{\substack{j=1 \\ j\neq i}}^{p} f_{ji} - f_{0i}, \qquad i = 1, 2, ..., p, \tag{3-1}$$

where $x_i(t)$ is the quantity or concentration of material in compartment i and f_{ij} is the material flow from compartment j to compartment i. The flows between compartments are positive. In physiological models the material flow f_{ij} is often directly proportional to the quantity of material in compartment j. In linear models, the constant of proportionality is denoted by k_{ij}, has dimension 1/time and is referred to as a rate constant. The state variables $x_i(t)$ have initial conditions $x_i(0)$ that may be unknown. The experimenter may observe one or more of the state variables themselves or some linear combinations of the state variables, possibly involving unknown parameters. Observation functions, also called outputs, in this thesis are denoted by $y(t)$.

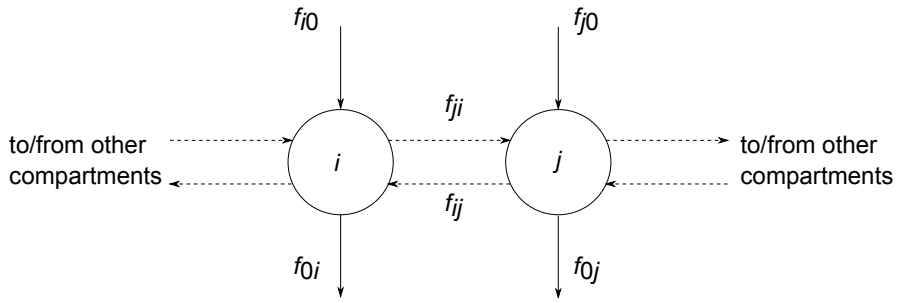

Figure 3-1 Schematic of the general form of a compartmental model, reproduced from Godfrey [2]

3.2 Data generation

Having derived a compartmental model of a biomedical system, parameter values must be determined in order for the model to be used for prediction. The process of inferring model structure and determining parameter values is often referred to as the 'inverse problem' [1].

In the pharmacokinetic context, experiments for determining parameter values usually involve administration of the drug (the 'input') and subsequent observations of the amount or concentration of substance in one or more compartments at selected time intervals (the 'output'). For example, the experimenter may administer a bolus intravenous injection of a drug and then take blood samples at time intervals after administration. Where the substance under investigation is also produced endogenously, for example Igs, labelling with radioactive isotopes allows the experimenter to distinguish between the endogenous substance and the administered dose [4–6]. The data collected from an individual subject typically consist of measurements of drug (or other substance) concentration in the blood (or other physiological compartment) at known time points. The data may also include known inputs at known time points, typically administered doses of drug. Multiple outputs can be observed for an individual, but for clarity a single output will be considered here.

3.3 Modelling the data of an individual subject

The solution of the compartmental model ordinary differential equations for the observation function, $y(t)$, gives the theoretical evolution of the quantity of interest in time. In practice, however, experimental data believed to arise from an underlying compartmental model are always observed with error. The observational error comprises both measurement error and the error caused by approximating a complex physiological system with a highly simplified model.

Taking into account inevitable errors, one observation for one individual can be expressed as $Y_j = y(t_j, \boldsymbol{\psi}) + e_j, 1 \leq j \leq J$, where J data points, Y_j, are measured at times t_j. $y(t_j, \boldsymbol{\psi})$ is the quantity predicted by the compartmental model, also known as the structural model, where $\boldsymbol{\psi}$ is the vector of parameter values. e_j is the residual error, representing the difference between the value predicted by the structural model, $y(t_j, \boldsymbol{\psi})$, and the value measured in practice, Y_j, at time t_j.

The residual errors themselves require a model to describe them. The simplest and most common models are the constant error model and the proportional error model. In the constant error model, $e_j = a\epsilon_j$, where ϵ_j is the normalised residual error and a is a constant. The normalised residual errors are usually assumed to be independently and identically distributed random variables drawn from a centred distribution, typically the normal distribution: $\epsilon_j \sim N(0, 1)$. In the proportional error model, $e_j = ay(t_j, \boldsymbol{\psi})\epsilon_j$. Now the residual error is assumed to be proportional to the value predicted by the model, $y(t_j, \boldsymbol{\psi})$ [7].

Distributional assumptions regarding the residual errors of the measured data are important when deciding upon the parameter estimation procedure to use. Pharmacokinetic data from individual subjects are typically analysed using nonlinear least squares, weighted least squares, or maximum likelihood (ML) approaches [7]. Where residual errors are assumed constant, least squares is appropriate; where the errors are assumed proportional to the model prediction, it is necessary to use weighted least squares or ML estimation. Depending upon the complexity of the structural model, a numerical ordinary differential equation solver may need to be employed if the model cannot be solved analytically [3].

3.4 Population approaches

Applying the approach in section 3.3 to the data generated by an individual subject, say subject i, yields an estimate for a vector of parameter values, $\boldsymbol{\psi}_i$, describing the evolution of their observation function, $y(t, \boldsymbol{\psi}_i)$, in time. If the same approach is applied to a second subject, it is unlikely that their parameter estimates will take the same values as those for subject i.

In a population approach, each individual is assumed to have a unique parameter vector, $\boldsymbol{\psi}_i$, that comes from a probability distribution. The 'typical' behaviour in the population is represented by $y(t, \boldsymbol{\psi}_{\text{pop}})$, where $\boldsymbol{\psi}_{\text{pop}}$ is the vector of so-called population parameters. Depending upon the distribution from which the individual parameters are assumed to be drawn, $\boldsymbol{\psi}_{\text{pop}}$ may be the mean or median of the distribution. The predicted behaviour of the individual subject i, $y(t, \boldsymbol{\psi}_i)$, deviates somewhat from the expected population behaviour due to deviation in their parameters, $\boldsymbol{\psi}_i$, from the population parameters, $\boldsymbol{\psi}_{\text{pop}}$ [8].

In pharmacokinetics, individual parameters are typically assumed to be drawn from a log-normal distribution, ensuring non-negative parameter values. For example, consider a rate constant, k. It is assumed that the individual parameters, k_i, are log-normally distributed, that is $\log(k_i) \sim N(\log\big(k_{\text{pop}}\big), \sigma_k^2)$, where k_{pop} is the population parameter and σ_k is the standard deviation of the parameter k. In this way, the individual parameter k_i can be decomposed into a fixed (population average) effect, k_{pop}, and random (individual) effect, η_i: $k_i = k_{\text{pop}} \exp(\eta_i)$, with $\eta_i \sim N(0, \sigma_k^2)$. The parameter vector of the individual i, $\boldsymbol{\psi}_i$, now has a fixed component $\boldsymbol{\psi}_{\text{pop}}$ and a random component $\boldsymbol{\eta}_i$, with $\boldsymbol{\eta}_i \sim N(0, \boldsymbol{\Omega})$. $\boldsymbol{\Omega}$ is the variance-covariance matrix of the random effects [7].

The population approach enables the measurement data from a sample of subjects to be described simultaneously by a single, nonlinear, mixed effects model. 'Mixed effects' refer to the population average parameters, considered as non-random or fixed variables, and subject specific effects, considered as random variables drawn from probability distributions. Parameter estimation uses the data from all of the subjects in the sample to estimate both population parameters and individual parameters, using ML estimation. There are a number of well-known software packages used in academia and industry for

this purpose, such as Monolix [9], NONMEM [10] and Phoenix NLME [11]; in this thesis Monolix is used.

The population approach is particularly useful in that it describes the average behaviour of a population and the variability within that population. When interest lies in the expected population behaviour of a system, estimated population parameters can be used to predict such behaviour. When interest lies in the variability within a population, the estimated standard deviations of the individual parameters provide a summary of the variability. A further advantage of population models is that they allow for dependence of individual parameters on relevant covariates such as body weight, however this is not considered in this thesis.

3.5 Structural identifiability of compartmental models

In some situations it may not be possible to uniquely estimate the model parameters from the available observations. Structural identifiability analysis addresses this question, under the assumption of the availability of ideal (i.e. noise-free) and continuous observational data [2]. The structural identifiability problem is first considered in terms of models describing the data from one individual, as in section 3.3.

A parameter is said to be globally identifiable if it can be uniquely determined from the given input-output structure of an experiment, locally identifiable if it takes one of a countable set of values, and unidentifiable if it can take any of an uncountable set (continuum) of values. A compartmental model is said to be structurally globally identifiable if all parameters are globally identifiable, locally identifiable if all parameters are locally identifiable and at least one is not globally identifiable, and unidentifiable if at least one parameter is not identifiable.

Consider the generic parameter vector of an individual, $\boldsymbol{\psi}$, which belongs to a space of feasible parameter vectors, $\boldsymbol{\Psi}$; that is $\boldsymbol{\psi} \in \boldsymbol{\Psi}$. Now consider a second parameter vector, $\overline{\boldsymbol{\psi}}$, that generates the same observation function as $\boldsymbol{\psi}$, such that $y(t, \boldsymbol{\psi}) = y(t, \overline{\boldsymbol{\psi}})$ for all t. If this equality requires that $\overline{\boldsymbol{\psi}} = \boldsymbol{\psi}$ in a neighbourhood N of the vector $\boldsymbol{\psi}$, then

the parameter vector $\boldsymbol{\psi}$ is locally structurally identifiable. If this is also true for $N = \boldsymbol{\Psi}$ then the parameter vector is globally structurally identifiable. If there are infinitely many values of $\overline{\boldsymbol{\psi}} \neq \boldsymbol{\psi}$ producing the same output $y(t, \overline{\boldsymbol{\psi}}) = y(t, \boldsymbol{\psi})$ then the parameter vector $\boldsymbol{\psi}$ is structurally unidentifiable [12].

Methods for assessing structural identifiability include the Laplace transform, Taylor series, similarity transformation, differential algebra, and observable normal form approaches [2; 13–16]. The Laplace transform approach can only be applied to linear systems. It is important to note that structural identifiability analysis only addresses the question of whether the input-output structure of the experiment allows for the parameter values to be uniquely determined or otherwise. Structural identifiability does not imply that model parameters can be estimated with an acceptable level of confidence in practice – that is the issue of practical, or numerical, identifiability.

In chapters 5 and 6 the Laplace transform approach is applied [17]. This approach is applicable to linear models that can be described in the form

$$\begin{aligned} \dot{\boldsymbol{x}}(t, \boldsymbol{\psi}) &= \boldsymbol{A}(\boldsymbol{\psi})\boldsymbol{x}(t, \boldsymbol{\psi}) + \boldsymbol{B}(\boldsymbol{\psi})\boldsymbol{u}(t, \boldsymbol{\psi}) \\ \boldsymbol{x}(t_0, \boldsymbol{\psi}) &= 0 \\ \boldsymbol{y}(t, \boldsymbol{\psi}) &= \boldsymbol{C}(\boldsymbol{\psi})\boldsymbol{x}(t, \boldsymbol{\psi}), \end{aligned} \tag{3-2}$$

where $\boldsymbol{x}(t, \boldsymbol{\psi})$ is the state of the system, $\boldsymbol{u}(t, \boldsymbol{\psi})$ is the input vector, $\boldsymbol{y}(t, \boldsymbol{\psi})$ is the observation function, and $\boldsymbol{A}(\boldsymbol{\psi})$, $\boldsymbol{B}(\boldsymbol{\psi})$ and $\boldsymbol{C}(\boldsymbol{\psi})$ are matrices with functions of the system parameters as their elements.

The input-output relationship of the system can be described in the form of $\boldsymbol{Y}(s) = \boldsymbol{G}(s)\boldsymbol{U}(s)$, where $\boldsymbol{Y}(s)$ is the Laplace transform of the observation $\boldsymbol{y}(t)$, $\boldsymbol{U}(s)$ is the Laplace transform of the input vector $\boldsymbol{u}(t)$ and $\boldsymbol{G}(s)$ is the transfer function, given by $\boldsymbol{G}(s) = \boldsymbol{C}(\boldsymbol{\psi})\left(s\boldsymbol{I} - \boldsymbol{A}(\boldsymbol{\psi})\right)^{-1}\boldsymbol{B}(\boldsymbol{\psi})$. The coefficients of s in $\boldsymbol{G}(s)$, denoted by $\boldsymbol{\Phi}(\boldsymbol{\psi}) = (\phi_1, \phi_2, ..., \phi_F)$ are functions of the system parameters, $\boldsymbol{\psi}$. Introducing a second parameter vector $\overline{\boldsymbol{\psi}}$, capable of generating the same output as $\boldsymbol{\psi}$, that is $y(t, \boldsymbol{\psi}) = y(t, \overline{\boldsymbol{\psi}})$, then $\boldsymbol{\Phi}(\boldsymbol{\psi}) = \boldsymbol{\Phi}(\overline{\boldsymbol{\psi}})$. If the only solution to $\boldsymbol{\Phi}(\boldsymbol{\psi}) = \boldsymbol{\Phi}(\overline{\boldsymbol{\psi}})$ is given by $\boldsymbol{\psi} = \overline{\boldsymbol{\psi}}$, then there is a unique parameter vector $\boldsymbol{\psi}$ and the system is structurally globally identifiable.

Structural identifiability is an a priori analysis, that is the analysis is performed before data are introduced. It is therefore also a generic, symbolic exercise, in general requir-

ing the computation of symbolic expressions and the solution of potentially nonlinear simultaneous algebraic equations. Symbolic computing packages are therefore extremely important when the model being analysed is large, in terms of its dimension and number of parameters, and can speed up the process of analysing small models. In chapters 5 and 6 structural identifiability analyses are performed in Mathematica [18].

3.5.1 Structural identifiability of mixed effects models

Recently methods have been developed that enable the structural identifiability of population models, as described in section 3.4, to be analysed [12; 19]. Previously structural identifiability analysis has only dealt with deterministic models describing the observation of an individual and was unable to handle the scenario in which individual parameters are assumed to be drawn from a distribution.

One of the new methods designed for mixed effects models is the Laplace transform mixed effects extension approach [12; 19]. As in the Laplace transform method for linear deterministic systems the input-output relationship is described by the transfer function, $\boldsymbol{G}(s)$. The Laplace transform mixed effects extension approach is based on the same principle, but now the parameters have both fixed and random effects, $\boldsymbol{\psi}_{\text{pop}}$ and $\boldsymbol{\eta}$, where $\boldsymbol{\eta} \sim N(0, \boldsymbol{\Omega})$. Now the coefficients of s in the transfer function are functions of both the fixed and random effects and are thus random variables, given by $\boldsymbol{Z}(\boldsymbol{\psi}_{\text{pop}}, \boldsymbol{\eta}) = (Z_1, Z_2, ..., Z_F)$. The structural identifiability problem amounts to determining whether the distributions of $\boldsymbol{Z}(\boldsymbol{\psi}_{\text{pop}}, \boldsymbol{\eta})$ are uniquely determined by the population parameter vector $\boldsymbol{\psi}_{\text{pop}}$ and the variance-covariance matrix $\boldsymbol{\Omega}$ [12].

An alternative population parameter vector $\overline{\boldsymbol{\psi}}_{\text{pop}}$ and an alternative variance-covariance matrix $\overline{\boldsymbol{\Omega}}$ are introduced. Statistical moments of the distributions are evaluated for both

$\{\boldsymbol{\psi}_{\text{pop}}, \boldsymbol{\Omega}\}$ and $\{\overline{\boldsymbol{\psi}}_{\text{pop}}, \overline{\boldsymbol{\Omega}}\}$, yielding a set of (nonlinear) algebraic equations

$$\begin{aligned}
\mathbb{E}\left(Z_1^l\left(\boldsymbol{\psi}_{\text{pop}}, \boldsymbol{\eta}\right)\right) &= \mathbb{E}\left(Z_1^l\left(\overline{\boldsymbol{\psi}}_{\text{pop}}, \bar{\boldsymbol{\eta}}\right)\right) \\
&\vdots \\
\mathbb{E}\left(Z_F^l\left(\boldsymbol{\psi}_{\text{pop}}, \boldsymbol{\eta}\right)\right) &= \mathbb{E}\left(Z_F^l\left(\overline{\boldsymbol{\psi}}_{\text{pop}}, \bar{\boldsymbol{\eta}}\right)\right) \\
\boldsymbol{\eta} &\sim N(0, \boldsymbol{\Omega}) \\
\bar{\boldsymbol{\eta}} &\sim N(0, \overline{\boldsymbol{\Omega}}),
\end{aligned} \tag{3-3}$$

where $\mathbb{E}(Z^l)$ denotes the l^{th} statistical moment of the distribution Z. If the solution of equations (3-3) requires that $\boldsymbol{\psi}_{\text{pop}} = \overline{\boldsymbol{\psi}}_{\text{pop}}$ and $\boldsymbol{\Omega} = \overline{\boldsymbol{\Omega}}$, then the mixed effects model is structurally globally identifiable [12].

3.6 Simulation and analysis

Using the methods thus far described, it is possible to derive a mathematical representation of the system under study, use data from human or animal subjects to estimate parameter values, and verify that the parameters are uniquely structurally identifiable. Once a model has been generated, it can be used for prediction and the system dynamics can be analysed in a realistic context.

Simulation of compartmental models more often than not involves numerical solution of ordinary differential equations. There are many specialist computer software packages that allow for simulation of compartmental models. In this thesis Berkeley Madonna [20] and Mathematica [18] are used to perform model simulations. Symbolic analyses, such as analyses of steady states, can be readily performed for generic parameters using Mathematica.

References

1. J. A. Jacquez, *Compartmental Analysis in Biology and Medicine* (Elsevier, Amsterdam, ed. 1, 1985), ISBN: 0444410465.
2. K. Godfrey, *Compartmental Models and their Application* (Academic Press, London, ed. 1, 1983), ISBN: 0122869702.
3. J. E. Riviere, *Comparative Pharmacokinetics: Principles, Techniques, and Applications* (John Wiley & Sons, Hoboken, ed. 2, 2011), ISBN: 9780813829937.
4. T. A. Waldmann, W. Strober, *Progress in Allergy* **13**, 1–110 (1969).
5. D. H. Anderson, *Compartmental Modeling and Tracer Kinetics* (Springer-Verlag, Berlin Heidelberg, ed. 1, 1983), ISBN: 9783540123033.
6. T. A. Waldmann, W. D. Terry, *The Journal of Clinical Investigation* **86**, 2093–2098 (1990).
7. P. L. Bonate, *Pharmacokinetic-Pharmacodynamic Modeling and Simulation* (Springer, New York, ed. 2, 2011), ISBN: 9781441994851.
8. T. K. L. Kiang, C. M. T. Sherwin, M. G. Spigarelli, M. H. H. Ensom, *Clinical Pharmacokinetics* **51**, 515–525 (2012).
9. Lixoft SAS, *Monolix version 2016R1*, Antony, 2016.
10. S. L. Beal, L. B. Sheiner, A. J. Boeckmann, R. J. Bauer, *NONMEM 7.3.0 User Guides*, Hanover, MD, 2013.
11. Certera, *Phoenix NLME*, Princeton.
12. D. L. Janzén, M. Jirstrand, M. J. Chappell, N. D. Evans, *Computer Methods and Programs in Biomedicine*, 329–339 (2016).
13. J. G. Hattersley, PhD thesis, University of Warwick, 2009.
14. M. J. Chappell, K. R. Godfrey, S. Vajda, *Mathematical Biosciences* **102**, 41–73 (1990).
15. A. Raksanyi, Y. Lecourtier, E. Walter, A. Venot, *Mathematical Biosciences* **77**, 245–266 (1985).
16. N. Evans et al., *Automatica* **49**, 48–57 (2013).
17. R. Bellman, K. Åström, *Mathematical Biosciences* **7**, 329–339 (1970).
18. Wolfram Research Inc., *Mathematica Version 11.1*, Champaign, IL, 2017.

19. D. Janzén, M. Jirstrand, N. D. Evans, M. Chappell, *IFAC-PapersOnLine* **48**, 563–568 (2015).

20. R. I. Macey, G. F. Oster, *Berkeley Madonna 8.3.18*, Berkeley, CA, 2009.

4

Survival analysis

In this chapter the basic concepts and definitions of survival analysis are introduced. The proportional hazards class of survival models [1] is introduced; these models are used in chapter 9 to describe the association between response markers and progression-free survival in multiple myeloma patients.

4.1 Survival data

Therapeutic strategies are frequently assessed by their effect on patient survival, that is the time until death, or the time until some other outcome of clinical importance such as, for example, disease progression. Event time outcomes also occur in other fields, such as failure times of engineering systems or components, but the following discussion will be restricted to the context of clinical research. Even though clinical events are not restricted to deaths, the terms 'event time' and 'survival time' are often used interchangeably and this will be the case throughout this thesis.

Event times have certain properties that must be considered in their analysis, for example they are always positive and are not appropriately described by normal distributions. Statistical methods also need to be able to handle patients for whom the event of interest does not occur before the end of the study. Such observations are called 'censored' and clearly cannot be disregarded.

Consider a patient who is recruited into a study at time t_0. In this hypothetical study

the endpoint of interest is death. This patient does not die during the study duration; however they die later at time $t_0 + t$. If the last contact with the patient is made at the end of the study, at time $t_0 + c$, then this time is called the censoring time. This type of censoring is known as right-censoring because the event is known to occur after the censoring time: $t > c$. Events can also, less commonly, be left-censored; however this type of censoring does not apply to the data used in this thesis. Survival data for a cohort of individuals usually consist of an event time and a binary variable indicating whether the event occurred or was censored at the given time, for each individual.

Subjects are frequently recruited into a study over a period of time, such that the study start date is different between individuals across the cohort. The time origin t_0 from which survival times are calculated is then different for each individual. The time origin may be the time at which the patient is recruited or begins treatment, for example.

At the time origin, by definition, no events have yet occurred and thus every subject is considered 'at risk'. At risk individuals are those individuals for whom the event has not yet occurred, assuming that the event can only occur once per subject, for example death. Models in which multiple events can occur are not considered in this thesis. At any time t there is a set of individuals who are at risk. When an event occurs for an individual they are removed from the set of at risk individuals at the event time. Similarly if an observation is censored then the individual is removed from the at risk set at the censoring time.

In clinical trials and in patient monitoring, clinicians desire a marker that is strongly correlated with patient survival. In this case the biomarker is considered as an explanatory variable and survival as the response variable, as in regression analysis. Due to the distribution of the survival times and censoring of observations, usual regression methods are not suitable [2]. Fortunately statistical models for survival times have been developed; but first, several functions need to be defined.

4.2 The survival function, hazard function and cumulative hazard function

In order to perform statistical analysis on survival data, the survival time of an individual is considered as a random variable, T, with probability density function $f(t)$. The cumulative distribution function $F(t)$, representing the probability that the survival time T takes a value less than t, is given by

$$F(t) = P(T \leq t) = \int_0^t f(u)\,\mathrm{d}u. \tag{4-1}$$

The survival function, $S(t)$, is defined as the probability that the survival time, T, is greater than some time, t, and is thus given by

$$S(t) = P(T > t) = 1 - F(t). \tag{4-2}$$

The survival function therefore represents the probability that an individual will survive beyond time t and is necessarily a nonincreasing function [3].

The hazard function is defined as the probability that an event occurs at time t, conditional on the event not having already occurred by that time. It can also be considered as the instantaneous rate of events at time t. It is defined by

$$h(t) = \lim_{\delta t \to 0} \frac{P(t \leq T < t + \delta t | T \geq t)}{\delta t}. \tag{4-3}$$

The hazard function is particularly important as it expresses the level of risk of the occurrence of an event over time. It is natural then to think of events occurring at certain times due to an underlying stochastic process with an associated hazard function. Unlike the survival function, the hazard function can increase or decrease over time. It is also possible that certain factors may influence the hazard rate, such as the patient's sex or treatment arm in a randomised clinical trial. This idea paves the way for proportional hazards models, also known as Cox models, introduced in section 4.3 [3].

Another function that is used in survival analysis is the cumulative hazard function, defined as the cumulative risk of an event occurring up to time t. It can also be interpreted as the expected number of events up to time t. It is defined by

$$H(t) = \int_0^t h(u)\,\mathrm{d}u, \tag{4-4}$$

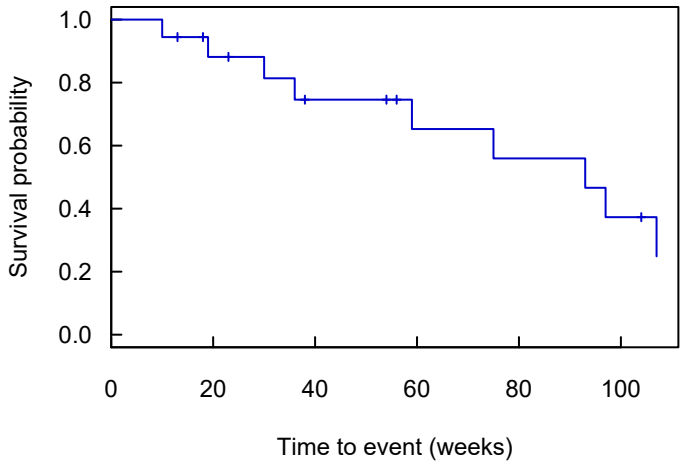

Figure 4-1 Plot of the Kaplan-Meier estimator of the survival function of discontinuation of intrauterine device use. Data from Collett [2, p. 5].

where $h(\cdot)$ is the hazard function as before.

The following relationships link the hazard function, $h(t)$, survival function, $S(t)$, and the probability density function, $f(t)$, of the event times [2]:

$$\begin{aligned} h(t) &= \frac{f(t)}{S(t)} \\ H(t) &= -\log S(t). \end{aligned} \tag{4-5}$$

4.2.1 The Kaplan-Meier survival estimator

A useful visualisation of event time data is the Kaplan-Meier survival estimator plot, which is frequently reported in the results of clinical trials [4]. The plot illustrates a non-parametric estimator of the survival function of a sample of individuals. An example survival plot is shown in figure 4-1. The survival plot is particularly useful as it is easy to interpret, with each step change representing the proportion of patients for whom the event has occurred at that time. The tick marks (+) represent the times at which individuals are censored.

The estimator is a step function, the value of which is assumed to be constant between observed events. The estimator takes into account right-censored observations by removing them from the 'at risk' subjects immediately prior to an observed event time in its calculation.

The Kaplan-Meier estimator over the time interval $t_k \leq t < t_{k+1}$ is given by

$$\hat{S}(t) = \prod_{j=1}^{k} \left(\frac{n_j - d_j}{n_j} \right), \tag{4-6}$$

for $k = 1, 2, ..., r$, where r is the total number of observed events, n_j is the number of at risk individuals immediately prior to the event time t_j, having removed any individuals that were censored during the preceding interval $t_{j-1} \leq t < t_j$, and d_j is the number of individuals for whom the event occurs at time t_j. Prior to time t_1 the value of $\hat{S}(t)$ is 1. t_{r+1} is 'infinity', such that after the final event has been observed the value of $\hat{S}(t)$ is zero for the rest of time. In the example plot shown in figure 4-1, two patients are censored at the final event time; in this case the survival estimator is undefined for $t > t_r = 107$ weeks.

The survival plot can also be stratified by a factor of interest, in order to compare the survival functions of the respective groups. For example in chapter 9 the survival functions of myeloma patients with immunoglobulin A (IgA) and immunoglobulin G (IgG) paraproteins are compared via survival plots.

It is also possible to test whether the survival functions of the two groups are significantly different using a hypothesis test. The log-rank test and the Wilcoxon test both test the null hypothesis that there is no difference between the survival functions of two groups [5; 6]. Rejection or non-rejection of the null hypothesis is not the most informative way to analyse the data; it only states whether or not there is sufficient evidence to reject the null hypothesis at a pre-specified significance level. A more informative approach would be to estimate the size of the difference between the two groups [2]. This requires a model-based approach which is introduced in the following section.

4.3 The proportional hazards model

The proportional hazards model, or Cox regression model, describes the relationship between the survival of patients and explanatory variables, such as the age of the patient and biomarkers measured at the time origin [1]. The model allows for comparison between groups, for example it may be that males have a worse prognosis than females. It may be possible to identify a biomarker cut-off value, such that patients with baseline biomarker

values larger than the cut-off have a worse prognosis than those with smaller values. There may also be a continuous relationship, where larger biomarker values are associated with a worse prognosis, for example.

The proportional hazards model postulates that the explanatory variables have a direct effect on the hazard rate $h(t)$, defined in section 4.2. Intuitively, the explanatory variable can be thought of as influencing the rate at which events happen. The rate of events, that is the hazard function $h(t)$, then determines the distribution of the survival times. For example, having a particular genetic risk factor could be seen as increasing the death rate, which in turn would mean that patients with the risk factor on average have shorter survival times.

According to the proportional hazards model the hazard function $h_i(t)$ of patient i, with p explanatory variables $x_{1i}, \ldots, x_{pi}$, is given by

$$h_i(t) = \exp\big(\beta_1 x_{1i} + \beta_2 x_{2i} + \cdots + \beta_p x_{pi}\big) h_0(t), \tag{4-7}$$

where $h_0(t)$ is the baseline hazard rate. The baseline hazard rate $h_0(t)$ is the hazard rate of a (possibly theoretical) patient for whom the term in parentheses in equation (4-7) evaluates to zero. This could represent for example a male whose biomarker levels are all zero. $\beta_1, \ldots, \beta_p$ are the coefficients of the explanatory variables, reflecting the size of their respective effects on the hazard function. From equation (4-7) it is clear why the model is called 'proportional hazards', as the hazard function for any patient i is proportional to the baseline hazard $h_0(t)$ and thus to every other patient represented by the model.

The model is usually fitted using a maximum likelihood method, such that the maximum likelihood estimator of the coefficients $\beta_1, \ldots, \beta_p$ and their standard errors are found. This approach allows for the estimation of confidence intervals and hypothesis tests on the values of the coefficients [2].

Equation (4-7) can be rearranged to give

$$\log\left(\frac{h_i(t)}{h_0(t)}\right) = \beta_1 x_{1i} + \beta_2 x_{2i} + \ldots + \beta_p x_{pi}. \tag{4-8}$$

Hazard functions and thus their ratios are necessarily positive. For a patient whose linear predictor (the right hand side of equation (4-8)) is zero, the ratio of $h_i(t)$ to $h_0(t)$ is equal to 1 and the patient's individual hazard rate is thus equal to the baseline hazard rate.

Likewise, if the patient's linear predictor is positive, then the ratio is greater than 1 and their hazard rate is greater than the baseline hazard rate. When the linear predictor is negative, then the ratio is between 0 and 1 and the hazard rate is smaller than the baseline hazard rate. The log of the ratio lies within the range $(-\infty, +\infty)$ and is linearly dependent on the explanatory variables.

Now in order to compare two groups of patients, rather than performing a hypothesis test with the null hypothesis that there is no difference between their survival functions, it is possible to estimate the size of the difference by fitting the proportional hazards model. For example, the survival of myeloma patients with IgA and IgG paraproteins, respectively, can be compared by considering the isotype of the monoclonal immunoglobulin as a factor with two levels, for IgA and IgG paraproteins, respectively. Then the proportional hazards model is expressed as

$$h_i(t) = \exp\left(\beta_{\mathrm{IgG}} x_{\mathrm{isotype},i}\right) h_0(t), \tag{4-9}$$

where $h_i(t)$ is the hazard function of patient i, $h_0(t)$ is the baseline hazard function for all subjects, $x_{\mathrm{isotype},i}$ is the value of an indicator variable X_{isotype} that takes the value 1 when the patient has an IgG paraprotein and 0 when the patient has an IgA paraprotein, and β_{IgG} is the effect on the hazard function of having an IgG paraprotein.

The model is parameterised such that the hazard function of a patient with an IgA paraprotein is given by $h_0(t)$ and the hazard function of an IgG patient is given by $\exp\big(\beta_{\mathrm{IgG}}\big)h_0(t)$. $\exp\big(\beta_{\mathrm{IgG}}\big)$ is thus the hazard ratio of IgG patients relative to IgA patients. Now, by estimating the coefficient β_{IgG}, it is possible to estimate the size of the difference between the survival of the two groups, rather than simply determining whether there is a difference at all.

The hazard functions of all individuals are assumed proportional to one another, but the hazard functions are not necessarily constant in time. The relationship between any two hazard functions *is* however constant in time, and fixed from the outset, depending only on those covariates that are measured at the defined time origin. There is a clear limitation here in that the hazard function of a patient cannot change, that is to say their outlook cannot improve or worsen after the pre-defined time origin [2].

4.3.1 Comparing alternative models

The methods that can be used to compare two models depend on whether one model is a nested form of the other, that is, whether one model is equivalent to setting one or more of the parameters in the second model equal to zero. Where models are nested, they can be compared using the likelihood ratio test.

Consider two models, M_1 and M_2, where M_1 is nested in M_2. The models can be compared using the statistic $-2\log\hat{L}$, where $\hat{L}$ is the maximised value of the likelihood function for each model, respectively. Let M_2 contain k additional parameters compared to M_1; therefore $\hat{L}_2$ is always greater than $\hat{L}_1$ and $-2\log\hat{L}_2$ is always smaller than $-2\log\hat{L}_1$, indicating that M_2 improves the goodness-of-fit of the model to the observed data. The question is whether the improvement is great enough to justify the inclusion of the k additional parameters that are present in M_2, but not in M_1.

This question can be addressed by the likelihood ratio test, with the test statistic

$$D = -2\log\left(\frac{\hat{L}_1}{\hat{L}_2}\right) = -2\log\hat{L}_1 + 2\log\hat{L}_2. \tag{4-10}$$

The larger the value of D, the greater the difference in adequacy between the two models. D has a chi-squared distribution under the null hypothesis that the additional parameters are all zero, with the degrees of freedom given by the number of additional parameters in M_2 compared to M_1, that is k. Therefore a hypothesis test can be performed to assess whether there is strong evidence to reject the simpler model M_1 [2].

The likelihood ratio test can only be performed when one model is nested in the other. Non-nested models can be compared using the Akaike Information Criterion (AIC), given by $-2\log\hat{L}+2k$. When comparing alternative models, the model with the smallest value of the AIC is considered to be the preferred model [7].

4.3.2 Time-varying covariates

An important quantity that is often reported in clinical trials is the number of patients achieving a certain level of response. In multiple myeloma there are several levels of response with corresponding criteria, given in section 2.2.1 of chapter 2. The criteria

for response are often reliant on measurements of some physiological quantity, or disease marker, representing the size of the effect of the treatment on the body. It is clear though that the response in itself can be achieved at different times for different patients.

Previously it was stated that the proportional hazards model is used to assess the effect on survival of explanatory variables known at the time origin of the survival times. If the survival times are calculated from the study entry date for each patient, then the values of explanatory variables must be known at the beginning of the study; such variables are called baseline covariates. However it is possible to incorporate a marker measured later in the study, as long as the survival times are then calculated from this new time point and the time point used is consistent across all patients. This is the simplest way to incorporate biomarkers that are strictly time-varying into a survival model and is known as landmark analysis [8; 9].

To give an example, it is possible to assess the influence of response on survival by determining whether or not response has occurred at a specific time point, such as six months after the beginning of treatment for each patient, and calculating survival times from this newly defined time origin. Those patients who have already died before six months are excluded from the analysis. It would not be legitimate to use survival times calculated from the beginning of the study and make a comparison between patients for whom response has or has not occurred at all [9].

Several methods have been developed specifically for the incorporation of time-varying covariates. These are time-varying Cox models and joint models for longitudinal and survival data [2; 3]. The assumption behind these models is fundamentally different from the standard proportional hazards model, in that the hazard function of an event at time t is associated with the values of explanatory variables at time t, not some earlier time from which survival times are calculated.

Time-varying Cox and joint models can be used to investigate, for example, whether a larger value of a biomarker at time t is associated with an increased risk of event at time t – this can provide information about which markers should be monitored in patient follow-up. A proportional hazards model however can be used to represent the association between the response to treatment at a given time and the risk of event at any time afterwards, where response to treatment is evaluated within a clinically relevant time

frame of therapy. Given that response assessment is the focus of this work, proportional hazards models, and not time-varying Cox or joint models, will be used in this thesis.

4.4 Computational tools

The methods discussed in this chapter can be implemented in many statistical software packages. In this thesis all survival analysis is performed using the R language and environment for statistical computing version 3.0.1 [10] and the Survival package version 2.37-4 [11]. Examples of the code used to perform the analyses in chapter 9 are provided in appendix A.

References

1. D. R. Cox, *Journal of the Royal Statistical Society, Series B (Methodological)* **34**, 187–220 (1972).
2. D. Collett, *Modelling Survival Data in Medical Research* (CRC Press (Taylor & Francis), Boca Raton, ed. 3, 2015), ISBN: 1584883251.
3. D. Rizopoulos, *Joint Models for Longitudinal and Time-to-Event Data: With Applications in R* (CRC Press (Taylor & Francis), Boca Raton, ed. 1, 2012), ISBN: 9781439872871.
4. E. L. Kaplan, P. Meier, *Journal of the American Statistical Association* **53**, 457–481 (1958).
5. N. Mantel, *Cancer Chemotherapy Reports* **50**, 163–170 (1966).
6. E. A. Gehan, *Biometrika* **52**, 203–224 (1965).
7. H. Akaike, in *Selected Papers of Hirotugu Akaike*, ed. by E. Parzen, K. Tanabe, G. Kitagawa (Springer, New York, ed. 1, 1998), ISBN: 9781461216940.
8. U. Dafni, *Circulation: Cardiovascular Quality and Outcomes* **4**, 363–371 (2011).
9. J. R. Anderson, K. C. Cain, R. D. Gelber, *Journal of Clinical Oncology* **1**, 710–719 (1983).
10. R Development Core Team, *R: A Language and Environment for Statistical Computing*, Vienna, Austria, 2013, (http://www.r-project.org).
11. T. M. Therneau, *A Package for Survival Analysis in S Version 2.3.8*, 2013, (http://cran.r-project.org/package=survival).

5

Parameter identification for a two-compartment model of immunoglobulin G metabolism

A mathematical model of immunoglobulin G (IgG) metabolism, with parameter values suitable for humans, is required in order to simulate plasma IgG responses during multiple myeloma treatment and relapse. In this chapter a previously published two-compartment model of IgG metabolism is analysed with respect to parameter identification. The model is nonlinear, employing Michaelis-Menten kinetics to describe the rate of recycling of IgG by neonatal Fc receptors (FcRn). Model parameters are estimated using data from radioactive tracer experiments in humans, also taken from the literature. The model has been previously presented by Waldmann et al. [1], Kim et al. [2] and Hattersley [3].

Several authors have suggested that the concentration-dependent metabolism of IgG means that monoclonal IgG responses in IgG myeloma patients may underestimate tumour responses to treatment [4; 5]. It is also possible that IgG patients may show slower monoclonal immunoglobulin (Ig) responses than immunoglobulin A (IgA) patients when the tumour response is comparable, due to the slower metabolism of IgG compared to IgA. However, these claims have not been investigated using simulations of IgA and IgG responses in patients. Based on a qualitative understanding of the biology these propositions have merit; however it is not known whether the differences in metabolic rates

between patients are so large as to cause meaningful differences in monoclonal Ig response rates.

Mathematical models of both IgA and IgG metabolism are available in the literature. The metabolism of systemic IgA is simple and can be described by a linear two-compartment model [6]. There is little data in the literature to support parameter estimation for the IgA model; however certain parameter values are available [1; 6]. In contrast, the literature provides data suitable for parameterising the model of IgG metabolism from several subjects. Ideally it would be useful to obtain a parameterised distribution of individual parameter values within the population, which would facilitate simulations of expected IgG responses to different tumour responses. This would also allow for simulations of a cohort of patients, as in a clinical trial, all with unique parameter vectors arising from a distribution.

In the following section the work of previous authors on which this chapter builds is briefly outlined. In section 5.2 the two-compartment model of IgG metabolism of Waldmann et al. [1], Kim et al. [2] and Hattersley [3] is described. In section 5.3 the data taken from the literature for parameter estimation are described. In section 5.4 the relationship between the experimental observations and the system model is described. In section 5.5 the data generation process and how errors manifest in the data are considered. A population approach to parameter identification using timecourse data is taken in section 5.6. In section 5.7 a naive pooled approach to parameter identification is taken, using fractional catabolic rate and half-life data. Parts of the work in this chapter have been published by the author [7].

5.1 Overview of the work of previous authors

The work presented in this chapter builds upon the work of previous authors, particularly Waldmann et al. [1], Kim et al. [2] and Hattersley [3]. Some descriptions of the work performed by previous authors are interspersed with original work within this chapter so that the text proceeds logically from one section to the next. In this section a brief description of the work drawn from previous authors is provided for clarity.

The model described in section 5.2 has been previously published by Kim et al. [2] and

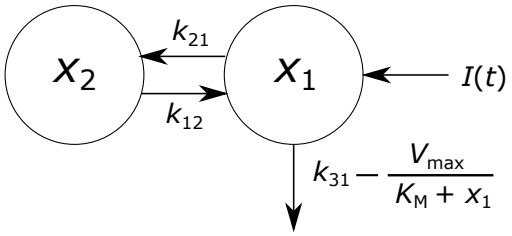

Figure 5-1 Schematic of the two-compartment model of IgG metabolism described in section 5.2

Hattersley et al. [6] and is based upon an expression for the fractional catabolic rate (equation (5-13)) first suggested by Waldmann et al. [1]. Section 5.2 (except for the equilibrium point and stability analysis) is therefore a description of the work of previous authors. No original data have been collected as part of this work; the data described in section 5.3 have been sourced by the author from the literature. In section 5.4.2 a linear model is derived from the nonlinear coupled model of unlabelled and labelled IgG dynamics. Authors Kim et al. [2] and Hattersley [3] have used this linear model of tracer dynamics ((5-10)–(5-12)) for parameter estimation; however previous authors have not considered the relationship between the linear and nonlinear models nor compared the two using simulations. Kim et al. [2] and Hattersley [3] have estimated parameters for individual subjects from timecourse data; their results are discussed and compared with the results presented in this chapter in section 5.8. Waldmann et al. [1] and Kim et al. [2] have used the expression for the fractional catabolic rate to estimate model parameters; again these results are discussed and compared with the results presented in this chapter in section 5.8.

5.2 System model

The two-compartment model of endogenous IgG metabolism, with the rate of recycling by FcRn receptors described by Michaelis-Menten kinetics [1; 2; 6], is given by

$$\begin{aligned} \dot{x}_1(t) &= -\left(k_{21} + k_{31} - \frac{V_{\max}}{K_M + x_1(t)}\right) x_1(t) + k_{12}x_2(t) + I(t) \\ \dot{x}_2(t) &= k_{21}x_1(t) - k_{12}x_2(t), \end{aligned} \tag{5-1}$$

where $x_1(t)$ and $x_2(t)$ represent the quantities in μmol of IgG in plasma and in a peripheral compartment, respectively. $I(t)$ represents the synthesis of IgG into plasma in

Table 5-1 States and parameters of two-compartment model of IgG metabolism

Name	Units	Physiological interpretation
x_1	µmol	Quantity of IgG in the central (plasma) compartment
x_2	µmol	Quantity of IgG in the peripheral (tissue) compartment
k_{21}	day^{-1}	Rate constant of flow of IgG from plasma to peripheral compartment
k_{31}	day^{-1}	Rate constant of flow of IgG from plasma into endosomes by pinocytosis
k_{12}	day^{-1}	Rate constant of flow of IgG from peripheral compartment to plasma
V_{max}	$\mu\text{mol}\,\text{day}^{-1}$	Maximum absolute recycling rate
K_{M}	µmol	Michaelis constant; the quantity of IgG in plasma at which the absolute recycling rate is half V_{max}

$\mu\text{mol}\,\text{day}^{-1}$. The rate constants k_{ij} represent material flow from compartment j to compartment i. The rate constant for the removal of IgG from the plasma compartment into intracellular endosomes for degradation is given by k_{31}, with the indices denoting the transfer from plasma to a third compartment representing intracellular endosomes. The endosome compartment is omitted from the model, as it is assumed that the rates of elimination and recycling of IgG can be expressed in terms of $x_1(t)$. The rate of FcRn-mediated recycling, as a fraction of the quantity of IgG in plasma, is given by $V_{\text{max}}/(K_{\text{M}} + x_1(t))$. The parameters V_{max} and K_{M} are the maximum absolute rate of FcRn-mediated recycling in $\mu\text{mol}\,\text{day}^{-1}$ and the Michaelis constant, representing the quantity of IgG in plasma in µmol at which the absolute recycling rate is half V_{max}. Those IgG molecules which are removed from the plasma compartment into intracellular endosomes and which are not recycled by FcRn are degraded in lysosomes. A schematic of the system model is shown in figure 5-1. Table 5-1 summarises the model states and parameters.

All states and parameters can only take non-negative values. The rate at which IgG is recycled cannot exceed the rate at which it leaves the plasma compartment; equivalently, the net elimination rate must be positive for all states and input rates, such that $k_{31} - \frac{V_{\text{max}}}{K_{\text{M}}} > 0$.

5.2.1 Stability anaysis

When the production rate of IgG is constant, $I(t) = I_0$, solving $\dot{x}_1(t) = 0$ and $\dot{x}_2(t) = 0$ simultaneously yields a single equilibrium point:

$$\begin{aligned} \hat{x}_1 &= \frac{-k_{31}K_\mathrm{M} + I_0 + V_\mathrm{max} + \sqrt{4k_{31}K_\mathrm{M}I_0 + (-k_{31}K_\mathrm{M} + I_0 + V_\mathrm{max})^2}}{2k_{31}} \\ \hat{x}_2 &= \frac{k_{21}}{k_{12}}\hat{x}_1. \end{aligned} \tag{5-2}$$

Note the positive sign before the square root to ensure that $\hat{x}_1$ and thus $\hat{x}_2$ are positive for all positive values of I_0.

Linearising the system about the equilibrium point gives

$$\begin{pmatrix} \dot{x}_1(t) \\ \dot{x}_2(t) \end{pmatrix} = \begin{pmatrix} -k_{21} - k_{31} - \frac{V_\mathrm{max}\hat{x}_1}{(K_\mathrm{M}+\hat{x}_1)^2} & k_{12} \\ k_{21} & -k_{12} \end{pmatrix} \begin{pmatrix} x_1(t) \\ x_2(t) \end{pmatrix}. \tag{5-3}$$

According to the Routh-Hurwitz stability criterion [8], the two-state system is stable provided the coefficients of the characteristic polynomial of the linearised system are positive. The coefficients of the characteristic polynomial are given by

$$\begin{aligned} a_2 &= 1 \\ a_1 &= \frac{k_{31}K_\mathrm{M}^2 - K_\mathrm{M}V_\mathrm{max} + 2k_{31}K_\mathrm{M}\hat{x}_1 + k_{31}\hat{x}_1^2 + k_{12}(K_\mathrm{M} + \hat{x}_1)^2 + k_{21}(K_\mathrm{M} + \hat{x}_1)^2}{(K_\mathrm{M} + \hat{x}_1)^2} \\ a_0 &= \frac{k_{12}\left(k_{31}\left(K_\mathrm{M} + \hat{x}_1\right)^2 - K_\mathrm{M}V_\mathrm{max}\right)}{\left(K_\mathrm{M} + \hat{x}_1\right)^2}. \end{aligned} \tag{5-4}$$

The denominator in the expressions for a_0 and a_1 is always positive. All parameters and the steady state $\hat{x}_1$ are positive. The sign of a_0 is thus given by the sign of $\left(k_{31}\left(K_\mathrm{M} + \hat{x}_1\right)^2 - K_\mathrm{M}V_\mathrm{max}\right)$. For stability of the equilibrium point it is necessary that $\left(k_{31}\left(K_\mathrm{M} + \hat{x}_1\right)^2 - K_\mathrm{M}V_\mathrm{max}\right) > 0$. This condition is met when $k_{31}K_\mathrm{M}^2 - K_\mathrm{M}V_\mathrm{max} > 0$, or equivalently $k_{31} - \frac{V_\mathrm{max}}{K_\mathrm{M}} > 0$.

The sign of a_1 is given by the sign of its numerator, $k_{31}K_\mathrm{M}^2 - K_\mathrm{M}V_\mathrm{max} + 2k_{31}K_\mathrm{M}\hat{x}_1 + k_{31}\hat{x}_1^2 + k_{12}(K_\mathrm{M} + \hat{x}_1)^2 + k_{21}(K_\mathrm{M} + \hat{x}_1)^2$. Once again, the sign of a_1 is positive provided that $k_{31} - \frac{V_\mathrm{max}}{K_\mathrm{M}} > 0$.

Both of the coefficients a_0 and a_1 are positive provided that all parameter values are positive and $k_{31} - \frac{V_\mathrm{max}}{K_\mathrm{M}} > 0$, which is the condition ensuring a positive IgG elimination

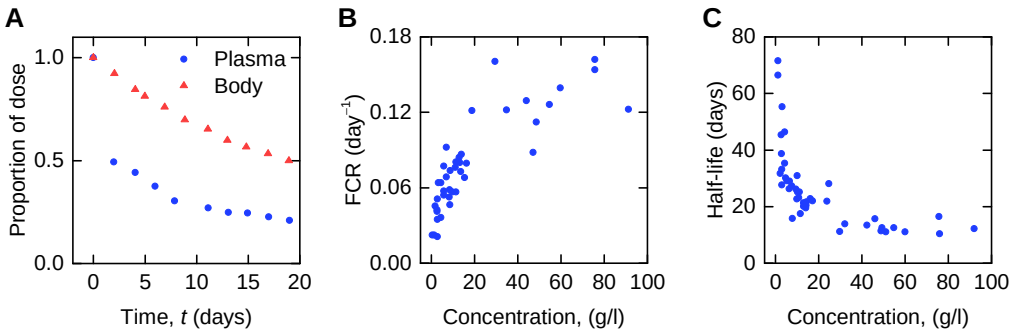

Figure 5-2 (A) Proportion of administered IgG remaining in plasma (blue circles) and the body (red triangles) in a typical normal subject; data from Solomon et al. [9]. Plasma concentration dependence of (B) fractional catabolic rate (FCR) and (C) half-life ($T_{1/2}$) of IgG; data from Waldmann et al. [1].

rate for all $x_1 > 0$. A negative elimination rate does not make sense physiologically and as such parameter values are not permitted which violate this condition. The equilibrium point is thus stable for all permitted parameter values.

5.3 Experimental data from the literature

Data for parameter estimation were obtained from tracer experiments reported in the literature. These studies entail intravenous administration of a bolus dose of radiolabelled IgG (the tracer) and monitoring the proportion of the dose remaining in the blood and in the body over time. In this way the administered dose is distinguishable (by the experimenter) from the subject's own endogenous IgG. The quantity of administered tracer is small, so as not to perturb the steady state of the endogenous IgG. The purpose of tracer experiments is to enable observation of the processes such as distribution and elimination undergone by the endogenous protein, whilst it is in steady state. The radioactive label (usually iodine) remains bound to the protein until the protein is degraded, at which point the label is released and rapidly excreted in urine. Several tracer studies were performed for IgG in humans in the middle of the last century and the results collated by Waldmann et al. [1], who also describe the methods in detail.

5.3.1 Timecourse data

The data from an individual subject consist of the timecourse of the proportion of an administered dose of radiolabelled IgG remaining in plasma and the proportion remaining in the whole body. An example is shown in figure 5-2A. The data have been extracted from a plot by Solomon et al. [9] using OriginPro [10]. Seven plots of this type have been found by the author in the literature. The data in these plots are assumed to arise from seven individuals to whom we refer as subjects A–G. The data for subjects A–D are taken from Solomon et al. [9], for subjects E and F from Waldmann et al. [11] and for subject G from Waldmann et al. [1]. Subjects A and C have IgG myeloma, subject D has macroglobulinemia and subject E has familial hypercatabolic hypoproteinemia. Subjects B, F and G are referred to as 'normal' subjects. No information is provided by the authors regarding the errors on these data; in section 5.5 expressions for measurement errors are derived based on assumptions about the experiment.

5.3.2 Fractional catabolic rate and half-life

In compartmental analysis, parameters are often considered as either micro constants or macro constants. The micro constants are dependent upon the assumed structure of the compartmental model, whereas the macro constants can be determined directly from the profile of concentration or radioactivity over time, such as the exponents of a multi-exponential profile, and do not assume a particular model structure [12]. Plots of the fractional catabolic rate (FCR) and half-life ($T_{1/2}$), respectively, vs. subjects' plasma concentrations of endogenous IgG, obtained from a group of individuals with a range of plasma IgG concentrations, are available in the literature [1]. Macro parameters are functions of the micro parameters of the assumed compartmental structure – therefore in this chapter the FCR and $T_{1/2}$ data are used in the estimation of the parameters of the underlying compartmental model.

The FCR is defined as the fraction of IgG in plasma that is degraded per day. In practice the FCR is calculated from the rate at which the tracer dose leaves the body at time t divided by the quantity of tracer in plasma at time t. The rate at which the dose leaves the body is given by the slope of the timecourse of the dose remaining in the whole body.

A plot of the FCR vs. the plasma concentration of endogenous IgG for 41 individuals provided by Waldmann et al. [1] is shown in figure 5-2B.

The half-life ($T_{1/2}$) is defined as the time taken for the quantity of tracer to halve, after the distribution phase is complete. The parameter $T_{1/2}$ is obtained from a plot of the timecourse of radioactivity remaining in plasma and in the body on a log scale. The slope of the curves is obtained for the latter part of the experiment, when distribution between the compartments is assumed to be complete, and the dynamics dominated by elimination and recycling. A plot of $T_{1/2}$ vs. the plasma concentration of endogenous IgG for 44 individuals provided by Waldmann et al. [1] is shown in figure 5-2C. All of the data described in this section were extracted from plots in the literature using the Digitizer tool in OriginPro [10]. Mathematical expressions for both the FCR and $T_{1/2}$ are provided in section 5.4.

5.4 Mathematical description of observations

In this section we consider how the experimental observations (timecourse of radioactivity, FCR and $T_{1/2}$) are defined in terms of the underlying system model. Tracer experiments are designed specifically so that the tracer-labelled protein observes linear kinetics, whether or not the underlying model is linear or nonlinear [13]. A linear model describing the timecourse observations is derived from the nonlinear model of coupled tracer and endogenous IgG dynamics. The linear model has been used by other authors for parameter estimation [1–3], however its use has not been previously validated by a formal consideration of its relationship with the full nonlinear model. The derivation of a new expression for the half-life makes data available that have previously not been used for parameter estimation.

5.4.1 Nonlinear structural model of coupled tracer and endogenous IgG dynamics

Assuming that the radiolabelled IgG dose and unlabelled endogenous IgG are indistinguishable by the system, both are described by the model given in equations (5-1). The in-

jected and endogenous IgG can be explicitly represented by letting $x_i(t) = x_{i,\mathrm{T}}(t) + x_{i,\mathrm{E}}(t)$ for $i = 1, 2$, with 'T' denoting tracer and 'E' denoting endogenous IgG. Then, from equations (5-1), the dynamics of labelled and unlabelled IgG are given by

$$\begin{aligned}
\dot{x}_{1,\mathrm{T}}(t) &= -\left(k_{21} + k_{31} - \frac{V_{\max}}{K_{\mathrm{M}} + x_{1,\mathrm{E}}(t) + x_{1,\mathrm{T}}(t)}\right) x_{1,\mathrm{T}}(t) + k_{12} x_{2,\mathrm{T}}(t) \\
\dot{x}_{2,\mathrm{T}}(t) &= k_{21} x_{1,\mathrm{T}}(t) - k_{12} x_{2,\mathrm{T}}(t) \\
\dot{x}_{1,\mathrm{E}}(t) &= -\left(k_{21} + k_{31} - \frac{V_{\max}}{K_{\mathrm{M}} + x_{1,\mathrm{E}}(t) + x_{1,\mathrm{T}}(t)}\right) x_{1,\mathrm{E}}(t) + k_{12} x_{2,\mathrm{E}}(t) + I_{\mathrm{E}} \\
\dot{x}_{2,\mathrm{E}}(t) &= k_{21} x_{1,\mathrm{E}}(t) - k_{12} x_{2,\mathrm{E}}(t),
\end{aligned} \tag{5-5}$$

where $x_{i,\mathrm{T}}(t)$ and $x_{i,\mathrm{E}}(t)$ represent the quantities in µmol of radiolabelled and endogenous IgG in compartment i, respectively, and I_{E} (µmol day^{-1}) represents the production rate of endogenous IgG, which is assumed constant.

The intravenous bolus injection of tracer can be treated as a non-zero initial condition for $x_{1,\mathrm{T}}(t)$; thus the initial conditions for the tracer are given by

$$\begin{aligned}
x_{1,\mathrm{T}}(0) &= D \\
x_{2,\mathrm{T}}(0) &= 0,
\end{aligned} \tag{5-6}$$

where D is the dose of tracer in µmol. The endogenous IgG is assumed to be in steady state at the beginning of the experiment and remain in steady state throughout, as verifiable by the experimenter. Waldmann et al. [11] state that 'serum immunoglobulin ... concentrations were obtained at intervals throughout the study period to verify that each patient was in a steady state.' Solomon et al. [9] do not make such a statement; however, they assume steady state when calculating the absolute synthetic rate of IgG from the fractional catabolic rate and the quantity of unlabelled IgG in plasma. Given that most methods for analysing tracer experiment data rest on the assumption that the endogenous protein is in steady state throughout the experiment [1], it is assumed that this was the case for each subject whose data are analysed in this chapter. The initial conditions for the endogenous IgG are therefore given by the equilibrium point in section 5.2, with $I_0 = I_{\mathrm{E}}$.

The experimenter observes the proportion of the initially injected radioactivity in plasma

and in the whole body. The observation functions are thus given by

$$\begin{aligned} y_1(t) &= x_{1,\mathrm{T}}(t)/D \\ y_2(t) &= \left(x_{1,\mathrm{T}}(t) + x_{2,\mathrm{T}}(t)\right)/D. \end{aligned} \tag{5-7}$$

5.4.2 Linearised structural model of tracer dynamics

A sufficiently small quantity of radiolabelled IgG, typically 0.5–1 mg (3.33×10^{-3}–6.67×10^{-3} µmol) [9], is administered into plasma such that the tracer-labelled protein obeys approximately linear kinetics. The dose is small enough so as not to perturb the steady state of the endogenous protein; thus $x_{1,\mathrm{E}}$ and $x_{2,\mathrm{E}}$ can be assumed constant. Then the equations describing the tracer dynamics are no longer coupled with those describing the endogenous IgG dynamics, giving

$$\begin{aligned} \dot{x}_{1,\mathrm{T}}(t) &= -\left(k_{21} + k_{31} - \frac{V_{\max}}{K_{\mathrm{M}} + x_{1,\mathrm{E}} + x_{1,\mathrm{T}}(t)}\right) x_{1,\mathrm{T}}(t) + k_{12} x_{2,\mathrm{T}}(t) \\ \dot{x}_{2,\mathrm{T}}(t) &= k_{21} x_{1,\mathrm{T}}(t) - k_{12} x_{2,\mathrm{T}}(t). \end{aligned} \tag{5-8}$$

A second assumption is required in order to derive a linear model: the quantity of tracer, $x_{1,\mathrm{T}}(t)$, is assumed to be much smaller than the quantity of the subject's endogenous IgG, $x_{1,\mathrm{E}}$. Thus the term $\frac{V_{\max}}{K_{\mathrm{M}}+x_{1,\mathrm{E}}+x_{1,\mathrm{T}}(t)}$ can be approximated by $\frac{V_{\max}}{K_{\mathrm{M}}+x_{1,\mathrm{E}}}$. In this way, the elimination rate of the tracer is determined by the subject's endogenous IgG only. The equations describing the tracer kinetics are now given by

$$\begin{aligned} \dot{x}_{1,\mathrm{T}}(t) &= -\left(k_{21} + k_{31} - \frac{V_{\max}}{K_{\mathrm{M}} + x_{1,\mathrm{E}}}\right) x_{1,\mathrm{T}}(t) + k_{12} x_{2,\mathrm{T}}(t) \\ \dot{x}_{2,\mathrm{T}}(t) &= k_{21} x_{1,\mathrm{T}}(t) - k_{12} x_{2,\mathrm{T}}(t), \end{aligned} \tag{5-9}$$

where $x_{1,\mathrm{T}}(t)$ and $x_{2,\mathrm{T}}(t)$ represent the quantities in µmol of radiolabelled IgG in the central and peripheral compartments, respectively. $x_{1,\mathrm{E}}$ represents the quantity of the subject's endogenous IgG in the central compartment, which is assumed to remain in steady state. All other parameters are defined as in section 5.2. The initial conditions and observation functions are given by equations (5-6) and (5-7), respectively.

We note that the parameters k_{31}, $V_{\max}$ and K_{M} only appear in the expression $\left(k_{31} - \frac{V_{\max}}{K_{\mathrm{M}}+x_{1,\mathrm{E}}}\right)$; therefore we can set this expression equal to a new constant and simplify the equations, effectively reparameterising the model. We also note that for the

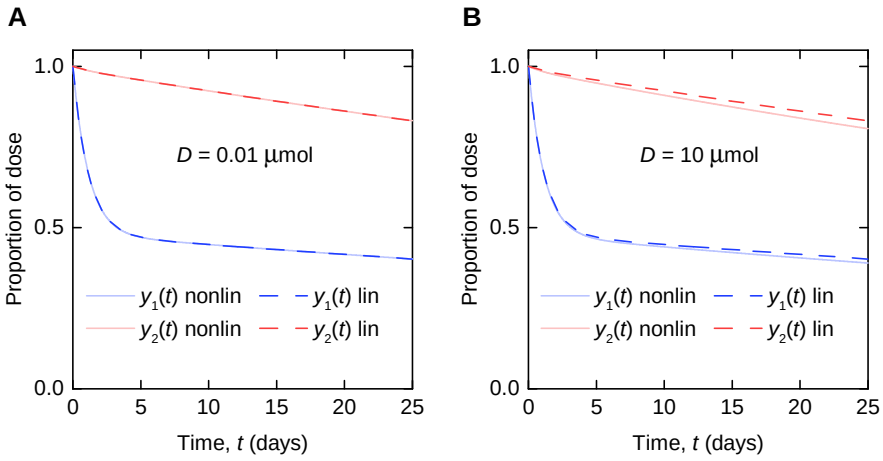

Figure 5-3 Simulations of timecourse responses $y_1(t)$ and $y_2(t)$ as described by equations (5-5)–(5-7) (nonlinear model – solid line) and equations (5-10)–(5-12) (linearised model – dashed line). The quantity of endogenous IgG in plasma at $t = 0$, $x_{1,\mathrm{E}}(0)$, is 5 µmol. The tracer dose D is (A) 0.01 µmol and (B) 10 µmol.

linear model, the initial conditions and observation gain cancel out; the tracer kinetics can therefore be described by

$$\begin{aligned} \dot{x}_{1,\mathrm{P}}(t) &= -\left(k_{21} + \mathrm{FCR}\right) x_{1,\mathrm{P}}(t) + k_{12} x_{2,\mathrm{P}}(t) \\ \dot{x}_{2,\mathrm{P}}(t) &= k_{21} x_{1,\mathrm{P}}(t) - k_{12} x_{2,\mathrm{P}}(t), \end{aligned} \tag{5-10}$$

where $x_{1,\mathrm{P}}(t)$ and $x_{2,\mathrm{P}}(t)$ represent the proportion of the radiolabelled IgG dose D in the central and peripheral compartments, respectively, at time t. The parameter FCR is the fractional catabolic rate (see section 5.4.3), equal to the expression noted in the preceding paragraph. All other parameters are defined as in section 5.2.

The initial conditions for the model are now given by

$$\begin{aligned} x_{1,\mathrm{P}}(0) &= 1 \\ x_{2,\mathrm{P}}(0) &= 0. \end{aligned} \tag{5-11}$$

The corresponding observation functions are given by

$$\begin{aligned} y_1(t) &= x_{1,\mathrm{P}}(t) \\ y_2(t) &= x_{1,\mathrm{P}}(t) + x_{2,\mathrm{P}}(t). \end{aligned} \tag{5-12}$$

The approximation of the nonlinear model (equations (5-5)–(5-7)) by the linearised model (equations (5-10)–(5-12)) relies on two assumptions:

- that the endogenous IgG can be considered in steady state,
- that the quantity $x_{1,\mathrm{T}}(t)$ can be neglected in the denominator of the Michaelis-Menten term.

Both assumptions require that the administered dose of tracer, D, is sufficiently smaller than the quantity of endogenous IgG in plasma, $x_{1,\mathrm{E}}(t)$. In figure 5-3 simulations of the nonlinear model and the linearised model are compared. The parameter values used in the simulations are estimated in this chapter and summarised in table 5-11. The production rate of endogenous IgG is set to $I_{\mathrm{E}} = 0.0727$ µmol day^{-1} to give $x_{1,\mathrm{E}}(0) = 5$ µmol for the nonlinear model and $x_{1,\mathrm{E}} = 5$ µmol for the linearised model, representing the lower limit of the quantities of endogenous IgG in plasma seen in the data. In figure 5-3A the tracer dose $D = 0.01$ µmol, representing the upper limit of administered tracer doses [9]. The nonlinear and linearised model responses are visually indistinguishable, illustrating that for typical tracer doses the linearised model is a valid approximation of the nonlinear model. In figure 5-3B the tracer dose $D = 10$ µmol, 1000 times larger; at this point the assumptions weaken and there is a small but noticeable difference between the responses of the two models.

5.4.3 Fractional catabolic rate and half-life

The fractional catabolic rate (FCR) is defined as the proportion of the radiolabelled IgG in plasma that is catabolised per day. From equation (5-9) this is equal to

$$\mathrm{FCR} = k_{31} - \frac{V_{\max}}{K_{\mathrm{M}} + x_{1,\mathrm{E}}}, \tag{5-13}$$

defined for non-negative values of $x_{1,\mathrm{E}}$. The maximal value of the FCR, as $x_{1,\mathrm{E}}$ tends to infinity, is equal to k_{31} day^{-1}; that is, the IgG cannot be catabolised faster than it is internalised into endosomes. The minimal value of the FCR, when $x_{1,\mathrm{E}} = 0$, is given by $\left(k_{31} - V_{\max}/K_{\mathrm{M}}\right)$ day^{-1}, where $V_{\max}/K_{\mathrm{M}}$ day^{-1} is the value to which the fractional recycling rate tends for small values of $x_{1,\mathrm{E}}$.

The terminal half-life, $T_{1/2}$, is related with the elimination phase of the kinetics, after the distribution phase is complete. The model described by equations (5-10)–(5-12) is a linear two-compartment model with the solutions of $x_{1,\mathrm{P}}(t)$ and $x_{2,\mathrm{P}}(t)$ given by the

bi-exponential functions

$$\begin{aligned} x_{1,\mathrm{P}}(t) &= A_{11}\exp(\lambda_1 t) + A_{12}\exp(\lambda_2 t) \\ x_{2,\mathrm{P}}(t) &= A_{21}\exp(\lambda_1 t) + A_{22}\exp(\lambda_2 t), \end{aligned} \tag{5-14}$$

where A_{ij} and λ_j are macro constants, with $|\lambda_1| > |\lambda_2|$. By definition, the terminal half-life is given by

$$T_{1/2} = -\frac{\log 2}{\lambda_2}. \tag{5-15}$$

Solving equations (5-10)–(5-12) for λ_2 and substituting into equation (5-15) gives the following expression for $T_{1/2}$:

$$T_{1/2} = \frac{2\log 2}{k_{12} + k_{21} + \mathrm{FCR} - \sqrt{-4k_{12}\mathrm{FCR} + (k_{12} + k_{21} + \mathrm{FCR})^2}}. \tag{5-16}$$

Substituting in the expression for FCR from (5-13) gives

$$\begin{aligned} T_{1/2} =& 2\log 2 \Bigg/ \left(k_{12} + k_{21} + k_{31} - \frac{V_{\max}}{K_{\mathrm{M}} + x_{1,\mathrm{E}}} \right. \\ & \left. - \sqrt{-4k_{12}\left(k_{31} - \frac{V_{\max}}{K_{\mathrm{M}} + x_{1,\mathrm{E}}}\right) + \left(k_{12} + k_{21} + k_{31} - \frac{V_{\max}}{K_{\mathrm{M}} + x_{1,\mathrm{E}}}\right)^2} \right). \end{aligned} \tag{5-17}$$

The maximal value of $T_{1/2}$, when $x_{1,\mathrm{E}} = 0$ and $\mathrm{FCR} = k_{31} - V_{\max}/K_{\mathrm{M}}$, is given by

$$\frac{2\log 2}{k_{12} + k_{21} + k_{31} - \frac{V_{\max}}{K_{\mathrm{M}}} - \sqrt{-4k_{12}\left(k_{31} - \frac{V_{\max}}{K_{\mathrm{M}}}\right) + \left(k_{12} + k_{21} + k_{31} - \frac{V_{\max}}{K_{\mathrm{M}}}\right)^2}}. \tag{5-18}$$

The minimal value to which $T_{1/2}$ tends, when $x_{1,\mathrm{E}}$ tends to infinity and FCR tends to k_{31}, is given by

$$\frac{2\log 2}{k_{12} + k_{21} + k_{31} - \sqrt{-4k_{12}k_{31} + (k_{12} + k_{21} + k_{31})^2}}. \tag{5-19}$$

5.5 Errors and the data generating process

In this section we consider how the timecourse data described in section 5.3 were calculated from measurements of radioactivity. We then consider where errors are likely to arise in data collection and calculation. It is assumed that $y_1(t)$ is observed with error at measurement times $t_1^{(1)}, \ldots, t_{N_1}^{(1)}$ and $y_2(t)$ is observed with error at measurement times $t_1^{(2)}, \ldots, t_{N_2}^{(2)}$, with $t_1^{(1)} = t_1^{(2)} = 0$. The superscripts (1) and (2) are used to allow for different sampling times between the two outputs.

5.5.1 Calculation of $y_1(t)$ from radioactivity measurements

The first timecourse observation, $y_1(t)$, represents the quantity of labelled IgG in plasma as a proportion of the administered IgG dose. In practice, the experimenters measure the radioactivity $A_{\text{PS}}(t)$ (microcurie; µCi) in a plasma sample of known volume $V_{\text{PS}}(t)$ (l), giving the resulting plasma radioactivity concentration $C_{\text{plasma}}(t)$ (µCi l^{-1}):

$$C_{\text{plasma}}(t) = \frac{A_{\text{PS}}(t)}{V_{\text{PS}}(t)}. \tag{5-20}$$

Values of $C_{\text{plasma}}(t)$ for blood samples taken within the first 30 minutes [9; 11] are extrapolated to time $t = 0$ to find the plasma radioactivity concentration at $t = 0$, $C_{\text{plasma}}(0)$. It is assumed that the plasma volume V_{plasma} is constant and is thus given by

$$V_{\text{plasma}} = \frac{A_{\text{dose}}}{C_{\text{plasma}}(0)}, \tag{5-21}$$

where A_{dose} is the radioactivity in µCi in the injected dose. Then the proportion of the dose of radioactivity in plasma at time t is given by

$$\frac{A_{\text{plasma}}(t)}{A_{\text{dose}}} = \frac{C_{\text{plasma}}(t)}{A_{\text{dose}}} \frac{A_{\text{dose}}}{C_{\text{plasma}}(0)} = \frac{C_{\text{plasma}}(t)}{C_{\text{plasma}}(0)}, \tag{5-22}$$

where $A_{\text{plasma}}(t)$ (µCi) is the total radioactivity in plasma at time t. The quantity of radioactivity is assumed to be directly proportional to the quantity of labelled IgG, with proportionality constant α (µCi µmol^{-1}),

$$A_{\text{plasma}}(t) = \alpha x_{1,\text{T}}(t), \tag{5-23}$$

such that

$$y_1(t) = \frac{\alpha x_{1,\text{T}}(t)}{\alpha D} = \frac{A_{\text{plasma}}(t)}{A_{\text{dose}}}, \tag{5-24}$$

where $x_{1,\text{T}}(t)$ (µmol) is the quantity of tracer in plasma at time t and D (µmol) is the tracer dose. The relationship between the model output $y_1(t)$ and the measurements taken at discrete sampling times is thus given by

$$y_1(t_j^{(1)}) = \begin{cases} 1 & j = 1 \\ \frac{C_{\text{plasma}}(t_j^{(1)})}{C_{\text{plasma}}(0)} & j = 2, \ldots, N_1. \end{cases} \tag{5-25}$$

5.5.2 Measurement errors relating to $y_1(t)$

The model output $y_1(t)$ is calculated from measurements of plasma radioactivity concentration, $C_{\text{plasma}}(t)$ ($\mu\text{Ci}\,\text{l}^{-1}$). Measurements of plasma radioactivity concentration have been assumed by other authors to have normally distributed, additive errors [14]. The errors have also been assumed or found (by taking replicate measurements) to be proportional to the size of the measurement, i.e. the coefficient of variation (CV) is constant [14; 15, p. 233–235]. From equations (5-23),

$$C_{\text{plasma}}(t) = \frac{A_{\text{plasma}}(t)}{V_{\text{plasma}}} = \frac{\alpha x_{1,\text{T}}(t)}{V_{\text{plasma}}}. \tag{5-26}$$

We now use tilde ($\tilde{\cdot}$) notation to denote quantities observed with error, as opposed to 'true' quantities. The plasma radioactivity concentration, measured with noise, is given by

$$\tilde{C}_{\text{plasma}}(t_j^{(1)}) = \frac{\alpha x_{1,\text{T}}(t_j^{(1)})}{V_{\text{plasma}}} + \epsilon_j^{(\text{P})}, \tag{5-27}$$

where $\epsilon_j^{(\text{P})}$ are independent, normally distributed residual errors, with superscript (P) referring to 'plasma'. The errors $\epsilon_j^{(\text{P})}$ are assumed to have zero mean and standard deviation proportional to the size of the true value of $C_{\text{plasma}}(t_j^{(1)})$.

The measured (with noise) values of the model output $y_1(t)$ are now given by

$$\tilde{y}_1(t_j^{(1)}) = \begin{cases} 1 & j = 1 \\ \dfrac{\tilde{C}_{\text{plasma}}(t_j^{(1)})}{\tilde{C}_{\text{plasma}}(0)} & j = 2, \ldots, N_1. \end{cases} \tag{5-28}$$

For $j = 2, \ldots, N_1$, $\tilde{y}_1(t_j^{(1)})$ is given by a random variable with a constant CV ($\tilde{C}_{\text{plasma}}(t_j^{(1)})$) divided by a random variable with a constant CV ($\tilde{C}_{\text{plasma}}(0)$). From the standard formulae for calculating propagation of errors [16], this means that the squared CV of $\tilde{y}_1(t_j^{(1)})$ is approximately equal to sum of the squared CV of $\tilde{C}_{\text{plasma}}(t_j^{(1)})$ and the squared CV of $\tilde{C}_{\text{plasma}}(0)$. The CV of $\tilde{y}_1(t_j^{(1)})$ is therefore constant. The division by a random variable, $\tilde{C}_{\text{plasma}}(0)$, means that the measured values of $\tilde{y}_1(t_j^{(1)})$ have a ratio distribution; however Q-Q (quantile-quantile) plots of simulated data show that the distribution is close to the normal distribution.

From equations (5-27) and (5-28), we have

$$\tilde{y}_1(t_j^{(1)}) = \frac{\frac{\alpha x_{1,\mathrm{T}}(t_j^{(1)})}{V_{\mathrm{plasma}}} + \epsilon_j^{(\mathrm{P})}}{\frac{\alpha x_{1,\mathrm{T}}(0)}{V_{\mathrm{plasma}}} + \epsilon_1^{(\mathrm{P})}} \qquad j = 2, \ldots, N_1. \tag{5-29}$$

Unfortunately, due to the error $\epsilon_1^{(\mathrm{P})}$ in the denominator of (5-29), a systematic error is introduced into every measured value of $\tilde{y}_1(t_j^{(1)}), j = 2, \ldots, N_1$; therefore the mean of the measured $\tilde{y}_1(t_j^{(1)})$ is not equal to the true value $y_1(t_j^{(1)})$, for $j = 2, \ldots, N_1$.

5.5.3 Calculation of $y_2(t)$ from radioactivity measurements

The second timecourse observation, $y_2(t)$, represents the quantity of labelled IgG in the body as a proportion of the administered IgG dose. The proportion of the dose of radioactivity remaining in the body can be obtained either by using a whole body counter or by subtracting the cumulative radioactivity in urine from the radioactivity in the administered dose [1]; Waldmann et al. [1], Waldmann et al. [11] and Solomon et al. [9] all state that urine collections were used. The experimenters measure the radioactivity, $A_{\mathrm{UC}}(t)$ (µCi), in urine collections and the total radioactivity in the injected dose, A_{dose} (µCi). The cumulative excreted radioactivity is calculated as the sum of the radioactivity in all urine collections up to the current time:

$$A_{\mathrm{urine}}(t_j^{(2)}) = \begin{cases} 0 & j = 1 \\ \sum_{k=2}^{k=j} A_{\mathrm{UC}}(t_k^{(2)}) & j = 2, \ldots, N_2. \end{cases} \tag{5-30}$$

The radioactivity in the body, $A_{\mathrm{body}}(t_j^{(2)})$, is calculated as the dose minus the cumulative excreted radioactivity:

$$A_{\mathrm{body}}(t_j^{(2)}) = A_{\mathrm{dose}} - A_{\mathrm{urine}}(t_j^{(2)}), \qquad j = 1, \ldots, N_2. \tag{5-31}$$

The radioactivity in the body is divided by the radioactivity in the dose to give the proportion of the radioactivity dose in the body:

$$\frac{A_{\mathrm{body}}(t_j^{(2)})}{A_{\mathrm{dose}}} = \frac{A_{\mathrm{dose}} - A_{\mathrm{urine}}(t_j^{(2)})}{A_{\mathrm{dose}}}, \qquad j = 1, \ldots, N_2. \tag{5-32}$$

Again the radioactivity is assumed to be directly proportional to the quantity of labelled IgG, with proportionality constant α (µCi µmol^{-1}), such that

$$y_2(t_j^{(2)}) = \frac{\alpha\left(x_{1,\mathrm{T}}(t_j^{(2)}) + x_{2,\mathrm{T}}(t_j^{(2)})\right)}{\alpha D} = \frac{A_{\mathrm{body}}(t_j^{(2)})}{A_{\mathrm{dose}}}. \tag{5-33}$$

The relationship between the model output $y_2(t)$ and the measurements taken at discrete sampling times is thus given by

$$y_2(t_j^{(2)}) = \begin{cases} 1 & j = 1 \\ \frac{A_{\text{dose}} - \sum_{k=2}^{k=j} A_{\text{UC}}(t_k^{(2)})}{A_{\text{dose}}} & j = 2, \ldots, N_2. \end{cases} \tag{5-34}$$

5.5.4 Measurement errors relating to $y_2(t)$

The model output $y_2(t)$ is calculated from measurements of radioactivity in urine collections, $A_{\text{UC}}(t)$ (µCi), and the radioactivity in the administered tracer dose, A_{dose} (µCi). Chen et al. [14] state that measurement noise primarily due to radioactive counting can be assumed to be normally distributed. It is assumed that, similar to measurements of plasma radioactivity concentration, the CVs of the measurements of $\tilde{A}_{\text{UC}}(t_k^{(2)}), j = 2, \ldots, N_2$, and $\tilde{A}_{\text{dose}}$ are constant. The activity in the dose is given by

$$A_{\text{dose}} = \alpha D. \tag{5-35}$$

It is assumed that the measured radioactivity in the tracer dose is given by

$$\tilde{A}_{\text{dose}} = \alpha D + \epsilon_j^{(\text{D})}, \tag{5-36}$$

where $\epsilon_j^{(\text{D})}$ is the normally distributed residual error, having zero mean and standard deviation proportional to the size of the true value of A_{dose}. Superscript (D) refers to 'dose'. We denote the standard deviation of $\epsilon_j^{(\text{D})}$ by σ_{D} and the CV by CV_{D}.

From (5-31), the cumulative excreted activity is given by

$$A_{\text{urine}}(t_j^{(2)}) = A_{\text{dose}} - A_{\text{body}}(t_j^{(2)}) = \alpha \left(D - x_{1,\text{T}}(t_j^{(2)}) - x_{2,\text{T}}(t_j^{(2)}) \right), \quad j = 1, \ldots, N_2. \tag{5-37}$$

The activity in each urine collection is given by

$$A_{\text{UC}}(t_j^{(2)}) = A_{\text{urine}}(t_j^{(2)}) - A_{\text{urine}}(t_{j-1}^{(2)}), \qquad j = 2, \ldots, N_2. \tag{5-38}$$

Substituting from equation (5-37) into equation (5-38) gives

$$A_{\text{UC}}(t_j^{(2)}) = \alpha \left(-x_{1,\text{T}}(t_j^{(2)}) - x_{2,\text{T}}(t_j^{(2)}) + x_{1,\text{T}}(t_{j-1}^{(2)}) + x_{2,\text{T}}(t_{j-1}^{(2)}) \right). \tag{5-39}$$

Again using tilde ($\tilde{\cdot}$) notation to denote quantities observed with error, as opposed to 'true' quantities, the measured radioactivity in a urine collection is given by

$$\tilde{A}_{\mathrm{UC}}(t_j^{(2)}) = \alpha\left(-x_{1,\mathrm{T}}(t_j^{(2)}) - x_{2,\mathrm{T}}(t_j^{(2)}) + x_{1,\mathrm{T}}(t_{j-1}^{(2)}) + x_{2,\mathrm{T}}(t_{j-1}^{(2)})\right) + \epsilon_j^{(\mathrm{UC})}, \qquad j = 2, \ldots, N_2, \tag{5-40}$$

where $\epsilon_j^{(\mathrm{UC})}$ are independent, normally distributed residual errors, with superscript (UC) referring to 'urine collection'. The errors $\epsilon_j^{(\mathrm{UC})}$ are assumed to have zero mean and standard deviation proportional to the size of the true value of $A_{\mathrm{UC}}(t_j^{(2)})$. We denote the standard deviation of $\epsilon_j^{(\mathrm{UC})}$ by $\sigma_{\mathrm{UC}}(t_j^{(2)})$ and the CV by $\mathrm{CV}_{\mathrm{UC}}$. The measured cumulative excreted activity is now given by

$$\tilde{A}_{\mathrm{urine}}(t_j^{(2)}) = \begin{cases} 0 & j = 1 \\ \sum_{k=2}^{k=j} A_{\mathrm{UC}}(t_k^{(2)}) + \epsilon_k^{(\mathrm{UC})} & j = 2, \ldots, N_2. \end{cases} \tag{5-41}$$

For $j = 2, \ldots, N_2$, measurements of $\tilde{A}_{\mathrm{urine}}(t_j^{(2)})$ are now given by sums of random variables, each having a constant CV, denoted by $\mathrm{CV}_{\mathrm{UC}}$. From standard propagation of error formulae, the variance of the sum of random variables is equal to the sum of variances of the summed variables [16]. The greater the value of j, that is the later the point in time, the more random variables are summed to obtain $\tilde{A}_{\mathrm{urine}}(t_j^{(2)})$; therefore the variance of $\tilde{A}_{\mathrm{urine}}(t_j^{(2)})$ increases with increasing j, and thus with increasing $A_{\mathrm{urine}}(t_j^{(2)})$. The CV of $\tilde{A}_{\mathrm{urine}}(t_j^{(2)})$, $\mathrm{CV}_{\mathrm{urine}}(t_j^{(2)})$, however is not constant. By definition,

$$\mathrm{CV}_{\mathrm{urine}}(t_j^{(2)}) = \frac{\sigma_{\mathrm{urine}}(t_j^{(2)})}{\mu_{\mathrm{urine}}(t_j^{(2)})}, \tag{5-42}$$

where $\sigma_{\mathrm{urine}}(t_j^{(2)})$ is the standard deviation of $\tilde{A}_{\mathrm{urine}}(t_j^{(2)})$ and $\mu_{\mathrm{urine}}(t_j^{(2)})$ is the mean value of $\tilde{A}_{\mathrm{urine}}(t_j^{(2)})$. From the propagation of error formula,

$$\sigma^2_{\mathrm{urine}}(t_j^{(2)}) \approx \sum_{k=2}^{j} \sigma^2_{\mathrm{UC}}(t_k^{(2)}), \qquad j = 2, \ldots, N_2. \tag{5-43}$$

Again, by definition,

$$\sigma_{\mathrm{UC}}(t_k^{(2)}) = \mathrm{CV}_{\mathrm{UC}} A_{\mathrm{UC}}(t_k^{(2)}), \tag{5-44}$$

where $A_{\mathrm{UC}}(t_k^{(2)})$ is the mean of $\tilde{A}_{\mathrm{UC}}(t_k^{(2)})$. $\tilde{A}_{\mathrm{urine}}(t_j^{(2)})$ is the sum of normally distributed variables; therefore $\tilde{A}_{\mathrm{urine}}(t_j^{(2)})$ is normally distributed and its mean is equal to the sum of the means of $\tilde{A}_{\mathrm{UC}}(t_k^{(2)})$. The mean of $\tilde{A}_{\mathrm{urine}}(t_j^{(2)})$ is therefore equal to its true value

$A_{\text{urine}}(t_j^{(2)})$, given by equation (5-30). Substituting from equations (5-30), (5-43) and (5-44) into equation (5-42) gives

$$\text{CV}_{\text{urine}}(t_j^{(2)}) \approx \text{CV}_{\text{UC}} \frac{\sqrt{\sum_{k=2}^{j} A_{\text{UC}}^2(t_k^{(2)})}}{\sum_{k=2}^{j} A_{\text{UC}}(t_k^{(2)})}, \qquad j = 2, \ldots, N_2. \tag{5-45}$$

Equation (5-45) shows that for increasing j, the magnitude of $\text{CV}_{\text{urine}}(t_j^{(2)})$ decreases.

From (5-34), the measured (with noise) values of the model output $y_2(t)$ are given by

$$\tilde{y}_2(t_j^{(2)}) = \begin{cases} 1 & j = 1 \\ 1 - \frac{\tilde{A}_{\text{urine}}(t_j^{(2)})}{\tilde{A}_{\text{dose}}} & j = 2, \ldots, N_2. \end{cases} \tag{5-46}$$

The division by a random variable, $\tilde{A}_{\text{dose}}$, means that the measured values of $\tilde{y}_2(t_j^{(2)})$ have a ratio distribution; however Q-Q (quantile-quantile) plots of simulated data show that the distribution is close to the normal distribution. The variance of $\tilde{y}_2(t_j^{(2)})$ is equal to the variance of $\frac{\tilde{A}_{\text{urine}}(t_j^{(2)})}{\tilde{A}_{\text{dose}}}$, for $j = 2, \ldots, N_2$. From the propagation of error formula,

$$\sigma_{y_2}^2(t_j^{(2)}) \approx \frac{\mu_{\text{urine}}^2(t_j^{(2)})}{A_{\text{dose}}^2} \left(\frac{\sigma_{\text{urine}}^2(t_j^{(2)})}{\mu_{\text{urine}}^2(t_j^{(2)})} + \frac{\sigma_{\text{dose}}^2}{A_{\text{dose}}^2} \right), \tag{5-47}$$

which is equivalent to

$$\sigma_{y_2}^2(t_j^{(2)}) \approx \frac{\sigma_{\text{urine}}^2(t_j^{(2)})}{A_{\text{dose}}^2} + \frac{\mu_{\text{urine}}^2(t_j^{(2)})\sigma_{\text{dose}}^2}{A_{\text{dose}}^4}. \tag{5-48}$$

Both $\sigma_{\text{urine}}^2(t_j^{(2)})$ and $\mu_{\text{urine}}^2(t_j^{(2)})$ increase with increasing $t_j^{(2)}$; thus $\sigma_{y_2}^2(t_j^{(2)})$ increases with increasing $t_j^{(2)}$. The mean of $\tilde{y}_2(t_j^{(2)})$ decreases with time and therefore its CV must also increase with time.

From (5-47), the CV of $\tilde{y}_2(t_j^{(2)})$ is given by

$$\text{CV}_{y_2}(t_j^{(2)}) = \frac{\sigma_{y_2}(t_j^{(2)})}{\mu_{y_2}(t_j^{(2)})} \approx \frac{\frac{\mu_{\text{urine}}(t_j^{(2)})}{A_{\text{dose}}} \sqrt{\text{CV}_{\text{urine}}^2(t_j^{(2)}) + \text{CV}_{\text{D}}^2}}{1 - \frac{\mu_{\text{urine}}(t_j^{(2)})}{A_{\text{dose}}}} \tag{5-49}$$

or

$$\text{CV}_{y_2}(t_j^{(2)}) \approx \frac{\left(1 - \mu_{y_2}(t_j^{(2)})\right) \sqrt{\text{CV}_{\text{urine}}^2(t_j^{(2)}) + \text{CV}_{\text{D}}^2}}{\mu_{y_2}(t_j^{(2)})}. \tag{5-50}$$

Consideration of the distribution and size of the errors in the data is important for selecting the most appropriate parameter estimation methods. This will be discussed in section 5.6.3.

5.6 Population approach to parameter identification using timecourse data

In this section model parameters are estimated using the timecourse data taken from the literature and described in section 5.3. It is assumed that the unique parameter vector of the i^{th} subject in the sample, $\boldsymbol{\psi}_i = \big(\text{FCR}_i, k_{12,i}, k_{21,i}\big)$, is drawn from a probability distribution. The parameters of this distribution are estimated by fitting the data from the seven available subjects simultaneously. The outputs $y_1(t)$ and $y_2(t)$ of the structural model described by equations (5-10)–(5-12) are fitted to the timecourse data. The population approach is implemented in the software package Monolix [17]. Monolix is a specialist software for estimating parameters of nonlinear mixed effects models. In Monolix an implementation of the stochastic approximation expectation maximization (SAEM) algorithm is used to maximise the likelihood function and thus generate maximum likelihoood (ML) parameter estimates.

5.6.1 The distribution of parameters in the population

The parameters for the individual subjects, or 'individual parameters', $\text{FCR}_i, k_{12,i}$ and $k_{21,i}$, are assumed to be log-normally distributed in the population to ensure positivity:

$$\begin{aligned} \log(\text{FCR}_i) &\sim N(\log\big(\text{FCR}_{\text{pop}}\big), \sigma^2_{\text{FCR}}) \\ \log\big(k_{12,i}\big) &\sim N(\log\big(k_{12,\text{pop}}\big), \sigma^2_{k_{12}}) \\ \log\big(k_{21,i}\big) &\sim N(\log\big(k_{21,\text{pop}}\big), \sigma^2_{k_{21}}), \end{aligned} \tag{5-51}$$

where $\log\big(\text{FCR}_{\text{pop}}\big)$, $\log\big(k_{12,\text{pop}}\big)$, and $\log\big(k_{21,\text{pop}}\big)$ are the means of the natural logarithms of the individual parameters and σ_{FCR}, $\sigma_{k_{12}}$ and $\sigma_{k_{21}}$ are the standard deviations of the natural logarithms of the individual parameters. FCR_{pop}, $k_{12,\text{pop}}$, and $k_{21,\text{pop}}$ are thus the medians of the log-normally distributed individual parameters. It is also assumed that the individual parameters are correlated with one another, with coefficients $\rho_{\text{FCR}k_{12}}$, $\rho_{\text{FCR}k_{21}}$ and $\rho_{k_{12}k_{21}}$ for the correlations between FCR_i and $k_{12,i}$, FCR_i and $k_{21,i}$, and $k_{12,i}$ and $k_{21,i}$, respectively. This general approach also allows for individual parameters to be uncorrelated when the relevant correlation coefficients are equal to zero.

The individual parameters can also be expressed as

$$\begin{aligned} \mathrm{FCR}_i &= \mathrm{FCR}_{\mathrm{pop}} \exp(\eta_{\mathrm{FCR}}) \\ k_{12,i} &= k_{12,\mathrm{pop}} \exp(\eta_{k_{12}}) \\ k_{21,i} &= k_{21,\mathrm{pop}} \exp(\eta_{k_{21}}), \end{aligned} \tag{5-52}$$

where now the individual parameters are decomposed into their fixed or population effects ($\mathrm{FCR}_{\mathrm{pop}}$, $k_{12,\mathrm{pop}}$ and $k_{21,\mathrm{pop}}$) and random or individual effects (η_{FCR}, $\eta_{k_{12}}$ and $\eta_{k_{21}}$). The random effects $\boldsymbol{\eta} = (\eta_{\mathrm{FCR}}, \eta_{k_{12}}, \eta_{k_{21}})$ are normally distributed:

$$\boldsymbol{\eta} \sim N(\mathbf{0}, \boldsymbol{\Omega}), \tag{5-53}$$

where $\boldsymbol{\Omega}$ is the variance-covariance matrix,

$$\boldsymbol{\Omega} = \begin{pmatrix} \sigma^2_{\mathrm{FCR}} & \rho_{\mathrm{FCR}k_{12}}\sigma_{\mathrm{FCR}}\sigma_{k_{12}} & \rho_{\mathrm{FCR}k_{21}}\sigma_{\mathrm{FCR}}\sigma_{k_{21}} \\ \rho_{\mathrm{FCR}k_{12}}\sigma_{k_{12}}\sigma_{\mathrm{FCR}} & \sigma^2_{k_{12}} & \rho_{k_{12}k_{21}}\sigma_{k_{12}}\sigma_{k_{21}} \\ \rho_{\mathrm{FCR}k_{21}}\sigma_{k_{21}}\sigma_{\mathrm{FCR}} & \rho_{k_{12}k_{21}}\sigma_{k_{21}}\sigma_{k_{12}} & \sigma^2_{k_{21}} \end{pmatrix}. \tag{5-54}$$

We refer to the parameter $\boldsymbol{\theta} = \left(\boldsymbol{\psi}_{\mathrm{pop}}, \boldsymbol{\Omega}\right)$, where $\boldsymbol{\psi}_{\mathrm{pop}} = \left(\mathrm{FCR}_{\mathrm{pop}}, k_{12,\mathrm{pop}}, k_{21,\mathrm{pop}}\right)$, as the population parameter, describing the distribution of the individuals' parameter values in the population. The parameter $\boldsymbol{\psi}_{\mathrm{pop}}$ represents the value of $\boldsymbol{\psi}_i$ in the absence of randomness. It is also considered to be the 'predicted' or typical value of the parameter $\boldsymbol{\psi}_i$ within the population.

5.6.2 Structural identifiability analysis

Before attempting to estimate the population parameter vector $\boldsymbol{\theta}$, it is necessary to establish whether the parameter vector is structurally identifiable given the available model outputs. The parameter $\boldsymbol{\psi}_{\mathrm{pop}}$, representing the fixed effect of the individual parameters, can be analysed using standard structural identifiability methods for deterministic systems. Standard methods do not however address whether the parameter $\boldsymbol{\Omega}$ is also structurally identifiable. Methods for analysing structural identifiability of mixed effects models have only recently been developed [18; 19]. Here the Laplace transform mixed effects extension approach of Janzén et al. [19] is applied.

Deterministic problem

In this section we confirm that the parameter $\boldsymbol{\psi} = (\text{FCR}, k_{12}, k_{21})$ is structurally uniquely identifiable from the timecourse outputs, $y_1(t)$ and $y_2(t)$, using the transfer function method [20]. Note that in this analysis the parameter $\boldsymbol{\psi}$ is considered to be a constant and not a random variable. The system described by equations (5-10)–(5-12) is re-written in vector-matrix notation as

$$\begin{aligned} \dot{\boldsymbol{x}}(t, \boldsymbol{\psi}) &= \boldsymbol{A}(\boldsymbol{\psi})\boldsymbol{x}(t, \boldsymbol{\psi}) + \boldsymbol{B}u(t) \\ \boldsymbol{x}(0, \boldsymbol{\psi}) &= 0 \\ \boldsymbol{y}(t, \boldsymbol{\psi}) &= \boldsymbol{C}\boldsymbol{x}(t, \boldsymbol{\psi}), \end{aligned} \tag{5-55}$$

where $\boldsymbol{x}(t, \boldsymbol{\psi}) = \big(x_{1,\text{P}}(t), x_{2,\text{P}}(t)\big)$ and $\boldsymbol{y}(t, \boldsymbol{\psi}) = \big(y_1(t), y_2(t)\big)$ are column vectors representing the state and the observation, respectively. $u(t)$ represents the single input to the system, a unit impulse applied at time $t = 0$, given by $u(t) = \delta(t)$. $\boldsymbol{A}(\boldsymbol{\psi})$ and $\boldsymbol{C}$ are 2×2 matrices and $\boldsymbol{B}$ is a column vector. $\boldsymbol{A}(\boldsymbol{\psi})$, $\boldsymbol{B}$ and $\boldsymbol{C}$ are given by

$$\boldsymbol{A}(\boldsymbol{\psi}) = \begin{pmatrix} -(k_{21} + \text{FCR}) & k_{12} \\ k_{21} & -k_{12} \end{pmatrix}, \boldsymbol{B} = \begin{pmatrix} 1 \\ 0 \end{pmatrix}, \boldsymbol{C} = \begin{pmatrix} 1 & 0 \\ 1 & 1 \end{pmatrix}. \tag{5-56}$$

Note that the administration of a bolus dose is now represented as an impulse at time $t = 0$, rather than a non-zero initial condition, such that $\boldsymbol{x}(0, \boldsymbol{\psi}) = 0$.

Taking Laplace transforms of equations (5-55), the input-output relation is described by $\boldsymbol{Y}(s) = \boldsymbol{G}(s)U(s)$, where $\boldsymbol{G}(s)$ is the transfer function matrix, given by $\boldsymbol{G}(s) = \boldsymbol{C}(s\boldsymbol{I} - \boldsymbol{A}(\boldsymbol{\psi}))^{-1}\boldsymbol{B}$, where $\boldsymbol{I}$ is the 2×2 identity matrix. $\boldsymbol{G}(s)$ has two elements, corresponding to the two measured outputs, which are given by

$$\begin{aligned} G_1(s) &= \frac{s + k_{12}}{s^2 + (\text{FCR} + k_{12} + k_{21})\, s + \text{FCR}k_{12}} \\ G_2(s) &= \frac{s + k_{12} + k_{21}}{s^2 + (\text{FCR} + k_{12} + k_{21})\, s + \text{FCR}k_{12}}. \end{aligned} \tag{5-57}$$

Let $\boldsymbol{\Phi}(\boldsymbol{\psi}) = (\phi_1(\boldsymbol{\psi}), ..., \phi_4(\boldsymbol{\psi}))$ denote the (distinct) coefficients of s in equations (5-57). The coefficients $\boldsymbol{\Phi}(\boldsymbol{\psi})$ are unique with respect to the input-output relationship of the

system and are given by

$$\begin{aligned}\phi_1(\boldsymbol{\psi}) &= k_{12}\\ \phi_2(\boldsymbol{\psi}) &= k_{12} + k_{21}\\ \phi_3(\boldsymbol{\psi}) &= \mathrm{FCR}k_{12}\\ \phi_4(\boldsymbol{\psi}) &= \mathrm{FCR} + k_{12} + k_{21}.\end{aligned} \tag{5-58}$$

Introducing an alternative parameter vector $\overline{\boldsymbol{\psi}} = (\overline{\mathrm{FCR}}, \bar{k}_{12}, \bar{k}_{21})$ and equating $\boldsymbol{\Phi}(\boldsymbol{\psi}) = \boldsymbol{\Phi}(\overline{\boldsymbol{\psi}})$ gives the following set of simultaneous equations:

$$\begin{aligned}k_{12} &= \bar{k}_{12}\\ k_{12} + k_{21} &= \bar{k}_{12} + \bar{k}_{21}\\ \mathrm{FCR}k_{12} &= \overline{\mathrm{FCR}}\bar{k}_{12}\\ \mathrm{FCR} + k_{12} + k_{21} &= \overline{\mathrm{FCR}} + \bar{k}_{12} + \bar{k}_{21}.\end{aligned} \tag{5-59}$$

Now equations (5-59) are solved for $\overline{\boldsymbol{\psi}}$. Immediately it can be seen from the first of equations (5-59) that the only solution for $\bar{k}_{12}$ is $\bar{k}_{12} = k_{12}$. Then from any pair of the remaining equations it can be seen that $\overline{\mathrm{FCR}} = \mathrm{FCR}$ and $\bar{k}_{21} = k_{21}$. It has thus been shown that $\boldsymbol{\Phi}(\boldsymbol{\psi}) = \boldsymbol{\Phi}(\overline{\boldsymbol{\psi}})$ requires $\overline{\boldsymbol{\psi}} = \boldsymbol{\psi}$ and therefore the parameter vector $\boldsymbol{\psi}$ is structurally globally identifiable. This analysis also proves that the population parameter $\boldsymbol{\psi}_{\mathrm{pop}} = \left(\mathrm{FCR}_{\mathrm{pop}}, k_{12,\mathrm{pop}}, k_{21,\mathrm{pop}}\right)$ is structurally globally identifiable [19].

Mixed effects problem

To extend the analysis to the mixed effects model, both the fixed and random effects of the parameters are now considered. The moment invariants of the system, $\boldsymbol{Z}(\boldsymbol{\psi}_{\mathrm{pop}}, \boldsymbol{\eta})$, where $\boldsymbol{\psi}_{\mathrm{pop}} = (\mathrm{FCR}_{\mathrm{pop}}, k_{12,\mathrm{pop}}, k_{21,\mathrm{pop}})$ and $\boldsymbol{\eta} = (\eta_{\mathrm{FCR}}, \eta_{k_{12}}, \eta_{k_{21}})$, are now given by

$$\begin{aligned}Z_1(\boldsymbol{\psi}_{\mathrm{pop}}, \boldsymbol{\eta}) &= k_{12,\mathrm{pop}} \exp(\eta_{k_{12}})\\ Z_2(\boldsymbol{\psi}_{\mathrm{pop}}, \boldsymbol{\eta}) &= k_{12,\mathrm{pop}} \exp(\eta_{k_{12}}) + k_{21,\mathrm{pop}} \exp(\eta_{k_{21}})\\ Z_3(\boldsymbol{\psi}_{\mathrm{pop}}, \boldsymbol{\eta}) &= \mathrm{FCR}_{\mathrm{pop}} \exp(\eta_{\mathrm{FCR}}) k_{12,\mathrm{pop}} \exp(\eta_{k_{12}})\\ Z_4(\boldsymbol{\psi}_{\mathrm{pop}}, \boldsymbol{\eta}) &= \mathrm{FCR}_{\mathrm{pop}} \exp(\eta_{\mathrm{FCR}}) + k_{12,\mathrm{pop}} \exp(\eta_{k_{12}}) + k_{21,\mathrm{pop}} \exp(\eta_{k_{21}}).\end{aligned} \tag{5-60}$$

The first order statistical moments are given by

$$\begin{aligned}
\mathbb{E}(Z_1) &= k_{12,\text{pop}} \exp\left(\frac{\sigma^2_{k_{12}}}{2}\right) \\
\mathbb{E}(Z_2) &= k_{12,\text{pop}} \exp\left(\frac{\sigma^2_{k_{12}}}{2}\right) + k_{21,\text{pop}} \exp\left(\frac{\sigma^2_{k_{21}}}{2}\right) \\
\mathbb{E}(Z_3) &= \text{FCR}_{\text{pop}} k_{12,\text{pop}} \exp\left(\frac{1}{2}\left(\sigma^2_{\text{FCR}} + \sigma^2_{k_{12}} + 2\sigma_{\text{FCR}}\sigma_{k_{12}}\rho_{\text{FCR}k_{12}}\right)\right) \\
\mathbb{E}(Z_4) &= \text{FCR}_{\text{pop}} \exp\left(\frac{\sigma^2_{\text{FCR}}}{2}\right) + k_{12,\text{pop}} \exp\left(\frac{\sigma^2_{k_{12}}}{2}\right) + k_{21,\text{pop}} \exp\left(\frac{\sigma^2_{k_{21}}}{2}\right).
\end{aligned} \tag{5-61}$$

Whereas in the deterministic problem the availability of noise-free continuous data is assumed, in the mixed-effects case we also assume the availability of an infinite number of subjects, such that full knowledge of the random variables $\boldsymbol{Z}(\boldsymbol{\psi}_{\text{pop}}, \boldsymbol{\eta})$ is obtained. Introducing an alternative parameter vector $\overline{\boldsymbol{\psi}}_{\text{pop}}$ and an alternative variance-covariance matrix $\overline{\boldsymbol{\Omega}}$ of the random effects $\overline{\boldsymbol{\eta}}$, the mixed effects structural identifiability analysis amounts to solving the system of equations given by

$$\begin{aligned}
\mathbb{E}(Z_1^l(\boldsymbol{\psi}_{\text{pop}}, \boldsymbol{\eta})) &= \mathbb{E}(Z_1^l(\overline{\boldsymbol{\psi}}_{\text{pop}}, \overline{\boldsymbol{\eta}})) \\
&\vdots \\
\mathbb{E}(Z_4^l(\boldsymbol{\psi}_{\text{pop}}, \boldsymbol{\eta})) &= \mathbb{E}(Z_4^l(\overline{\boldsymbol{\psi}}_{\text{pop}}, \overline{\boldsymbol{\eta}})) \\
\boldsymbol{\eta} &\sim N(0, \boldsymbol{\Omega}) \\
\overline{\boldsymbol{\eta}} &\sim N(0, \overline{\boldsymbol{\Omega}}),
\end{aligned} \tag{5-62}$$

where $\mathbb{E}(Z^l)$ denotes the l^{th} statistical moment of the distribution Z, for the parameters in the vector $\overline{\boldsymbol{\psi}}_{\text{pop}}$ and the matrix $\overline{\boldsymbol{\Omega}}$.

Equating the first order statistical moments evaluated for $\overline{\boldsymbol{\psi}}_{\text{pop}}$ and $\overline{\boldsymbol{\Omega}}$ with the first order moments evaluated for $\boldsymbol{\psi}_{\text{pop}}$ and $\boldsymbol{\Omega}$ gives

$$k_{12,\text{pop}} \exp\left(\frac{\sigma^2_{k_{12}}}{2}\right) = \bar{k}_{12,\text{pop}} \exp\left(\frac{\bar{\sigma}^2_{k_{12}}}{2}\right), \tag{5-63}$$

$$\begin{aligned}
k_{12,\text{pop}} \exp\left(\frac{\sigma^2_{k_{12}}}{2}\right) + k_{21,\text{pop}} \exp\left(\frac{\sigma^2_{k_{21}}}{2}\right) \\
= \bar{k}_{12,\text{pop}} \exp\left(\frac{\bar{\sigma}^2_{k_{12}}}{2}\right) + \bar{k}_{21,\text{pop}} \exp\left(\frac{\bar{\sigma}^2_{k_{21}}}{2}\right),
\end{aligned} \tag{5-64}$$

$$\mathrm{FCR}_{\mathrm{pop}} k_{12,\mathrm{pop}} \exp\left(\frac{1}{2}\left(\sigma^2_{\mathrm{FCR}} + \sigma^2_{k_{12}} + 2\sigma_{\mathrm{FCR}}\sigma_{k_{12}}\rho_{\mathrm{FCR}k_{12}}\right)\right) = \overline{\mathrm{FCR}}_{\mathrm{pop}} \bar{k}_{12,\mathrm{pop}} \exp\left(\frac{1}{2}\left(\bar{\sigma}^2_{\mathrm{FCR}} + \bar{\sigma}^2_{k_{12}} + 2\bar{\sigma}_{\mathrm{FCR}}\bar{\sigma}_{k_{12}}\bar{\rho}_{\mathrm{FCR}k_{12}}\right)\right), \quad (5\text{-}65)$$

and

$$\mathrm{FCR}_{\mathrm{pop}} \exp\left(\frac{\sigma^2_{\mathrm{FCR}}}{2}\right) + k_{12,\mathrm{pop}} \exp\left(\frac{\sigma^2_{k_{12}}}{2}\right) + k_{21,\mathrm{pop}} \exp\left(\frac{\sigma^2_{k_{21}}}{2}\right) = \overline{\mathrm{FCR}}_{\mathrm{pop}} \exp\left(\frac{\bar{\sigma}^2_{\mathrm{FCR}}}{2}\right) + \bar{k}_{12,\mathrm{pop}} \exp\left(\frac{\bar{\sigma}^2_{k_{12}}}{2}\right) + \bar{k}_{21,\mathrm{pop}} \exp\left(\frac{\bar{\sigma}^2_{k_{21}}}{2}\right). \quad (5\text{-}66)$$

Now equations (5-63) to (5-66) are solved for $\overline{\boldsymbol{\psi}}_{\mathrm{pop}}$ and $\overline{\boldsymbol{\Omega}}$. It is already known from the deterministic structural identifiability analysis that the population parameters are structurally identifiable, that is $\overline{\mathrm{FCR}}_{\mathrm{pop}} = \mathrm{FCR}_{\mathrm{pop}}$, $\bar{k}_{12,\mathrm{pop}} = k_{12,\mathrm{pop}}$ and $\bar{k}_{21,\mathrm{pop}} = k_{21,\mathrm{pop}}$. From equation (5-63), given $\bar{k}_{12,\mathrm{pop}} = k_{12,\mathrm{pop}}$, it can be seen that $\bar{\sigma}_{k_{12}}$ must be equal to $\sigma_{k_{12}}$. $\bar{\sigma}_{k_{12}} = -\sigma_{k_{12}}$ is also a solution of (5-63), but $\sigma_{k_{12}}$ is a standard deviation and therefore can only be positive. Then from equation (5-64), with $\bar{k}_{12,\mathrm{pop}} = k_{12,\mathrm{pop}}$, $\bar{\sigma}_{k_{12}} = \sigma_{k_{12}}$ and $\bar{k}_{21,\mathrm{pop}} = k_{21,\mathrm{pop}}$ known, the solution for $\bar{\sigma}_{k_{21}}$ is given by $\bar{\sigma}_{k_{21}} = \sigma_{k_{21}}$. Now solving equation (5-66) gives $\bar{\sigma}_{\mathrm{FCR}} = \sigma_{\mathrm{FCR}}$. Finally solving equation (5-65) for $\bar{\rho}_{\mathrm{FCR}k_{12}}$ gives $\bar{\rho}_{\mathrm{FCR}k_{12}} = \rho_{\mathrm{FCR}k_{12}}$.

The remaining parameters $\rho_{k_{12}k_{21}}$ and $\rho_{\mathrm{FCR}k_{21}}$ do not feature in the first order statistical moments given in equations (5-61); therefore the second order moments of the moment invariants $Z_2(\boldsymbol{\psi}_{\mathrm{pop}}, \boldsymbol{\eta})$ and $Z_4(\boldsymbol{\psi}_{\mathrm{pop}}, \boldsymbol{\eta})$ are required in order to assess whether the system is structurally globally identifiable. These are given by

$$\mathbb{E}(Z_2^2) = k^2_{12,\mathrm{pop}} \exp\left(2\sigma^2_{k_{12}}\right) + k^2_{21,\mathrm{pop}} \exp\left(2\sigma^2_{k_{21}}\right) + 2k_{12,\mathrm{pop}}k_{21,\mathrm{pop}} \exp\left(\frac{1}{2}\left(\sigma^2_{k_{12}} + \sigma^2_{k_{21}} + 2\sigma_{k_{12}}\sigma_{k_{21}}\rho_{k_{12}k_{21}}\right)\right) \quad (5\text{-}67)$$

and

$$\begin{aligned}\mathbb{E}(Z_4^2) = {} & \mathrm{FCR}^2_{\mathrm{pop}} \exp\left(2\sigma^2_{\mathrm{FCR}}\right) + k^2_{12,\mathrm{pop}} \exp\left(2\sigma^2_{k_{12}}\right) + k^2_{21,\mathrm{pop}} \exp\left(2\sigma^2_{k_{21}}\right) \\ & + 2\mathrm{FCR}_{\mathrm{pop}}k_{12,\mathrm{pop}} \exp\left(\frac{1}{2}\left(\sigma^2_{\mathrm{FCR}} + \sigma^2_{k_{12}} + 2\sigma_{\mathrm{FCR}}\sigma_{k_{12}}\rho_{\mathrm{FCR}k_{12}}\right)\right) \\ & + 2k_{12,\mathrm{pop}}k_{21,\mathrm{pop}} \exp\left(\frac{1}{2}\left(\sigma^2_{k_{12}} + \sigma^2_{k_{21}} + 2\sigma_{k_{12}}\sigma_{k_{21}}\rho_{k_{12}k_{21}}\right)\right) \\ & + 2k_{21,\mathrm{pop}}\mathrm{FCR}_{\mathrm{pop}} \exp\left(\frac{1}{2}\left(\sigma^2_{k_{21}} + \sigma^2_{\mathrm{FCR}} + 2\sigma_{k_{21}}\sigma_{\mathrm{FCR}}\rho_{\mathrm{FCR}k_{21}}\right)\right). \quad (5\text{-}68)\end{aligned}$$

Equating $\mathbb{E}\left(Z_2^2(\boldsymbol{\psi}_{\text{pop}}, \boldsymbol{\eta})\right)$ with $\mathbb{E}\left(Z_2^2(\overline{\boldsymbol{\psi}}_{\text{pop}}, \overline{\boldsymbol{\eta}})\right)$ gives

$$\begin{aligned} &k_{12,\text{pop}}^2 \exp\left(2\sigma_{k_{12}}^2\right) + k_{21,\text{pop}}^2 \exp\left(2\sigma_{k_{21}}^2\right) \\ &\quad + 2k_{12,\text{pop}}k_{21,\text{pop}} \exp\left(\frac{1}{2}\left(\sigma_{k_{12}}^2 + \sigma_{k_{21}}^2 + 2\sigma_{k_{12}}\sigma_{k_{21}}\rho_{k_{12}k_{21}}\right)\right) = \bar{k}_{12,\text{pop}}^2 \exp\left(2\bar{\sigma}_{k_{12}}^2\right) \\ &+ \bar{k}_{21,\text{pop}}^2 \exp\left(2\bar{\sigma}_{k_{21}}^2\right) + 2\bar{k}_{12,\text{pop}}\bar{k}_{21,\text{pop}} \exp\left(\frac{1}{2}\left(\bar{\sigma}_{k_{12}}^2 + \bar{\sigma}_{k_{21}}^2 + 2\bar{\sigma}_{k_{12}}\bar{\sigma}_{k_{21}}\bar{\rho}_{k_{12}k_{21}}\right)\right). \end{aligned} \tag{5-69}$$

With $k_{12,\text{pop}}$, $k_{21,\text{pop}}$, $\sigma_{k_{12}}$ and $\sigma_{k_{21}}$ already shown to be structurally identifiable, solving equation (5-69) for $\bar{\rho}_{k_{12}k_{21}}$ gives $\bar{\rho}_{k_{12}k_{21}} = \rho_{k_{12}k_{21}}$. Last of all, equating $\mathbb{E}\left(Z_4^2(\boldsymbol{\psi}_{\text{pop}}, \boldsymbol{\eta})\right)$ with $\mathbb{E}\left(Z_4^2(\overline{\boldsymbol{\psi}}_{\text{pop}}, \overline{\boldsymbol{\eta}})\right)$ and solving for $\bar{\rho}_{k_{21}\text{FCR}}$ gives $\bar{\rho}_{k_{21}\text{FCR}} = \rho_{\text{FCR}k_{21}}$.

It has thus been shown that the system of equations in (5-62) requires $\overline{\boldsymbol{\Omega}} = \boldsymbol{\Omega}$; therefore both population parameters $\boldsymbol{\psi}_{\text{pop}}$ and $\boldsymbol{\Omega}$ are structurally globally identifiable. The Mathematica [21] code used to perform the mixed effects structural identifiability analysis is provided in appendix B.

5.6.3 Error models

The structural identifiability analysis shows that in the absence of errors on the observations, a set of continuous trajectories of $y_1(t, \boldsymbol{\psi}_i)$ and $y_2(t, \boldsymbol{\psi}_i)$, $i = 1, \ldots, n$, for some n subjects, must arise from a unique parameter $\boldsymbol{\theta}$. In reality, however, model outputs are observed with error at discrete timepoints. The measured quantities with error are denoted by $\tilde{y}_k(t_{ij}^{(k)}, \boldsymbol{\psi}_i)$, $k = 1, 2$, for subjects $i = 1, \ldots, n$. It is assumed that $\tilde{y}_k(t_{ij}^{(k)}, \boldsymbol{\psi}_i)$ is measured at discrete timepoints $t_{ij}^{(k)}, j = 1, \ldots, N_{ik}$, with $t_{i1}^{(k)} = t_{i1}^{(k)} = 0$.

From section 5.5, there are several features of the data that may cause problems when attempting to estimate parameters. Firstly, systematic errors are introduced in the calculation of $\tilde{y}_1(t_{ij}^{(1)}, \boldsymbol{\psi}_i)$ and $\tilde{y}_2(t_{ij}^{(2)}, \boldsymbol{\psi}_i)$ due to division by quantities measured with error at time $t = 0$. This means that the observations are not symmetric about their predicted or 'true' value. Secondly, it is assumed that $\tilde{y}_2(t_{ij}^{(2)}, \boldsymbol{\psi}_i)$ is calculated by summing daily urine collections, such that the errors on individual measurements of $\tilde{y}_2(t_{ij}^{(2)}, \boldsymbol{\psi}_i)$ are no longer independent. Finally, the calculation of $\tilde{y}_2(t_{ij}^{(2)}, \boldsymbol{\psi}_i)$ leads to a non-standard relationship between variance of $\tilde{y}_2(t_{ij}^{(2)}, \boldsymbol{\psi}_i)$ and its mean, as shown in the expression for the CV in equation (5-50).

In order to estimate model parameters, it is necessary to make assumptions regarding the data that are in actuality violated, as described above. The importance of violating these assumptions will be assessed in section 5.6.5 by using the estimation method on synthetic data for which the true parameter values are known. It is therefore assumed that the observed measurements for the i^{th} subject are given by

$$\tilde{y}_k(t_{ij}^{(k)}, \boldsymbol{\psi}_i) = y_k(t_{ij}^{(k)}, \boldsymbol{\psi}_i) + g_k(t_{ij}^{(k)}, \boldsymbol{\psi}_i, \boldsymbol{\xi})\epsilon_{ij}^{(k)}, \qquad j = 1, \ldots, N_{ik}, \qquad k = 1, 2, \tag{5-70}$$

where $\epsilon_{ij}^{(k)}$ are independent and identically distributed random variables following the normal distribution: $\epsilon_{ij}^{(k)} \sim N(0, 1)$. The error model is represented by $g_k(t_{ij}^{(k)}, \boldsymbol{\psi}_i, \boldsymbol{\xi})$, allowing for possible dependence of the residual errors on time, the individual's true parameter vector, and an additional error model parameter $\boldsymbol{\xi}$.

The population parameters are estimated by ML estimation. In order to use ML estimation it is necessary to specify the error model for the observations, the most common being normally distributed errors with constant variance (constant error model) and normally distributed errors with standard deviation proportional to the size of the predicted value (proportional error model). The constant error model is given by

$$g_k(t_{ij}^{(k)}, \boldsymbol{\psi}_i, \xi) = a_k. \tag{5-71}$$

The proportional error model is given by

$$g_k(t_{ij}^{(k)}, \boldsymbol{\psi}_i, \xi) = b_k y_k(t_{ij}^{(k)}, \boldsymbol{\psi}_i). \tag{5-72}$$

The two model outputs $\tilde{y}_k(t_{ij}^{(k)}, \boldsymbol{\psi}_i)$, $k = 1, 2$, need not have the same error model; however the error model for each output ($k = 1$ or 2) is assumed to apply to all individuals in the population.

These models assume that the observations are symmetrically distributed around their predicted value, which is not strictly true for the data used here due to the systematic error described above. They also assume that the errors are independent, whereas we believe the errors on the calculated $\tilde{y}_2(t_{ij}^{(2)}, \boldsymbol{\psi}_i)$ to be autocorrelated. It is assumed, based on information about the data collection, that $\tilde{y}_1(t_{ij}^{(1)}, \boldsymbol{\psi}_i)$ has a constant CV and that $\tilde{y}_2(t_{ij}^{(2)}, \boldsymbol{\psi}_i)$ has a more complex relationship between its variance and its mean that may not be possible to specify in a standard form; we are therefore consigned to misspecify the

error model for $\tilde{y}_2(t_{ij}^{(2)}, \boldsymbol{\psi}_i)$. The problems identified here mean that several assumptions underlying the estimation method will be violated by these data and the estimation may yield biased parameter estimates.

The suitability of different assumed error models can be compared by estimating the population parameters from multiple synthetic datasets and assessing the performance of each method in recovering the true parameter values, which in this scenario are known. Bonate states that, 'before undertaking anything, the question of whether it is worth the effort to find a residual variance model must be answered', and offers the rule of thumb that a correct error model is required when the ratio of the largest to the smallest standard deviation of the errors exceeds 3 [22, p. 133].

Given the issues discussed in this section, synthetic data will be used to compare two methods:

- Method 1, in which a proportional error model is assumed to apply to both $\tilde{y}_1(t_{ij}^{(1)}, \boldsymbol{\psi}_i)$ and $\tilde{y}_2(t_{ij}^{(2)}, \boldsymbol{\psi}_i)$;
- Method 2, in which a proportional error model is assumed to apply to $\tilde{y}_1(t_{ij}^{(1)}, \boldsymbol{\psi}_i)$ and a constant error model to $\tilde{y}_2(t_{ij}^{(2)}, \boldsymbol{\psi}_i)$.

Firstly Method 1 is applied to the real data in order to estimate the population parameters in section 5.6.4; these parameter estimates are then used to simulate data in section 5.6.5. The population parameters are then estimated from the synthetic data using both Method 1 and Method 2 in section 5.6.6.

5.6.4 Parameter estimation

The population parameter vector $\boldsymbol{\theta} = \left(\boldsymbol{\psi}_{\text{pop}}, \boldsymbol{\Omega}\right)$ is estimated by maximising the observed likelihood of $\boldsymbol{\theta}$ given the data for the seven subjects. The data for the i^{th} individual are assumed to be described by equation (5-70), with the proportional error model for both outputs, given by equation (5-72). For brevity, the data for an individual are denoted by $\boldsymbol{y}_i$ and the data for the sample of individuals are denoted by $\boldsymbol{y}$. The measurement times for all observations are denoted by $\boldsymbol{t}$, where $\boldsymbol{t} = t_{ij}^{(k)}, i = 1, \ldots, n; k = 1, 2; j = 1, \ldots, N_{ik}$.

Table 5-2 Initial values for SAEM algorithm

Parameter	Units	Initial value
FCR_{pop}	day^{-1}	1
$k_{12,\text{pop}}$	day^{-1}	1
$k_{21,\text{pop}}$	day^{-1}	1
σ_{FCR}	day^{-1}	1
$\sigma_{k_{12}}$	day^{-1}	1
$\sigma_{k_{21}}$	day^{-1}	1
b_1	–	0.3
b_2	–	0.3

Table 5-3 Maximum likelihood (ML) parameter estimates, standard errors (S.E.) and relative standard error (R.S.E.) as a % of the value of the estimate

Parameter	Units	ML estimate	S.E.	R.S.E. (%)
FCR_{pop}	day^{-1}	0.0778	0.02	26
$k_{12,\text{pop}}$	day^{-1}	0.422	0.12	27
$k_{21,\text{pop}}$	day^{-1}	0.441	0.083	19
σ_{FCR}	day^{-1}	0.685	0.18	27
$\sigma_{k_{12}}$	day^{-1}	0.713	0.19	27
$\sigma_{k_{21}}$	day^{-1}	0.498	0.13	27
$\rho_{\text{FCR}k_{12}}$	–	0.872	0.092	11
$\rho_{\text{FCR}k_{21}}$	–	0.608	0.24	39
$\rho_{k_{12}k_{21}}$	–	0.739	0.17	23
b_1	–	0.0814	0.0065	8
b_2	–	0.0222	0.0016	7

The likelihood of $\boldsymbol{\theta}$ given $\boldsymbol{y}$ is given by

$$\mathcal{L}(\boldsymbol{\theta}; \boldsymbol{y}, \boldsymbol{t}) = f(\boldsymbol{y}; \boldsymbol{\theta}, \boldsymbol{t}), \tag{5-73}$$

where $f(\boldsymbol{y}; \boldsymbol{\theta}, \boldsymbol{t})$ is the probability density function of $\boldsymbol{y}$, parameterised by $\boldsymbol{\theta}$ and $\boldsymbol{t}$.

The population parameters were estimated by fitting the timecourse data from seven subjects (see section 5.3) using the software package Monolix [17]. Initial values for the parameters provided to the SAEM algorithm are given in table 5-2. The population parameter ML estimates and their standard errors are summarised in table 5-3.

The individual parameters are estimated by estimating the distribution of the individual parameter vector $\boldsymbol{\psi}_i$, conditional on the individual data $\boldsymbol{y}_i$ and parameterised by the ML estimate of the population parameter vector, $\hat{\boldsymbol{\theta}}$, for each individual, using the Metropolis-Hastings algorithm. The modes of the conditional distributions are found by numerical

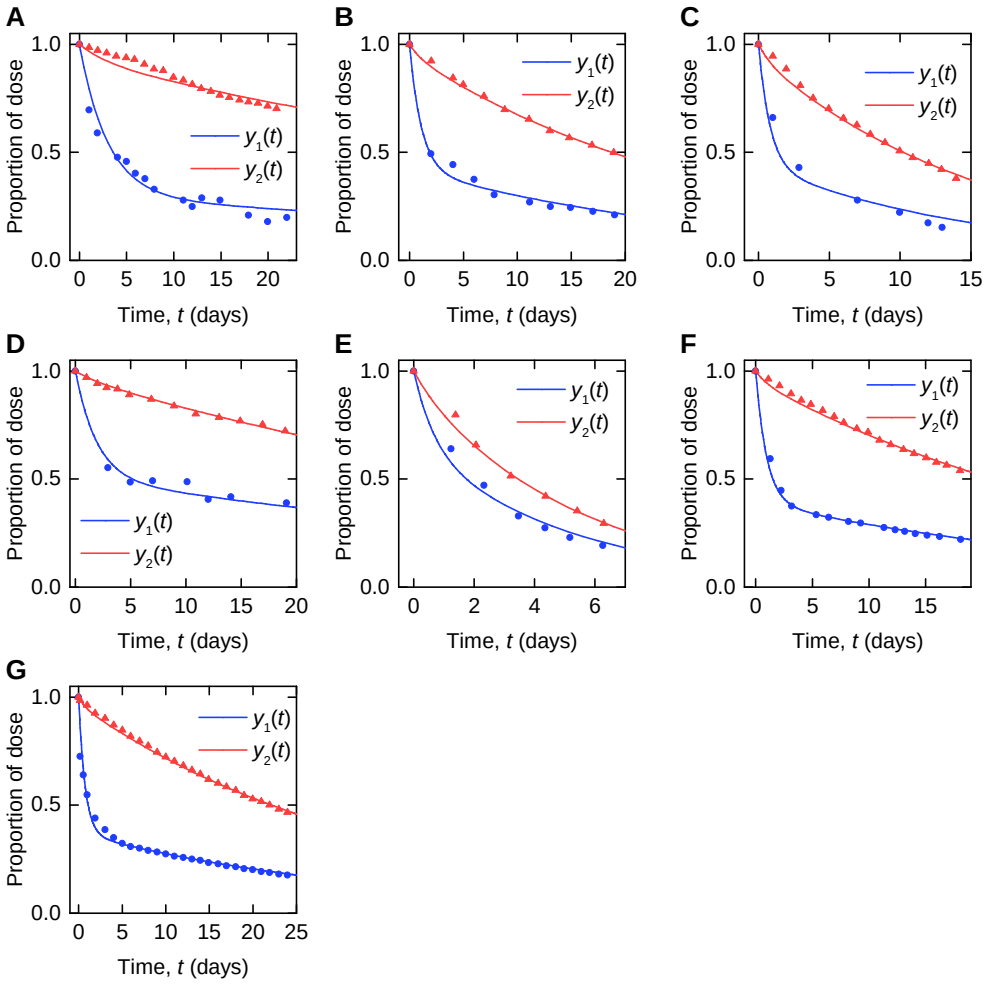

Figure 5-4 Timecourse fits: model described by equations (5-10)–(5-12) fitted to timecourse data for (A–D) subjects A–D (data from [9]), (E–F) subjects E–F (data from [11]), and (G) subject G (data from [1]), by the population approach described in section 5.6

Table 5-4 Individual parameter estimates

Subject	FCR_i (day^{-1})	$k_{12,i}$ (day^{-1})	$k_{21,i}$ (day^{-1})
A	0.03589	0.11643	0.21413
B	0.077272	0.40364	0.46188
C	0.13218	0.62103	0.62127
D	0.030666	0.27822	0.2388
E	0.27073	1.6953	0.66285
F	0.074878	0.43395	0.57506
G	0.077297	0.52945	0.80139

maximisation. These conditional modes represent the estimated individual parameter vectors and are provided in table 5-4. The model outputs are plotted for the estimated individual parameter vectors alongside the data in figure 5-4.

As stated in section 5.3, several subjects have IgG myeloma, macroglobulinemia or familial hypercatabolic hypoproteinemia. Patients with familial hypercatabolic hypoproteinemia do not express FcRn, explaining the large value of the FCR (0.27 day^{-1}) for subject E. The parameter $V_{\max}$ (not estimated here) for subject E should be equal to zero, reflecting the absence of recycling receptors. Subjects A and C have IgG myeloma and subject D has macroglobulinemia. The high or low values of the FCR in these patients may be explained by the concentration-dependent catabolism of IgG, as described by equation (5-13), with abnormally high or low plasma IgG concentrations likely occurring as symptoms of the respective disease.

5.6.5 Synthetic data simulation

In this section it is assumed that the parameter estimates for $\boldsymbol{\psi}_{\text{pop}}$ and $\boldsymbol{\Omega}$ in table 5-3 are the true population parameters for seven hypothetical subjects. Data were simulated with these population parameters in order to test how well the true parameter values can be recovered in Monolix, taking into account the errors in the data and the small sample of subjects available. Population parameters are estimated from the synthetic data in section 5.6.6.

Seven individual parameter vectors $\boldsymbol{\psi}_i, i = 1, \ldots, 7$, were drawn from the parameterised lognormal distribution. The experimental data for each individual parameter vector $\boldsymbol{\psi}_i$ were simulated 10 times, yielding 10 unique datasets for the same sample of seven individuals. Since the sample size of $n = 7$ may be small for estimating the population parameters, the process was repeated for five different samples of seven individual parameter vectors $\boldsymbol{\psi}_i, i = 1, \ldots, 7$. The individual parameter vectors are tabulated in table 5-5. In total $5 \times 10 = 50$ datasets to be fitted by a population approach were simulated, each of seven subjects.

Data were simulated according to the equations and assumptions given in section 5.5. Data for $\tilde{y}_1(t_{ij}^{(1)}, \boldsymbol{\psi}_i)$ were generated by first simulating the plasma radioactivity concen-

Table 5-5 True individual parameter values for the seven subjects in each of five samples, for whom data were simulated

		Subject number, i						
		1	2	3	4	5	6	7
Sample 1	FCR_i	0.110984975	0.179022118	0.416445474	0.140046278	0.042490161	0.297597056	0.091545732
	$k_{12,i}$	0.577924426	0.680583598	3.632129902	0.561378088	0.207230189	0.90208813	0.619241405
	$k_{21,i}$	0.53221047	0.332086484	0.92700592	0.302140328	0.261303137	0.783250661	0.561366815
Sample 2	FCR_i	0.038102176	0.041663693	0.084583507	0.126985597	0.073098181	0.028028037	0.0340121
	$k_{12,i}$	0.09330052	0.264287512	0.182981488	0.864572255	0.475266716	0.123687218	0.232631827
	$k_{21,i}$	0.139111835	0.366803897	0.278437758	0.729767545	0.8231428	0.379733231	0.621086268
Sample 3	FCR_i	0.075505969	0.225431461	0.07190829	0.083094083	0.038178905	0.049781932	0.056795114
	$k_{12,i}$	1.32718538	1.910523519	0.285251404	0.947762901	0.192667415	0.220377271	0.169079559
	$k_{21,i}$	1.266685187	1.053054063	0.195643213	0.748559935	0.133500771	0.410446241	0.238353978
Sample 4	FCR_i	0.065701025	0.102613006	0.029847141	0.073268156	0.151423804	0.027887747	0.101710455
	$k_{12,i}$	0.314681321	0.487770168	0.194480467	0.610676399	0.562160173	0.285784722	0.66122055
	$k_{21,i}$	0.386736952	0.432089394	0.17667979	0.583309366	0.388046681	0.345315908	0.746369857
Sample 5	FCR_i	0.083260871	0.066260186	0.058434785	0.037116266	0.089870319	0.014216423	0.041865056
	$k_{12,i}$	0.474629657	0.444656782	0.267908687	0.107578224	0.331561656	0.052473962	0.194705474
	$k_{21,i}$	0.945166455	0.364942643	0.415110773	0.093591273	0.292122172	0.174690329	0.368286271

Table 5-6 Experiment parameters used for simulating tracer experiment data

Parameter	Units	Value	Reference
D	µmol	0.005	Solomon et al. [9]
V_{plasma}	l	3	Solomon et al. [9]
α	µCi µmol^{-1}	45	Solomon et al. [9]

tration $\tilde{C}_{\text{plasma}}(t_{ij}^{(1)}, \boldsymbol{\psi}_i)$ with constant CV, denoted by $\text{CV}_{\text{plasma}}$, from which $\tilde{y}_1(t_{ij}^{(1)}, \boldsymbol{\psi}_i)$ was calculated. Data for $\tilde{y}_2(t_{ij}^{(2)}, \boldsymbol{\psi}_i)$ were generated by simulating the radioactivity in urine collections, $\tilde{A}_{\text{UC}}(t_k^{(2)}), k = 2, \ldots, N_2$, with constant CV, denoted by CV_{UC}, and the radioactivity in the administered tracer dose, $\tilde{A}_{\text{dose}}$, with constant CV, denoted by CV_{D}. The data were simulated in Mathematica [21] using the script provided in appendix C.

In order to simulate the data it is necessary to assign values to the tracer dose D (µmol), plasma volume V_{plasma} (l), and proportionality constant α (µCi µmol^{-1}). The values used, for all simulations, are provided in table 5-6. Three coefficients of variation must be specified, which determine the magnitudes of the errors. These are $\text{CV}_{\text{plasma}}$, CV_{UC} and CV_{D}. Cobelli et al. [15, p. 233–235] provide a value of 0.02 for the CV of plasma radioactivity concentrations. The variability in the activity in the dose is assumed to be similar to that of the activity in plasma; thus it is assumed that $\text{CV}_{\text{D}} = \text{CV}_{\text{plasma}}$. The summation of radioactivity measurements in urine collections in the calculation of $\tilde{y}_2(t_{ij}^{(2)}, \boldsymbol{\psi}_i)$ results in autocorrelated errors and thus very smooth trajectories of the measured values of $\tilde{y}_2(t_{ij}^{(2)}, \boldsymbol{\psi}_i)$. Therefore larger values of CV_{UC} are required in order to achieve similar variability to that seen in the real data. By a process of trial and error, values of $\text{CV}_{\text{D}} = \text{CV}_{\text{plasma}} = 0.07$ and $\text{CV}_{\text{UC}} = 0.3$ were chosen.

It is assumed that measurements of both model outputs were taken daily. It is also assumed that subjects showing faster metabolism would be observed over a shorter time period. The following simple linear relationship between the individual values of FCR_i and the final observation time was used:

$$f = -70 \times \text{FCR}_i + 24. \tag{5-74}$$

The relationship was obtained by fitting a straight line to the final observation times for the real subjects and their estimated values of FCR, obtained by an individual approach. The obtained value of f was rounded to the next whole number and, if smaller than 7,

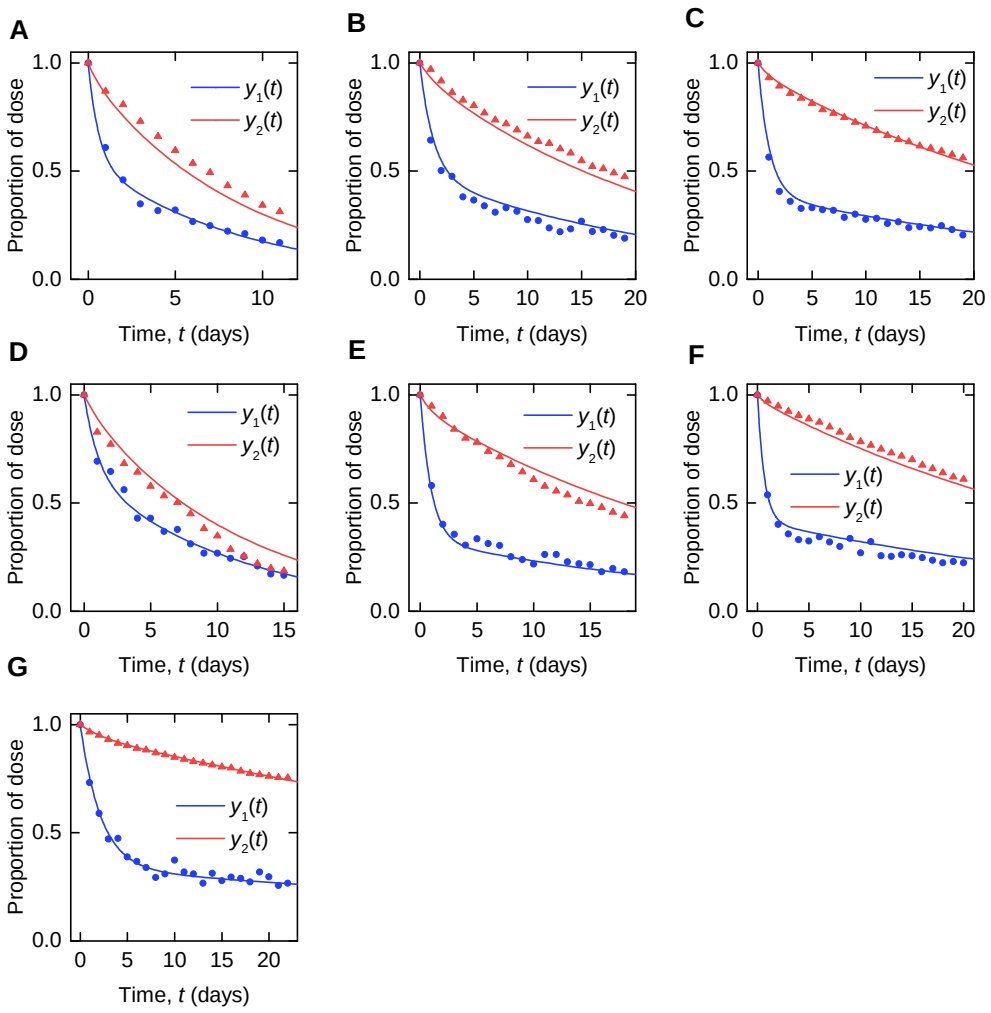

Figure 5-5 Example of synthetic data for seven individuals. Simulation process described in section 5.6.5.

replaced by 7, giving the value of $T_{\max,i}$ (days) that was used for the i^{th} subject:

$$T_{\max,i} = \max\left(\lceil f(\text{FCR}_i)\rceil, 7\right). \tag{5-75}$$

An example of one simulated dataset for one sample of seven individuals is shown in figure 5-5. The true trajectories are also shown in the plots.

5.6.6 Parameter estimation using synthetic data

In this section the population parameters are estimated from the synthetic data simulated in section 5.6.5. The aim of this exercise is to find out how well the population parameters are estimated in Monolix, by looking at properties of the parameter estimates, such as

the mean, standard deviation and bias. We also wish to ascertain the importance of the error model that is assumed for $y_2(t)$ when estimating the population parameters; therefore the estimation is performed, firstly, assuming a proportional error model for both $y_1(t_{ij}^{(1)}, \boldsymbol{\psi}_i)$ and $y_2(t_{ij}^{(2)}, \boldsymbol{\psi}_i)$ (Method 1) and, secondly, assuming a proportional error model for $y_1(t_{ij}^{(1)}, \boldsymbol{\psi}_i)$ and a constant error model for $y_2(t_{ij}^{(2)}, \boldsymbol{\psi}_i)$ (Method 2). Aside from the choice of error model, each of the 50 datasets were estimated by the same approach as in section 5.6.4. When the constant error model is assumed, an initial value of 0.0251 for the error model parameter a_2 is used. This is the default value provided by Monolix for the first dataset analysed.

Four properties of the parameter estimates of the k^{th} parameter are calculated: sample mean (μ_k), sample standard deviation ($S.D._k$), bias (b_k) and variability (v_k). The bias is given by

$$b_k = \mu_k - p_k^0, \tag{5-76}$$

where μ_k is the mean of the estimates and $p_k^{(0)}$ is the true value of the parameter. The variability of the k^{th} parameter is given by

$$v_k = \frac{\sqrt{\text{S.D.}_k^2 + b_k^2}}{p_k^{(0)}}. \tag{5-77}$$

Variability as defined here has been used by Chen et al. [14] to evaluate the performance of estimation methods when the assumptions relied upon by the methods, in particular relating to noise, are violated. A larger value of v_k represents a worse performance of an estimation method. Chen et al. [14] also define the overall variability of a method V as

$$V = \frac{\sum_{k=1}^{N_p} v_k}{N_p}, \tag{5-78}$$

where N_p is the total number of parameters estimated. The properties of the parameter estimates are calculated for each sample of seven subjects. Since the sample size $n = 7$ is small, the parameter estimates might vary significantly depending on which sample is used.

Method 1: proportional error models assumed for both $y_1(t)$ and $y_2(t)$

The sample mean, sample standard deviation, bias and variability of the parameter estimates are tabulated in table 5-7. The population parameter estimates as a proportion

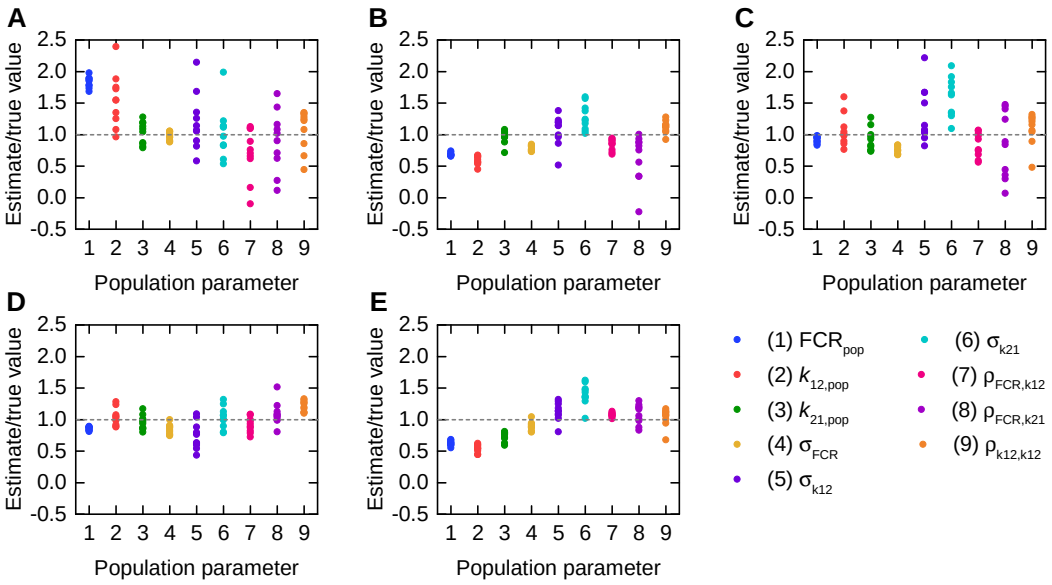

Figure 5-6 Plots illustrating the distributions of population parameter estimates relative to their true values for (A–E) samples 1 to 5 of seven individual parameters $\boldsymbol{\psi}_i$, when estimated by Method 1. Details in section 5.6.6.

Table 5-7 Mean, standard deviation (S.D.), bias and variability of the parameter estimates for five samples of seven individual parameter vectors. Data were simulated 10 times for each sample and population parameters estimated from each of the 10 datasets. A proportional error model was assumed for both $y_1(t)$ and $y_2(t)$ (Method 1).

		Population parameter								
		FCR_{pop}	$k_{12,pop}$	$k_{21,pop}$	σ_{FCR}	$\sigma_{k_{12}}$	$\sigma_{k_{21}}$	$\rho_{FCR k_{12}}$	$\rho_{FCR k_{21}}$	$\rho_{k_{12} k_{21}}$
Sample 1	Mean	0.1411	0.6531	0.4517	0.6661	0.8556	0.5157	0.61202	0.54441	0.7974
	S.D.	0.0075638	0.177309	0.0784518	0.044725	0.320203	0.202313	0.353596	0.292445	0.23481
	Bias	0.0633	0.2311	0.0107	-0.0189	0.1426	0.0177	-0.25998	-0.06359	0.0584
	Variability	0.819413	0.690244	0.179542	0.0708824	0.491614	0.407802	0.503308	0.492234	0.32742
Sample 2	Mean	0.05334	0.2487	0.4262	0.5375	0.7554	0.6355	0.7339	0.3808	0.8286
	S.D.	0.0019665	0.0292842	0.0464107	0.0285939	0.172537	0.102896	0.0775148	0.232178	0.0720111
	Bias	-0.02446	-0.1733	-0.0148	-0.1475	0.0424	0.1375	-0.1381	-0.2272	0.0896
	Variability	0.31541	0.416485	0.110461	0.219337	0.249188	0.344855	0.181614	0.534291	0.15555
Sample 3	Mean	0.07125	0.4487	0.4048	0.5097	0.9353	0.7943	0.7302	0.5149	0.8093
	S.D.	0.00397639	0.104905	0.0805437	0.041414	0.311434	0.157657	0.169444	0.322123	0.186995
	Bias	-0.00655	0.0267	-0.0362	-0.1753	0.2223	0.2963	-0.1418	-0.0931	0.0703
	Variability	0.0984899	0.256516	0.200238	0.262957	0.536653	0.673962	0.253382	0.551491	0.270329
Sample 4	Mean	0.0667	0.4367	0.4202	0.5779	0.5268	0.513	0.7973	0.6625	0.8973
	S.D.	0.00217715	0.057219	0.0506443	0.0538526	0.153113	0.0863147	0.104402	0.112183	0.0626206
	Bias	-0.0111	0.0147	-0.0208	-0.1071	-0.1862	0.015	-0.0747	0.0545	0.1583
	Variability	0.145392	0.139993	0.124148	0.175003	0.338105	0.17592	0.147218	0.205132	0.23036
Sample 5	Mean	0.04845	0.2273	0.3238	0.6096	0.8034	0.6963	0.9397	0.6587	0.7668
	S.D.	0.0031135	0.0256993	0.0328458	0.0502531	0.106104	0.0851914	0.0299149	0.0954033	0.105973
	Bias	-0.02935	-0.1947	-0.1172	-0.0754	0.0904	0.1983	0.0677	0.0507	0.0278
	Variability	0.379366	0.465376	0.275999	0.13228	0.195501	0.433384	0.0848794	0.177695	0.148252

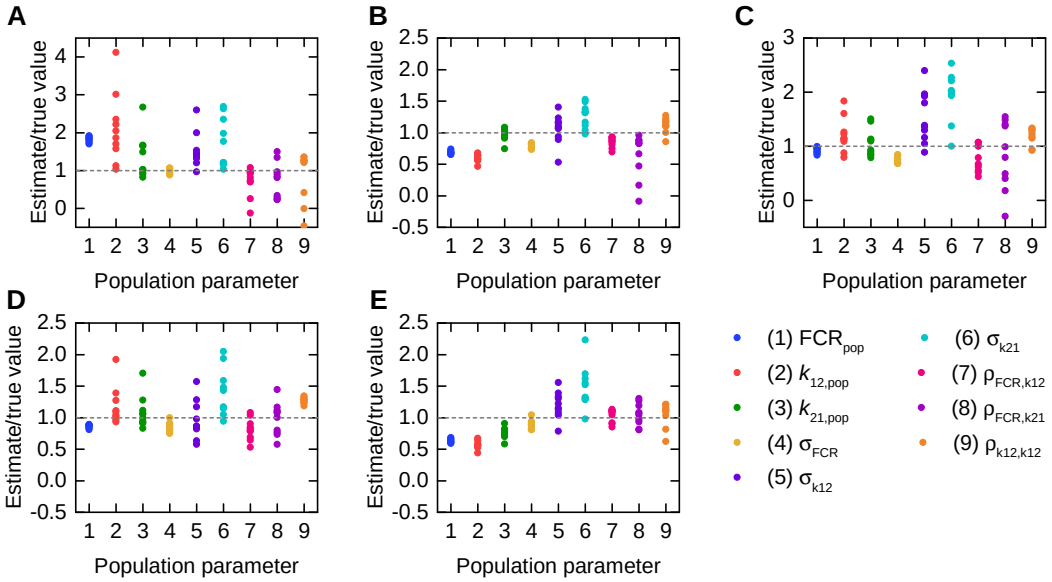

Figure 5-7 Plots illustrating the distributions of population parameter estimates relative to their true values for (A–E) samples 1 to 5 of seven individual parameters $\boldsymbol{\psi}_i$, when estimated by Method 2. Details in section 5.6.6.

such as systematic errors and other issues discussed in section 5.6.3.

Method 2: proportional error model assumed for $y_1(t)$ and constant error model for $y_2(t)$

The sample mean, sample standard deviation, bias and variability of the parameter estimates are tabulated in table 5-9. The population parameter estimates as a proportion of the true population parameter values are plotted in figure 5-7. Comparing tables 5-7 and 5-9 and figures 5-6 and 5-7, overall the results of the parameter estimation are similar whether a proportional or constant error model is assumed for model output $\tilde{y}_2(t_{ij}^{(2)}, \boldsymbol{\psi}_i)$.

Table 5-8 Overall variability of Method 1 and Method 2 for samples 1–5

	Sample				
	1	2	3	4	5
Method 1	0.442	0.288	0.345	0.187	0.255
Method 2	0.705	0.272	0.443	0.284	0.283

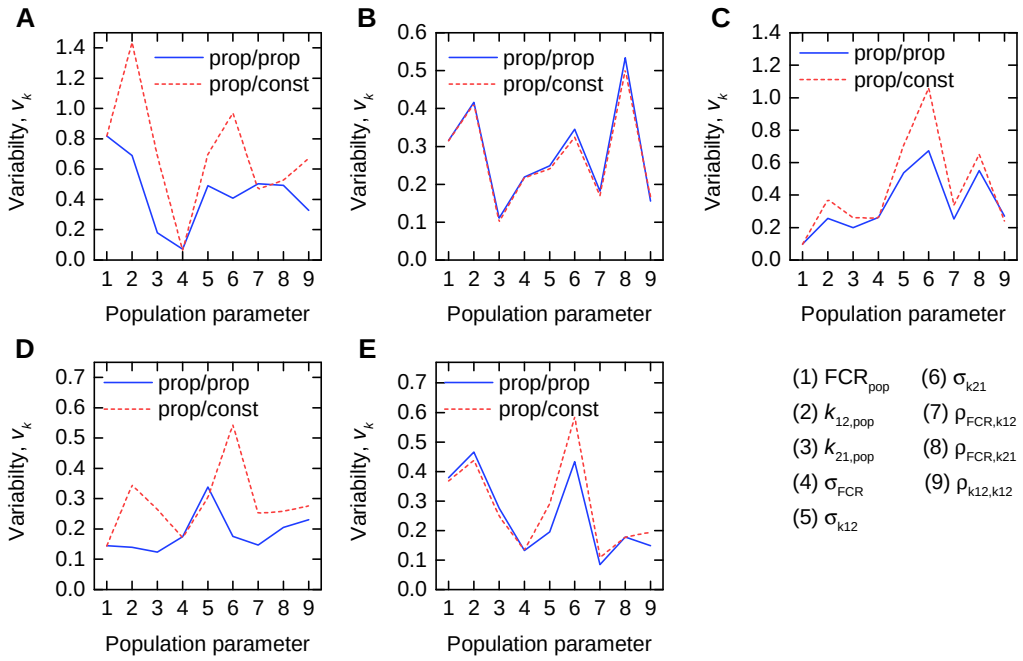

Figure 5-8 Variability of population parameter estimates when estimated by Method 1 (blue solid lines) and Method 2 (red dashed lines), for (A–E) samples 1 to 5 of seven individual parameter vectors

Table 5-9 Mean, standard deviation (S.D.), bias and variability of the parameter estimates for five samples of seven individual parameter vectors. Data were simulated 10 times for each sample and population parameters estimated from each of the 10 datasets. A proportional error model was assumed for $y_1(t)$ and a constant error model for $y_2(t)$ (Method 2).

		Population parameter								
		FCR_{pop}	$k_{12,pop}$	$k_{21,pop}$	σ_{FCR}	$\sigma_{k_{12}}$	$\sigma_{k_{21}}$	$\rho_{FCR k_{12}}$	$\rho_{FCR k_{21}}$	$\rho_{k_{12} k_{21}}$
Sample 1	Mean	0.1413	0.8878	0.6106	0.6761	1.09	0.856	0.6337	0.4521	0.656092
	S.D.	0.00569698	0.387486	0.251132	0.0420673	0.325055	0.325865	0.331798	0.280094	0.488291
	Bias	0.0635	0.4658	0.1696	-0.0089	0.377	0.358	-0.2383	-0.1559	-0.082908
	Variability	0.819474	1.43578	0.687159	0.0627714	0.698155	0.972086	0.46847	0.527233	0.670202
Sample 2	Mean	0.05341	0.25	0.4295	0.5388	0.7538	0.6305	0.7405	0.39066	0.8259
	S.D.	0.00197678	0.0250333	0.04287	0.0275834	0.166625	0.0922078	0.0686444	0.213858	0.0863423
	Bias	-0.02439	-0.172	-0.0115	-0.1462	0.0408	0.1325	-0.1315	-0.21734	0.0869
	Variability	0.314524	0.411877	0.100648	0.217196	0.240599	0.32415	0.170113	0.501502	0.165766
Sample 3	Mean	0.07152	0.5101	0.4668	0.5129	1.0841	0.9746	0.6715	0.5076	0.8765
	S.D.	0.00410983	0.130705	0.111839	0.0426209	0.34115	0.226613	0.215252	0.38352	0.110987
	Bias	-0.00628	0.0881	0.0258	-0.1721	0.3711	0.4766	-0.2005	-0.1004	0.1375
	Variability	0.0964688	0.373518	0.260264	0.258831	0.706987	1.0597	0.337347	0.652046	0.239112
Sample 4	Mean	0.06683	0.4946	0.4768	0.5806	0.686	0.6949	0.7086	0.5943	0.9399
	S.D.	0.00211977	0.126096	0.110904	0.0538789	0.215703	0.186224	0.14712	0.156045	0.0345365
	Bias	-0.01097	0.0726	0.0358	-0.1044	-0.027	0.1969	-0.1634	-0.0137	0.2009
	Variability	0.143611	0.344793	0.264261	0.171508	0.30489	0.544207	0.252147	0.25764	0.275842
Sample 5	Mean	0.04925	0.2391	0.338	0.6084	0.8537	0.737	0.9013	0.6369	0.7757
	S.D.	0.00243139	0.0259463	0.0381372	0.0497576	0.152958	0.166705	0.0905134	0.1047	0.138956
	Bias	-0.02855	-0.1829	-0.103	-0.0766	0.1407	0.239	0.0293	0.0289	0.0367
	Variability	0.368295	0.437752	0.249056	0.133346	0.291484	0.585132	0.109103	0.178644	0.194481

The variability v_k of the estimates of the k^{th} population parameter combines both the bias and the spread of the estimates. The variability v_k is plotted in figure 5-8. Figures 5-8A to 5-8E represent samples 1–5, each of seven individual parameter vectors. Blue solid lines represent the variability of the population parameter estimates when they are estimated by Method 1; red dashed lines represent the variability when the parameters are estimated by Method 2. The variabilities of the parameter estimates for samples B, C and E follow the same trend regardless of the error model assumed for $\tilde{y}_2(t_{ij}^{(2)}, \boldsymbol{\psi}_i)$, with the peak in the red line in figure 5-8C showing a particularly large variability in the estimates for $\sigma_{k_{21}}$, when the constant error model is assumed for $\tilde{y}_2(t_{ij}^{(2)}, \boldsymbol{\psi}_i)$. For samples A and D, the difference between the two methods is more apparent, with Method 2 resulting in substantially greater variability for several population parameters. The overall variability V, defined in equation 5-78, is tabulated for each sample and for both methods in table 5-8. The overall variability is greater for Method 2 for each sample, except for sample B, for which the variabilities are close for both methods.

5.7 Naive pooled approach to parameter identification using fractional catabolic rate and half-life data

The parameters k_{31}, $V_{\max}$ and K_{M} are structurally unidentifiable from an individual subject's timecourse data, assuming the linearised model given by equations (5-10)–(5-12) (see section 5.4.2). It is therefore necessary to make use of the relationships between FCR and $T_{1/2}$, respectively, and the quantity of endogenous IgG in plasma, $x_{1,\text{E}}$. Unfortunately, these relationships are not known for an individual subject; obtaining them would require performing the tracer experiment over a range of different plasma concentrations of endogenous IgG within an individual subject, which is not practically feasible. Parameter values are therefore estimated from the FCR and $T_{1/2}$ measurements taken from a sample of patients with a wide range of endogenous IgG plasma concentrations, as though the data arose from an individual subject, in what may be described as a naive pooled approach [23]. By this approach it is not however possible to gain a sense of the distribution of the parameters k_{31}, $V_{\max}$ and K_{M} within the population.

5.7.1 Structural identifiability analysis

Fractional catabolic rate

The relationship between the FCR and $x_{1,\mathrm{E}}$ is given by equation (5-13). The SolveAlways function was used in Mathematica [21] to determine whether the parameter vector $\boldsymbol{\phi} = (k_{31}, V_{\max}, K_{\mathrm{M}})$ is uniquely identifiable given the relationship in equation (5-13). Introducing an alternative parameter vector $\overline{\boldsymbol{\phi}} = \left(\bar{k}_{31}, \overline{V}_{\max}, \overline{K}_{\mathrm{M}}\right)$ and solving the equation

$$k_{31} - \frac{V_{\max}}{K_{\mathrm{M}} + x_{1,\mathrm{E}}} = \bar{k}_{31} - \frac{\overline{V}_{\max}}{\overline{K}_{\mathrm{M}} + x_{1,\mathrm{E}}}, \tag{5-79}$$

over all values of $x_{1,\mathrm{E}}$, gives $\left(\bar{k}_{31}, \overline{V}_{\max}, \overline{K}_{\mathrm{M}}\right) = (k_{31}, V_{\max}, K_{\mathrm{M}})$ as the only solution for the unknown parameters. $\mathrm{FCR}(x_{1,\mathrm{E}}, \boldsymbol{\phi}) = \mathrm{FCR}(x_{1,\mathrm{E}}, \overline{\boldsymbol{\phi}})$ requires $\boldsymbol{\phi} = \overline{\boldsymbol{\phi}}$; therefore the parameters k_{31}, $V_{\max}$ and K_{M} are structurally globally identifiable given the relationship between FCR and $x_{1,\mathrm{E}}$.

Half-life

The relationship between $T_{1/2}$ and $x_{1,\mathrm{E}}$ is given by equation (5-17). We now wish to know whether the parameter vector $\boldsymbol{\phi} = (k_{12}, k_{21}, k_{31}, V_{\max}, K_{\mathrm{M}})$ is structurally identifiable with respect to the relationship in equation (5-17). From equation (5-15), this is equivalent to asking whether $\boldsymbol{\phi}$ is structurally identifiable with respect to the relationship between λ_2 and $x_{1,\mathrm{E}}$, given by

$$\begin{aligned}\lambda_2 = \frac{1}{2}\Bigg(& -k_{12} - k_{21} - k_{31} + \frac{V_{\max}}{K_{\mathrm{M}} + x_{1,\mathrm{E}}} \\ & + \sqrt{-4k_{12}\left(k_{31} - \frac{V_{\max}}{K_{\mathrm{M}} + x_{1,\mathrm{E}}}\right) + \left(k_{12} + k_{21} + k_{31} - \frac{V_{\max}}{K_{\mathrm{M}} + x_{1,\mathrm{E}}}\right)^2}\Bigg).\end{aligned} \tag{5-80}$$

The structural identifiability problem amounts to determining whether there exists an alternative parameter vector $\overline{\boldsymbol{\phi}}$ such that $\lambda_2(x_{1,\mathrm{E}}, \boldsymbol{\phi}) = \lambda_2(x_{1,\mathrm{E}}, \overline{\boldsymbol{\phi}})$ with $\boldsymbol{\phi} \neq \overline{\boldsymbol{\phi}}$. λ_2 is one of the roots of the characteristic polynomial equation, given by

$$\lambda^2 + \left(k_{12} + k_{21} + k_{31} - \frac{V_{\max}}{K_{\mathrm{M}} + x_{1,\mathrm{E}}}\right)\lambda + k_{12}\left(k_{31} - \frac{V_{\max}}{K_{\mathrm{M}} + x_{1,\mathrm{E}}}\right) = 0. \tag{5-81}$$

We wish to know whether there exists an alternative parameter vector $\overline{\boldsymbol{\phi}} \neq \boldsymbol{\phi}$, such that

$$\begin{aligned}\lambda^2 + \left(k_{12} + k_{21} + k_{31} - \frac{V_{\max}}{K_{\mathrm{M}} + x_{1,\mathrm{E}}}\right)\lambda + k_{12}\left(k_{31} - \frac{V_{\max}}{K_{\mathrm{M}} + x_{1,\mathrm{E}}}\right) \\ = \lambda^2 + \left(\bar{k}_{12} + \bar{k}_{21} + \bar{k}_{31} - \frac{\overline{V}_{\max}}{\overline{K}_{\mathrm{M}} + x_{1,\mathrm{E}}}\right)\lambda + \bar{k}_{12}\left(\bar{k}_{31} - \frac{\overline{V}_{\max}}{\overline{K}_{\mathrm{M}} + x_{1,\mathrm{E}}}\right).\end{aligned} \tag{5-82}$$

From the uniqueness of interpolating polynomials [24, p. 98], the coefficients of the quadratic are unique, therefore

$$\begin{aligned}k_{12} + k_{21} + k_{31} - \frac{V_{\max}}{K_{\mathrm{M}} + x_{1,\mathrm{E}}} &= \bar{k}_{12} + \bar{k}_{21} + \bar{k}_{31} - \frac{\overline{V}_{\max}}{\overline{K}_{\mathrm{M}} + x_{1,\mathrm{E}}} \\ k_{12}\left(k_{31} - \frac{V_{\max}}{K_{\mathrm{M}} + x_{1,\mathrm{E}}}\right) &= \bar{k}_{12}\left(\bar{k}_{31} - \frac{\overline{V}_{\max}}{\overline{K}_{\mathrm{M}} + x_{1,\mathrm{E}}}\right).\end{aligned} \tag{5-83}$$

The only solution to equations (5-83), over all values of $x_{1,\mathrm{E}}$ and for generic positive parameter values, is $\boldsymbol{\phi} = \overline{\boldsymbol{\phi}}$. Therefore the parameters $k_{12}, k_{21}, k_{31}, V_{\max}$ and K_{M} are structurally globally identifiable given the relationship between $T_{1/2}$ and $x_{1,\mathrm{E}}$.

5.7.2 Parameter estimation

The parameters k_{12}, k_{21}, k_{31}, $V_{\max}$ and K_{M} were estimated from FCR vs. $x_{1,\mathrm{E}}$ and $T_{1/2}$ vs. $x_{1,\mathrm{E}}$ data, simultaneously. Waldmann et al. [1] provide plots of FCR and $T_{1/2}$ vs. plasma endogenous IgG concentration in $\mathrm{g\,l^{-1}}$. The data were extracted using the Digitizer tool in OriginPro [10]. The plasma IgG concentration in $\mathrm{g\,l^{-1}}$ was converted to $\mu\mathrm{mol\,l^{-1}}$ by dividing by the molar mass of IgG, 0.15 $\mathrm{g\,\mu mol^{-1}}$. The concentration was then multiplied by an average plasma volume of 3 l [9] to obtain the quantity $x_{1,\mathrm{E}}$ in µmol.

The FCR and $T_{1/2}$ data were fitted simultaneously by the model outputs described in equations (5-13) and (5-17). The parameter values were estimated by minimising the sum of squared residual errors between the model outputs and the measured values, using the function NonlinearModelFit in Mathematica [21]. Due to the different scales for the parameters ($0.02 < \mathrm{FCR} < 0.17$ $\mathrm{day^{-1}}$; $10 < T_{1/2} < 72$ days) the $T_{1/2}$ data points were assigned different weights to the FCR data points. It is assumed that the residual errors on the FCR measurements have a constant standard deviation, σ_{F}, and that the residual errors on the $T_{1/2}$ measurements have a constant standard deviation, $\sigma_{T_{1/2}}$. It is assumed that the ratio of the two standard deviations is equal to the ratio of the means

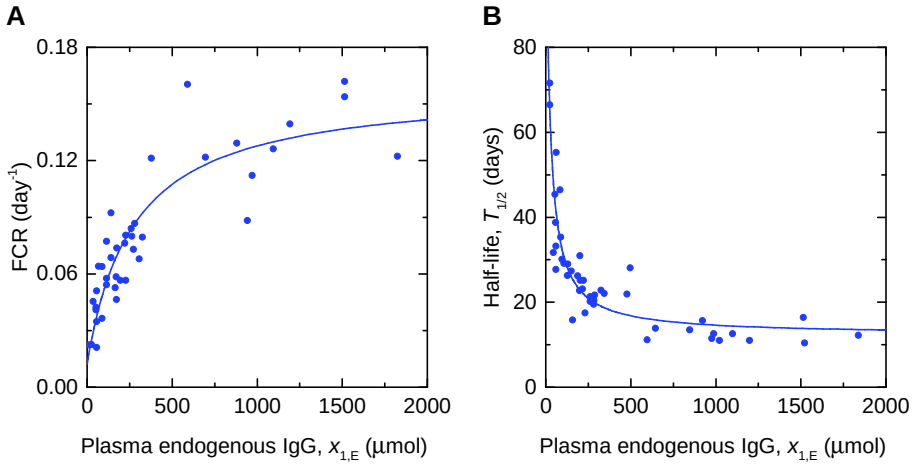

Figure 5-9 Expressions for (A) FCR (equation (5-13)) and (B) $T_{1/2}$ (equation (5-17)) fitted to data from [1]

Table 5-10 Parameter estimates and standard errors estimated from FCR and $T_{1/2}$ data

Parameter	Units	Estimate	Standard error (SE)	95% confidence interval
k_{31}	day^{-1}	0.159	0.0111	$(0.137, 0.181)$
$V_{\max}$	$\mu\text{mol}\,\text{day}^{-1}$	40.0	10.5	$(19.1, 60.9)$
K_{M}	µmol	272	55.4	$(162, 382)$
k_{12}	day^{-1}	0.158	0.155	$(-0.150, 0.467)$
k_{21}	day^{-1}	0.187	0.231	$(-0.273, 0.647)$

of the measured values, as follows:

$$\frac{\sigma_{T_{1/2}}}{\sigma_{\text{F}}} = \frac{\overline{T_{1/2}}}{\overline{\text{FCR}}}, \tag{5-84}$$

where $\overline{\text{FCR}}$ and $\overline{T_{1/2}}$ are the sample means of the measured values of FCR and $T_{1/2}$, respectively. The relative weighting of each data point is assumed to be inversely proportional to its error variance, therefore

$$\frac{w_{\text{F}}}{w_{T_{1/2}}} = \frac{\sigma^2_{T_{1/2}}}{\sigma^2_{\text{F}}} = \frac{\overline{T_{1/2}}^2}{\overline{\text{FCR}}^2} = 1.08 \times 10^5, \tag{5-85}$$

where w_{F} and $w_{T_{1/2}}$ are the weights assigned to the FCR data points and the $T_{1/2}$ data points, respectively. The weights given to the FCR data points were set to 1.08×10^5 and the weights given to the $T_{1/2}$ data points were set to 1.

The data and model fits are shown in figure 5-9. The parameter estimates and their standard errors are given in table 5-10. The standard errors are almost as large as, or

Table 5-11 Comparison with published parameter values

Parameter	Units	Previously published values			This thesis
		Waldmann et al. [1]	Kim et al. [2]	Hattersley et al. [6]	
k_{12}	day^{-1}	–	0.158	0.41	0.422
k_{21}	day^{-1}	–	0.156	0.51	0.441
k_{31}	day^{-1}	0.18	0.18†	0.13	0.159
$V_{\max}$	$\mu\text{mol}\,\text{day}^{-1}$	68.6*	68.6*†	103	40.0
K_{M}	µmol	–	420**	530	272

*Assuming 70 kg human. **Assuming 3 l plasma volume. †Taken from Waldmann et al. [1].

larger than, the estimates themselves for the parameters k_{12} and k_{21}, indicating that these parameters cannot be estimated with a reasonable level of precision.

The correlation matrix of the parameter estimates is given by

$$\begin{array}{c} \\ k_{31} \\ V_{\max} \\ K_{\text{M}} \\ k_{12} \\ k_{21} \end{array} \begin{array}{c} \begin{array}{ccccc} k_{31} & V_{\max} & K_{\text{M}} & k_{12} & k_{21} \end{array} \\ \begin{pmatrix} 1 & 0.928 & 0.839 & -0.290 & -0.300 \\ 0.928 & 1 & 0.976 & -0.228 & -0.253 \\ 0.839 & 0.976 & 1 & -0.0890 & -0.115 \\ -0.290 & -0.228 & -0.0890 & 1 & 0.996 \\ -0.300 & -0.253 & -0.115 & 0.996 & 1 \end{pmatrix} \end{array}.$$

The parameters k_{31}, $V_{\max}$ and K_{M} are highly correlated pairwise, with the strongest correlation between K_{M} and $V_{\max}$. k_{12} and k_{21} are highly correlated with one another (correlation coefficient of 0.996) and not with the other parameters, explaining why they cannot be estimated with a reasonable level of precision from these data.

5.8 Comparison with previously published parameter values

Table 5-11 compares previously published parameter values alongside the parameter values estimated in this chapter. For the parameters k_{12} and k_{21} the estimated population parameters $k_{12,\text{pop}}$ and $k_{21,\text{pop}}$ are provided; for the parameters k_{31}, $V_{\max}$ and K_{M} the values estimated from FCR and $T_{1/2}$ vs. $x_{1,\text{E}}$ data from many subjects are taken to rep-

resent the population average. At first glance the newly estimated parameter values are reasonably similar to the previously published values.

Waldmann et al. [1] give values of $k_{31} = 0.18\ \text{day}^{-1}$ and $V_{\max}/w = 147\ \text{mg}\,\text{day}^{-1}\,\text{kg}^{-1}$, where w is body weight in kg. Assuming a 70 kg human, this is equivalent to $V_{\max} = 68.6$ µmol day^{-1}. The value of k_{31} was obtained 'from the asymptotic value of the plot of the IgG fractional catabolic rate versus its concentration' [1]. These are the same data that were utilised in this paper as described in section 5.3. The authors subtracted the value of the FCR for each individual from 0.18 to find the fractional recycling rate. The fractional recycling rate is thus given by

$$\text{FRR} = k_{31} - \text{FCR} = k_{31} - \left(k_{31} - \frac{V_{\max}}{K_{\text{M}} + x_{1,\text{E}}}\right) = \frac{V_{\max}}{K_{\text{M}} + x_{1,\text{E}}}. \tag{5-86}$$

They then multiplied the plasma concentration of endogenous IgG by the plasma volume per kg of body weight for each individual to get the quantity of endogenous IgG in plasma per kg of body weight, $x_{1,\text{E}}/w$. Finally the authors multiplied the fractional recycling rate by $x_{1,\text{E}}/w$ to obtain the absolute recycling rate per kg of body weight, which is denoted here by ARR. They then plotted the reciprocal of the ARR against the reciprocal of $x_{1,\text{E}}/w$ to obtain a straight line relationship, given by

$$\frac{1}{\text{ARR}} = \frac{K_{\text{M}}}{V_{\max}}\frac{w}{x_{1,\text{E}}} + \frac{w}{V_{\max}}. \tag{5-87}$$

From the intercept the authors obtained the value of $V_{\max}/w = 147\ \text{mg}\,\text{kg}^{-1}\,\text{day}^{-1}$.

Kim et al. [2] provide values for all model parameters. Again using the FCR vs. endogenous IgG concentration data first published by Waldmann et al. [1] and described here in section 5.3, Kim et al. [2] estimate K_{M}/w using a least-squares fitting. The equation fitted to the data is

$$\text{FCR} = k_{31} - \frac{V_{\max}/w}{\frac{v_1}{w}\left(\frac{K_{\text{M}}}{v_1} + \frac{x_{1,\text{E}}}{v_1}\right)}, \tag{5-88}$$

where v_1 is the plasma volume. The authors fit equation (5-88) to FCR vs. $x_{1,\text{E}}/v_1$ to obtain K_{M}/v_1 whilst fixing the remaining parameters as follows: $k_{31} = 0.18\ \text{day}^{-1}$ [1], $V_{\max}/w = 0.98$ µmol kg^{-1} [1], and $v_1/w = 0.042$ l kg^{-1} [11]. By this approach the authors obtain a value of $K_{\text{M}}/v_1 = 140$ µmol l^{-1}. Assuming a plasma volume of 3 l this equates to $K_{\text{M}} = 420$ µmol. The authors also estimate the parameters k_{12} and k_{21} by curve fitting to tracer experiment data from Waldmann et al. [11].

The parameter values provided by Hattersley et al. [6] were obtained by methods described in Hattersley [3], which involved estimating the parameters k_{12} and k_{21} by fitting the model to tracer experiment data in [1]. For the remaining model parameters, k_{31}, $V_{\max}$ and K_{M}, the author takes a completely different approach, fitting the model directly to serum IgG data from an IgG myeloma patient, assuming a delayed logistic function to describe the production of tumour-produced IgG. For this approach, the parameters k_{12}, k_{21} and v_1 were fixed.

The values provided by Hattersley et al. [6] and Kim et al. [2] for k_{12} and k_{21} are similar to the individual parameter values estimated in this chapter, given in table 5-4. The value for parameter k_{31} estimated here is between previously estimated values. The estimated values for parameters $V_{\max}$ and K_{M} are both significantly smaller than previously published values, although the value of $V_{\max} = 68.6\ \mu\mathrm{mol\,day}^{-1}$ assumes a body weight of 70 kg, which may be too high for multiple myeloma patients.

5.9 Conclusions

The aim of this chapter was to analyse a previously published model of endogenous IgG metabolism and available measurements in humans with respect to parameter identification. The model was linearised to replicate experimental conditions in which small doses of administered IgG exhibit linear timecourse responses and a new expression for the half-life of the tracer was derived. The linearised model was then analysed in terms of parameter structural identifiability, both for individual parameters and population parameters. Certain important parameters are not structurally identifiable from an individual's timecourse response, namely, k_{31}, $V_{\max}$, and K_{M}; however they are structurally identifiable using the relationships between the FCR and $T_{1/2}$, respectively, and the quantity of endogenous IgG in plasma, which is assumed to remain in steady state.

It is not known whether the parameters k_{31}, $V_{\max}$ and K_{M} are structurally identifiable in the nonlinear model of coupled radiolabelled and endogenous IgG responses given by equations (6-7)–(5-7). There are two reasons this approach was not pursued here: firstly, structural identifiability analysis of a four-state nonlinear model with rational terms presents a more challenging problem; secondly, if the nonlinear model were found to

be structurally identifiable, then the responses available nonetheless do not demonstrate nonlinear behaviour due to the small doses of radiolabelled IgG administered (see figure 5-3) – therefore the parameters representing nonlinear behaviour may not be practically identifiable by fitting the nonlinear model and there would be an increased risk of fitting the noise in the data with the increased model complexity.

The parameters estimated using Monolix were validated by estimating the same parameters from synthetic data. The sources of experimental errors were considered in order to simulate the data. This simulation study showed how the population parameter estimates may be biased, dependent largely on the sample of individual parameter values. This result suggests that whilst the population parameter estimates may represent the studied sample, future experiments would benefit from a larger sample of individuals in order to more accurately estimate the population parameters. A future analysis may involve estimating parameters directly from the simulated data for the radioactivity in plasma, urine collections and the tracer dose, to explore the impact of misspecification of the error model in estimating the parameters. If future experiments were permitted, the distributions of errors on these observations could be validated by taking replicate measurements. By performing a simulation study it would be possible to make recommendations for future experiments, by determining whether the correct specification of the error model or an increase in the sample size would produce more accurate parameters; the benefit of these measures could then be weighed up against their respective costs. Using a naive pooled approach to parameter estimation, the parameter k_{31} was estimated with higher precision than $V_{\max}$ and K_{M}, possibly due to the very high correlation between $V_{\max}$ and K_{M}. A recommendation for future work is to estimate these parameters from synthetic data for FCR and $T_{1/2}$ to assess the stability of their parameter estimates.

In this chapter population parameters have been estimated, which will be used in chapter 8 for predicting cancer marker responses in patients with IgG multiple myeloma. In section 5.8, the parameter values obtained in this chapter are compared with previously published values and the parameter estimation methods used by previous authors are briefly described. Parameter values obtained from individual subjects' data can be quite different, for example the values for k_{21} and k_{12} obtained by Hattersley et al. [6] and Kim et al. [2], respectively. The population approach taken in this chapter has provided estimates

of the average parameter values in the population, which can be used to predict average responses. The simulation study performed in this chapter also provides an indication of the level of variability within population parameter estimates for the FCR, k_{21} and k_{12}.

References

1. T. A. Waldmann, W. Strober, *Progress in Allergy* **13**, 1–110 (1969).
2. J. Kim, W. L. Hayton, J. M. Robinson, C. L. Anderson, *Clinical Immunology* **122**, 146–155 (2007).
3. J. G. Hattersley, PhD thesis, University of Warwick, 2009.
4. P. W. Sullivan, S. E. Salmon, *The Journal of Clinical Investigation* **51**, 1697–1708 (1972).
5. A. Bradwell, *Hematology Reports* **2**, 16–18 (2010).
6. J. G. Hattersley et al., *Computer Methods and Programs in Biomedicine* **109**, 126–133 (2013).
7. F. Kendrick et al., *Frontiers in Physiology* **8** (2017).
8. E. J. Routh, *A Treatise on the Stability of a Given State of Motion: Particularly Steady Motion* (Macmillan, London, ed. 1, 1877).
9. A. Solomon, T. Waldmann, J. Fahey, *The Journal of Laboratory and Clinical Medicine* **62**, 1–17 (1963).
10. OriginLab Corporation, *OriginPro 2016*, Northampton, 2016.
11. T. A. Waldmann, W. D. Terry, *The Journal of Clinical Investigation* **86**, 2093–2098 (1990).
12. J. E. Riviere, *Comparative Pharmacokinetics: Principles, Techniques, and Applications* (John Wiley & Sons, Hoboken, ed. 2, 2011), ISBN: 9780813829937.
13. D. H. Anderson, *Compartmental Modeling and Tracer Kinetics* (Springer-Verlag, Berlin Heidelberg, ed. 1, 1983), ISBN: 9783540123033.
14. K. W. Chen, S. C. Huang, D. C. Yu, *Physics in Medicine and Biology* **36**, 1183–1200 (1991).
15. C. Cobelli, D. Foster, G. Toffolo, *Tracer Kinetics in Biomedical Research* (Springer, New York, ed. 1, 2002), ISBN: 0306468336.
16. H. Ku, *Journal of Research of the National Bureau of Standards, Section C: Engineering and Instrumentation* **70C**, 263–273 (1966).
17. Lixoft SAS, *Monolix version 2016R1*, Antony, 2016.
18. D. Janzén, M. Jirstrand, N. D. Evans, M. Chappell, *IFAC-PapersOnLine* **48**, 563–568 (2015).

19. D. L. Janzén, M. Jirstrand, M. J. Chappell, N. D. Evans, *Computer Methods and Programs in Biomedicine*, 329–339 (2016).
20. R. Bellman, K. Åström, *Mathematical Biosciences* **7**, 329–339 (1970).
21. Wolfram Research Inc., *Mathematica Version 11.1*, Champaign, IL, 2017.
22. P. L. Bonate, *Pharmacokinetic-Pharmacodynamic Modeling and Simulation* (Springer, New York, ed. 2, 2011), ISBN: 9781441994851.
23. P. Wright, *British Journal of Anaesthesia* **80**, 488–501 (1998).
24. P. C. Biswal, *Numerical Analysis* (PHI Learning, New Delhi, ed. 1, 2008), ISBN: 9788120334441.

6

Parameter identification for a four-compartment model of immunoglobulin G metabolism

In this chapter a four-compartment model of immunoglobulin G (IgG) metabolism is analysed with respect to parameter identification using data from radioactive tracer experiments. The previously published model [1; 2] is semi-mechanistic, with binding of neonatal Fc receptor (FcRn) and IgG in endosomes represented by nonlinear receptor-ligand binding kinetics. The model has been previously presented by Kim et al. [1] and Hattersley [2]. The principles of this model have been extended to physiologically based pharmacokinetic models of IgG-based monoclonal antibodies by a number of authors [3–6]. The four-compartment model represents a compromise between complex, physiologically based models and the two-compartment model [1; 2; 7] analysed in chapter 5.

The purpose of modelling IgG metabolism in this thesis is to be able to predict responses of plasma IgG in multiple myeloma patients; mechanistic models are desirable when the purpose is prediction beyond readily available datasets. Mechanistic models can also be used to explain why certain behaviours arise in terms of underlying biological processes. With accurate parameter values, it may be possible to draw meaningful interpretations regarding FcRn-mediated recycling based upon binding kinetics. In addition, using a

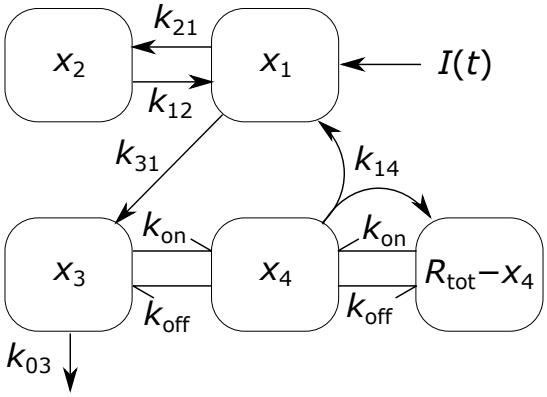

Figure 6-1 Schematic of the four-compartment model of IgG metabolism. Arrows represent material flow between compartments and hooked arrows represent nonlinear receptor-ligand binding.

simpler, descriptive or phenomenological model to describe data can result in biased parameter estimates [8].

The aim of this chapter is to determine whether parameter values can be estimated using the limited in vivo human data available in the literature. In section 6.1 the four-compartment model is described. In section 6.2 the model is linearised and relationships between available experimental observations and the system model are described. In section 6.3 parameters are estimated from the timecourse data of six individuals from tracer experiments reported in the literature. In section 6.4 a naive-pooled approach is used to estimate parameters for a reparameterised model. All of the data used in this chapter are taken from Solomon et al. [9], Waldmann et al. [7] and Waldmann et al. [10]. The four-compartment model presented in section 6.1 has been previously published by Kim et al. [1] and Hattersley [2]. The remainder of the work presented in this chapter represents original work by the author.

6.1 System model

The four-compartment model of IgG metabolism [1; 2] has four state variables ($x_1(t)$, $x_2(t)$, $x_3(t)$ and $x_4(t)$), nine parameters and an input function, $I(t)$, representing the

Table 6-1 States and parameters of four-compartment model of IgG metabolism, with parameter values sourced in the literature

Name	Units	Literature value	Physiological interpretation
x_1	µmol	–	Quantity of IgG in the central (plasma) compartment
x_2	µmol	–	Quantity of IgG in the peripheral compartment
x_3	µmol	–	Quantity of unbound IgG in intracellular endosomes
x_4	µmol	–	Quantity of IgG-FcRn complexes in intracellular endosomes
v_1	l	2.9*	Plasma volume
v_2	l	–	Volume of peripheral compartment
v_3	l	0.34†	Total volume of endosomes
k_{21}	day^{-1}	0.51‡	Rate constant of flow of IgG from plasma to peripheral compartment
k_{31}	day^{-1}	0.18§	Rate constant of flow of IgG from plasma into endosomes by pinocytosis
k_{12}	day^{-1}	0.41‡	Rate constant of flow of IgG from peripheral compartment to plasma
k_{14}	day^{-1}	5.0¶	Rate constant of flow of recycled IgG from endosomes back into plasma
k_{03}	day^{-1}	3.0‖	Rate constant of degradation of unbound IgG in endosomes
k_{on}	$\text{l}\,\mu\text{mol}^{-1}\,\text{day}^{-1}$	1000**	Association rate constant of IgG-FcRn binding
R_{tot}	µmol	14¶	Total quantity of FcRn receptors, bound and unbound
k_{off}	day^{-1}	100**	Dissociation rate constant of IgG-FcRn binding

*Solomon et al. [9], †Shah et al. [5], ‡Hattersley et al. [11], §Waldmann et al. [7], ¶Ferl et al. [3], ‖Hansen et al. [12], **Chen et al. [13]

synthesis rate of IgG. The model equations are given by

$$\begin{aligned}
\dot{x}_1(t) &= -(k_{21}+k_{31})x_1(t) + k_{12}x_2(t) + k_{14}x_4(t) + I(t)\\
\dot{x}_2(t) &= k_{21}x_1(t) - k_{12}x_2(t)\\
\dot{x}_3(t) &= k_{31}x_1(t) - k_{03}x_3(t) - \frac{k_{\text{on}}}{v_3}x_3(t)(R_{\text{tot}} - x_4(t)) + k_{\text{off}}x_4(t)\\
\dot{x}_4(t) &= \frac{k_{\text{on}}}{v_3}x_3(t)(R_{\text{tot}} - x_4(t)) - (k_{14}+k_{\text{off}})x_4(t),
\end{aligned} \tag{6-1}$$

where $x_1(t)$, $x_2(t)$, $x_3(t)$ and $x_4(t)$ represent the quantities in micromoles (µmol) of IgG in plasma, IgG in a peripheral compartment, unbound IgG in endosomes and IgG bound to FcRn in endosomes, respectively. $I(t)$ represents the synthesis rate of IgG in plasma in micromoles per day ($\mu\text{mol}\,\text{day}^{-1}$). The rate constants, k_{ij}, represent material flow from compartment j to compartment i, with the convention that 0 represents the environment outside the system. The parameters k_{on} and k_{off} are the receptor-ligand binding constants of IgG and FcRn. The volumes of plasma, the peripheral compartment and the

endosomes are denoted by v_1, v_2 and v_3, respectively. We notice that the parameters k_{on} and v_3 appear in the equations only as the fraction k_{on}/v_3; therefore we immediately can conclude that these two parameters are not uniquely structurally identifiable. We assume a constant total (bound and unbound) quantity of FcRn, R_{tot}, as other authors have done [3]. This means that the quantity of unbound FcRn is represented by $(R_{\text{tot}} - x_4(t))$. The model states and physiological interpretations of the parameters are summarised in table 6-1. Note that all states and parameters can only take non-negative values. We refer to figure 6-1 for a schematic of the model.

6.1.1 Stability analysis

When the production rate of IgG is constant, $I(t) = I_0$, the system has an equilibrium point given by

$$\begin{aligned}
\hat{x}_1 &= \frac{I_0\left(k_{03}k_{14}v_3 + k_{03}k_{\text{off}}v_3 + k_{\text{on}}I_0 + k_{14}k_{\text{on}}R_{\text{tot}}\right)}{k_{31}\left(k_{03}v_3(k_{14}+k_{\text{off}}) + k_{\text{on}}I_0\right)} \\
\hat{x}_2 &= \frac{k_{21}}{k_{12}}\hat{x}_1 \\
\hat{x}_3 &= \frac{I_0}{k_{03}} \\
\hat{x}_4 &= \frac{k_{\text{on}}I_0R_{\text{tot}}}{k_{03}v_3(k_{14}+k_{\text{off}}) + k_{\text{on}}I_0}.
\end{aligned} \tag{6-2}$$

Linearising the system about the equilibrium point gives

$$\begin{pmatrix} \dot{x}_1(t) \\ \dot{x}_2(t) \\ \dot{x}_3(t) \\ \dot{x}_4(t) \end{pmatrix} = \begin{pmatrix} -k_{21}-k_{31} & k_{12} & 0 & k_{14} \\ k_{21} & -k_{12} & 0 & 0 \\ k_{31} & 0 & a_{33} & k_{\text{off}} + \frac{k_{\text{on}}I_0}{k_{03}v_3} \\ 0 & 0 & a_{43} & -k_{14}-k_{\text{off}} - \frac{k_{\text{on}}I_0}{k_{03}v_3} \end{pmatrix} \begin{pmatrix} x_1(t) \\ x_2(t) \\ x_3(t) \\ x_4(t) \end{pmatrix}, \tag{6-3}$$

where

$$\begin{aligned}
a_{33} &= -\frac{k_{03}(k_{\text{on}}(I_0 + (k_{14}+k_{\text{off}})\,R_{\text{tot}}) + k_{03}v_3\,(k_{14}+k_{\text{off}})}{k_{\text{on}}I_0 + k_{03}v_3\,(k_{14}+k_{\text{off}})} \\
a_{43} &= \frac{k_{03}k_{\text{on}}R_{\text{tot}}\,(k_{14}+k_{\text{off}})}{k_{\text{on}}I_0 + k_{03}v_3\,(k_{14}+k_{\text{off}})}.
\end{aligned} \tag{6-4}$$

The coefficients of the characteristic polynomial for this matrix are given by

$$\begin{aligned}
c_1 = \frac{1}{k_{03}v_3\big(k_{\text{on}}I_0 + k_{03}v_3(k_{14}+k_{\text{off}})\big)}\Big(&I_0^2k_{\text{on}}^2 + I_0k_{03}(k_{03}+k_{12}+2k_{14}+k_{21}+k_{31} \\
&+ 2k_{\text{off}})k_{\text{on}}v_3 + k_{03}^2(k_{14}+k_{\text{off}})v_3\big(k_{\text{on}}R_{\text{tot}} + (k_{03}+k_{12}+k_{14}+k_{21}+k_{31}+k_{\text{off}})v_3\big)\Big)
\end{aligned}$$

$$c_2 = \frac{1}{k_{03}v_3\big(k_{\text{on}}I_0 + k_{03}v_3(k_{14}+k_{\text{off}})\big)}\Bigg(I_0^2(k_{03}+k_{12}+k_{21}+k_{31})k_{\text{on}}^2 + I_0k_{03}\big(2(k_{21}+k_{31})(k_{14}+k_{\text{off}}) + k_{12}(2k_{14}+k_{31}+2k_{\text{off}}) + k_{03}(k_{12}+2k_{14}+k_{21}+k_{31} + 2k_{\text{off}})\big)k_{\text{on}}v_3 + k_{03}^2(k_{14}+k_{\text{off}})v_3\Big(k_{21}k_{\text{on}}R_{\text{tot}} + k_{31}k_{\text{on}}R_{\text{tot}} + k_{03}k_{21}v_3 + k_{03}k_{31}v_3 + k_{03}k_{\text{off}}v_3 + k_{21}k_{\text{off}}v_3 + k_{31}k_{\text{off}}v_3 + k_{14}\big(k_{\text{on}}R_{\text{tot}} + (k_{03}+k_{21}+k_{31})v_3\big) + k_{12}\big(k_{\text{on}}R_{\text{tot}} + (k_{03}+k_{14}+k_{31}+k_{\text{off}})v_3\big)\Big)\Bigg)$$

$$c_3 = \frac{1}{k_{03}v_3\big(k_{\text{on}}I_0 + k_{03}v_3(k_{14}+k_{\text{off}})\big)}\Bigg(I_0^2\big(k_{12}k_{31} + k_{03}(k_{12}+k_{21}+k_{31})\big)k_{\text{on}}^2 + I_0k_{03}\Big(2k_{12}k_{31}(k_{14}+k_{\text{off}}) + k_{03}\big(2(k_{21}+k_{31})(k_{14}+k_{\text{off}}) + k_{12}(2k_{14}+k_{31}+2k_{\text{off}})\big)\Big)k_{\text{on}}v_3 + k_{03}^2(k_{14}+k_{\text{off}})v_3\Big(k_{03}(k_{21}+k_{31})k_{\text{off}}v_3 + k_{14}(k_{21}k_{\text{on}}R_{\text{tot}} + k_{03}k_{21}v_3 + k_{03}k_{31}v_3) + k_{12}\Big(k_{03}k_{\text{off}}v_3 + k_{14}\big(k_{\text{on}}R_{\text{tot}} + (k_{03} + k_{31})v_3\big) + k_{31}\big(k_{\text{on}}R_{\text{tot}} + (k_{03}+k_{\text{off}})v_3\big)\Big)\Big)\Big)\Bigg)$$

$$c_4 = \frac{k_{12}k_{31}\left(k_{03}v_3\left(k_{14}+k_{\text{off}}\right) + k_{\text{on}}I_0\right)}{v_3}. \tag{6-5}$$

According to the Routh-Hurwitz stability criterion [14], the four-state system is stable provided the coefficients of the characteristic polynomial of the linearised system satisfy the conditions:

$$\begin{gathered} c_1, c_3, c_4 > 0 \\ c_1c_2c_3 > c_3^2 + c_1^2c_4. \end{gathered} \tag{6-6}$$

All parameters, including the input I_0, can only take positive values. The conditions given by the first inequality in 6-6 can easily be checked by noticing that none of the terms in equations 6-5 are preceded by a minus sign. The second inequality was tested in Mathematica [15] using the code:

```
Assuming[Table[parameters[[i]] > 0, {i, 10}], FullSimplify[c1*c2*c3 > c3^2 +
    c4*c1^2]
```

Both conditions are found to be met, showing that the equilibrium point of the system is stable.

6.2 Mathematical description of observations

The data available in the literature that may be used for parameter estimation are described in section 5.3 of chapter 5. The data for subject E, who has familial hypercatabolic hypoproteinemia, are unsuitable for estimating all of the parameters of the four-compartment model: subjects with familial hypercatabolic hypoproteinemia do not express FcRn receptors and therefore the compartments for IgG-FcRn complexes and unbound FcRn receptors can be eliminated from the model described in section 6.1, leaving a three-compartment model with parameters k_{21}, k_{12}, k_{31} and k_{03}. This sub-model could potentially be used to estimate some of the model parameters; however this is not investigated in this thesis.

In this section we consider how the available experimental observations are defined in terms of the underlying system model. A linear model describing the timecourse observations is derived from the nonlinear model of coupled tracer and endogenous IgG dynamics. Expressions for the fractional catabolic rate (FCR) and half-life ($T_{1/2}$) are then derived from the linear model of the timecourse observations.

6.2.1 Nonlinear structural model of coupled tracer and endogenous IgG dynamics

The administered tracer and the endogenous IgG are assumed to be indistinguishable by the system, that is they exhibit identical kinetic behaviour – a standard assumption in tracer studies [16]. It is thus assumed that the kinetics of both tracer and endogenous IgG are described by the model in (6-1). From (6-1), letting $x_i(t) = x_{i,\mathrm{T}}(t) + x_{i,\mathrm{E}}(t)$, $i = 1, \ldots, 4$, where subscript 'T' denotes tracer, and subscript 'E' denotes endogenous

IgG, respectively, gives

$$\begin{aligned}
\dot{x}_{1,\mathrm{T}}(t) &= -(k_{21}+k_{31})x_{1,\mathrm{T}}(t) + k_{12}x_{2,\mathrm{T}}(t) + k_{14}x_{4,\mathrm{T}}(t)\\
\dot{x}_{2,\mathrm{T}}(t) &= k_{21}x_{1,\mathrm{T}}(t) - k_{12}x_{2,\mathrm{T}}(t)\\
\dot{x}_{3,\mathrm{T}}(t) &= k_{31}x_{1,\mathrm{T}}(t) - k_{03}x_{3,\mathrm{T}}(t) - \frac{k_{\mathrm{on}}}{v_3}x_{3,\mathrm{T}}(t)(R_{\mathrm{tot}} - x_{4,\mathrm{E}}(t) - x_{4,\mathrm{T}}(t)) + k_{\mathrm{off}}x_{4,\mathrm{T}}(t)\\
\dot{x}_{4,\mathrm{T}}(t) &= \frac{k_{\mathrm{on}}}{v_3}x_{3,\mathrm{T}}(t)(R_{\mathrm{tot}} - x_{4,\mathrm{E}}(t) - x_{4,\mathrm{T}}(t)) - (k_{14}+k_{\mathrm{off}})x_{4,\mathrm{T}}(t)\\
\dot{x}_{1,\mathrm{E}}(t) &= -(k_{21}+k_{31})x_{1,\mathrm{E}}(t) + k_{12}x_{2,\mathrm{E}}(t) + k_{14}x_{4,\mathrm{E}}(t) + I_{\mathrm{E}}\\
\dot{x}_{2,\mathrm{E}}(t) &= k_{21}x_{1,\mathrm{E}}(t) - k_{12}x_{2,\mathrm{E}}(t)\\
\dot{x}_{3,\mathrm{E}}(t) &= k_{31}x_{1,\mathrm{E}}(t) - k_{03}x_{3,\mathrm{E}}(t) - \frac{k_{\mathrm{on}}}{v_3}x_{3,\mathrm{E}}(t)(R_{\mathrm{tot}} - x_{4,\mathrm{E}}(t) - x_{4,\mathrm{T}}(t)) + k_{\mathrm{off}}x_{4,\mathrm{E}}(t)\\
\dot{x}_{4,\mathrm{E}}(t) &= \frac{k_{\mathrm{on}}}{v_3}x_{3,\mathrm{E}}(t)(R_{\mathrm{tot}} - x_{4,\mathrm{E}}(t) - x_{4,\mathrm{T}}(t)) - (k_{14}+k_{\mathrm{off}})x_{4,\mathrm{E}}(t),
\end{aligned} \tag{6-7}$$

where $x_{i,\mathrm{T}}(t)$ and $x_{i,\mathrm{E}}(t)$ represent the quantities in µmol of radiolabelled and endogenous IgG in compartment i, respectively, and I_{E} (µmol day^{-1}) represents the production rate of endogenous IgG, which is assumed constant. All other parameters are as defined in section 6.1.

The dose of tracer administered at time $t = 0$ is treated as a non-zero initial condition for $x_{1,\mathrm{T}}(t)$. Tracer is administered to the plasma compartment ($i = 1$) only, therefore the initial conditions for the remaining tracer compartments are zero. The endogenous IgG is assumed to be in steady state at the beginning of the experiment and remain in steady state throughout, as verifiable by the experimenter, such that the initial conditions of the endogenous IgG are given by the steady states in equation (6-2), with $I_0 = I_{\mathrm{E}}$. In summary, the initial conditions are given by

$$\begin{aligned}
x_{1,\mathrm{T}}(0) &= D\\
x_{2,\mathrm{T}}(0) &= x_{3,\mathrm{T}}(0) = x_{4,\mathrm{T}}(0) = 0\\
x_{1,\mathrm{E}}(0) &= \hat{x}_1\\
x_{2,\mathrm{E}}(0) &= \hat{x}_2\\
x_{3,\mathrm{E}}(0) &= \hat{x}_3\\
x_{4,\mathrm{E}}(0) &= \hat{x}_4,
\end{aligned} \tag{6-8}$$

where D (µmol) is the administered dose of tracer.

The experimenter observes the proportion of the dose remaining in plasma and in the

body during the experiment. The observation functions are thus given by

$$\begin{aligned} y_1(t) &= \frac{x_{1,\mathrm{T}}(t)}{D} \\ y_2(t) &= \frac{x_{1,\mathrm{T}}(t) + x_{2,\mathrm{T}}(t) + x_{3,\mathrm{T}}(t) + x_{4,\mathrm{T}}(t)}{D}. \end{aligned} \tag{6-9}$$

6.2.2 Linearised structural model of tracer dynamics

Provided that the administered dose of tracer is sufficiently small, the tracer kinetics can be approximated using a Taylor series expansion of the model state about the equilibrium point [17]. In this way a linear model of the experiment is derived. The derivation of a linearised model for tracer dynamics from a general compartmental model is provided by Anderson [18].

The dynamics of endogenous IgG and FcRn receptors are described by

$$\begin{aligned} \dot{x}_{1,\mathrm{E}}(t) &= -(k_{21} + k_{31})x_{1,\mathrm{E}}(t) + k_{12}x_{2,\mathrm{E}}(t) + k_{14}x_{4,\mathrm{E}}(t) + I_{\mathrm{E}} \\ \dot{x}_{2,\mathrm{E}}(t) &= k_{21}x_{1,\mathrm{E}}(t) - k_{12}x_{2,\mathrm{E}}(t) \\ \dot{x}_{3,\mathrm{E}}(t) &= k_{31}x_{1,\mathrm{E}}(t) - k_{03}x_{3,\mathrm{E}}(t) - \frac{k_{\mathrm{on}}}{v_3}x_{3,\mathrm{E}}(t)x_{5,\mathrm{E}}(t) + k_{\mathrm{off}}x_{4,\mathrm{E}}(t) \\ \dot{x}_{4,\mathrm{E}}(t) &= \frac{k_{\mathrm{on}}}{v_3}x_{3,\mathrm{E}}(t)x_{5,\mathrm{E}}(t) - (k_{14} + k_{\mathrm{off}})x_{4,\mathrm{E}}(t) \\ \dot{x}_{5,\mathrm{E}}(t) &= -\frac{k_{\mathrm{on}}}{v_3}x_{3,\mathrm{E}}(t)x_{5,\mathrm{E}}(t) + (k_{14} + k_{\mathrm{off}})x_{4,\mathrm{E}}(t), \end{aligned} \tag{6-10}$$

where $x_{i,\mathrm{E}}(t)$, $i = 1, \ldots, 4$, is the quantity of unlabelled IgG in compartment i (for details see section 6.1) and $x_{5,\mathrm{E}}(t)$ is the quantity of unbound FcRn receptors in intracellular endosomes. The total quantity of FcRn, $x_{4,\mathrm{E}}(t) + x_{5,\mathrm{E}}(t)$, is constant and given by R_{tot}, therefore the equation for the rate of change of $x_{5,\mathrm{E}}(t)$ is not actually required in equations (6-10). However, in order to linearise the model, all endogenous quantities are assumed to be in steady state, including the endogenous FcRn receptors. Including the equation for $x_{5,\mathrm{E}}(t)$ makes this assumption more straightforward later. Prior to administration of the tracer dose, the system is assumed to be in steady state, where $\hat{x}_i$, $i = 1, \ldots, 4$, is the quantity of IgG in compartment i in steady state, as given by (6-2) with I_0 set to I_{E}. The steady state of unbound FcRn is given by $\hat{x}_5 = R_{\mathrm{tot}} - \hat{x}_4$. For convenience equations

(6-10) are re-written as follows:

$$\begin{aligned}
\dot{x}_{1,\mathrm{E}}(t) &= F_1(x_{1,\mathrm{E}}(t), x_{2,\mathrm{E}}(t), x_{3,\mathrm{E}}(t), x_{4,\mathrm{E}}(t), x_{5,\mathrm{E}}(t)) + I_{\mathrm{E}} \\
\dot{x}_{2,\mathrm{E}}(t) &= F_2(x_{1,\mathrm{E}}(t), x_{2,\mathrm{E}}(t), x_{3,\mathrm{E}}(t), x_{4,\mathrm{E}}(t), x_{5,\mathrm{E}}(t)) \\
\dot{x}_{3,\mathrm{E}}(t) &= F_3(x_{1,\mathrm{E}}(t), x_{2,\mathrm{E}}(t), x_{3,\mathrm{E}}(t), x_{4,\mathrm{E}}(t), x_{5,\mathrm{E}}(t)) \\
\dot{x}_{4,\mathrm{E}}(t) &= F_4(x_{1,\mathrm{E}}(t), x_{2,\mathrm{E}}(t), x_{3,\mathrm{E}}(t), x_{4,\mathrm{E}}(t), x_{5,\mathrm{E}}(t)) \\
\dot{x}_{5,\mathrm{E}}(t) &= F_5(x_{1,\mathrm{E}}(t), x_{2,\mathrm{E}}(t), x_{3,\mathrm{E}}(t), x_{4,\mathrm{E}}(t), x_{5,\mathrm{E}}(t)).
\end{aligned} \tag{6-11}$$

The administration of a small bolus dose of labelled IgG is treated as a perturbation of the steady state at time $t = 0$. The input of tracer is denoted by $u(t)$. Now the dynamics of the total quantity of both labelled and unlabelled IgG are described by

$$\begin{aligned}
\dot{q}_1(t) &= -(k_{21} + k_{31})q_1(t) + k_{12}q_2(t) + k_{14}q_4(t) + I_{\mathrm{E}} + u(t) \\
\dot{q}_2(t) &= k_{21}q_1(t) - k_{12}q_2(t) \\
\dot{q}_3(t) &= k_{31}q_1(t) - k_{03}q_3(t) - \frac{k_{\mathrm{on}}}{v_3}q_3(t)x_{5,\mathrm{E}}(t) + k_{\mathrm{off}}q_4(t) \\
\dot{q}_4(t) &= \frac{k_{\mathrm{on}}}{v_3}q_3(t)x_{5,\mathrm{E}}(t) - (k_{14} + k_{\mathrm{off}})q_4(t) \\
\dot{x}_{5,\mathrm{E}}(t) &= -\frac{k_{\mathrm{on}}}{v_3}q_3(t)x_{5,\mathrm{E}}(t) + (k_{14} + k_{\mathrm{off}})q_4(t),
\end{aligned} \tag{6-12}$$

where $q_i(t) = x_{i,\mathrm{E}}(t) + x_{i,\mathrm{T}}(t)$, $i = 1, \ldots, 4$ is the total quantity of labelled and unlabelled IgG in compartment i.

Assuming that the tracer dose is sufficiently small, we have $x_{i,\mathrm{T}}(t) = q_i(t) - \hat{x}_i$, $i = 1, \ldots, 4$, where $x_{i,\mathrm{T}}(t)$ is the quantity of tracer, $q_i(t)$ is the total quantity of tracer and endogenous IgG, and $\hat{x}_i$ is the quantity of IgG in steady state, in compartment i, respectively. Since the FcRn receptors are endogenous to the system they are assumed to be in steady state, such that $x_{5,\mathrm{E}}(t) = \hat{x}_5$, where $\hat{x}_5 = R_{\mathrm{tot}} - \hat{x}_4$ is the quantity of unbound FcRn receptors in equilibrium. The rate of change of the total quantity of IgG in compartment i is given by

$$\dot{q}_i(t) = \frac{\mathrm{d}}{\mathrm{d}t}\left(x_{i,\mathrm{T}}(t) + \hat{x}_i\right) = \dot{x}_{i,\mathrm{T}}(t), \qquad i = 1, \ldots, 4. \tag{6-13}$$

From (6-12) and (6-13) we have that

$$\begin{aligned}
\dot{x}_{1,\mathrm{T}}(t) &= -(k_{21}+k_{31})(x_{1,\mathrm{T}}(t)+\hat{x}_1)+k_{12}(x_{2,\mathrm{T}}(t)+\hat{x}_2)+k_{14}(x_{4,\mathrm{T}}(t)+\hat{x}_4)+I_{\mathrm{E}} \\
&\qquad\qquad\qquad\qquad\qquad\qquad\qquad\qquad\qquad\qquad\qquad\qquad + u(t) \\
\dot{x}_{2,\mathrm{T}}(t) &= k_{21}(x_{1,\mathrm{T}}(t)+\hat{x}_1)-k_{12}(x_{2,\mathrm{T}}(t)+\hat{x}_2) \\
\dot{x}_{3,\mathrm{T}}(t) &= k_{31}(x_{1,\mathrm{T}}(t)+\hat{x}_1)-k_{03}(x_{3,\mathrm{T}}(t)+\hat{x}_3)-\frac{k_{\mathrm{on}}}{v_3}(x_{3,\mathrm{T}}(t)+\hat{x}_3)\hat{x}_5 \\
&\qquad\qquad\qquad\qquad\qquad\qquad\qquad\qquad\qquad\qquad + k_{\mathrm{off}}(x_{4,\mathrm{T}}(t)+\hat{x}_4) \\
\dot{x}_{4,\mathrm{T}}(t) &= \frac{k_{\mathrm{on}}}{v_3}(x_{3,\mathrm{T}}(t)+\hat{x}_3)\hat{x}_5-(k_{14}+k_{\mathrm{off}})(x_{4,\mathrm{T}}(t)+\hat{x}_4).
\end{aligned} \tag{6-14}$$

It is now possible to approximate the right hand sides of (6-14) using the Taylor series expansion. Equations (6-14) are re-written to give

$$\begin{aligned}
\dot{x}_{1,\mathrm{T}}(t) &= F_1(\hat{x}_1+x_{1,\mathrm{T}}(t),\hat{x}_2+x_{2,\mathrm{T}}(t),\hat{x}_3+x_{3,\mathrm{T}}(t),\hat{x}_4+x_{4,\mathrm{T}}(t),\hat{x}_5)+I_{\mathrm{E}}+u(t) \\
\dot{x}_{2,\mathrm{T}}(t) &= F_2(\hat{x}_1+x_{1,\mathrm{T}}(t),\hat{x}_2+x_{2,\mathrm{T}}(t),\hat{x}_3+x_{3,\mathrm{T}}(t),\hat{x}_4+x_{4,\mathrm{T}}(t),\hat{x}_5) \\
\dot{x}_{3,\mathrm{T}}(t) &= F_3(\hat{x}_1+x_{1,\mathrm{T}}(t),\hat{x}_2+x_{2,\mathrm{T}}(t),\hat{x}_3+x_{3,\mathrm{T}}(t),\hat{x}_4+x_{4,\mathrm{T}}(t),\hat{x}_5) \\
\dot{x}_{4,\mathrm{T}}(t) &= F_4(\hat{x}_1+x_{1,\mathrm{T}}(t),\hat{x}_2+x_{2,\mathrm{T}}(t),\hat{x}_3+x_{3,\mathrm{T}}(t),\hat{x}_4+x_{4,\mathrm{T}}(t),\hat{x}_5).
\end{aligned} \tag{6-15}$$

The Taylor series expansion of the right hand side of (6-15) is given by

$$\begin{aligned}
&F_i(\hat{x}_1+x_{1,\mathrm{T}}(t),\hat{x}_2+x_{2,\mathrm{T}}(t),\hat{x}_3+x_{3,\mathrm{T}}(t),\hat{x}_4+x_{4,\mathrm{T}}(t),\hat{x}_5) \\
&\quad = F_i(\hat{x}_1,\hat{x}_2,\hat{x}_3,\hat{x}_4,\hat{x}_5)+x_{1,\mathrm{T}}(t)\frac{\partial F_i}{\partial x_{1,\mathrm{E}}}(\hat{x}_1,\hat{x}_2,\hat{x}_3,\hat{x}_4,\hat{x}_5) \\
&\qquad + x_{2,\mathrm{T}}(t)\frac{\partial F_i}{\partial x_{2,\mathrm{E}}}(\hat{x}_1,\hat{x}_2,\hat{x}_3,\hat{x}_4,\hat{x}_5)+x_{3,\mathrm{T}}(t)\frac{\partial F_i}{\partial x_{3,\mathrm{E}}}(\hat{x}_1,\hat{x}_2,\hat{x}_3,\hat{x}_4,\hat{x}_5) \\
&\qquad + x_{4,\mathrm{T}}(t)\frac{\partial F_i}{\partial x_{4,\mathrm{E}}}(\hat{x}_1,\hat{x}_2,\hat{x}_3,\hat{x}_4,\hat{x}_5)+\mathrm{H.O.T},
\end{aligned} \tag{6-16}$$

where H.O.T are higher order terms. Expanding (6-15) using (6-16) gives

$$\begin{aligned}
\dot{x}_{1,\mathrm{T}}(t) &\approx -(k_{21}+k_{31})x_{1,\mathrm{T}}(t)+k_{12}x_{2,\mathrm{T}}(t)+k_{14}x_{4,\mathrm{T}}(t)+u(t) \\
\dot{x}_{2,\mathrm{T}}(t) &\approx k_{21}x_{1,\mathrm{T}}(t)-k_{12}x_{2,\mathrm{T}}(t) \\
\dot{x}_{3,\mathrm{T}}(t) &\approx k_{31}x_{1,\mathrm{T}}(t)-k_{03}x_{3,\mathrm{T}}(t)-\frac{k_{\mathrm{on}}}{v_3}\hat{x}_5x_{3,\mathrm{T}}(t)+k_{\mathrm{off}}x_{4,\mathrm{T}}(t) \\
\dot{x}_{4,\mathrm{T}}(t) &\approx \frac{k_{\mathrm{on}}}{v_3}\hat{x}_5x_{3,\mathrm{T}}(t)-(k_{14}+k_{\mathrm{off}})x_{4,\mathrm{T}}(t).
\end{aligned} \tag{6-17}$$

It is assumed that the tracer dose is small enough so that higher order terms in the Taylor series expansion can be neglected. We also recall that $\hat{x}_5 = R_{\mathrm{tot}} - \hat{x}_4$. Finally a linear

model for the tracer dynamics is obtained, given by

$$\begin{aligned}
\dot{x}_{1,\mathrm{T}}(t) &= -(k_{21}+k_{31})x_{1,\mathrm{T}}(t) + k_{12}x_{2,\mathrm{T}}(t) + k_{14}x_{4,\mathrm{T}}(t) + u(t)\\
\dot{x}_{2,\mathrm{T}}(t) &= k_{21}x_{1,\mathrm{T}}(t) - k_{12}x_{2,\mathrm{T}}(t)\\
\dot{x}_{3,\mathrm{T}}(t) &= k_{31}x_{1,\mathrm{T}}(t) - k_{03}x_{3,\mathrm{T}}(t) - k_{43}x_{3,\mathrm{T}}(t) + k_{34}x_{4,\mathrm{T}}(t)\\
\dot{x}_{4,\mathrm{T}}(t) &= k_{43}x_{3,\mathrm{T}}(t) - (k_{14}+k_{34})x_{4,\mathrm{T}}(t),
\end{aligned} \tag{6-18}$$

where k_{34} and k_{43} are given by

$$\begin{aligned}
k_{34} &= k_{\mathrm{off}}\\
k_{43} &= \frac{k_{\mathrm{on}}(R_{\mathrm{tot}} - \hat{x}_4)}{v_3} = \frac{k_{\mathrm{on}}R_{\mathrm{tot}}k_{03}(k_{14}+k_{\mathrm{off}})}{I_{\mathrm{E}}k_{\mathrm{on}} + k_{03}v_3(k_{14}+k_{\mathrm{off}})}.
\end{aligned} \tag{6-19}$$

The input $u(t)$ can be treated as a non-zero initial condition for $x_{1,\mathrm{T}}(t)$. The linear equations describing the tracer kinetics are then given by

$$\begin{aligned}
\dot{x}_{1,\mathrm{T}}(t) &= -(k_{21}+k_{31})x_{1,\mathrm{T}}(t) + k_{12}x_{2,\mathrm{T}}(t) + k_{14}x_{4,\mathrm{T}}(t)\\
\dot{x}_{2,\mathrm{T}}(t) &= k_{21}x_{1,\mathrm{T}}(t) - k_{12}x_{2,\mathrm{T}}(t)\\
\dot{x}_{3,\mathrm{T}}(t) &= k_{31}x_{1,\mathrm{T}}(t) - k_{03}x_{3,\mathrm{T}}(t) - k_{43}x_{3,\mathrm{T}}(t) + k_{34}x_{4,\mathrm{T}}(t)\\
\dot{x}_{4,\mathrm{T}}(t) &= k_{43}x_{3,\mathrm{T}}(t) - (k_{14}+k_{34})x_{4,\mathrm{T}}(t),
\end{aligned} \tag{6-20}$$

where $x_{1,\mathrm{T}}(t)$, $x_{2,\mathrm{T}}(t)$, $x_{3,\mathrm{T}}(t)$ and $x_{4,\mathrm{T}}(t)$ represent the quantities of radiolabelled IgG in the central compartment, in the peripheral compartment, unbound in intracellular endosomes, and bound to FcRn in intracellular endosomes, respectively. The new parameters k_{34} and k_{43} are given by equation (6-19) and all other parameters are defined as in section 6.1.

The initial conditions are given by

$$\begin{aligned}
x_{1,\mathrm{T}}(0) &= D\\
x_{2,\mathrm{T}}(0) &= x_{3,\mathrm{T}}(0) = x_{4,\mathrm{T}}(0) = 0.
\end{aligned} \tag{6-21}$$

The observation functions are given by

$$\begin{aligned}
y_1(t) &= \frac{x_{1,\mathrm{T}}(t)}{D}\\
y_2(t) &= \frac{x_{1,\mathrm{T}}(t) + x_{2,\mathrm{T}}(t) + x_{3,\mathrm{T}}(t) + x_{3,\mathrm{T}}(t)}{D}.
\end{aligned} \tag{6-22}$$

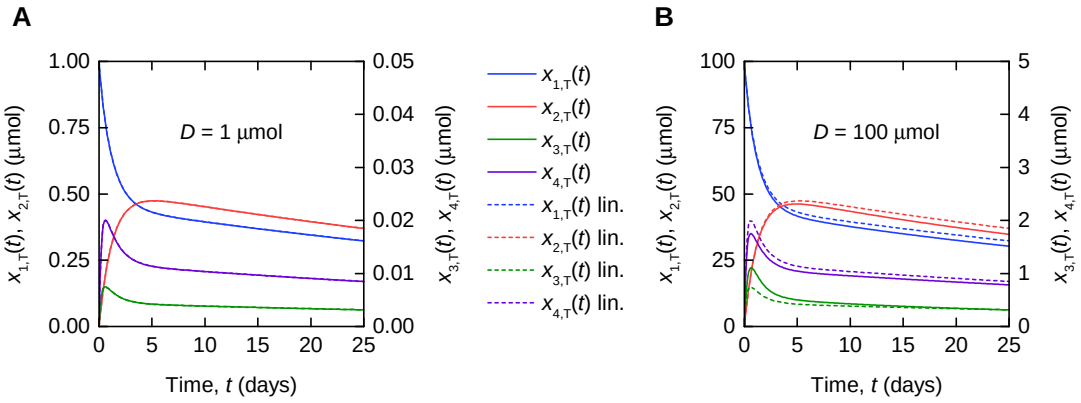

Figure 6-2 Simulations of the quantities of tracer in each compartment after administration at $t = 0$ days, for a tracer dose of (A) 1 µmol and (B) 100 µmol. The nonlinear model is represented by solid lines and the linearised model by dashed lines ('lin.'). In (A) the dashed lines overlay the solid lines; hence the linearised model is valid for the smaller dose (A) but not for the larger dose (B). Note the different scales for $x_{1,\mathrm{T}}(t)$ and $x_{2,\mathrm{T}}(t)$ (left axis), and $x_{3,\mathrm{T}}(t)$ and $x_{4,\mathrm{T}}(t)$ (right axis), respectively.

6.2.3 Comparison of the nonlinear and linearised models for large tracer doses

The linearisation of the model of tracer and endogenous IgG dynamics relies on the assumption of a sufficiently small dose of tracer, such that the endogenous IgG can be assumed to remain in steady state. A typical tracer dose is 3×10^{-3} µmol – 7×10^{-3} µmol [9]. Simulations of the quantity of tracer in each compartment are shown in figure 6-2. The nonlinear model, described by equations (6-7)–(6-8), is represented by solid lines and the linearised model, described by equations (6-20)–(6-21), is represented by dashed lines. In figure 6-2A a dose of $D = 1$ µmol is assumed and in figure 6-2B a dose of $D = 100$ µmol is assumed. The parameter values in table 6-1 are used. A normal IgG synthesis rate of $I_{\mathrm{E}} = 15\,\mu\mathrm{mol\,day}^{-1}$ was used; however the conclusion drawn was the same when very small values of I_{E} were used. The simulations illustrate that, for a dose of 1 µmol and the particular parameter values used, the linearised model is a valid approximation of the full nonlinear model over a 25-day simulated time course. When the dose is increased to 100 µmol, the assumption that the steady state is not perturbed by the administered dose no longer holds, and the two models give different simulation results for the quantities of tracer. For $D = 1$ µmol, which is more than 100 times typical tracer doses, the maximal

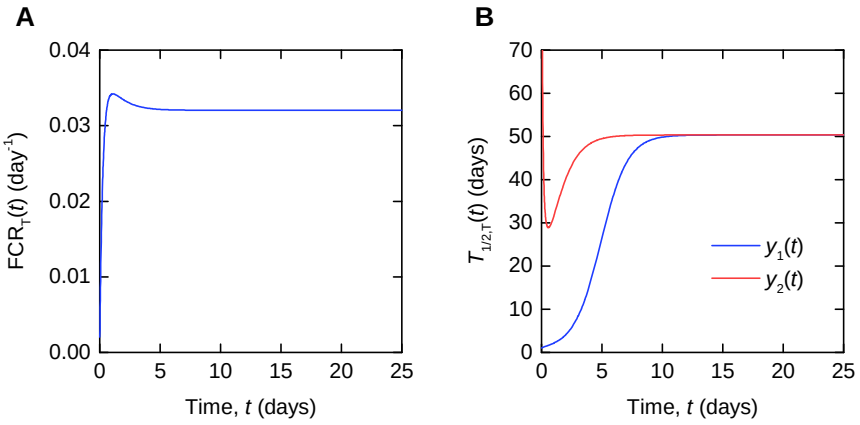

Figure 6-3 (A) Simulation of $\mathrm{FCR_T}(t)$ given by equations (6-23) and (6-24), for the parameter values in table 6-1 and dose $D = 0.01$ µmol. (B) Simulations of $T_{1/2,\mathrm{T}}(t)$ given by equation (6-30), for the parameter values in table 6-1 with normal endogenous IgG production rate $I_\mathrm{E} = 15$ µmol day^{-1} [7].

difference between the linear model and nonlinear model simulations is less than 0.7%. The extremely large dose of $D = 100$ µmol was chosen specifically to show the dynamics of the linearised model when it is not a valid approximation of the nonlinear model.

6.2.4 Fractional catabolic rate

The fractional catabolic rate (FCR) is defined as the elimination rate of IgG as a fraction of the quantity of IgG in plasma. The FCR can be defined with respect to the tracer, denoted here by $\mathrm{FCR_T}$, or with respect to the endogenous IgG, denoted here by $\mathrm{FCR_E}$. $\mathrm{FCR_T}$ and $\mathrm{FCR_E}$ have units of µmol day^{-1}.

As there is only elimination from the system and no input after time $t = 0$, $\mathrm{FCR_T}$ is given by the rate of change of radiolabelled IgG in all compartments, divided by the quantity of radiolabelled IgG in plasma:

$$\mathrm{FCR_T}(t) = \frac{-\left(\dot{x}_{1,\mathrm{T}}(t) + \dot{x}_{2,\mathrm{T}}(t) + \dot{x}_{3,\mathrm{T}}(t) + \dot{x}_{4,\mathrm{T}}(t)\right)}{x_{1,\mathrm{T}}(t)} = \frac{-\dot{y}_2(t)}{y_1(t)}. \tag{6-23}$$

From equation (6-23), it can be seen that in practice $\mathrm{FCR_T}$ is obtained from the slope of the observation $y_2(t)$ divided by $y_1(t)$. Substituting equations (6-20) into equation (6-23) gives

$$\mathrm{FCR_T}(t) = \frac{k_{03} x_{3,\mathrm{T}}(t)}{x_{1,\mathrm{T}}(t)}, \tag{6-24}$$

where $x_{3,\mathrm{T}}(t)$ and $x_{1,\mathrm{T}}(t)$ are given by the solution of equations (6-20)–(6-21).

Whilst a single value of FCR_T is measured for an individual subject (see section 5.3 in chapter 5), in actuality FCR_T is not constant, as shown by the dependence on time in equations (6-23) and (6-24). A simulation of $\mathrm{FCR}_\mathrm{T}(t)$ during the experiment is shown in figure 6-3A. After around day 5 (for the particular parameter values used) $\mathrm{FCR}_\mathrm{T}(t)$ approaches a steady state value, which is denoted here by $\mathrm{FCR}_{\mathrm{T},\infty}$:

$$\mathrm{FCR}_{\mathrm{T},\infty} = \lim_{t\to\infty} \frac{k_{03}x_{3,\mathrm{T}}(t)}{x_{1,\mathrm{T}}(t)}. \tag{6-25}$$

Solving equations (6-20)–(6-21) gives

$$x_{i,\mathrm{T}}(t) = A_{i1}\exp(\lambda_1 t) + A_{i2}\exp(\lambda_2 t) + A_{i3}\exp(\lambda_3 t) + A_{i4}\exp(\lambda_4 t), \tag{6-26}$$

assuming, without loss of generality, $|\lambda_1| > |\lambda_2| > |\lambda_3| > |\lambda_4|$. After sufficient time, $x_{i,\mathrm{T}}(t)$ can be approximated by $A_{i4}\exp(\lambda_4 t)$; thus, $\mathrm{FCR}_{\mathrm{T},\infty}$ is given by

$$\mathrm{FCR}_{\mathrm{T},\infty} = k_{03}\frac{A_{34}\exp(\lambda_4 t)}{A_{14}\exp(\lambda_4 t)} = k_{03}\frac{A_{34}}{A_{14}}, \tag{6-27}$$

where A_{34} and A_{14} are expressions in terms of the model parameters. The expressions for A_{34} and A_{14} are extremely long. The Mathematica [15] code for generating the expressions is provided in appendix D.

It is also possible to derive an expression for the FCR with respect to the endogenous IgG, FCR_E. If the endogenous IgG is assumed to remain in steady state, then from the definition of the FCR,

$$\mathrm{FCR}_\mathrm{E} = \frac{k_{03}\hat{x}_3}{\hat{x}_1}, \tag{6-28}$$

where $\hat{x}_1$ and $\hat{x}_3$ are the quantities of IgG in compartments 1 and 3 in steady state, given by (6-2). Substituting the expression for $\hat{x}_3$ from (6-2) into (6-28), eliminating I_0 in favour of $\hat{x}_1$ using the first equation of (6-2), and setting $\hat{x}_1 = x_{1,\mathrm{E}}$, gives the following expression for the FCR_E in terms of the quantity of IgG in plasma, $x_{1,\mathrm{E}}$:

$$\begin{aligned}\mathrm{FCR}_\mathrm{E} = \frac{1}{2k_{\mathrm{on}}x_{1,\mathrm{E}}}\Big(&k_{31}k_{\mathrm{on}}x_{1,\mathrm{E}} - k_{14}k_{\mathrm{on}}R_{\mathrm{tot}} - k_{03}k_{14}v_3 - k_{03}k_{\mathrm{off}}v_3 \\ &+ \Big\{4k_{03}k_{31}(k_{14}+k_{\mathrm{off}})k_{\mathrm{on}}x_{1,\mathrm{E}}v_3 \\ &+ (-k_{31}k_{\mathrm{on}}x_{1,\mathrm{E}} + k_{14}k_{\mathrm{on}}R_{\mathrm{tot}} + k_{03}k_{14}v_3 + k_{03}k_{\mathrm{off}}v_3)^2\Big\}^{1/2}\Big).\end{aligned} \tag{6-29}$$

6.2.5 Half-life

The half-life is obtained from the slope of either timecourse observation, $y_1(t)$ or $y_2(t)$, plotted on a log scale. The half-life is thus given by

$$T_{1/2,i}(t) = \frac{-\log(2)}{\mathrm{d}(\log y_i(t))\,/\,\mathrm{d}t}, \tag{6-30}$$

for $i = 1$ or $i = 2$, depending on whether $y_1(t)$ or $y_2(t)$ is used. Simulations of $T_{1/2,1}(t)$ and $T_{1/2,2}(t)$ are plotted in figure 6-3B. After sufficient time, the slopes of $\log\big(y_1(t)\big)$ and $\log\big(y_2(t)\big)$ approach the same value and therefore so do $T_{1/2,1}(t)$ and $T_{1/2,2}(t)$. Experimenters measure the value towards which $T_{1/2,1}(t)$ and $T_{1/2,2}(t)$ tend for increasing values of t, which we will call $T_{1/2,\infty}$:

$$T_{1/2,\infty} = \lim_{t\to\infty} \frac{-\log 2}{\mathrm{d}(\log y_i(t))\,/\,\mathrm{d}t}, \qquad i = 1, 2. \tag{6-31}$$

For the linear model described by equations (6-20)–(6-22), $T_{1/2,\infty}$ is given by

$$T_{1/2,\infty} = \lim_{t\to\infty} \frac{-\log 2}{\mathrm{d}(\log y_i(t))\,/\,\mathrm{d}t} = \frac{-\log 2}{\lambda_4}, \tag{6-32}$$

where λ_4 is the negative terminal slope of the timecourse observations plotted on a log scale. The expression for λ_4 is large and omitted for brevity. The Mathematica [15] code for generating the expression is provided in appendix D. Henceforth $\mathrm{FCR}_{\mathrm{T},\infty}$ and $T_{1/2,\infty}$ will be referred to simply as $\mathrm{FCR}_{\mathrm{T}}$ and $T_{1/2,\mathrm{T}}$.

6.3 Individual approach to parameter identification using timecourse data

In this section we investigate parameterisation of the model by fitting the linearised model outputs described in section 6.2.2 to the timecourse data described in section 5.3 of chapter 5. Firstly, a structural identifiability analysis is performed in order to determine which, if any, of the model parameters are structurally identifiable. The parameters are then estimated from the data by fitting the linearised model described by equations (6-20)–(6-22). The simulation in figure 6-2 illustrates that, for typical doses, the solution to the linear approximation is practically indistinguishable from the solution to the full nonlinear model. It is therefore sufficient to perform the fitting on the linear model.

6.3.1 Structural identifiability analysis

Structural identifiability addresses the question of whether model parameters can be uniquely identified from available observations, under the assumption of the availability of ideal (i.e. noise-free) and continuous observational data. Here we determine which of the model parameters are structurally uniquely identifiable from the observations $y_1(t)$ and $y_2(t)$ for an individual subject, given by equations (6-20)–(6-22). The parameter vector is given by $\boldsymbol{\theta} = (k_{21}, k_{31}, k_{12}, k_{14}, k_{03}, k_{43}, k_{34})^{\mathrm{T}}$.

Here the transfer function method is used [19]. To apply this approach the system described by equations (6-20)–(6-22) is re-written in vector-matrix notation as

$$\begin{aligned} \dot{\boldsymbol{x}}_{\mathrm{T}}(t, \boldsymbol{\theta}) &= \boldsymbol{A}(\boldsymbol{\theta})\boldsymbol{x}_{\mathrm{T}}(t) + \boldsymbol{B}(\boldsymbol{\theta})u(t) \\ \boldsymbol{x}_{\mathrm{T}}(0, \boldsymbol{\theta}) &= 0 \\ \boldsymbol{y}(t, \boldsymbol{\theta}) &= \boldsymbol{C}(\boldsymbol{\theta})\boldsymbol{x}_{\mathrm{T}}(t), \end{aligned} \tag{6-33}$$

where $\boldsymbol{x}_{\mathrm{T}}(t) = \big(x_{1,\mathrm{T}}(t), x_{2,\mathrm{T}}(t), x_{3,\mathrm{T}}(t), x_{4,\mathrm{T}}(t)\big)^{\mathrm{T}}$ and $\boldsymbol{y}(t, \boldsymbol{\theta}) = \big(y_1(t, \boldsymbol{\theta}), y_2(t, \boldsymbol{\theta})\big)^{\mathrm{T}}$ are column vectors representing the state and the observation, respectively. $u(t)$ represents the single input to the system, an impulse at time $t = 0$, given by $u(t) = \delta(t)$. $\boldsymbol{A}(\boldsymbol{\theta})$ is a 4×4 matrix, $\boldsymbol{C}(\boldsymbol{\theta})$ is a 2×4 matrix and $\boldsymbol{B}(\boldsymbol{\theta})$ is a column vector. $\boldsymbol{A}(\boldsymbol{\theta})$, $\boldsymbol{B}(\boldsymbol{\theta})$ and $\boldsymbol{C}(\boldsymbol{\theta})$ are given by

$$\begin{aligned} \boldsymbol{A}(\boldsymbol{\theta}) &= \begin{pmatrix} -(k_{21}+k_{31}) & k_{12} & 0 & k_{14} \\ k_{21} & -k_{12} & 0 & 0 \\ k_{31} & 0 & -(k_{03}+k_{43}) & k_{34} \\ 0 & 0 & k_{43} & -(k_{14}+k_{34}) \end{pmatrix}, \\ \boldsymbol{B}(\boldsymbol{\theta}) &= \begin{pmatrix} D \\ 0 \\ 0 \\ 0 \end{pmatrix}, \boldsymbol{C}(\boldsymbol{\theta}) = \begin{pmatrix} \frac{1}{D} & 0 & 0 & 0 \\ \frac{1}{D} & \frac{1}{D} & \frac{1}{D} & \frac{1}{D} \end{pmatrix}. \end{aligned} \tag{6-34}$$

Note that the administration of a bolus dose is now represented as an impulse at time $t = 0$, rather than a non-zero initial condition, such that $\boldsymbol{x}_{\mathrm{T}}(0, \boldsymbol{\theta}) = (0, 0, 0, 0)^{\mathrm{T}}$.

Taking Laplace transforms of equations (6-33), the input-output relation is given by $\boldsymbol{Y}(s) = \boldsymbol{G}(s)U(s)$, where $\boldsymbol{G}(s)$ is the transfer function matrix, given by $\boldsymbol{G}(s) = \boldsymbol{C}(\boldsymbol{\theta})(s\boldsymbol{I} -$

$\boldsymbol{A}(\boldsymbol{\theta}))^{-1}\boldsymbol{B}(\boldsymbol{\theta})$, where $\boldsymbol{I}$ is the 4×4 identity matrix. $\boldsymbol{G}(s)$ has two elements, corresponding to the two observed outputs, which are given by

$$\begin{aligned} G_1(s) &= \frac{\phi_1 + \phi_2 s + \phi_3 s^2 + s^3}{\phi_4 + \phi_5 s + \phi_6 s^2 + \phi_7 s^3 + s^4} \\ G_2(s) &= \frac{\phi_8 + \phi_9 s + \phi_{10} s^2 + s^3}{\phi_{11} + \phi_{12} s + \phi_{13} s^2 + \phi_{14} s^3 + s^4}, \end{aligned} \tag{6-35}$$

where the coefficients of s, $\boldsymbol{\Phi}(\boldsymbol{\theta}) = (\phi_1(\boldsymbol{\theta}), \phi_2(\boldsymbol{\theta}), ..., \phi_{14}(\boldsymbol{\theta}))^{\mathrm{T}}$, are nonlinear expressions in the parameters. The coefficients of s, $\boldsymbol{\Phi}(\boldsymbol{\theta})$, are given by

$$\begin{aligned}
\phi_1(\boldsymbol{\theta}) &= k_{12}\left(k_{03}\left(k_{14}+k_{34}\right)+k_{14}k_{43}\right) \\
\phi_2(\boldsymbol{\theta}) &= k_{03}\left(k_{12}+k_{14}+k_{34}\right)+k_{14}k_{43}+k_{12}\left(k_{14}+k_{34}+k_{43}\right) \\
\phi_3(\boldsymbol{\theta}) &= k_{03}+k_{12}+k_{14}+k_{34}+k_{43} \\
\phi_4(\boldsymbol{\theta}) &= \phi_{11}(\boldsymbol{\theta}) = k_{03}k_{12}k_{31}(k_{14}+k_{34}) \\
\phi_5(\boldsymbol{\theta}) &= \phi_{12}(\boldsymbol{\theta}) = k_{03}((k_{21}+k_{31})(k_{14}+k_{34})+k_{12}(k_{14}+k_{31}+k_{34}))+k_{14}k_{21}k_{43} \\
&\quad + k_{12}(k_{14}(k_{31}+k_{43})+k_{31}(k_{34}+k_{43})) \\
\phi_6(\boldsymbol{\theta}) &= \phi_{13}(\boldsymbol{\theta}) = k_{14}k_{21}+k_{14}k_{31}+k_{21}k_{34}+k_{31}k_{34}+k_{03}(k_{12}+k_{14}+k_{21}+k_{31} \\
&\quad + k_{34})+k_{14}k_{43}+k_{21}k_{43}+k_{31}k_{43}+k_{12}(k_{14}+k_{31}+k_{34}+k_{43}) \\
\phi_7(\boldsymbol{\theta}) &= \phi_{10}(\boldsymbol{\theta}) = \phi_{14}(\boldsymbol{\theta}) = k_{03}+k_{12}+k_{14}+k_{21}+k_{31}+k_{34}+k_{43} \\
\phi_8(\boldsymbol{\theta}) &= k_{03}(k_{12}+k_{21})(k_{14}+k_{34})+k_{14}k_{21}k_{43}+k_{12}(k_{14}(k_{31}+k_{43})+k_{31}(k_{34} \\
&\quad + k_{43})) \\
\phi_9(\boldsymbol{\theta}) &= k_{14}k_{21}+k_{14}k_{31}+k_{21}k_{34}+k_{31}k_{34}+k_{03}(k_{12}+k_{14}+k_{21}+k_{34})+k_{14}k_{43} \\
&\quad + k_{21}k_{43}+k_{31}k_{43}+k_{12}(k_{14}+k_{31}+k_{34}+k_{43}).
\end{aligned} \tag{6-36}$$

The coefficients $\boldsymbol{\Phi}(\boldsymbol{\theta})$ are unique with respect to the input-output relationship represented by the transfer function. Introducing an alternative parameter vector $\bar{\boldsymbol{\theta}} = (\bar{k}_{21}, \bar{k}_{31}, \bar{k}_{12}, \bar{k}_{14}, \bar{k}_{03}, \bar{k}_{43}, \bar{k}_{34})^{\mathrm{T}}$ and equating $\boldsymbol{\Phi}(\boldsymbol{\theta}) = \boldsymbol{\Phi}(\bar{\boldsymbol{\theta}})$, the resulting set of simultaneous equations is solved for $\boldsymbol{\theta}$ using the Solve function in Mathematica [15]. The only solution is $\boldsymbol{\theta} = \bar{\boldsymbol{\theta}}$; therefore all of the parameters in $\boldsymbol{\theta}$ are structurally uniquely identifiable.

6.3.2 The parameter estimation problem

The 'true' parameter vector for an individual is denoted by $\boldsymbol{\theta}_0$. For an individual subject it is assumed that $y_i(t, \boldsymbol{\theta_0}), i = 1, 2$, is observed with error at measurement times $t_1^{(i)}, \ldots, t_{N_i}^{(i)}, i = 1, 2$, where $t_1^{(1)} = t_1^{(2)} = 0$. The observed (with error) values of $y_i(t, \boldsymbol{\theta_0}), i = 1, 2$, are now denoted by $\tilde{y}_i(t_j^{(i)}, \boldsymbol{\theta_0})$ for $i = 1, 2$ and $j = 1, \ldots, N_i$.

Assumptions regarding data generation and collection and the resulting errors are outlined in section 5.5 of chapter 5. The assumptions that applied to the two-compartment model also apply to the four-compartment model; however now $y_1(t)$, $y_2(t)$ and $x_{1,\mathrm{T}}(t)$ are defined by equations (6-20)–(6-22). Where $x_{2,\mathrm{T}}(t)$ appears in sections 5.5.3 and 5.5.4, it is replaced by $x_{2,\mathrm{T}}(t) + x_{3,\mathrm{T}}(t) + x_{4,\mathrm{T}}(t)$ for the four-compartment model.

From section 5.5, it is assumed that observation $\tilde{y}_1(t_j^{(1)}, \boldsymbol{\theta_0})$ has standard deviation proportional to its mean, or a constant coefficient of variation. The standard deviation of $\tilde{y}_2(t_j^{(2)}, \boldsymbol{\theta_0})$ however has a more complex relationship with its mean. It is also assumed that there are systematic errors and autocorrelation between errors present as a result of calculations from raw measurements. Any of the standard estimation methods is strictly not valid due to the presence of systematic errors; therefore when estimating parameter values from the data by any method, it will be necessary to validate the method against synthetic data with known true parameter values.

In section 6.3.3 the parameter vector $\boldsymbol{\theta}$ is estimated for each subject using unweighted least squares, by fitting the timecourse data described in section 5.3 of chapter 5. Unweighted least squares is used initially because it is the simplest method and can be used to investigate whether it is possible to fit the data before refining the error model.

In order to estimate the parameters, it is assumed that the observed measurements for an individual are given by

$$\tilde{y}_i(t_j^{(i)}, \boldsymbol{\theta_0}) = y_i(t_j^{(i)}, \boldsymbol{\theta_0}) + b\epsilon_i(t_j^{(i)}), \qquad j = 1, \ldots, N_i, \qquad i = 1, 2, \tag{6-37}$$

where $\epsilon_i(t_j^{(i)})$ are independent and identically distributed random variables following the normal distribution, $\epsilon(x_{1,\mathrm{E},j}) \sim N(0, 1)$. The standard deviation of the errors is denoted by b. It is assumed that b does not depend on time or on i.

Both outputs y_1 and y_2 were fitted simultaneously, therefore the cost functional for $\boldsymbol{\theta}$ is

Table 6-2 Parameters for differential evolution

	Subject					
	A	B	C	D	F	G
Scaling factor (F)	0.5	0.5	0.7	0.5	0.5	0.7
Crossover probability (CR)	0.9	0.9	0.95	0.9	0.9	0.95

given by

$$J(\boldsymbol{\theta}_0, \boldsymbol{\theta}) = \sum_{i=1}^{2} J_i(\boldsymbol{\theta}_0, \boldsymbol{\theta}), \tag{6-38}$$

where

$$J_i(\boldsymbol{\theta}_0, \boldsymbol{\theta}) = \sum_{j=1}^{N_i} \left(\tilde{y}_i(t_j^{(i)}, \boldsymbol{\theta_0}) - y_i(t_j^{(i)}, \boldsymbol{\theta}) \right)^2. \tag{6-39}$$

Since the model parameters can only take positive values it is assumed that $\boldsymbol{\theta}_0, \boldsymbol{\theta} \in \mathbb{R}_+^7$.

6.3.3 Parameter estimation

Differential evolution was implemented using the NonlinearModelFit function in Mathematica [15] to minimise of the cost functional in equation (6-38). The differential evolution algorithm was chosen because there is little information available about the parameters, in particular k_{14}, k_{03}, k_{43} and k_{34}. Differential evolution is a stochastic, global minimisation algorithm that does not require the user to specify initial guesses for the parameter values [20]. All parameters were constrained to be positive, by providing the constraints to NonlinearModelFit. The maximum number of iterations was increased up to a maximum of 5000, which was sufficient for the algorithm to converge in all cases. In differential evolution an initial population of parameter vectors is generated randomly. The algorithm was run for each subject's data with integer seeds for the pseudorandom number generator between 1 and 10; thus ten estimates for each parameter were obtained for each subject.

Differential evolution maintains a population of parameter vectors which evolves iteratively. For each new generation of the algorithm, a mutant and trial vector are produced from the current generation and the trial vector is compared with a target vector from the current generation. Either the target or trial vector is selected to move forward to the new generation based on which has the smallest value of the cost function to be

minimised. The scaling factor (F) is used to produce the mutant vector and generally a larger value of F means a broader search of the parameter space. The crossover probability (CR) is the probability that each element of the mutant vector is used to produce the trial vector, rather than the corresponding element of the target vector. F and CR were tuned by trial and error for each subject. The parameters were initially set to $F = 0.5$, as recommended by Storn et al. [20], and $CR = 0.9$, as recommended by Storn et al. [20] for faster convergence. For subjects C and G the algorithm either took a very long time to converge or gave larger residual sums of squares than local methods that were previously tried; therefore the parameters were adjusted to $F = 0.7$, for a broader search of the parameter space, and $CR = 0.95$, to speed convergence.

Differential evolution is a stochastic minimisation method: each run with a unique seed for the pseudorandom number generator can produce unique parameter estimates; it is therefore recommended to perform multiple runs with unique, randomly chosen starting populations of parameter vectors [20]. The parameter estimates and root mean square error (RMSE) for each run and each subject are tabulated in tables 6-3 to 6-5. The parameter estimates from multiple runs should be close to one another so that they can be averaged [20; 21]; however, for the data fitted here, the different runs give very different parameter estimates, implying that the algorithm has difficulty finding the global minimum and that there may be many local minima. It is therefore not certain that the global minimum has been found for each subject. It is also likely that certain parameters are highly correlated, such that different parameter vectors produce very similar model outputs. This is reflected in the diversity of parameter vectors obtained within subjects using differential evolution.

In some cases parameters are estimated to be zero, or very close to zero, for example k_{34} for subject B, k_{12} and k_{14} for subject C, k_{34} for subject D, and k_{21} and k_{14} for subject F. For each of these subjects the data can be well represented by a reduced model in which either IgG-FcRn binding is irreversible ($k_{34} = 0$), there is no transfer from the peripheral compartment to plasma ($k_{12} = 0$) or vice versa ($k_{21} = 0$), or bound IgG molecules are not recycled into plasma ($k_{14} = 0$). None of these scenarios is consistent with the biology.

The data and the model outputs using the parameter estimates in tables 6-3 to 6-5 are plotted in figure 6-4. In each panel of figure 6-4, the model outputs $y_1(t)$ and $y_2(t)$ are

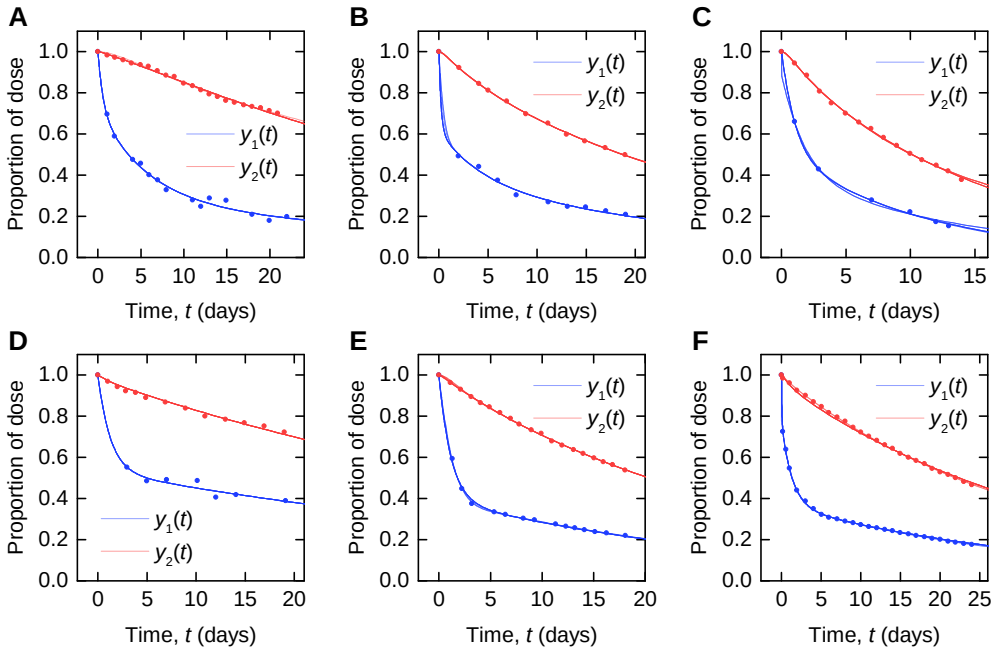

Figure 6-4 Tracer experiment data ($y_1(t)$ blue circles; $y_2(t)$ red circles) and model fits ($y_1(t)$ blue line; $y_2(t)$ red line) for (A–F) subjects A–D, F and G

Table 6-3 Estimated parameter values from multiple runs; subjects A and B

	Run	Parameter							RMSE
		k_{21} (day^{-1})	k_{31} (day^{-1})	k_{12} (day^{-1})	k_{14} (day^{-1})	k_{03} (day^{-1})	k_{43} (day^{-1})	k_{34} (day^{-1})	
Subject A	1	0.39119	0.157878	1.28693	0.0627919	0.260824	1.88308	0.206295	0.0123609
	2	0.390745	0.158698	1.29161	0.0623367	0.29449	2.22981	0.216064	0.01236
	3	0.390487	0.159263	1.29333	0.0616348	0.341147	2.6961	0.224638	0.0123598
	4	0.38958	0.159262	1.28763	0.0612125	0.363375	2.90857	0.227123	0.0123599
	5	0.388328	0.139006	1.10777	0.0698655	0.0880881	0.208648	0.0279417	0.0122732
	6	0.391029	0.159866	1.29897	0.0611406	0.395192	3.24859	0.232921	0.0123601
	7	0.391508	0.159861	1.30286	0.0616297	0.364982	2.95008	0.229264	0.01236
	8	0.386326	0.158598	1.26971	0.0614646	0.327351	2.54105	0.221117	0.0123603
	9	0.390512	0.159204	1.29311	0.0616972	0.336033	2.64455	0.22378	0.0123598
	10	0.389696	0.158633	1.28534	0.0619406	0.307191	2.34694	0.217706	0.0123599
Subject B	1	1.71644	0.174093	2.95564	0.151315	1.04088	1.22565	1.0875×10^{-16}	0.00858265
	2	0.100606	0.731658	0.14714	3.18125	0.208244	1.7168	0.	0.00858943
	3	0.0986298	1.09096	0.146438	2.48661	0.408062	20.1932	7.16228	0.00864507
	4	1.734	0.174091	2.98353	0.151317	1.04436	1.22956	0.	0.00858265
	5	1.71644	0.174093	2.95564	0.151315	1.04088	1.22565	0.	0.00858265
	6	1.71644	0.174093	2.95564	0.151315	1.04088	1.22565	0.	0.00858265
	7	1.71644	0.174093	2.95564	0.151315	1.04088	1.22565	0.	0.00858265
	8	1.71644	0.174093	2.95564	0.151315	1.04088	1.22565	$3.688\,03 \times 10^{-15}$	0.00858265
	9	0.100606	0.731658	0.14714	3.18125	0.208244	1.7168	0.	0.00858943
	10	1.71619	0.174078	2.95504	0.151295	1.04094	1.22553	0.	0.00858265

Table 6-4 Estimated parameter values from multiple runs; subjects C and D

	Run	Parameter							RMSE
		k_{21} (day^{-1})	k_{31} (day^{-1})	k_{12} (day^{-1})	k_{14} (day^{-1})	k_{03} (day^{-1})	k_{43} (day^{-1})	k_{34} (day^{-1})	
Subject C	1	0.0217371	0.438343	6.4685×10^{-16}	0.527361	0.580325	2.10374	0.331603	0.00681915
	2	0.346192	0.159615	0.536837	0.	1.3126	0.446687	0.0880231	0.00552995
	3	0.0217371	0.438343	$9.748\,08 \times 10^{-15}$	0.527361	0.580325	2.10374	0.331603	0.00681915
	4	1104.9	0.349394	8586.71	0.2537	0.764531	1.72415	0.140787	0.00780007
	5	0.346192	0.159615	0.536837	$2.807\,85 \times 10^{-16}$	1.3126	0.446687	0.0880231	0.00552995
	6	202.854	0.349347	1576.2	0.253697	0.764203	1.72264	0.140666	0.00780007
	7	0.0217371	0.438343	$1.509\,99 \times 10^{-16}$	0.527361	0.580325	2.10374	0.331603	0.00681915
	8	0.0217371	0.438343	$4.653\,98 \times 10^{-15}$	0.527361	0.580325	2.10374	0.331603	0.00681915
	9	284.447	0.349385	2210.37	0.253656	0.765017	1.72557	0.140863	0.00780007
	10	0.0217371	0.438343	$2.747\,36 \times 10^{-15}$	0.527361	0.580325	2.10374	0.331603	0.00681915
Subject D	1	0.346344	0.153825	0.432311	$2.732\,79 \times 10^{7}$	20.3408	80.1561	0.0549054	0.0136333
	2	0.346115	1.50133	0.432278	1.4454×10^{9}	15.3493	725.205	68.6663	0.0136105
	3	0.345524	0.15922	0.432213	$4.845\,87 \times 10^{16}$	9.08349	37.3264	94575.2	0.0136749
	4	0.345826	0.172752	0.432204	$1.985\,65 \times 10^{7}$	11.5164	52.3632	1183.85	0.0136546
	5	0.346178	0.102262	0.431988	$2.121\,37 \times 10^{17}$	22.1847	50.6702	0.	0.0136437
	6	0.343936	1.94633	0.432605	$1.157\,36 \times 10^{7}$	3.89904	239.768	207.839	0.0136425
	7	0.345699	0.0999169	0.431651	1.2234×10^{6}	15.4357	34.0737	3.06844	0.0136652
	8	0.345878	0.950743	0.432202	$2.160\,62 \times 10^{11}$	12.8357	379.272	1705.63	0.0136156
	9	0.133928	0.241859	0.428493	0.434878	5.48696	37.1081	0.	0.0136694
	10	0.34689	0.141799	0.432315	$4.140\,53 \times 10^{8}$	163.322	581.028	0.	0.0136031

Table 6-5 Estimated parameter values from multiple runs; subjects F and G

	Run	Parameter							RMSE
		k_{21} (day^{-1})	k_{31} (day^{-1})	k_{12} (day^{-1})	k_{14} (day^{-1})	k_{03} (day^{-1})	k_{43} (day^{-1})	k_{34} (day^{-1})	
Subject F	1	0.412129	0.116792	0.361135	0.272648	0.994852	1.01853	0.326048	0.00550167
	2	$1.402\,57 \times 10^{-6}$	0.444537	141.642	0.452248	0.148064	0.69255	0.00603218	0.00378963
	3	$2.195\,54 \times 10^{-13}$	0.444528	8.71379	0.452283	0.148045	0.692391	0.00600534	0.00378963
	4	0.454367	0.0795007	0.362001	$7.119\,19 \times 10^{-8}$	4.51354	5.30071	1.10612	0.00549635
	5	0.454351	0.0794952	0.361966	$2.965\,81 \times 10^{-12}$	5.39512	6.75573	1.14185	0.0054954
	6	0.454415	0.07951	0.362082	0.000022722	3.41001	3.51726	1.03978	0.00549893
	7	0.	0.454276	$6.907\,69 \times 10^{7}$	0.418849	0.175345	0.94755	0.0586333	0.00402419
	8	0.454348	0.0795006	0.361985	0.	4.11203	4.66027	1.08929	0.00549701
	9	0.454432	0.0795174	0.362085	0.0000416412	3.21347	3.20078	1.02184	0.00549978
	10	0.45423	0.0794697	0.36176	$5.405\,78 \times 10^{-7}$	51.2404	83.9639	1.30387	0.0054928
Subject G	1	0.455651	4.21715	0.372039	19.2778	0.956271	$1.445\,75 \times 10^{7}$	$5.368\,35 \times 10^{6}$	0.00686157
	2	$1.234\,56 \times 10^{10}$	0.531781	4.2902×10^{10}	0.359708	1692.03	15306.6	0.213966	0.00286239
	3	0.455565	4.21228	0.371993	14.6467	6.23104	$1.205\,04 \times 10^{8}$	$5.223\,45 \times 10^{6}$	0.00686157
	4	0.455598	4.21346	0.372012	17.0521	1.46728	$1.700\,37 \times 10^{7}$	$3.643\,04 \times 10^{6}$	0.00686157
	5	0.455584	4.21184	0.372002	15.4307	2.86613	$1.402\,61 \times 10^{8}$	$1.392\,69 \times 10^{7}$	0.00686157
	6	0.455577	4.2128	0.371991	17.5851	1.28423	$1.538\,39 \times 10^{7}$	$3.884\,15 \times 10^{6}$	0.00686157
	7	0.455807	4.15569	0.372092	47.9845	0.364451	184.906	407.172	0.00686531
	8	0.455568	4.21544	0.371981	16.1167	2.01938	$1.415\,04 \times 10^{7}$	$1.415\,04 \times 10^{7}$	0.00686157
	9	$4.969\,67 \times 10^{8}$	0.531465	$1.726\,38 \times 10^{9}$	0.359917	33602.9	303849.	0.21395	0.00286184
	10	0.455544	4.21255	0.371978	15.6524	2.51039	$1.435\,87 \times 10^{8}$	$1.650\,85 \times 10^{7}$	0.00686157

Table 6-6 Relative standard deviations of parameter estimates obtained from ten runs using differential evolution, for each of the subjects A–D, F and G

Parameter	Relative standard deviation					
	A	B	C	D	F	G
k_{21}	0.00404	0.634	2.18	0.206	0.691	3.03
k_{31}	0.0405	0.905	0.312	1.24	0.907	0.446
k_{12}	0.0458	0.642	2.18	0.00277	3.16	3.03
k_{14}	0.0417	1.38	0.643	2.58	1.33	0.792
k_{03}	0.280	0.461	0.373	1.71	2.12	3.00
k_{43}	0.360	1.85	0.399	1.15	2.32	1.14
k_{34}	0.305	3.16	0.502	3.05	0.758	1.01

plotted for each of the estimated parameter vectors from ten runs. The model outputs are very similar for all of the estimated parameter vectors for an individual. For some subjects there are noticeably different trajectories within the fits, for example: in the first and last five days of $y_2(t)$ for subject A; in the first two days of $y_1(t)$ for subject B; for all of $y_1(t)$ and the latter part of $y_2(t)$ for subject C; between days 2 and 6 for $y_1(t)$ and the initial two days of $y_2(t)$ for subject F; and the first twelve days and final five days of $y_2(t)$ for subject G. The similarity between the outputs for the parameter estimates obtained in different runs is shown by the similar values of RMSE within each subject. The model appears to fit the data reasonably well and in some subjects extremely well.

The results of the multiple runs of differential evolution show that in many cases, highly different parameter vectors can produce very similar model outputs. The spread of the parameter estimates from multiple runs is conveyed using the relative standard deviation, that is, the standard deviation of the estimates of a parameter from ten runs, divided by the mean of those estimates. The relative standard deviations are tabulated in table 6-6. For some parameters and subjects, the estimates for the parameters have a small relative standard deviation, for example the first four parameters for subject A and parameter k_{12} for subject D. In other instances however the relative standard deviation is much larger, reflecting the highly different estimates obtained for these parameters. The similarly high quality fits produced by diverse parameter vectors implies that, whilst the parameters are structurally identifiable, they are not practically identifiable for the quality of data that are available.

It must be noted again that, based on assumptions about the data collection and subsequent calculations, the data do not meet the assumptions on which the parameter estimation method is based. Violation of the assumptions of the estimation method leads to biased parameter estimates with decreased precision [8]. However, if the parameter estimators are insensitive to true parameter values or are highly correlated, this will cause problems in estimating true parameter values regardless of the true error model. It is possible to assess the degree of bias and variability in parameter estimates for various estimation methods based on different assumptions about the error model, by simulating data with plausible parameter values and estimating the parameters from those data; however, given the practical identifiability issue, this approach was not taken.

6.4 Naive pooled approach to parameter identification using fractional catabolic rate data

Authors who have studied a two-compartment model of IgG metabolism have estimated parameters from FCR vs. plasma IgG concentration data [1; 7]. The purpose of this section is to investigate whether it is possible to estimate parameters of the four-compartment model from these data. The data are described in section 5.3 of chapter 5. In section 6.2.4 two expressions for the FCR were introduced: the FCR of the tracer, $\mathrm{FCR_T}$ (6-27), and the FCR of the endogenous IgG in steady state, $\mathrm{FCR_E}$ (6-29). In practice $\mathrm{FCR_T}$ is measured, however it is difficult to obtain a closed form expression for $\mathrm{FCR_T}$. In contrast, we can easily obtain an expression for $\mathrm{FCR_E}$ in terms of the model parameters and the quantity of endogenous IgG in plasma, $x_{1,\mathrm{E}}$, as given by equation (6-29).

$\mathrm{FCR_T}$ and $\mathrm{FCR_E}$ are not equal for this model. $\mathrm{FCR_T}$ vs. $x_{1,\mathrm{E}}$ and $\mathrm{FCR_E}$ vs. $x_{1,\mathrm{E}}$ are plotted alongside one another in figure 6-5A. The difference between $\mathrm{FCR_T}$ and $\mathrm{FCR_E}$ as a proportion of $\mathrm{FCR_T}$ is plotted in figure 6-5B. Both $\mathrm{FCR_E}$ and $\mathrm{FCR_T}$ are evaluated for the parameter values from the literature, given in table 6-1. Since in practice subjects were observed for up to around 25 days, the $\mathrm{FCR_T}$ was calculated at time $t = 10$ days, using

$$\mathrm{FCR_T} = \frac{k_{03} x_{3,\mathrm{T}}(10)}{x_{1,\mathrm{T}}(10)}, \tag{6-40}$$

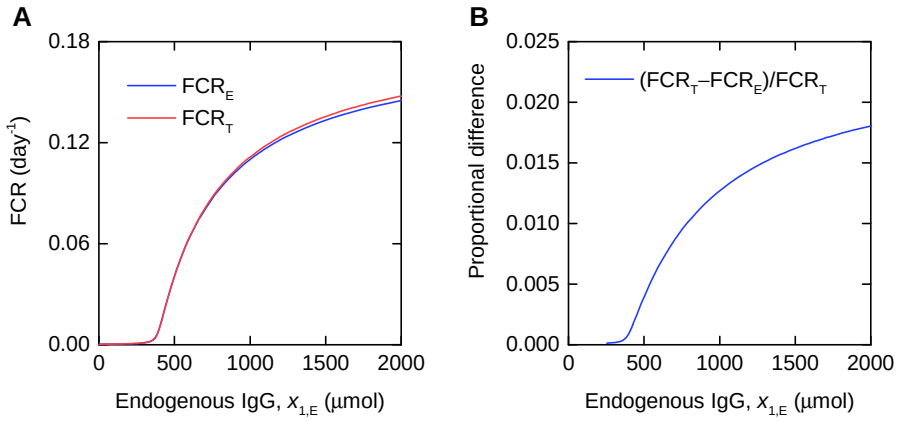

Figure 6-5 (A) Comparison of $\mathrm{FCR_E}$ and $\mathrm{FCR_T}$. (B) The difference between $\mathrm{FCR_T}$ and $\mathrm{FCR_E}$ as a proportion of $\mathrm{FCR_T}$. Both simulations were produced using the literature parameter values in table 6-1.

where $x_{3,\mathrm{T}}(10)$ and $x_{1,\mathrm{T}}(10)$ were obtained by numerically solving the system of equations given by (6-20)–(6-21). The simulation was performed multiple times for values of I_E between 0 and 295 µmol day^{-1}, giving different values of $\mathrm{FCR_T}$. The quantity of endogenous IgG in plasma, $x_{1,\mathrm{E}}$, was calculated from equation (6-2) for each value of I_E. For the particular parameter values used, the difference between $\mathrm{FCR_T}$ and $\mathrm{FCR_E}$ is within 2% of the true value of $\mathrm{FCR_T}$. In this section model parameters are estimated by fitting the expression for $\mathrm{FCR_E}$ vs. $x_{1,\mathrm{E}}$ (6-29) to the $\mathrm{FCR_T}$ vs. $x_{1,\mathrm{E}}$ data. $\mathrm{FCR_T}$ is simulated for the estimated parameter values, in order to assess the difference between $\mathrm{FCR_T}$ and $\mathrm{FCR_E}$.

6.4.1 Structural identifiability analysis

The relationship between $\mathrm{FCR_E}$ and $x_{1,\mathrm{E}}$ is given by equation (6-29). Given that the parameters k_{on} and v_3 only appear in the model equations (6-7) as the ratio k_{on}/v_3, we re-write equation (6-29), defining $\phi_1 = k_{\mathrm{on}}/v_3$, giving

$$\mathrm{FCR_E} = \frac{1}{2\phi_1 x_{1,\mathrm{E}}}\Bigg(k_{31}\phi_1 x_{1,\mathrm{E}} - k_{14}\phi_1 R_{\mathrm{tot}} - k_{03}k_{14} - k_{03}k_{\mathrm{off}} + \sqrt{4k_{03}k_{31}\left(k_{14}+k_{\mathrm{off}}\right)\phi_1 x_{1,\mathrm{E}} + \left(-k_{31}\phi_1 x_{1,\mathrm{E}} + k_{14}\phi_1 R_{\mathrm{tot}} + k_{03}\left(k_{14}+k_{\mathrm{off}}\right)\right)^2}\Bigg). \tag{6-41}$$

We wish to know whether the parameter vector $\boldsymbol{\phi} = (\phi_1, k_{31}, k_{14}, R_{\mathrm{tot}}, k_{03}, k_{\mathrm{off}})$ is structurally identifiable with respect to the relationship in equation (6-41). The structural

identifiability problem amounts to determining whether there exists an alternative parameter vector $\overline{\boldsymbol{\phi}} = \left(\bar{\phi}_1, \bar{k}_{31}, \bar{k}_{14}, \overline{R}_{\text{tot}}, \bar{k}_{03}, \bar{k}_{\text{off}}\right)$ such that $\text{FCR}_\text{E}(x_{1,\text{E}}, \boldsymbol{\phi}) = \text{FCR}_\text{E}(x_{1,\text{E}}, \overline{\boldsymbol{\phi}})$.

From equations (6-28) and (6-2)

$$\text{FCR}_\text{E} = \frac{I_0}{\hat{x}_1}. \tag{6-42}$$

I_0 is given in terms of $\hat{x}_1$ by the solution of the following quadratic equation, obtained by rearranging the first equation of (6-2) and setting $\phi_1 = k_{\text{on}}/v_3$:

$$-\phi_1 I_0^2 + \left(-k_{03}(k_{14}+k_{\text{off}}) + \phi_1(k_{31}\hat{x}_1 - k_{14}R_{\text{tot}})\right) I_0 + k_{03}k_{31}(k_{14}+k_{\text{off}})\hat{x}_1 = 0. \tag{6-43}$$

Substituting $\text{FCR}_\text{E}\hat{x}_1$ in place of I_0 and setting $\hat{x}_1 = x_{1,\text{E}}$ gives the following quadratic equation in FCR_E:

$$\begin{aligned}-\phi_1 x_{1,\text{E}}^2\text{FCR}_\text{E}^2 + \left(-k_{03}(k_{14}+k_{\text{off}}) + \phi_1(k_{31}x_{1,\text{E}} - k_{14}R_{\text{tot}})\right) x_{1,\text{E}}\text{FCR}_\text{E} \\ +k_{03}k_{31}(k_{14}+k_{\text{off}})x_{1,\text{E}} = 0.\end{aligned} \tag{6-44}$$

Dividing (6-44) throughout by the coefficient of FCR_E^2 gives

$$\text{FCR}_\text{E}^2 + \left(\frac{k_{03}\left(k_{14}+k_{\text{off}}\right) - k_{31}\phi_1 x_{1,\text{E}} + k_{14}\phi_1 R_{\text{tot}}}{\phi_1 x_{1,\text{E}}}\right)\text{FCR}_\text{E} - \frac{k_{03}k_{31}\left(k_{14}+k_{\text{off}}\right)}{\phi_1 x_{1,\text{E}}} = 0. \tag{6-45}$$

The expression for FCR_E given by equation (6-41) is one of the two solutions of equation (6-45). We therefore wish to know whether there exists an alternative parameter vector $\overline{\boldsymbol{\phi}}$ such that:

$$\begin{aligned}&\text{FCR}_\text{E}^2 + \left(\frac{k_{03}\left(k_{14}+k_{\text{off}}\right) - k_{31}\phi_1 x_{1,\text{E}} + k_{14}\phi_1 R_{\text{tot}}}{\phi_1 x_{1,\text{E}}}\right)\text{FCR}_\text{E} - \frac{k_{03}k_{31}\left(k_{14}+k_{\text{off}}\right)}{\phi_1 x_{1,\text{E}}} \\ &= \text{FCR}_\text{E}^2 + \left(\frac{\bar{k}_{03}\left(\bar{k}_{14}+\bar{k}_{\text{off}}\right) - \bar{k}_{31}\bar{\phi}_1 x_{1,\text{E}} + \bar{k}_{14}\bar{\phi}_1\overline{R}_{\text{tot}}}{\bar{\phi}_1 x_{1,\text{E}}}\right)\text{FCR}_\text{E} - \frac{\bar{k}_{03}\bar{k}_{31}\left(\bar{k}_{14}+\bar{k}_{\text{off}}\right)}{\bar{\phi}_1 x_{1,\text{E}}}.\end{aligned} \tag{6-46}$$

The coefficients of the quadratic in (6-45) are unique, therefore the problem amounts to solving the simultaneous equations:

$$\begin{aligned}\frac{k_{03}\left(k_{14}+k_{\text{off}}\right) - k_{31}\phi_1 x_{1,\text{E}} + k_{14}\phi_1 R_{\text{tot}}}{\phi_1 x_{1,\text{E}}} &= \frac{\bar{k}_{03}\left(\bar{k}_{14}+\bar{k}_{\text{off}}\right) - \bar{k}_{31}\bar{\phi}_1 x_{1,\text{E}} + \bar{k}_{14}\bar{\phi}_1\overline{R}_{\text{tot}}}{\bar{\phi}_1 x_{1,\text{E}}} \\ -\frac{k_{03}k_{31}\left(k_{14}+k_{\text{off}}\right)}{\phi_1 x_{1,\text{E}}} &= -\frac{\bar{k}_{03}\bar{k}_{31}\left(\bar{k}_{14}+\bar{k}_{\text{off}}\right)}{\bar{\phi}_1 x_{1,\text{E}}}.\end{aligned} \tag{6-47}$$

The solution was found using the SolveAlways function in Mathematica. The only solution to equation (6-47), for all values of $x_{1,\mathrm{E}}$, is given by

$$\begin{aligned} \bar{k}_{31} &= k_{31} \\ \bar{k}_{14}\bar{R}_{\mathrm{tot}} &= k_{14}R_{\mathrm{tot}} \\ \frac{\bar{k}_{03}\left(\bar{k}_{14}+\bar{k}_{\mathrm{off}}\right)}{\bar{\phi}_1} &= \frac{k_{03}\left(k_{14}+k_{\mathrm{off}}\right)}{\phi_1}. \end{aligned} \tag{6-48}$$

Therefore the parameter k_{31} and the expressions $k_{14}R_{\mathrm{tot}}$ and $k_{03}\left(k_{14}+k_{\mathrm{off}}\right)/\phi_1$ are structurally identifiable with respect to the relationship between $\mathrm{FCR_E}$ and $x_{1,\mathrm{E}}$.

6.4.2 Parameter estimation

Having analysed the structural identifiability of the expression for $\mathrm{FCR_E}$ vs. $x_{1,\mathrm{E}}$, it becomes clear that we can rewrite the expression by combining parameters into structurally identifiable parameter combinations, as follows:

$$\begin{aligned} \mathrm{FCR_E}(x_{1,\mathrm{E}},\boldsymbol{\psi}) = \frac{1}{2x_{1,\mathrm{E}}}\Bigg(& k_{31}x_{1,\mathrm{E}} - \psi_1 - \psi_2 \\ &+ \sqrt{k_{31}^2x_{1,\mathrm{E}}^2 + 2k_{31}x_{1,\mathrm{E}}\left(\psi_1-\psi_2\right) + \left(\psi_1+\psi_2\right)^2}\Bigg), \end{aligned} \tag{6-49}$$

where

$$\begin{aligned} \psi_1 &= \frac{k_{03}v_3\left(k_{14}+k_{\mathrm{off}}\right)}{k_{\mathrm{on}}} \\ \psi_2 &= k_{14}R_{\mathrm{tot}} \end{aligned} \tag{6-50}$$

are uniquely identifiable parameter combinations. ψ_1 and ψ_2 have units of $\mu\mathrm{mol\,day^{-1}}$. The parameter vector to be estimated is now $\boldsymbol{\psi} = (k_{31}, \psi_1, \psi_2)$.

It is assumed that (6-49) is a close approximation to the relationship between the measured $\mathrm{FCR_T}$ and $x_{1,\mathrm{E}}$. The 'true' or 'nominal' parameter vector is denoted by $\boldsymbol{\psi}_0$. It is assumed that $\mathrm{FCR_E}(x_{1,\mathrm{E}},\boldsymbol{\psi}_0)$ is observed with error for values of $x_{1,\mathrm{E}}$ given by $x_{1,\mathrm{E},0},\ldots,x_{1,\mathrm{E},N}$. It is thus assumed that the observed measurements are given by

$$Y_{\mathrm{FCR}}(x_{1,\mathrm{E},j},\boldsymbol{\psi}_0) = \mathrm{FCR_E}(x_{1,\mathrm{E},j},\boldsymbol{\psi}_0) + b\epsilon(x_{1,\mathrm{E},j}), \qquad j=1,\ldots,N, \tag{6-51}$$

where $\epsilon(x_{1,\mathrm{E},j})$ are independent and identically distributed random variables following the normal distribution, $\epsilon(x_{1,\mathrm{E},j}) \sim N(0,1)$. The standard deviation of the errors is denoted by b. It is assumed that b does not depend on $x_{1,\mathrm{E}}$.

Table 6-7 Parameter estimates from fitting $\mathrm{FCR_E}$ expression to $\mathrm{FCR_T}$ vs. $x_{1,\mathrm{E}}$ data

Parameter	Units	Estimate	Standard error	95% confidence interval
ψ_1	$\mu\mathrm{mol\,day^{-1}}$	7.46556	2.73608	$(1.92666, 13.0045)$
ψ_2	$\mu\mathrm{mol\,day^{-1}}$	25.729	6.65578	$(12.255, 39.2029)$
k_{31}	$\mathrm{day^{-1}}$	0.15419	0.00969072	$(0.134572, 0.173808)$

Parameters values were estimated using unweighted least squares, by numerically minimising the cost functional

$$J(\boldsymbol{\psi}_0, \boldsymbol{\psi}) = \sum_{j=1}^{N} \left(Y_{\mathrm{FCR}}(x_{1,\mathrm{E},j}, \boldsymbol{\psi}_0) - \mathrm{FCR_E}(x_{1,\mathrm{E},j}, \boldsymbol{\psi}) \right)^2 . \tag{6-52}$$

The estimated parameters were constrained to be positive: $\boldsymbol{\psi}_0, \boldsymbol{\psi} \in \mathbb{R}^3_+$.

Waldmann et al. [7] provide $\mathrm{FCR_T}$ vs. plasma IgG concentration data. The plasma concentrations of endogenous IgG were multiplied by the average plasma volume v_1, from table 6-1, in order to obtain the quantity of endogenous IgG in plasma, $x_{1,\mathrm{E}}$. The data for $\mathrm{FCR_T}$ vs. $x_{1,\mathrm{E}}$ were then fitted using the interior point algorithm implemented within the NonlinearModelFit function in Mathematica. The starting value for the minimisation was set to 1 for each parameter. To verify that the estimates were insensitive to the starting values, the parameters were also estimated using the differential evolution algorithm, with ten different seeds for the random number generator, to find the global minimum of the residual sum of squares. The parameter estimates for each method were equal to at least four significant figures and the residual sums of squares were equal to six significant figures.

The parameter estimates and their standard errors are provided in table 6-7. The fitted expression given by (6-49) is plotted alongside the data in figure 6-6A. The residuals vs. the fitted values are plotted in figure 6-6B. On inspection, the model appears to fit the data well. The residuals appear reasonably homoscedastic and there is no obvious autocorrelation. The parameter correlation matrix is given by

$$\begin{array}{c} \\ \psi_1 \\ \psi_2 \\ k_{31} \end{array} \begin{array}{c} \begin{array}{ccc} \psi_1 & \psi_2 & k_{31} \end{array} \\ \begin{pmatrix} 1. & 0.886758 & 0.626202 \\ 0.886758 & 1. & 0.868569 \\ 0.626202 & 0.868569 & 1. \end{pmatrix} \end{array} .$$

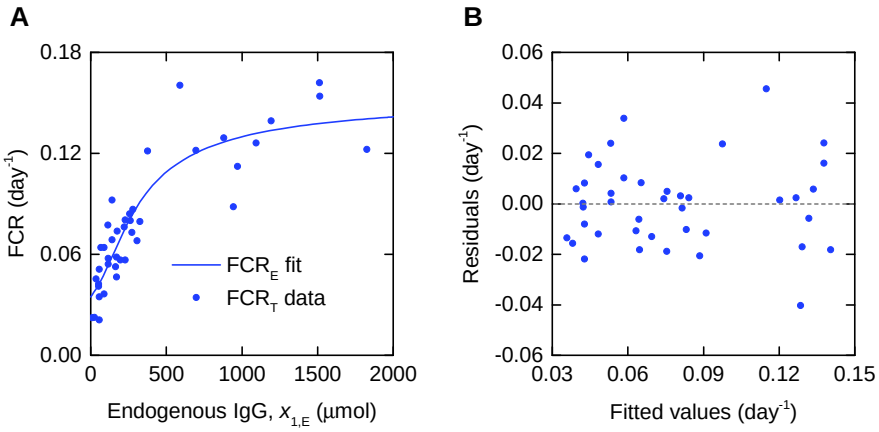

Figure 6-6 (A) Expression for $\mathrm{FCR_E}$ vs. $x_{1,\mathrm{E}}$, given by equation (6-49), fitted to $\mathrm{FCR_T}$ vs. $x_{1,\mathrm{E}}$ data from Waldmann et al. [7]. (B) Residuals vs. fitted values.

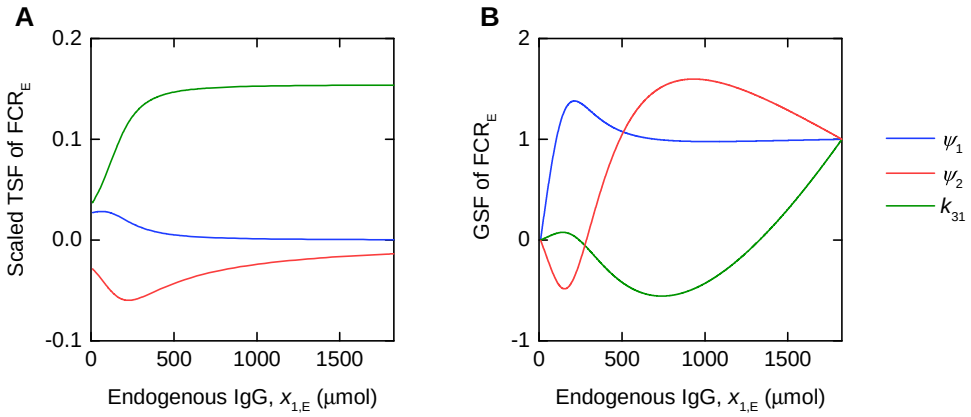

Figure 6-7 (A) Scaled traditional sensitivity functions (TSFs) and (B) generalised sensitivity functions for $\mathrm{FCR_E}$ vs. $x_{1,\mathrm{E}}$, evaluated for the parameter values estimated in section 6.4.2 and provided in table 6-7

6.4.3 Sensitivity analysis

We now consider a hypothetical problem in which we know the true parameter vector $\boldsymbol{\psi}_0$ and investigate the sensitivity of the output $\mathrm{FCR_E}(x_{1,\mathrm{E}}, \boldsymbol{\psi})$ to the elements of $\boldsymbol{\psi}$, when $\boldsymbol{\psi} = \boldsymbol{\psi}_0$. It is assumed that the true parameter vector is given by those values estimated in the previous section, such that $\boldsymbol{\psi}_0 = (7.46556, 25.729, 0.15419)$. It is assumed that measurements are available on the interval $\left[x_{1,\mathrm{E},1}, x_{1,\mathrm{E},N}\right] = [10, 1826]$, reflecting the range of values of $x_{1,\mathrm{E}}$ that are available in the real data.

The traditional sensitivity function (TSF) of $\mathrm{FCR_E}(x_{1,\mathrm{E}}, \boldsymbol{\psi}_0)$ with respect to a parameter

ψ_k, is given by

$$s_{\mathrm{FCR},\psi_k}(x_{1,\mathrm{E}}, \boldsymbol{\psi}_0) = \frac{\partial \mathrm{FCR}_{\mathrm{E}}(x_{1,\mathrm{E}}, \boldsymbol{\psi}_0)}{\partial \psi_k}, \tag{6-53}$$

where $\psi_k, k = 1, \ldots, 3$, are the elements of $\boldsymbol{\psi}$. Due to the different orders of magnitude of the TSFs with respect to the parameters ψ_1, ψ_2 and k_{31}, respectively, each TSF is scaled by the true value of the parameter, giving

$$\tilde{s}_{\mathrm{FCR},\psi_k}(x_{1,\mathrm{E}}, \boldsymbol{\psi}_0) = \frac{\partial \mathrm{FCR}_{\mathrm{E}}(x_{1,\mathrm{E}}, \boldsymbol{\psi}_0)}{\partial \psi_k} \times \psi_{k,0}, \tag{6-54}$$

where $\psi_{k,0}$ is the true value of the parameter ψ_k.

The scaled TSFs, $\tilde{s}_{\mathrm{FCR},\psi_k}(x_{1,\mathrm{E}}, \boldsymbol{\psi}_0)$, of $\mathrm{FCR}_{\mathrm{E}}(x_{1,\mathrm{E}}, \boldsymbol{\psi_0})$ are plotted in figure 6-7A. The scaled TSFs show that the output $\mathrm{FCR}_{\mathrm{E}}(x_{1,\mathrm{E}}, \boldsymbol{\psi}_0)$ is only sensitive to the parameter ψ_1 for small values of $x_{1,\mathrm{E}}$, implying that measurements on a subinterval of $x_{1,\mathrm{E}}$ close to zero are important for estimating this parameter. $\mathrm{FCR}_{\mathrm{E}}(x_{1,\mathrm{E}}, \boldsymbol{\psi}_0)$ is also more sensitive to the parameter ψ_2 for small values of $x_{1,\mathrm{E}}$, but is less sensitive to k_{31} for small values of $x_{1,\mathrm{E}}$.

Generalised sensitivity functions (GSFs), which better represent correlations between parameters, are plotted in figure 6-7B. In order to plot smooth GSFs which are more easily interpreted, it is assumed that measurements are taken on a uniform sampling grid given by

$$x_{1,\mathrm{E},j} = j + 9, \qquad j = 1, \ldots, N = 1817 \tag{6-55}$$

on the interval $\left[x_{1,\mathrm{E},1}, x_{1,\mathrm{E},N}\right] = [10, 1826]$. The $N \times N$ diagonal matrix D is given by

$$D = \mathrm{diag}\left(\frac{1}{\sigma^2}, \ldots, \frac{1}{\sigma^2}\right), \tag{6-56}$$

where $\sigma^2 = 0.000281693$ is the variance of the residuals obtained by fitting the real data.

The Fisher information matrix $\mathscr{F}_{\mathrm{FCR}}(\boldsymbol{\psi}_0)$ for the model output is given by

$$\mathscr{F}_{\mathrm{FCR}}(\boldsymbol{\psi}_0) = (\mathcal{D}_{\boldsymbol{\psi}} \boldsymbol{F}_{\mathrm{FCR}}(\boldsymbol{\psi}_0))^{\mathrm{T}} D \mathcal{D}_{\boldsymbol{\psi}} \boldsymbol{F}_{\mathrm{FCR}}(\boldsymbol{\psi}_0), \tag{6-57}$$

where $\boldsymbol{F}_{\mathrm{FCR}}(\boldsymbol{\psi}_0) = (\mathrm{FCR}_{\mathrm{E}}(x_{1,\mathrm{E},1}, \boldsymbol{\psi}_0), \ldots, \mathrm{FCR}_{\mathrm{E}}(x_{1,\mathrm{E},N}, \boldsymbol{\psi}_0))^{\mathrm{T}}$ is the column vector of model outputs.

The generalised sensitivity matrix for one observation function [22] is given by

$$\mathscr{G}(x_{1,\mathrm{E},j}, \boldsymbol{\psi}_0) = \mathscr{F}(\boldsymbol{\psi}_0)^{-1} \mathscr{F}^{(j)}(\boldsymbol{\psi}_0), \qquad j = 1, \ldots, N, \tag{6-58}$$

where $\mathscr{F}(\boldsymbol{\psi}_0)$ is the Fisher information matrix for the parameter estimation problem and $\mathscr{F}^{(j)}(\boldsymbol{\psi}_0)$ is the Fisher information matrix for the parameter estimation problem where only measurements up to $x_{1,\mathrm{E},j}$ are available. The diagonal elements of $\mathscr{G}(x_{1,\mathrm{E},j}, \boldsymbol{\psi}_0)$ are the GSFs with respect to each parameter ψ_k in $\boldsymbol{\psi}$, which are denoted by

$$g_{\psi_k}(x_{1,\mathrm{E},j}, \boldsymbol{\psi}_0) = \mathscr{G}(x_{1,\mathrm{E},j}, \boldsymbol{\psi}_0)_{(k,k)}, \qquad k = 1, \ldots, 3. \tag{6-59}$$

The GSFs as defined by equations (6-55)–(6-59) are plotted in figure 6-7B. The GSFs show that the interval on which measurements are available can be divided into three subintervals corresponding to each parameter. The information on the parameters ψ_1, ψ_2 and k_{31}, respectively, is available on the approximate subintervals $[10, 200]$, $[200, 800]$ and $[800, 1826]$. The GSFs suggest that it should be possible to estimate the true parameter values, provided that valid assumptions were made and that sufficient data points were available on the subintervals identified.

6.4.4 Comparison of endogenous IgG and tracer fractional catabolic rates for estimated parameter values

It is important to recall that the $\mathrm{FCR_E}$ as defined by equations (6-29) and (6-49) is not measured in practice. By definition, measuring $\mathrm{FCR_E}$ requires measurement of the quantities of IgG in plasma and unbound in endosomes in steady state, along with knowledge of the value of the parameter k_{03} (see equation (6-28)). Assuming the endogenous IgG is in steady state, it is possible to measure the steady state quantity of IgG in plasma, $\hat{x}_1$, however to the author's knowledge it is not practically feasible to obtain $\hat{x}_3$ as intracellular endosomes are not easily accessible to measurement. Since it is difficult to obtain a closed form expression for $\mathrm{FCR_T}$, the $\mathrm{FCR_E}$ expression was fitted to the $\mathrm{FCR_T}$ vs. $x_{1,\mathrm{E}}$ data.

In figure 6-5, $\mathrm{FCR_E}$ and $\mathrm{FCR_T}$ are plotted using the parameter values from the literature; however, having fitted the real $\mathrm{FCR_T}$ data, it is clear that the parameter values from the literature do not fit the data well. It is possible that, for the parameter values estimated in section 6.4.2, the difference between $\mathrm{FCR_E}$ and $\mathrm{FCR_T}$ is large; therefore in this section the plot in figure 6-5B is reproduced for the parameter values estimated in section 6.4.2. $\mathrm{FCR_E}$ was calculated from equation (6-29). $\mathrm{FCR_T}$ was calculated from equation (6-40),

as described at the beginning of section 6.4. $\mathrm{FCR_T}$ cannot be defined by the parameters k_{31}, ψ_1 and ψ_2 alone: firstly, the solution of equations (6-20)–(6-22) requires the additional parameters k_{21} and k_{12}; secondly, ψ_1 and ψ_2 do not provide values for the individual parameters k_{03}, R_{tot}, k_{off}, k_{14} and k_{on}/v_3.

Parameter vectors which satisfy $\psi_1 = 7.46556\ \mu\mathrm{mol\,day^{-1}}$ and $\psi_2 = 25.729\ \mu\mathrm{mol\,day^{-1}}$ can be found by fixing three parameters (not including both R_{tot} and k_{14}) out of k_{03}, R_{tot}, k_{off}, k_{14} and k_{on}/v_3, yielding a linear system of two equations and two unknowns. Equation (6-50) is then solved for the remaining two parameters. Three parameters of k_{03}, R_{tot}, k_{off}, k_{14} and k_{on}/v_3 were fixed to randomly generated values and the remaining two calculated. Each value was generated by assuming a lognormal distribution, in order to ensure positivity, with median given by the parameter value from the literature, given in table 6-1, and variance 1. Random values for k_{21} and k_{12} were also generated in this way. k_{31} was set to the estimated value in table 6-7. There are seven sets of three parameters from k_{03}, R_{tot}, k_{off}, k_{14} and k_{on}/v_3, which can be fixed to give the remaining two parameters. Parameters were generated ten times for each of these seven sets, giving seventy parameter vectors in total, which are tabulated in tables 6-8 to 6-11. The parameters which were not randomly generated are labelled with an asterisk ($*$). For each of the parameter vectors, the parameters estimated in section 6.4.2 are equal to their estimated values: $(\psi_1, \psi_2, k_{31}) = (7.46556, 25.729, 0.15419)$.

In figure 6-8, both $\mathrm{FCR_E}$ and $\mathrm{FCR_T}$ are plotted for the parameter vectors in tables 6-8 to 6-11. In each of the seven plots, a different set of parameters was randomly generated and the remaining parameters calculated. The difference between $\mathrm{FCR_T}$ and $\mathrm{FCR_E}$ is highly dependent on the parameter values. Whilst it may be possible to estimate the parameters $\psi_1 = k_{03}v_3\left(k_{14} + k_{\mathrm{off}}\right)/k_{\mathrm{on}}$, $\psi_2 = k_{14}R_{\mathrm{tot}}$ and k_{31} by fitting the $\mathrm{FCR_E}$ vs. $x_{1,\mathrm{E}}$ relationship to $\mathrm{FCR_T}$ vs. $x_{1,\mathrm{E}}$ data, individual model parameter values would also need to be known in order to validate the approximation of $\mathrm{FCR_T}$ by $\mathrm{FCR_E}$.

6.5 Conclusions

In this chapter parameter identification for a four-compartment model of IgG metabolism has been investigated, using in vivo human data obtained from tracer experiments and

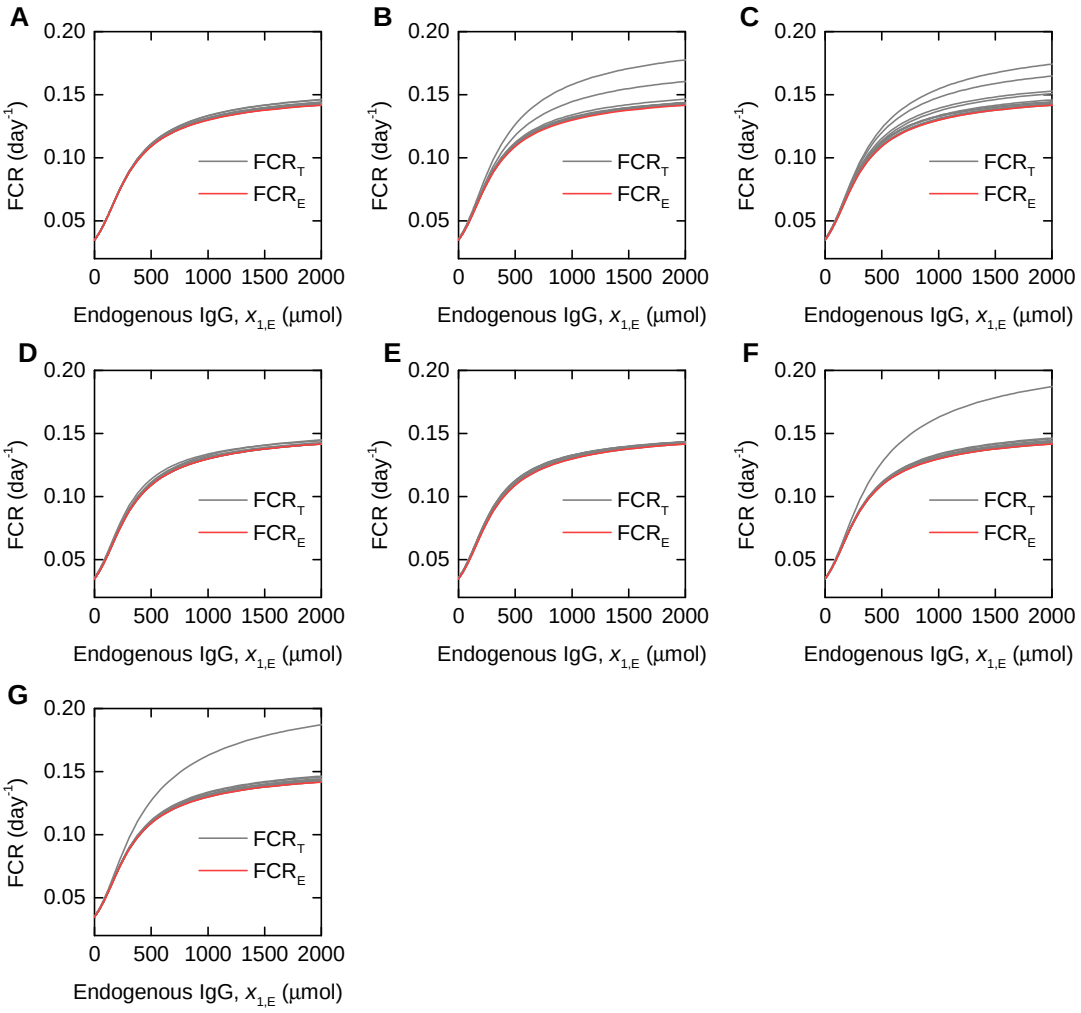

Figure 6-8 FCR_E and FCR_T evaluated for the parameter vectors in (A–B) table 6-8, (C–D) table 6-9, (E–F) table 6-10, and (G) 6-11. The parameter vectors used in panel (A) are labelled A1–A10, and likewise for the other panels.

Table 6-8 Parameters used for comparing FCR_E and FCR_T

	k_{21} (day^{-1})	k_{31} (day^{-1})*	k_{12} (day^{-1})	k_{14} (day^{-1})	k_{03} (day^{-1})	k_{on}/v_3 ($\mu mol^{-1}\,day^{-1}$)*	R_{tot} (µmol)*	k_{off} (day^{-1})
A1	0.1856345921	0.1541900000	0.1097537128	14.95919855	30.82311663	751.3749429	1.719945084	167.0287161
A2	0.4895880322	0.1541900000	1.074255468	19.82491140	3.102060329	18.14343259	1.297811601	23.83990173
A3	0.1435674005	0.1541900000	0.4010150060	2.400327761	16.54449597	2485.765410	10.71895281	1119.279707
A4	0.3864796452	0.1541900000	0.09962847246	3.499839508	0.6765305842	6.474389427	7.351479958	67.94547850
A5	1.716833969	0.1541900000	0.04939591400	1.384847410	4.377473729	26.41884511	18.57894221	43.67115647
A6	0.6758131115	0.1541900000	0.1278125097	9.667682902	3.824106865	101.3775527	2.661340909	188.2452493
A7	0.3206851069	0.1541900000	0.1033674177	3.980573768	1.798150222	11.88590563	6.463641047	45.36732860
A8	2.341018666	0.1541900000	0.8801037899	4.570220219	7.673700016	116.8162923	5.629706835	109.0775687
A9	0.09830406964	0.1541900000	0.1619128974	12.38998997	3.485032976	32.21972227	2.076595709	56.63038129
A10	0.1343257412	0.1541900000	0.3989146114	15.04220163	0.3610727119	2.926553736	1.710454403	45.46739046
	k_{21} (day^{-1})	k_{31} (day^{-1})*	k_{12} (day^{-1})	k_{14} (day^{-1})	k_{03} (day^{-1})	k_{on}/v_3 ($\mu mol^{-1}\,day^{-1}$)	R_{tot} (µmol)*	k_{off} (day^{-1})*
B1	0.6943884374	0.1541900000	0.6209714527	1.613456446	2.895702089	4330.950116	15.94651040	11164.23405
B2	0.4208673089	0.1541900000	0.2467496600	12.86710689	5.270940166	1654.590347	1.999594798	2330.631988
B3	0.6869401743	0.1541900000	0.01468724713	3.773131082	1.742624869	3189.540769	6.819005076	13660.50333
B4	0.3595315002	0.1541900000	0.1535438196	3.170010552	11.62314125	1040.487125	8.116376769	665.1363356
B5	0.4518490717	0.1541900000	0.8449208561	4.991633460	4.417643647	17567.29327	5.154424941	29682.70897
B6	0.1932362745	0.1541900000	0.09794711818	1.964934988	1.888215170	930.8187838	13.09407189	3678.274261
B7	0.5642193322	0.1541900000	0.1850012768	5.507296574	0.9493875002	14421.76604	4.671802155	113400.8306
B8	0.2090607604	0.1541900000	0.7380873774	8.931821715	5.739142103	7772.132214	2.880599369	10101.17145
B9	1.103987485	0.1541900000	0.3118039830	1.734556175	0.9084503385	632.2258592	14.83318925	5193.838482
B10	0.6467637266	0.1541900000	0.1707292613	2.943052822	1.532151189	1356.577960	8.742282778	6607.118821

Table 6-9 Parameters used for comparing FCR_E and FCR_T

	k_{21} (day^{-1})	k_{31} (day^{-1})*	k_{12} (day^{-1})	k_{14} (day^{-1})*	k_{03} (day^{-1})	k_{on}/v_3 ($\mu mol^{-1}\,day^{-1}$)	R_{tot} (µmol)*	k_{off} (day^{-1})
C1	0.1004069159	0.1541900000	0.2135941627	1460.336688	15.05177191	3089.824705	0.01761853977	72.19196518
C2	0.5873451339	0.1541900000	0.1615523506	328.4497418	14.65187750	1195.450685	0.07833466350	280.6673365
C3	0.2829075719	0.1541900000	0.1345545947	1078.454692	4.767150876	933.2375554	0.02385728412	383.0348106
C4	1.975178924	0.1541900000	0.5464299446	10922.21534	1.581068051	2328.372728	0.002355657638	72.00232291
C5	4.652530259	0.1541900000	0.2634046016	122000.4134	2.373034683	38799.33400	0.0002108927281	62.17510883
C6	0.4202074295	0.1541900000	1.391932462	406.3499633	8.628225540	541.1454798	0.06331734299	61.87540110
C7	0.5095934759	0.1541900000	0.2944506661	17240.81092	1.444834913	3465.426860	0.001492331197	665.2847338
C8	0.3740153789	0.1541900000	0.08552095699	6287.928030	4.857029137	4342.562308	0.004091808920	386.8640192
C9	2.955511860	0.1541900000	0.7179231654	67788.99191	0.7877116273	7159.027302	0.0003795453993	60.89886058
C10	1.411376086	0.1541900000	0.5862088346	862.8750460	2.516207642	604.3192635	0.02981775880	930.1334661
	k_{21} (day^{-1})	k_{31} (day^{-1})*	k_{12} (day^{-1})	k_{14} (day^{-1})*	k_{03} (day^{-1})	k_{on}/v_3 ($\mu mol^{-1}\,day^{-1}$)*	R_{tot} (µmol)	k_{off} (day^{-1})
D1	0.6953416343	0.1541900000	0.1480967541	14.57172812	4.138551492	53.65851124	1.765679388	82.22320989
D2	0.1921416066	0.1541900000	0.2766639527	0.9544293027	7.544456560	47.54254062	26.95747074	46.09093265
D3	0.1261409549	0.1541900000	0.05368335660	1.506888773	2.024864366	29.76850170	17.07425289	108.2478875
D4	0.08498647642	0.1541900000	0.2147443285	4.483863783	0.6727814283	4.674721754	5.738131497	47.38947021
D5	0.06372162209	0.1541900000	0.1775017503	0.9455567461	0.3895396600	4.284423911	27.21042402	81.16578403
D6	0.2248886645	0.1541900000	0.1135637469	0.9252852626	3.544196371	53.62932028	27.80655982	112.0404950
D7	1.606231307	0.1541900000	0.7093851811	1.795263795	10.38304041	77.54470049	14.33159855	53.96052559
D8	0.3554974363	0.1541900000	0.5934760799	2.807590666	6.591148559	15.05829607	9.164085176	14.24840675
D9	0.1910162739	0.1541900000	0.08664274150	3.137066577	3.851953137	35.21908301	8.201611082	65.12185766
D10	0.4402451744	0.1541900000	0.3459107874	1.189812915	1.797917569	8.593572477	21.62440807	34.49359773

Table 6-10 Parameters used for comparing FCR_E and FCR_T

	k_{21} (day^{-1})	k_{31} (day^{-1})*	k_{12} (day^{-1})	k_{14} (day^{-1})*	k_{03} (day^{-1})	k_{on}/v_3 ($\mu mol^{-1}\,day^{-1}$)	R_{tot} (µmol)	k_{off} (day^{-1})*
E1	0.3138078505	0.1541900000	1.175442511	1.748916629	0.5413273486	1607.857406	14.71139309	22172.55276
E2	0.1993513894	0.1541900000	2.039783388	1.990790155	0.8608245468	2810.638211	12.92401409	24373.46212
E3	1.479692405	0.1541900000	0.9421116766	0.7721965104	0.7137028436	10405.82200	33.31923889	108847.4539
E4	0.6036061886	0.1541900000	0.8710609460	0.7261548338	15.18549936	14039.52211	35.43183740	6901.443619
E5	1.271117171	0.1541900000	2.789337774	5.492748273	12.61318112	1888.315982	4.684176067	1112.174249
E6	0.3650575250	0.1541900000	0.3086189409	0.4954434537	5.651685939	9954.484398	51.93125433	13148.81988
E7	1.178608732	0.1541900000	24.48785817	6.265789430	4.583971770	9282.806225	4.106266303	15111.92217
E8	0.05137643134	0.1541900000	1.284805476	10.64866561	2.055590318	8028.505703	2.416171278	29147.54035
E9	1.024144690	0.1541900000	0.7682659939	3.470167911	10.04658341	4541.245229	7.414338631	3371.103788
E10	1.237277457	0.1541900000	0.04668542959	2.336393286	16.29472491	777.4977702	11.01227270	353.8804981
	k_{21} (day^{-1})	k_{31} (day^{-1})*	k_{12} (day^{-1})	k_{14} (day^{-1})	k_{03} (day^{-1})*	k_{on}/v_3 ($\mu mol^{-1}\,day^{-1}$)	R_{tot} (µmol)*	k_{off} (day^{-1})
F1	0.4227979497	0.1541900000	0.5847978719	2.175288467	590.0174200	3196.129134	11.82785658	38.26571041
F2	0.4881123798	0.1541900000	1.652660655	67.04644452	100.0399314	2528.777345	0.3837489099	121.6655901
F3	0.7637183865	0.1541900000	1.724180793	2.314080011	4.673562055	478.5463675	11.11845739	762.1171135
F4	0.2176901897	0.1541900000	0.6355392693	1.163775383	220.7883037	5766.184777	22.10821811	193.8094080
F5	2.369273527	0.1541900000	0.4811737286	2.695987864	69.82344860	933.5275171	9.543440585	97.11726729
F6	0.7728110410	0.1541900000	0.1313636229	18.93111429	405.4594059	4289.925975	1.359085345	60.05755708
F7	0.3962002241	0.1541900000	1.511500544	0.5936060006	50.03634540	2357.717632	43.34356454	351.1843327
F8	0.6423813098	0.1541900000	0.09057099241	11.16852970	924.1355728	10491.09504	2.303705205	73.58299573
F9	2.049426746	0.1541900000	1.896558855	2.649676358	87.12501574	1400.131731	9.710242506	117.3246772
F10	0.5225569819	0.1541900000	0.4813453981	2.497344610	137.3366784	6286.402084	10.30254291	339.2286421

Table 6-11 Parameters used for comparing FCR_E and FCR_T

	k_{21} (day^{-1})	k_{31} (day^{-1})*	k_{12} (day^{-1})	k_{14} (day^{-1})*	k_{03} (day^{-1})*	k_{on}/v_3 ($\mu mol^{-1}\,day^{-1}$)	R_{tot} (µmol)	k_{off} (day^{-1})
G1	0.6858589725	0.1541900000	0.7755310870	0.4899032028	58.59066140	2136.674363	52.51853805	271.7628804
G2	0.08521829759	0.1541900000	1.156906451	2.815779948	27.89464102	518.4547255	9.137432780	135.9404370
G3	0.4302125295	0.1541900000	0.5491562190	0.5205815942	1871.149288	8390.147288	49.42356834	32.95464585
G4	0.9412978335	0.1541900000	0.7717423546	4.815221139	181.1848430	1909.147373	5.343264464	73.84949510
G5	0.9133212014	0.1541900000	0.2738199714	0.6612078409	454.6407214	18974.98671	38.91212174	310.9230720
G6	0.2135381053	0.1541900000	0.1857331628	0.7805893660	84.14355890	3767.588162	32.96099220	333.4952107
G7	0.2697199607	0.1541900000	0.5450843786	1.313670204	33.69332961	1189.674114	19.58558542	262.2869766
G8	0.6924590204	0.1541900000	2.208729760	0.7601887407	229.4283338	5541.378783	33.84554206	179.5553595
G9	3.081751624	0.1541900000	0.2649774411	2.122118852	221.4273895	2754.264912	12.12420311	90.73960888
G10	0.5113141025	0.1541900000	0.7624342094	1.868746436	152.6193438	1384.804507	13.76805301	65.87064280

available in the literature. Two observed model outputs were considered: the timecourse of the proportion of a dose of IgG remaining in plasma and in the body of an individual subject; and the FCR vs. the quantity of endogenous IgG in plasma, measured in a cohort of subjects with a range of plasma IgG concentrations. The stability of the model steady state has also been analysed.

In section 6.3 parameters were estimated using data for the timecourse of an administered dose of radiolabelled IgG in plasma and in the body. All parameters of the linearised model were found to be structurally globally identifiable. Whilst the model is capable of fitting the data well, the results of ten runs of differential evolution suggest that the parameter estimates are unstable. Highly different parameter vectors, as illustrated by the relative standard deviations of parameter estimates from ten runs, produce similarly excellent fits to the data. These results suggest that certain parameters are highly correlated and that the available data do not support the complexity of the model.

The structural identifiability of the relationship between $\mathrm{FCR_E}$ and the quantity of endogenous IgG in plasma, $x_{1,\mathrm{E}}$, was analysed. It was found that the parameter k_{31} and parameter combinations $\psi_1 = (k_{03}v_3\,(k_{14} + k_{\mathrm{off}}))/k_{\mathrm{on}}$ and $\psi_2 = k_{14}R_{\mathrm{tot}}$ are structurally globally identifiable. These parameters were estimated using unweighted least squares. Sensitivity analysis, assuming that the estimated parameter values were the known, true parameter values, using TSFs and GSFs, shows that the parameter estimators are sensitive to the true parameter values. The GSFs also highlighted sub-intervals of $x_{1,\mathrm{E}}$ on which additional data points would improve the precision of individual parameter estimates. The parameters k_{31} and ψ_2 have physiological meaning, with k_{31} being the rate at which plasma IgG is internalised into intracellular endosomes, and ψ_2 being the maximal rate of recycling of IgG from endosomes into plasma. The 95% confidence interval for k_{31} (0.135–0.174 day^{-1}) is similar to other values reported in the literature (0.13 day^{-1} [2]; 0.18 day^{-1} [7]) and overlaps with the 95% confidence interval (0.137–0.181 day^{-1}) estimated with respect to the two-compartment model in chapter 5. The 95% confidence interval for ψ_2 (12.3–39.2 $\mu\mathrm{mol\,day}^{-1}$) is considerably smaller than previously reported values (68.6 $\mu\mathrm{mol\,day}^{-1}$ [1]; 103 $\mu\mathrm{mol\,day}^{-1}$ [2]); however it overlaps with the 95% confidence interval (19.1–60.9 day^{-1}) estimated with respect to the two-compartment model in chapter 5.

In applications in which the behaviour of the variables $x_3(t)$ and $x_4(t)$, representing unbound and bound IgG in intracellular endosomes, respectively, are of great importance, clearly parameter values are required which determine this behaviour, including receptor-ligand binding (k_{on}/v_3, k_{off} and R_{tot}), recycling of bound IgGs into plasma (k_{14}) and degradation of unbound IgGs (k_{03}). Unfortunately, the results presented in this chapter suggest that it may not be possible to estimate these parameters from the available data. For example, the data for subject D are fitted well by the model when $k_{34} = k_{\text{off}} = 5.49 \times 10^{-2}$ day^{-1} and 9.46×10^{4} day^{-1}. Similarly, in section 6.4.4, it is shown that the parameters listed above can be varied enormously whilst having a minimal effect on the relationship between the FCR_{T} and $x_{1,\text{E}}$. For investigations limited to behaviour of IgG in plasma, the two-compartment model analysed in chapter 5 may be sufficient. However, the relationship between the four-compartment model and the two-compartment model is not clear and it is not known whether the two models produce equivalent responses in relevant simulations; this will be the subject of chapter 7.

References

1. J. Kim, W. L. Hayton, J. M. Robinson, C. L. Anderson, *Clinical Immunology* **122**, 146–155 (2007).
2. J. G. Hattersley, PhD thesis, University of Warwick, 2009.
3. G. Z. Ferl, A. M. Wu, J. J. DiStefano, *Annals of Biomedical Engineering* **33**, 1640–1652 (2005).
4. S. Urva, V. Yang, J. Balthasar, *Journal of Pharmaceutical Sciences* **99**, 1582–1600 (2010).
5. D. K. Shah, A. M. Betts, *Journal of Pharmacokinetics and Pharmacodynamics* **39**, 67–86 (2012).
6. L. Li, I. Gardner, M. Dostalek, M. Jamei, *The AAPS journal* **16**, 1097–1109 (2014).
7. T. A. Waldmann, W. Strober, *Progress in Allergy* **13**, 1–110 (1969).
8. P. L. Bonate, *Pharmacokinetic-Pharmacodynamic Modeling and Simulation* (Springer, New York, ed. 2, 2011), ISBN: 9781441994851.
9. A. Solomon, T. Waldmann, J. Fahey, *The Journal of Laboratory and Clinical Medicine* **62**, 1–17 (1963).
10. T. A. Waldmann, W. D. Terry, *The Journal of Clinical Investigation* **86**, 2093–2098 (1990).
11. J. G. Hattersley et al., *Computer Methods and Programs in Biomedicine* **109**, 126–133 (2013).
12. R. J. Hansen, J. P. Balthasar, *Journal of Pharmaceutical Sciences* **92**, 1206–1215 (2003).
13. Y. Chen, J. P. Balthasar, *The AAPS Journal* **14**, 850–859 (2012).
14. E. J. Routh, *A Treatise on the Stability of a Given State of Motion: Particularly Steady Motion* (Macmillan, London, ed. 1, 1877).
15. Wolfram Research Inc., *Mathematica Version 11.1*, Champaign, IL, 2017.
16. C. Cobelli, D. Foster, G. Toffolo, *Tracer Kinetics in Biomedical Research* (Springer, New York, ed. 1, 2002), ISBN: 0306468336.
17. F. Kendrick, S. Harding, M. J. Chappell, N. D. Evans, *IFAC-PapersOnLine* **48**, 106–111 (2015).

18. D. H. Anderson, *Compartmental Modeling and Tracer Kinetics* (Springer-Verlag, Berlin Heidelberg, ed. 1, 1983), ISBN: 9783540123033.
19. R. Bellman, K. Åström, *Mathematical Biosciences* **7**, 329–339 (1970).
20. R. Storn, K. Price, *Journal of Global Optimization* **11**, 341–359 (1997).
21. S. Ghosh, *Computers in Biology and Medicine* **46**, 51–60 (2014).
22. K. Thomaseth, C. Cobelli, *Annals of Biomedical Engineering* **27**, 607–616 (1999).

7

Comparison of two- and four-compartment models of immunoglobulin G metabolism

The aim of this chapter is to clarify the relationship between the two models of immunoglobulin G (IgG) metabolism studied in chapters 5 and 6. A derivation of the two-compartment model from the four-compartment model is taken from Hattersley [1] and the assumptions for the derivation are investigated with simulations. Simulations of IgG responses during multiple myeloma are compared for the two respective models, using the parameter values estimated in chapters 5 and 6.

The derivation presented in section 7.1 is reproduced from Hattersley [1]. Section 7.3 summarises the classical Michaelis-Menten approximation for an enzyme reaction, first presented by Michaelis et al. [2]. A similar summary can be found in many biochemistry and mathematical biology texts; an extended mathematical introduction can be found in Murray [3, ch. 6]. The remainder of this chapter comprises original work by the author.

7.1 Derivation of two-compartment model

A derivation of the two-compartment model of IgG metabolism (chapter 5) from the four-compartment model (chapter 6) is provided by Hattersley [1]. Hattersley [1] states:

'if a quasi-steady state assumption is made regarding the bound IgG, namely that the bound IgG dynamics are much faster than the free IgG in the endosome, the IgG bound in the endosome can be considered in steady state'.

The four-compartment model equations are given by

$$\begin{aligned}
\dot{x}_1(t) &= -(k_{21}+k_{31})x_1(t) + k_{12}x_2(t) + k_{14}x_4(t) + I(t) \\
\dot{x}_2(t) &= k_{21}x_1(t) - k_{12}x_2(t) \\
\dot{x}_3(t) &= k_{31}x_1(t) - k_{03}x_3(t) - \frac{k_{\text{on}}}{v_3}x_3(t)(R_{\text{tot}} - x_4(t)) + k_{\text{off}}x_4(t) \\
\dot{x}_4(t) &= \frac{k_{\text{on}}}{v_3}x_3(t)(R_{\text{tot}} - x_4(t)) - (k_{14}+k_{\text{off}})x_4(t).
\end{aligned} \tag{7-1}$$

Details including physiological interpretations of states and parameters are provided in section 6.1 of chapter 6.

The steady state is given by

$$\begin{aligned}
\hat{x}_1 &= \frac{I_0\left(k_{03}k_{14}v_3 + k_{03}k_{\text{off}}v_3 + k_{\text{on}}I_0 + k_{14}k_{\text{on}}R_{\text{tot}}\right)}{k_{31}\left(k_{03}v_3(k_{14}+k_{\text{off}}) + k_{\text{on}}I_0\right)} \\
\hat{x}_2 &= \frac{k_{21}}{k_{12}}\hat{x}_1 \\
\hat{x}_3 &= \frac{I_0}{k_{03}} \\
\hat{x}_4 &= \frac{k_{\text{on}}I_0R_{\text{tot}}}{k_{03}v_3(k_{14}+k_{\text{off}}) + k_{\text{on}}I_0},
\end{aligned} \tag{7-2}$$

where $\hat{x}_i$ is the equilibrium point for $x_i(t)$.

By setting $\dot{x}_4(t) = 0$, Hattersley [1] rearranges the ordinary differential equation for $x_4(t)$ in order to obtain an expression for the quantity $x_4(t)$:

$$x_4(t) = \frac{\frac{k_{\text{on}}}{v_3}R_{\text{tot}}x_3(t)}{k_{\text{off}} + k_{14} + \frac{k_{\text{on}}}{v_3}x_3(t)}. \tag{7-3}$$

Hattersley [1] then assumes that the concentrations of unbound IgG in plasma and in endosomes are equal, such that $x_1(t)/v_1 = x_3(t)/v_3$, where v_1 is the plasma volume and v_3 is the total volume of the endosomes, then

$$x_4(t) = \frac{\frac{k_{\text{on}}}{v_3}R_{\text{tot}}\frac{v_3}{v_1}x_1(t)}{k_{\text{off}} + k_{14} + \frac{k_{\text{on}}}{v_3}\frac{v_3}{v_1}x_1(t)}. \tag{7-4}$$

The expression for the rate at which IgG is recycled into plasma is then given by

$$k_{14}x_4(t) = \frac{k_{14}k_{\text{on}}R_{\text{tot}}\frac{1}{v_1}x_1(t)}{k_{\text{off}} + k_{14} + k_{\text{on}}\frac{1}{v_1}x_1(t)}. \tag{7-5}$$

Several parameters are then lumped together to give

$$k_{14}x_4(t) = \frac{V_{\max}x_1(t)}{K_{\mathrm{M}} + x_1(t)}, \tag{7-6}$$

where

$$V_{\max} = k_{14}R_{\mathrm{tot}} \tag{7-7}$$

and

$$K_{\mathrm{M}} = \frac{v_1(k_{14} + k_{\mathrm{off}})}{k_{\mathrm{on}}}. \tag{7-8}$$

Substituting equation (7-6) into the first equation of (7-1) gives the reduced two-compartment model:

$$\begin{aligned} \dot{x}_1(t) &= -\left(k_{21} + k_{31} - \frac{V_{\max}}{K_{\mathrm{M}} + x_1(t)}\right) x_1(t) + k_{12}x_2(t) + I(t) \\ \dot{x}_2(t) &= k_{21}x_1(t) - k_{12}x_2(t). \end{aligned} \tag{7-9}$$

The equilibrium point for the two-compartment model is given by

$$\begin{aligned} \hat{x}_1 &= \frac{-k_{31}K_{\mathrm{M}} + I_0 + V_{\max} + \sqrt{4k_{31}K_{\mathrm{M}}I_0 + (-k_{31}K_{\mathrm{M}} + I_0 + V_{\max})^2}}{2k_{31}} \\ \hat{x}_2 &= \frac{k_{21}}{k_{12}}\hat{x}_1. \end{aligned} \tag{7-10}$$

7.2 Four-compartment model non-dimensional analysis

In the following non-dimensional analysis, the following assumptions are made, based upon the general relations between estimated parameter values found in chapter 6:

$$\begin{aligned} \frac{R_{\mathrm{tot}}}{x_1(0)} &\ll 1 \\ \frac{k_{\mathrm{on}}}{v_3} &> k_{\mathrm{off}} \\ k_{\mathrm{on}}, k_{\mathrm{off}} &> k_{12}, k_{31}, k_{14}, k_{21}. \end{aligned} \tag{7-11}$$

The four-compartment model given by equations (7-1) can be non-dimensionalised [4] by making the following substitutions,

$$\begin{aligned} \hat{t} = \frac{k_{\mathrm{on}}R_{\mathrm{tot}}t}{v_3}, \quad \hat{x}_1 = \frac{x_1}{x_1(0)}, \quad \hat{x}_2 = \frac{x_2}{x_1(0)}, \quad \hat{x}_3 = \frac{x_3}{x_1(0)}, \quad \hat{x}_4 = \frac{x_4}{R_{\mathrm{tot}}}, \\ \beta = \frac{R_{\mathrm{tot}}}{x_1(0)}, \quad \gamma = \frac{v_3}{k_{\mathrm{on}}R_{\mathrm{tot}}x_1(0)}, \end{aligned} \tag{7-12}$$

and defining the following parameters,

$$K = \frac{k_{21}v_3}{k_{\text{on}}R_{\text{tot}}}, \quad L = \frac{k_{\text{on}}}{v_3 x_1(0)}, \quad M = \frac{k_{14}v_3}{x_1(0)k_{\text{on}}}, \quad N = \frac{k_{\text{off}}v_3}{x_1(0)k_{\text{on}}},$$
$$P = \frac{k_{31}v_3}{k_{\text{on}}R_{\text{tot}}}, \quad Q = \frac{k_{12}v_3}{k_{\text{on}}R_{\text{tot}}}, \quad R = \frac{k_{03}v_3}{k_{\text{on}}R_{\text{tot}}}. \tag{7-13}$$

The non-dimensional system is obtained by using

$$\frac{\mathrm{d}x_1}{\mathrm{d}t} = \frac{\mathrm{d}x_1}{\mathrm{d}\hat{t}}\frac{\mathrm{d}\hat{t}}{\mathrm{d}t} = \frac{k_{\text{on}}R_{\text{tot}}}{v_3}x_1(0)\frac{\mathrm{d}\hat{x}_1}{\mathrm{d}\hat{t}}. \tag{7-14}$$

Similarly for x_2, x_3 and x_4, we have

$$\begin{aligned}
\frac{\mathrm{d}x_2}{\mathrm{d}t} &= \frac{k_{\text{on}}R_{\text{tot}}x_1(0)}{v_3}\frac{\mathrm{d}\hat{x}_2}{\mathrm{d}\hat{t}} \\
\frac{\mathrm{d}x_3}{\mathrm{d}t} &= \frac{k_{\text{on}}R_{\text{tot}}x_1(0)}{v_3}\frac{\mathrm{d}\hat{x}_3}{\mathrm{d}\hat{t}} \\
\frac{\mathrm{d}x_4}{\mathrm{d}t} &= \frac{k_{\text{on}}R_{\text{tot}}^2}{v_3}\frac{\mathrm{d}\hat{x}_4}{\mathrm{d}\hat{t}}.
\end{aligned} \tag{7-15}$$

Using equations (7-14) and (7-15), and making the substitutions in equations (7-12) and (7-13), gives the following non-dimensional system equations,

$$\begin{aligned}
\frac{\mathrm{d}\hat{x}_1}{\mathrm{d}\hat{t}} &= -(K+P)\hat{x}_1 + Q\hat{x}_2 + M\hat{x}_4 + \gamma I(t) \\
\frac{\mathrm{d}\hat{x}_2}{\mathrm{d}\hat{t}} &= K\hat{x}_1 - Q\hat{x}_2 \\
\frac{\mathrm{d}\hat{x}_3}{\mathrm{d}\hat{t}} &= P\hat{x}_1 - R\hat{x}_3 - \hat{x}_3\left(1-\hat{x}_4\right) + N\hat{x}_4 \\
\beta\frac{\mathrm{d}\hat{x}_4}{\mathrm{d}\hat{t}} &= \hat{x}_3\left(1-\hat{x}_4\right) - (M+N)\hat{x}_4.
\end{aligned} \tag{7-16}$$

A series solution is assumed, such that

$$\hat{x}_1 = \sum_{n=0}^{\infty}\hat{x}_1^{(n)}\beta^n, \quad \hat{x}_2 = \sum_{n=0}^{\infty}\hat{x}_2^{(n)}\beta^n, \quad \hat{x}_3 = \sum_{n=0}^{\infty}\hat{x}_3^{(n)}\beta^n, \quad \hat{x}_4 = \sum_{n=0}^{\infty}\hat{x}_4^{(n)}\beta^n, \tag{7-17}$$

where superscript (n) indicates the n^{th} derivative. Substituting (7-17) into the ordinary differential equation for $\hat{x}_4$ in (7-16) gives

$$\beta\sum_{n=0}^{\infty}\hat{x}_4^{(n+1)}\beta^n = \sum_{n=0}^{\infty}\hat{x}_3^{(n)}\beta^n\left(1-\sum_{n=0}^{\infty}\hat{x}_4^{(n)}\beta^n\right) - (M+N)\sum_{n=0}^{\infty}\hat{x}_4^{(n)}\beta^n. \tag{7-18}$$

Assuming $\beta \ll 1$, higher order terms ($n \geq 1$) can be neglected, giving

$$0 = \hat{x}_3\left(1-\hat{x}_4\right) - (M+N)\,\hat{x}_4. \tag{7-19}$$

By reverting back to the original dimensional variables, equation (7-19) gives $\dot{x}_4(t) = 0$ and thus allows for the algebraic approximation for $x_4(t)$ in equation (7-3), provided that $\beta \ll 1$.

7.3 Classical Michaelis-Menten kinetics

The model reduction provided by Hattersley [1] and re-produced in section 7.1 depends on two simplifying assumptions. Firstly, Hattersley [1] states that a quasi-steady state (QSS) assumption enables the setting of the rate of change of bound IgG in endosomes ($x_4(t)$ in equations (7-1)) to zero. In order to investigate the validity of this assumption under different conditions, the four-compartment model of IgG kinetics is compared with the classical model of Michaelis-Menten kinetics, which is briefly summarised here.

Classical Michaelis-Menten kinetics deals with a reaction scheme in which an enzyme (E) and substrate (S) bind reversibly to form a complex (C), which irreversibly goes on to form a product (P), within a closed system, as given by

$$E + S \underset{k_{-1}}{\overset{k_1}{\rightleftharpoons}} C \underset{k_2}{\rightarrow} P. \tag{7-20}$$

The reaction is described by the following ordinary differential equations and initial conditions

$$\begin{aligned}
\dot{e}(t) &= -k_1 e(t)s(t) + k_{-1}c(t) + k_2 c(t) \\
\dot{s}(t) &= -k_1 e(t)s(t) + k_{-1}c(t) \\
\dot{c}(t) &= k_1 e(t)s(t) - k_{-1}c(t) - k_2 c(t) \\
\dot{p}(t) &= k_2 c(t) \\
e(0) &= e_0 \\
s(0) &= s_0 \\
c(0) &= 0 \\
p(0) &= 0,
\end{aligned} \tag{7-21}$$

where lower case denotes concentration and e_0 and s_0 are the initial concentrations of the enzyme and substrate, respectively. The total quantity of enzyme, in both free and bound form, is constant, that is $e(t) + c(t) = e_0$. This allows $e(t)$ to be eliminated from the equations, giving

$$\begin{aligned}
\dot{s}(t) &= -k_1(e_0 - c(t))s(t) + k_{-1}c(t) \\
\dot{c}(t) &= k_1(e_0 - c(t))s(t) - k_{-1}c(t) - k_2 c(t) \\
\dot{p}(t) &= k_2 c(t).
\end{aligned} \tag{7-22}$$

Table 7-1 Parameters for simulations of enzyme reaction

	k_1	k_{-1}	k_2	e_0	s_0	ϵ
Good approximation	1	1	1	0.05	50	0.001
Poor approximation	1	1	1	25	50	0.5

When the ratio $e_0/s_0 \ll 1$, it can be assumed that the initial formation of complex is fast, after which the complex is approximately in equilibrium, i.e. $\dot{c}(t) \approx 0$. This provides the following approximation for $c(t)$,

$$c(t) = \frac{e_0 s(t)}{s(t) + K_{\mathrm{M}}}, \tag{7-23}$$

where

$$K_{\mathrm{M}} = \frac{k_{-1} + k_2}{k_1}. \tag{7-24}$$

The rate of product formation is then given by

$$\dot{p}(t) = k_2 c(t) = \frac{k_2 e_0 s(t)}{s(t) + K_{\mathrm{M}}}. \tag{7-25}$$

This is known as the quasi-steady state (QSS) approximation and is valid for $\epsilon \ll 1$, where

$$\epsilon = \frac{e_0}{s_0 + K_{\mathrm{M}}}. \tag{7-26}$$

Simulations of the reaction are shown in figure 7-1. The parameters for the simulations in panels (A) and (C) (good approximation) and (B) and (D) (poor approximation), respectively, are provided in table 7-1. In figure 7-1A the initial enzyme concentration is 0.001 times the initial substrate concentration. There is an initial stage in which enzyme and substrate rapidly bind to form complexes, after which point the complexes can be considered to be in approximate equilibrium. During the second stage the rate at which substrate is 'used up' effectively equals the rate of product formation. In figure 7-1B the initial enzyme concentration is now half the initial substrate concentration and $\epsilon = 0.5$ is no longer much smaller than 1. Whilst there are still two timescales at play, the initial binding is slower and takes up a larger proportion (half) of the substrate. Figures 7-1C and 7-1D show simulations of $c(t)$ and the QSS approximation to $c(t)$, given by equation (7-23). In the initial fast binding stage the approximation is poor for both sets of parameter values, but in the second stage it is good for $\epsilon = 0.001$ (figure 7-1C) and poor for $\epsilon = 0.5$ (figure 7-1D).

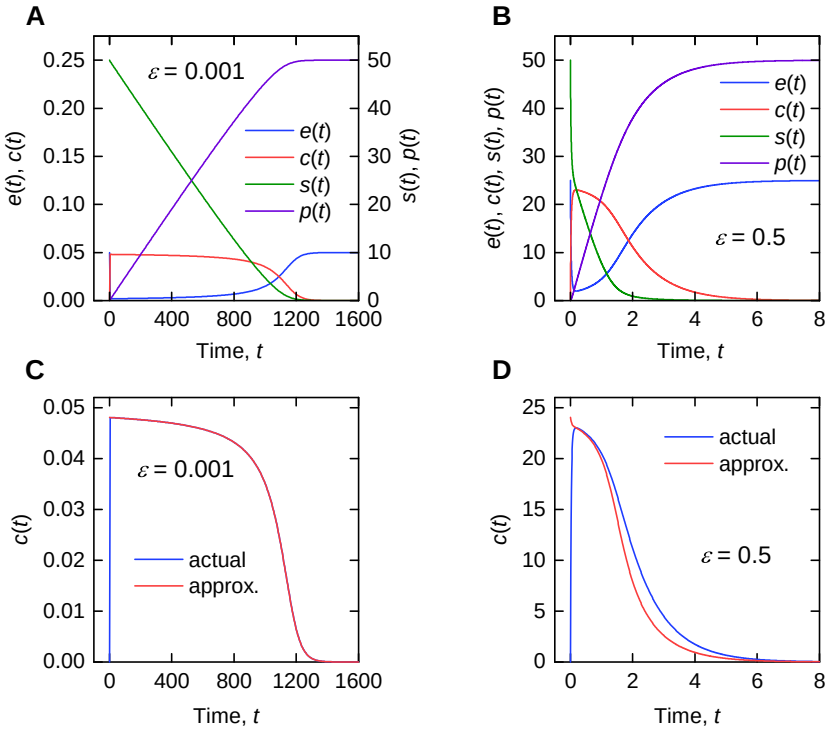

Figure 7-1 (A, B) Simulations of $e(t)$, $c(t)$, $s(t)$ and $p(t)$. (C, D) Simulations of $c(t)$ and the approximation to $c(t)$ based on a QSS assumption. In panels (A) and (C) the QSS approximation is good and in panels (B) and (D) it is poor. Parameter values for the simulations are given in table 7-1. Note the two different scales used for $e(t)$ and $c(t)$ (left axis) and $s(t)$ and $p(t)$ (right axis) in (A).

7.4 Quasi-steady state assumption in the four-compartment model of IgG kinetics

In this section the QSS assumption with respect to the four-compartment model of IgG metabolism is investigated, by comparing the four-compartment model with the enzyme reaction model discussed in 7.3. Figure 7-2 shows how the classical Michaelis-Menten model is a sub-model within the four-compartment model. The parameters k_1, k_{-1} and k_2 in the enzyme reaction model are equivalent to the parameters k_{on}, k_{off} and k_{14}, respectively, in the IgG model. The quantities E, S, C and P correspond to x_5, x_3, x_4 and x_1, respectively. Concentrations e, s, c and p correspond to x_5/v_3, x_3/v_3, x_4/v_3 and x_1/v_1, respectively, where v_1 is the plasma volume and v_3 is the total volume of the endosomes. x_5 represents the quantity of unbound neonatal Fc receptors (FcRn) in

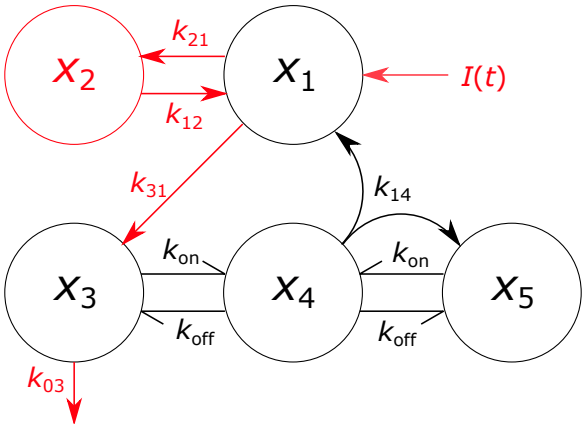

Figure 7-2 Schematic showing the relationship between the four-compartment model of IgG kinetics and the original enzyme reaction model that can be simplified using Michaelis-Menten kinetics. The original enzyme reaction model is shown in black and the additional compartments and flows required for the four-compartment model are shown in red.

intracellular endosomes; it is eliminated from the IgG metabolism model in the same way that e is eliminated from the enzyme reaction equations in (7-22), leaving a four-compartment rather than five-compartment model.

When simulating the four-compartment model with feasible parameter values, steady state initial conditions and realistic models (developed in chapter 8) for the IgG production rate, it is difficult to violate the QSS assumption. We therefore attempt to find conditions under which the QSS assumption is not valid for the four-compartment model, by drawing comparison with the original enzyme reaction model. In section 7.3, it was shown that the QSS is not valid for the 'poor approximation' parameter values given in table 7-1, for which $\epsilon = 0.5$. We now consider the four-compartment model in which the equivalent parameter values and initial conditions are set to the 'poor approximation' parameter values in table 7-1. The initial condition for $x_4(t)$ is set to zero, as in the enzyme reaction model.

The main differences between the enzyme reaction model and the four-compartment model are the elimination from the 'substrate' compartment ($x_3(t)$) with rate constant k_{03}, the flow from the 'product' compartment ($x_1(t)$) to the 'substrate' compartment ($x_3(t)$) with rate constant k_{31}, the interaction between $x_1(t)$ and $x_2(t)$, and the input of new product, $I(t)$. The QSS assumption for $x_4(t)$ can therefore be violated in a trivial sense, by choosing parameter values and initial conditions which violate the condition

Table 7-2 Parameter values and initial conditions for simulations of the four-compartment model in which the QSS assumption is violated by setting the parameter k_{31} to be small

Parameter	Units	Value	
k_{21}	day^{-1}	0.51	Value from the literature [5]
k_{31}	day^{-1}	1×10^{-6}	Chosen to be small
k_{12}	day^{-1}	0.41	Value from the literature [5]
k_{14}	day^{-1}	1	Fixed for large ϵ
k_{03}	day^{-1}	1×10^{-6}	Chosen to be small
k_{on}	$\text{l}\,\mu\text{mol}^{-1}\,\text{day}^{-1}$	1	Fixed for large ϵ
R_{tot}	μmol	25	Fixed for large ϵ
k_{off}	day^{-1}	1	Fixed for large ϵ
v_1	l	2.9	Value from the literature [6]
v_3	l	0.34	Value from the literature [7]
$x_1(0)$	μmol	500	Chosen to be large
$x_2(0)$	μmol	621.951	In steady state with respect to $x_1(0)$
$x_3(0)$	μmol	50	Fixed for large ϵ
$x_4(0)$	μmol	0	Fixed for large ϵ

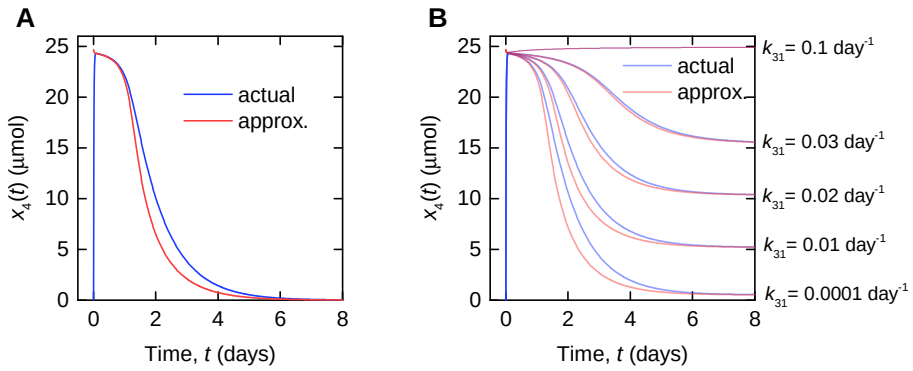

Figure 7-3 (A) Simulation of $x_4(t)$ given by equations (7-1) (actual) and the approximation given by equation (7-3) (approx.), for the parameter values in table 7-2. (B) The same simulation as in (A), but now varying the parameter k_{31}.

$\epsilon \ll 1$ and then setting the parameters k_{03} and k_{31}, the initial conditions $x_1(0)$ and $x_2(0)$, and the IgG production rate $I(t)$ close to zero, such that there is little interaction between the Michaelis-Menten sub-model and the additional compartments or the environment.

Figure 7-3A shows a simulation of $x_4(t)$ given by solving equations (7-1) (actual) and given by the approximation in equation (7-3) (approx.). The production rate of IgG, $I(t)$, is assumed to be zero. All parameter values and initial conditions for the simulation are provided in table 7-2. The values of k_{14}, k_{on}, R_{tot}, k_{off}, $x_3(0)$ and $x_4(0)$ are fixed in order to

replicate the dynamics of the simulation shown in figures 7-1B and 7-1D, in which $\epsilon = 0.5$. The values for parameters k_{31} and k_{03} were chosen, by trial and error, to be sufficiently small such that the interaction between the Michaelis-Menten sub-model and additional compartments is minimal and the QSS assumption remains violated. Parameters k_{21}, k_{12}, v_1 and v_3 are fixed to values from the literature. The initial condition for $x_1(t)$ is set to $x_1(0) = 500$ µmol; this value is chosen somewhat arbitrarily and the importance of $x_1(0)$ will be investigated later. The initial condition for $x_2(t)$ is given by its steady state with respect to $x_1(t)$, $\hat{x}_2 = k_{21}x_1(0)/k_{12}$, with values for $x_1(0)$, k_{21} and k_{12} given in table 7-2.

As expected, the dynamics shown by $x_4(t)$ and its approximation in figure 7-3A are similar to those shown by $c(t)$ and its approximation in figure 7-1D. Even though there is a large pool of IgG in the system (1122 µmol initially between $x_1(0)$ and $x_2(0)$), it is not made available to the 'substrate' compartment, due to the 'small' value of $k_{31} = 1 \times 10^{-6}$ day^{-1}. The effect of increasing the value of k_{31} is shown in figure 7-3B. The parameter k_{31} is varied between the simulations and is labelled next to each pair of curves on the plot. As the value of k_{31} is increased between 0.0001 day^{-1} and 0.1 day^{-1}, the approximation to $x_4(t)$ given by equation (7-3) becomes closer to the true value of $x_4(t)$, until the two outputs are indistinguishable, by inspection, for the second phase of the simulation. The initial, fast binding stage of the reaction lasts less than 0.1 days. Increasing k_{31} has the effect of slowing down the dynamics of the second stage, after initial fast binding has occurred; the two models are still indistinguishable by inspection when simulated over a longer timecourse, for example from 0.1 to 8000 days.

In the classical enzyme reaction model, the QSS assumption is valid for $\epsilon \ll 1$ (for example $\epsilon = 0.001$), where ϵ is given by equation (7-26). Therefore the QSS assumption is valid when the total quantity of enzyme is much smaller than the initial quantity of substrate. For the simulation shown in figure 7-3A, the QSS is violated by having an initial quantity of $x_3(t)$ (substrate) that is only twice the total quantity of receptors (enzyme). This is still the case for the simulations shown in figure 7-3B; now however there is a constant flow of 'substrate' from the first compartment to the third compartment due to k_{31}. In the classical enzyme reaction, the substrate is used up such that a steady state concentration of complexes cannot be maintained indefinitely: the complex concentration falls during the reaction until it eventually reaches zero, when all of the substrate has been converted

Table 7-3 Parameters and initial conditions for simulations of the four-compartment model in which the QSS assumption is violated by setting initial conditions $x_1(0)$ and $x_2(0)$ to be small

Parameter	Units	Value	
k_{21}	day^{-1}	0.51	Value from the literature [5]
k_{31}	day^{-1}	0.1	Value for which QSS is valid, with large $x_1(0)$
k_{12}	day^{-1}	0.41	Value from the literature [5]
k_{14}	day^{-1}	1	Fixed for large ϵ
k_{03}	day^{-1}	1×10^{-6}	Chosen to be small
k_{on}	$\text{l}\,\mu\text{mol}^{-1}\,\text{day}^{-1}$	1	Fixed for large ϵ
R_{tot}	µmol	25	Fixed for large ϵ
k_{off}	day^{-1}	1	Fixed for large ϵ
v_1	l	2.9	Value from the literature [6]
v_3	l	0.34	Value from the literature [7]
$x_1(0)$	µmol	1	Chosen to be small
$x_2(0)$	µmol	1.2439	In steady state with respect to $x_1(0)$
$x_3(0)$	µmol	50	Fixed for large ϵ
$x_4(0)$	µmol	0	Fixed for large ϵ

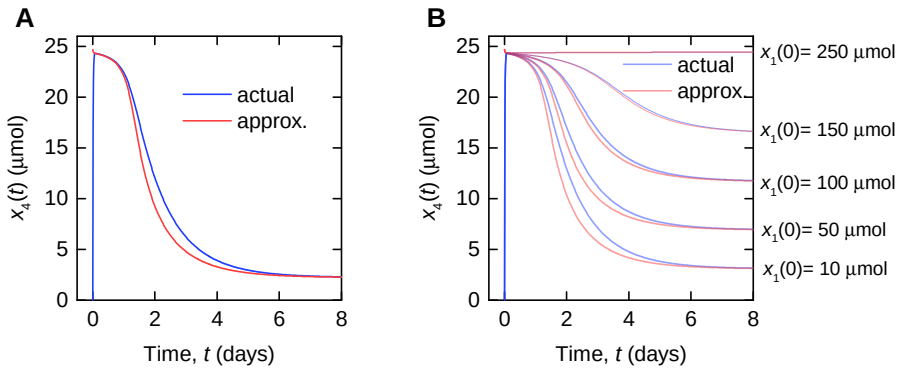

Figure 7-4 (A) Simulation of $x_4(t)$ given by equations (7-1) (actual) and the approximation given by equation (7-3) (approx.), for the parameter values in table 7-3. (B) The same simulation as in (A), but now varying the initial conditions for $x_1(0)$ and $x_2(0)$.

to product (see figure 7-1). At the same time, having rapidly bound to substrate in the initial fast stage, the enzyme recovers its initial concentration by the end of the experiment. In the four-compartment model however, there is a positive flow from $x_1(t)$ to $x_3(t)$ (the 'substrate' compartment); as such the substrate is not used up and there is enough unbound substrate to maintain a QSS quantity of complexes. Likewise the receptors remain in a bound state and do not recover their initial unbound concentration during the simulation.

The effect of the initial conditions for $x_1(t)$ and $x_2(t)$ on the validity of the QSS assumption is now investigated. In figure 7-3B, the QSS assumption was valid for $k_{31} = 0.1$ day^{-1}. Despite the small ratio of 'substrate' to 'enzyme' initially, violating the condition $\epsilon \ll 1$, the transfer of IgG from $x_1(t)$ to $x_3(t)$ meant that there was a constant supply of IgG to bind to receptors. This implies that, if $k_{31} = 0.1$ day^{-1} but there is little IgG in the plasma and peripheral compartments initially, relative to the size of k_{31}, the QSS assumption will be similarly invalidated. This scenario is simulated in figure 7-4A, in which the parameter k_{31} is 0.1 day^{-1} and the initial condition for $x_1(t)$ is small, with $x_1(0) = 1$ µmol; all other parameters and initial conditions are given in table 7-3. In figure 7-4A, the QSS assumption is poor due to the 'small' values of $x_1(0) = 1$ µmol and $x_2(0) = 1.24$ µmol, relative to the size of k_{31}. The effect of increasing $x_1(0)$ and $x_2(0)$ is shown in figure 7-4B. As $x_1(0)$ is increased from 10 µmol to 250 µmol, the validity of the QSS approximation improves.

The effect of including the elimination of substrate, parameterised by k_{03}, in the model is to speed up the dynamics of the second stage of the simulation (after the fast binding stage), since 'substrate' that would have been converted to 'product' is now removed from the system. The inclusion of this flow has the opposite effect, qualitatively, to the inclusion of a pool of IgG ($x_1(t)$) which flows to the 'substrate' compartment ($x_3(t)$). If the model is simulated instead with parameter values that give a small value of $\epsilon = 0.001$, such that the QSS approximation ought to be valid, increasing the value of k_{03} makes the approximation progressively worse.

The simulations in this section show that additions to the classical enzyme reaction model which serve to feed the substrate compartment ($x_3(t)$) will have the effect of improving the approximation to $x_4(t)$, given by equation (7-3). Additions which serve to remove substrate from $x_3(t)$ will have the effect of worsening the approximation of $x_4(t)$. In the simulations seen in this section, parameter values and initial conditions have been set to certain values in order to give $\epsilon = 0.5$, to purposely violate the QSS assumption. However, when simulating responses in IgG multiple myeloma, the system is assumed to be in steady state, or at least near to steady state, prior to any intervention. This is fundamentally different to the classical enzyme reaction scheme, in which the concentration of complex is initially zero and substrate and enzyme rapidly bind at the onset of the reaction. The

Table 7-4 Parameter values and initial conditions for the simulations of the four-compartment model and the two-compartment reduced model in section 7.5

Parameter	Units	Value	
k_{21}	day^{-1}	0.441	Estimated for two-compartment model in chapter 5
k_{31}	day^{-1}	0.15419	Estimated for four-compartment model in chapter 6
k_{12}	day^{-1}	0.422	Estimated for two-compartment model in chapter 5
k_{14}	day^{-1}	14.9592	See section 6.4.4 in chapter 6
k_{03}	day^{-1}	30.8231	See section 6.4.4 in chapter 6
k_{on}	$\text{l}\,\mu\text{mol}^{-1}\,\text{day}^{-1}$	255.467	See section 6.4.4 in chapter 6
R_{tot}	μmol	1.71994	See section 6.4.4 in chapter 6
k_{off}	day^{-1}	167.029	See section 6.4.4 in chapter 6
v_1	l	2.9	Value from the literature [6]
v_3	l	0.34	Value from the literature [7]
k_{kill}	day^{-1}	0.055	Chosen for realistic tumour response
I_0	$\mu\text{mol}\,\text{day}^{-1}$	76	Chosen for realistic tumour response
I_∞	$\mu\text{mol}\,\text{day}^{-1}$	26.5	Chosen for realistic tumour response

simulations in this section show that it is possible to violate the QSS assumption, however the conditions required to achieve this are unlikely to occur in practice.

7.5 The relationship between plasma and endosomal concentrations of IgG

The second assumption used by Hattersley [1] to derive the two-compartment model from the four-compartment model is that the concentration of unbound IgG in endosomes is equal to the concentration of IgG in plasma. Hattersley [1] states that 'pinocytosis is assumed to be a constant extraction and recycling process, which ensures that the concentrations of IgG in the endosome and plasma are constant'. In this section the four-compartment model is simulated with feasible parameter values to see whether this assumption is likely to hold in practice. The two-compartment model is then simulated using the parameter values calculated from the four-compartment parameter values.

The four-compartment model, given by equations (7-1), was simulated with feasible parameter values (see table 7-4) and a model for the IgG production rate that produces IgG responses that are typically observed in patients. The IgG production rate, $I(t)$, is

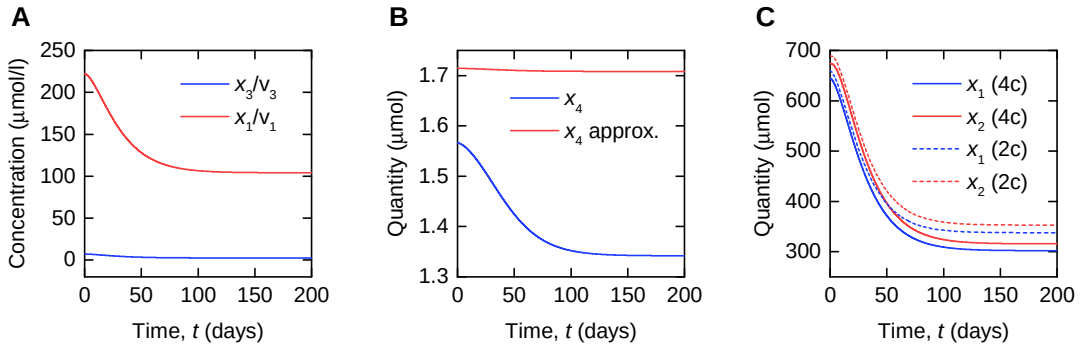

Figure 7-5 (A) Plasma and endosomal concentrations of unbound IgG. (B) Quantity of bound IgG in endosomes and an approximation, assuming both QSS and equality of plasma and endosomal concentrations of IgG. (C) Quantities of IgG in the plasma and peripheral compartments, for the four-compartment model and the two-compartment model, parameterised according to Hattersley's [1] derivation.

assumed to be given by

$$I(t) = (I_0 - I_\infty)\exp(-k_{\text{kill}}t) + I_\infty. \tag{7-27}$$

This model is discussed in section 8.2 of chapter 8. At the beginning of the simulation, when $t = 0$ days, the system is assumed to be in steady state. The initial conditions for the model states are therefore given by the equilibrium point in equation (7-2).

The parameter values used to produce the simulation are given in table 7-4. The values for k_{21} and k_{12} were estimated for the two-compartment model in chapter 5. The parameter k_{31} was estimated for the four-compartment model in chapter 6. The values for k_{14}, k_{03}, k_{on}, R_{tot} and k_{off} are taken from row A1 of table 6-8 in chapter 6 and their generation is discussed in section 6.4.4 of that chapter.

Figure 7-5A shows the plasma and endosomal concentrations of IgG, given by $x_1(t)/v_1$ and $x_3(t)/v_3$, respectively, for the simulation described. According to the derivation of the two-compartment model in section 7.1, these two quantities are required to be equal, however this is clearly not the case for the current simulation. This means that the approximation of $x_4(t)$, based on this assumption and given by equation (7-4), is a poor one, as shown in figure 7-5B.

Figure 7-5C shows the quantities of IgG in plasma ($x_1(t)$) and in the peripheral compartment ($x_2(t)$), simulated from the four-compartment model and from the reduced model.

The reduced model, given by equations (7-9), was simulated assuming the same model for IgG production, given by equation (7-27). Again the system was assumed to be in steady state at $t = 0$ days; therefore the initial conditions for the reduced model are given by equation (7-10). The parameters $V_{\max}$ and K_{M} were calculated using equations (7-7) and (7-8); all other parameter values are given in table 7-4. Figure 7-5C shows that there is a small difference in $x_1(t)$ and $x_2(t)$ between the two models at $t = 0$ days, around 2%, which increases to around 12% by the end of the simulation. This difference is due to the poor approximation of $x_4(t)$ shown in figure 7-5B, based upon an assumption that is not supported by the model, with feasible parameter values.

The simulations shown in figure 7-5 show that the dynamics of $x_1(t)$ and $x_3(t)$ are not the same and therefore, assuming a constant total volume of endosomes, the concentrations are not equal. However, if we are to assume that the concentrations are equal based on the biological process of pinocytosis, then clearly the total volume of the endosomes must vary with time. Pinocytosis is nonspecific, that is, the cell internalises a small quantity of the surrounding fluid and its contents, without targeting certain molecules. It is therefore not unreasonable to suggest that the concentration of IgG within endosomes would equal that of the environment outside the cell. From the point of view of the model, this would mean that the total volume of the endosomes must become a variable which changes such that $x_1(t)/v_1 = x_3(t)/v_3(t)$.

The suggestion that the total volume of the endosomes containing IgG may vary is not unreasonable: the total volume is made up of many individual endosomes, some of which may not manage to capture IgG molecules when there is less IgG available in the system. This modification to the model is easy to achieve by including an additional ordinary differential equation for $v_3(t)$, which satisfies the second assumption of Hattersley's [1] derivation. However, this assumption requires us to consider endosomes as separate entities. A simplified diagram of FcRn-mediated recycling is provided in figure 2-3 in chapter 2. This diagram shows the transit of IgG through a cell within an endosome. When the IgG is first internalised, the endosomal concentration of unbound IgG may be assumed to be equal to its concentration in plasma; however once the endosome has acidified, IgG-FcRn binding takes place and as such the concentration of unbound IgG within that particular endosome must decrease. The concentration of unbound IgG

within an individual endosome therefore changes during its transit through the cell. Due to the difficulty in validating this assumption, a model in which v_3 is time-varying is not presented here, but may be the subject of future work.

7.6 Simulations of IgG responses in multiple myeloma

As discussed in section 7.5, the second assumption required for the equivalence of the four- and two-compartment models, namely that the concentrations of free IgG in plasma and endosomes are equal, is unlikely to be valid for feasible parameter values. Having discovered that the reduced model is not a good approximation to the full model, in this section we investigate whether the two models can nonetheless produce similar predictions, when the identifiable parameters $V_{\max}$ and K_{M} are no longer calculated from equations (7-7) and (7-8), but are estimated from experimental data. In this section IgG responses during multiple myeloma treatment are compared for the two- and four-compartment models, using the parameter values estimated in chapters 5 and 6, respectively. The two-compartment model can no longer be considered as a reduced form of the four-compartment model and simulated responses will not be identical.

The parameter identification problem was considered for the four-compartment model in chapter 6. Whilst individual parameter values were difficult to estimate, certain expressions in terms of the underlying parameters could be estimated (see section 6.4). By generating certain parameter values randomly and calculating the remaining parameters, feasible parameter vectors were generated; these are tabulated in tables 6-8–6-11. These parameter values are used in the simulations in this section.

7.6.1 Models for monoclonal and polyclonal IgG dynamics in multiple myeloma

In order to simulate monoclonal IgG responses in IgG multiple myeloma, the models of IgG metabolism need to explicitly account for monoclonal IgG produced by the malignant plasma cells and polyclonal IgG produced by healthy plasma cells, since both types of IgG

undergo the same processes of recycling and elimination and therefore one is influenced by the other. For the two-compartment model, the dynamics of monoclonal and polyclonal IgG in an IgG myeloma patient are described by

$$\begin{aligned}
\dot{x}_{1\mathrm{m}}(t) &= -\left(k_{21} + k_{31} - \frac{V_{\max}}{K_{\mathrm{M}} + x_{1\mathrm{m}}(t) + x_{1\mathrm{p}}(t)}\right) x_{1\mathrm{m}}(t) + k_{12} x_{2\mathrm{m}}(t) + I_{\mathrm{m}}(t) \\
\dot{x}_{2\mathrm{m}}(t) &= k_{21} x_{1\mathrm{m}}(t) - k_{12} x_{2\mathrm{m}}(t) \\
\dot{x}_{1\mathrm{p}}(t) &= -\left(k_{21} + k_{31} - \frac{V_{\max}}{K_{\mathrm{M}} + x_{1\mathrm{m}}(t) + x_{1\mathrm{p}}(t)}\right) x_{1\mathrm{p}}(t) + k_{12} x_{2\mathrm{p}}(t) + I_{\mathrm{p}} \\
\dot{x}_{2\mathrm{p}}(t) &= k_{21} x_{1\mathrm{p}}(t) - k_{12} x_{2\mathrm{p}}(t),
\end{aligned} \tag{7-28}$$

where $x_{1\mathrm{m}}(t)$ and $x_{2\mathrm{m}}(t)$ are the quantities in µmol of monoclonal IgG in plasma and in the peripheral space, respectively, $x_{1\mathrm{p}}(t)$ and $x_{2\mathrm{p}}(t)$ are the quantities in µmol of polyclonal IgG in plasma and in the peripheral space, respectively, $I_{\mathrm{m}}(t)$ is the production rate of monoclonal IgG in $\mu\mathrm{mol\,day}^{-1}$, and I_{p} is the production rate of polyclonal IgG in $\mu\mathrm{mol\,day}^{-1}$, which is assumed to be constant. All other parameters are as defined in chapter 5. The total quantity of IgG in each compartment is given by

$$x_{i\mathrm{tot}}(t) = x_{i\mathrm{m}}(t) + x_{i\mathrm{p}}(t), \qquad i = 1, \ldots, 2. \tag{7-29}$$

At the beginning of each simulation, the system is assumed to be in steady state. The initial conditions are thus given by

$$\begin{aligned}
x_{i\mathrm{m}}(0) &= \frac{I_{\mathrm{m0}}}{I_0} \hat{x}_i \\
x_{i\mathrm{p}}(0) &= \frac{I_{\mathrm{p}}}{I_0} \hat{x}_i,
\end{aligned} \tag{7-30}$$

for $i = 1, 2$, where $\hat{x}_1$ and $\hat{x}_2$ are given by equation (7-10) and $I_0 = I_{\mathrm{m0}} + I_{\mathrm{p}}$.

The monoclonal IgG response, $y_{\mathrm{m}}(t)$, is given by

$$y_{\mathrm{m}}(t) = \frac{x_{1\mathrm{m}}(t)}{x_{1\mathrm{m}}(0)}. \tag{7-31}$$

For the four-compartment model, the dynamics of monoclonal and polyclonal IgG in an

IgG myeloma patient are described by

$$\begin{aligned}
\dot{x}_{1\mathrm{m}}(t) &= -(k_{21}+k_{31})x_{1\mathrm{m}}(t) + k_{12}x_{2\mathrm{m}}(t) + k_{14}x_{4\mathrm{m}}(t) + I_{\mathrm{m}}(t)\\
\dot{x}_{2\mathrm{m}}(t) &= k_{21}x_{1\mathrm{m}}(t) - k_{12}x_{2\mathrm{m}}(t)\\
\dot{x}_{3\mathrm{m}}(t) &= k_{31}x_{1\mathrm{m}}(t) - k_{03}x_{3\mathrm{m}}(t) - \frac{k_{\mathrm{on}}}{v_3}x_{3\mathrm{m}}(t)(R_{\mathrm{tot}} - x_{4\mathrm{m}}(t) - x_{4\mathrm{p}}(t)) + k_{\mathrm{off}}x_{4\mathrm{m}}(t)\\
\dot{x}_{4\mathrm{m}}(t) &= \frac{k_{\mathrm{on}}}{v_3}x_{3\mathrm{m}}(t)(R_{\mathrm{tot}} - x_{4\mathrm{m}}(t) - x_{4\mathrm{p}}(t)) - (k_{14}+k_{\mathrm{off}})x_{4\mathrm{m}}(t)\\
\dot{x}_{1\mathrm{p}}(t) &= -(k_{21}+k_{31})x_{1\mathrm{p}}(t) + k_{12}x_{2\mathrm{p}}(t) + k_{14}x_{4\mathrm{p}}(t) + I_{\mathrm{p}}\\
\dot{x}_{2\mathrm{p}}(t) &= k_{21}x_{1\mathrm{p}}(t) - k_{12}x_{2\mathrm{p}}(t)\\
\dot{x}_{3\mathrm{p}}(t) &= k_{31}x_{1\mathrm{p}}(t) - k_{03}x_{3\mathrm{p}}(t) - \frac{k_{\mathrm{on}}}{v_3}x_{3\mathrm{p}}(t)(R_{\mathrm{tot}} - x_{4\mathrm{m}}(t) - x_{4\mathrm{p}}(t)) + k_{\mathrm{off}}x_{4\mathrm{p}}(t)\\
\dot{x}_{4\mathrm{p}}(t) &= \frac{k_{\mathrm{on}}}{v_3}x_{3\mathrm{p}}(t)(R_{\mathrm{tot}} - x_{4\mathrm{m}}(t) - x_{4\mathrm{p}}(t)) - (k_{14}+k_{\mathrm{off}})x_{4\mathrm{p}}(t),
\end{aligned} \tag{7-32}$$

where $x_{1\mathrm{m}}(t)$ and $x_{1\mathrm{p}}(t)$ are the quantities of monoclonal and polyclonal IgG in plasma, $x_{2\mathrm{m}}(t)$ and $x_{2\mathrm{p}}(t)$ are the quantities of monoclonal and polyclonal IgG in the peripheral space, $x_{3\mathrm{m}}(t)$ and $x_{3\mathrm{p}}(t)$ are the quantities of unbound monoclonal and polyclonal IgG in endosomes, and $x_{4\mathrm{m}}(t)$ and $x_{4\mathrm{p}}(t)$ are the quantities of monoclonal and polyclonal IgG bound to FcRn in endosomes. All quantities have units of µmol. $I_{\mathrm{m}}(t)$ is the production rate of monoclonal IgG in $\mu\mathrm{mol\,day}^{-1}$ and I_{p} is the production rate of polyclonal IgG in $\mu\mathrm{mol\,day}^{-1}$, which is assumed to be constant. All other parameters are as defined in table 6-1 in chapter 6. The total quantity of IgG in each compartment is given by

$$x_{i\mathrm{tot}}(t) = x_{i\mathrm{m}}(t) + x_{i\mathrm{p}}(t), \qquad i = 1,\ldots,4. \tag{7-33}$$

At the beginning of each simulation, the system is assumed to be in steady state. The initial conditions are thus given by

$$\begin{aligned}
x_{i\mathrm{m}}(0) &= \frac{I_{\mathrm{m0}}}{I_0}\hat{x}_i\\
x_{i\mathrm{p}}(0) &= \frac{I_{\mathrm{p}}}{I_0}\hat{x}_i,
\end{aligned} \tag{7-34}$$

for $i = 1,\ldots,4$, where $\hat{x}_i$ is given by equation (7-2) and $I_0 = I_{\mathrm{m0}} + I_{\mathrm{p}}$.

The monoclonal IgG response, $y_{\mathrm{m}}(t)$, is given by

$$y_{\mathrm{m}}(t) = \frac{x_{1\mathrm{m}}(t)}{x_{1\mathrm{m}}(0)}. \tag{7-35}$$

Table 7-5 Parameter values for monoclonal and polyclonal IgG production for the simulations in section 7.6.2

Parameter	Units	A	B	C	D	E	F
I_{m0}	µmol day^{-1}	61	152	116	68	105	53
$I_{m\infty}$	µmol day^{-1}	11.5	5	2.5	0	24	5
k_{kill}	day^{-1}	0.055	0.03	0.07	0.007	0.0065	0.01
I_p	µmol day^{-1}	15	15	15	15	15	15

Table 7-6 Parameter values for the simulations of the two-compartment model in section 7.6

Parameter	Units	Value	
k_{21}	day^{-1}	0.441	Estimated for two-compartment model in chapter 5
k_{31}	day^{-1}	0.159	Estimated for two-compartment model in chapter 5
k_{12}	day^{-1}	0.422	Estimated for two-compartment model in chapter 5
V_{max}	µmol day^{-1}	40.0	Estimated for two-compartment model in chapter 5
K_M	µmol	272	Estimated for two-compartment model in chapter 5
v_1	l	2.9	Value from the literature [6]
v_3	l	0.34	Value from the literature [7]

Table 7-7 Parameter values for the simulations of the four-compartment model in section 7.6

	k_{31} (day^{-1})	k_{14} (day^{-1})	k_{03} (day^{-1})	k_{on}/v_3 (µmol^{-1} day^{-1})	R_{tot} (µmol)	k_{off} (day^{-1})
A1	0.15419	14.9592	30.8231	751.375	1.71994	167.029
B1	0.15419	1.61346	2.89570	4330.95	15.9465	11164.2
C1	0.15419	1460.34	15.0518	3089.82	0.0176185	72.1920
D1	0.15419	14.5717	4.13855	53.6585	1.765680	82.2232
E1	0.15419	1.74892	0.541327	1607.86	14.7114	22172.6
F1	0.15419	2.17529	590.017	3196.13	11.8279	38.2657
G1	0.15419	0.489903	58.5907	2136.67	52.5185	271.763

Assuming a constant rate of IgG synthesis per plasma cell, the tumour response, $y_T(t)$, is defined as

$$y_T(t) = \frac{I_m(t)}{I_m(0)}. \tag{7-36}$$

7.6.2 Simulations of responses to a decreasing tumour burden

The simulation in figure 7-6 shows the responses of monoclonal, polyclonal and total IgG in plasma and the peripheral compartment, respectively, for both the two- and

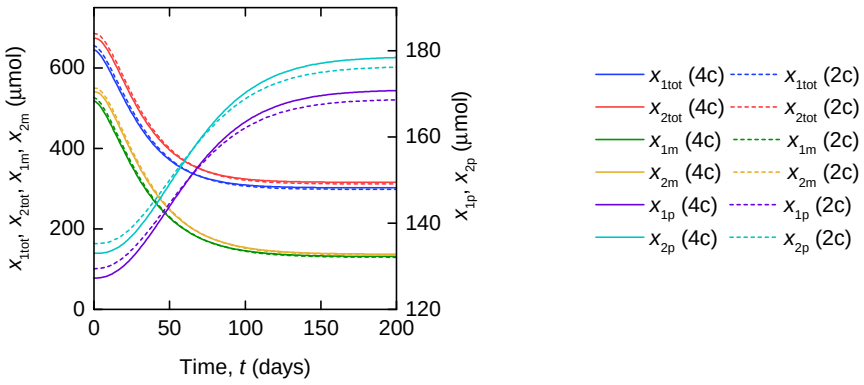

Figure 7-6 Monoclonal, polyclonal and total IgG, in compartments 1 and 2, simulated using the two-compartment model (dashed lines) and the four-compartment model (solid lines). Note the different scales for total and monoclonal quantities (left axis) and polyclonal quantities (right axis).

four-compartment models. The simulations were produced using equations (7-28) for the two-compartment model and equations (7-32) for the four-compartment model. The monoclonal IgG production rate, $I_{\mathrm{m}}(t)$, is given by equation (7-27) with parameter values from column 'A' in table 7-5. The system is assumed to be in steady state at time $t = 0$. The parameter values for the two-compartment model are those estimated in chapter 5, summarised here in table 7-6. The values for parameters k_{21}, k_{12}, v_1 and v_3 are assumed to be the same for both models. The remaining parameter values used in simulating the four-compartment model are given by row 'A1' in table 7-7. The values in table 7-7 are taken from tables 6-8 to 6-11 in chapter 6.

The simulation in figure 7-6 shows that the trajectories of a quantity of IgG produced by the two- and four-compartment models are, as expected, not identical. The two-compartment model over-estimates all quantities of IgG by 1.7% at the beginning of the simulated time interval and underestimates them by 1.3% at the end of the time interval. We note that the quantities of polyclonal IgG are plotted on a different quantity scale as they represent a small proportion of the total IgG.

Clinicians are most interested in the monoclonal IgG response in terms of the proportional change during treatment. Figure 7-7 shows the tumour response, given by equation (7-36), and the monoclonal IgG responses for the two- and four-compartment models, given by equations (7-31) and (7-35), respectively. The monoclonal IgG response is used as a surrogate for the tumour response in clinical practice. The simulation shows that,

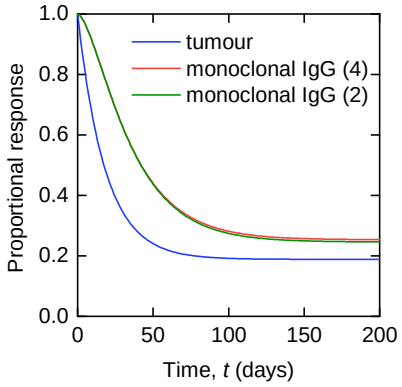

Figure 7-7 The monoclonal IgG response to a falling tumour burden, simulated for both the two-compartment model and the four-compartment model

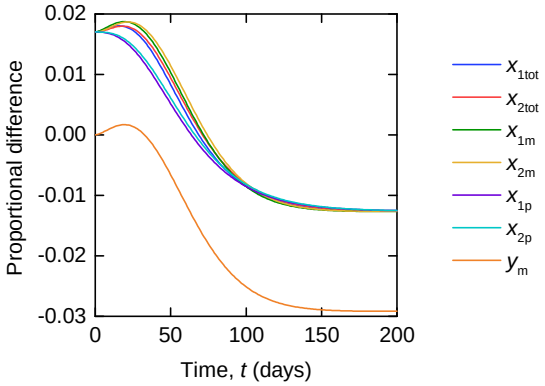

Figure 7-8 Proportional differences between the four-compartment model and the two-compartment model, for monoclonal, polyclonal and total quantities of IgG and the monoclonal IgG response

for both models, the monoclonal IgG response underestimates the depth of the tumour response, with a maximum difference of 0.3 between the tumour and monoclonal IgG responses at time $t = 21$ days. For the four-compartment model, the underestimation of the tumour response is slightly greater.

Figure 7-8 shows the proportional differences between the responses produced by the two- and four-compartment models. Allowing q to represent each of the variables ($x_{i\text{tot}}$, $x_{i\text{m}}$, $x_{i\text{p}}$ and y_{m}, for $i = 1, 2$), the proportional difference, q_{diff}, is given by

$$q_{\text{diff}} = \frac{q^{(2)} - q^{(4)}}{q^{(4)}}, \tag{7-37}$$

where superscripts (2) and (4) denote the two-compartment model and four-compartment model, respectively. The plot shows that the percentage difference for the quantities in

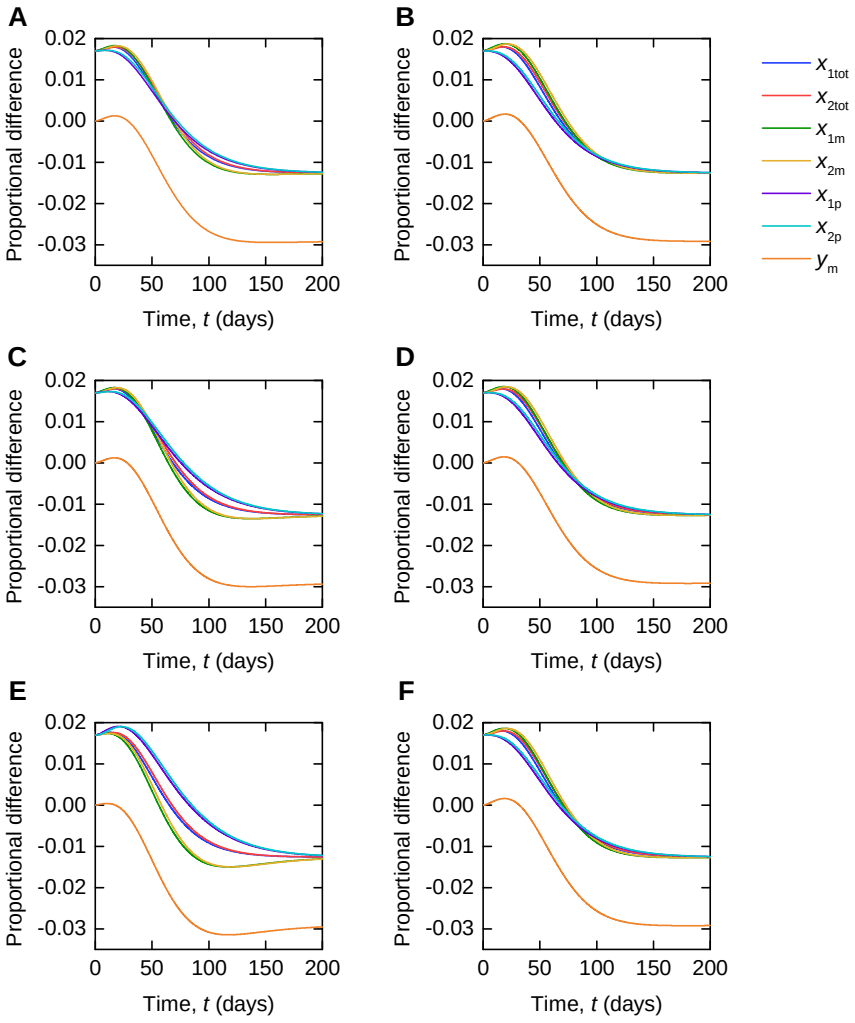

Figure 7-9 Proportional differences between the four-compartment model and the two-compartment model, for monoclonal, polyclonal and total quantities of IgG and the monoclonal IgG response. The four-compartment model parameter values for each simulation are given by rows (A) B1, (B) C1, (C) D1, (D) E1, (E) F1, and (F) G1, in table 7-7.

µmol is between -1.3% and 1.9% over the whole simulation. The percentage difference in the monoclonal IgG response, $y_{\mathrm{m}}(t)$, reaches its maximal absolute value of around 2.9% at $t = 200$ days, when $y_{\mathrm{m}}(t) = 0.254$ for the four-compartment model and $y_{\mathrm{m}}(t) = 0.246$ for the two-compartment model. Whilst these differences seem small, they may be important in future predictions, depending on the scenario that is being investigated.

In chapter 6, it was discovered that a wide range of parameter values for the four-compartment model produce similar behaviour in the observed model outputs. The different sets of parameter values in table 7-7 all produce similar behaviour in plasma

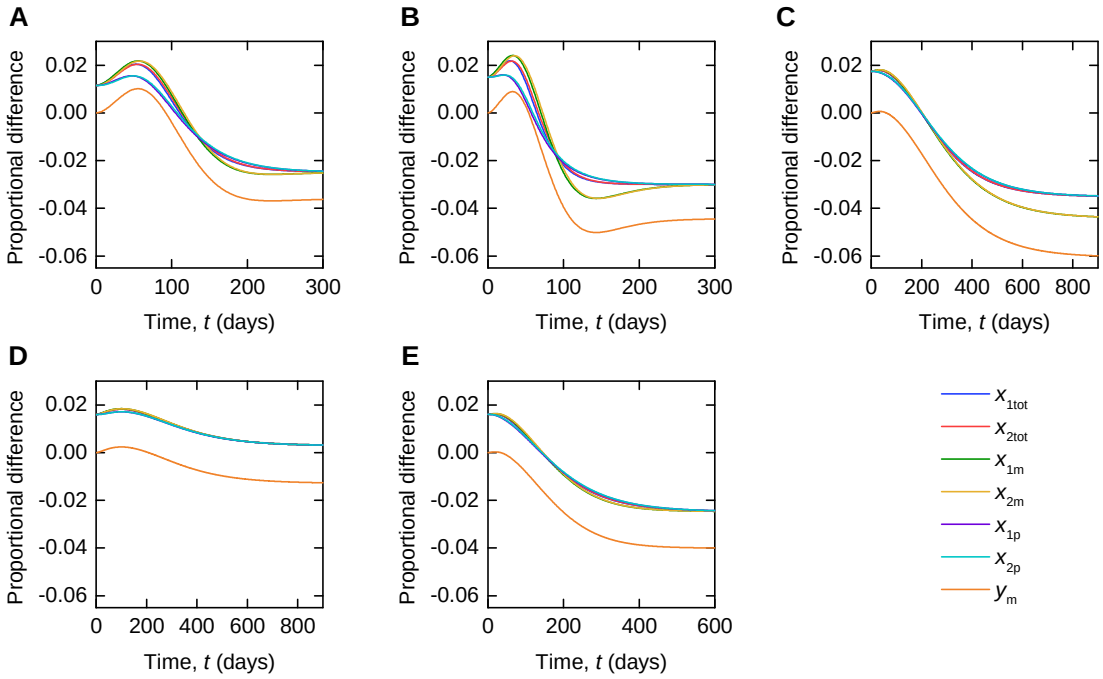

Figure 7-10 Proportional differences between the four-compartment model and the two-compartment model, for monoclonal, polyclonal and total quantities of IgG and the monoclonal IgG response. The monoclonal IgG production parameter values for each simulation are given by columns (A) B, (B) C, (C) D, (D) E, and (E) F, from table 7-5.

and peripheral IgG ($x_1(t)$ and $x_2(t)$), despite having some extremely different individual values. The simulation of proportional differences, shown in figure 7-8, is therefore repeated in figure 7-9 for each of the parameter vectors in table 7-7. All other details of the simulation remain the same. There is some variation between the plots in figures 7-9A to 7-9F; however all of the parameter vectors show a similar pattern in terms of the differences between the two- and four-compartment model responses.

The differences between the predictions of the two metabolism models are also dependent on the assumed model for the monoclonal IgG production rate. Figure 7-10 shows the same simulation of proportional differences between the responses produced by the two- and four-compartment models, now using parameter values from columns B–F in table 7-5. The four-compartment model parameters are given by row 'A1' in table 7-7. Now, whilst the basic pattern shown remains the same, there is much more variation between the simulations, for example, we note that the time axis is no longer the same for each plot, due to the different timescales of the dynamics shown.

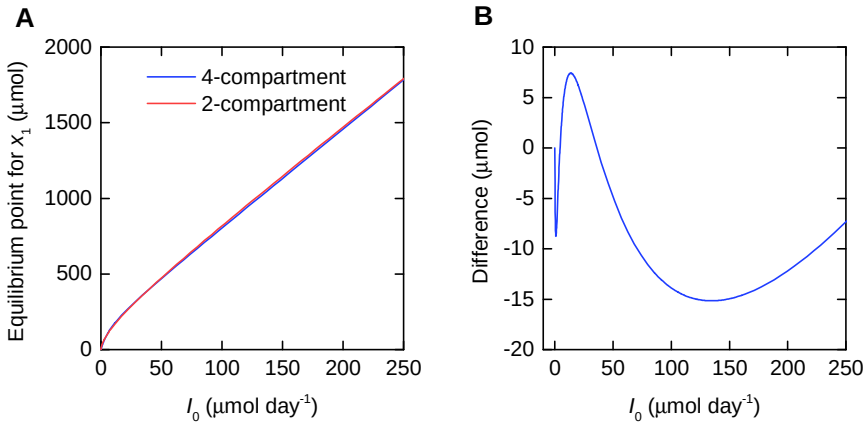

Figure 7-11 (A) The relationship between the total IgG production rate and the plasma IgG equilibrium point, for both the four- and two-compartment models. (B) The difference between the plasma IgG equilibrium points for the four- and two-compartment models.

In each simulation shown in figures 7-8–7-10, the basic pattern is the same: the percentage difference for IgG quantities is between 1% and 2% at $t = 0$ days, there then is some positive fluctuation seen, followed by a steady decline then a negative fluctuation, before reaching a steady state at a negative value for the proportional difference. In this simulation, the system both begins and ends in steady state. Clinicians are most interested in these 'final' responses, which are used to assess what proportion of the tumour has been killed during therapy. The relationship between the steady states of the two models therefore is important.

Figure 7-11A shows the relationship between the total IgG production rate and the plasma IgG equilibrium point, for both the four- and two-compartment models, given by equations (7-2) and (7-10), respectively. The parameter values used to plot the two-compartment model equilibrium point are given in table 7-6. The four-compartment model equilibrium point for $x_1(t)$ can be simplified, giving

$$\hat{x}_1 = \frac{(\psi_1 + \psi_2 + I_0)\, I_0}{k_{31}\,(\psi_1 + I_0)}, \tag{7-38}$$

where

$$\begin{aligned} \psi_1 &= \frac{k_{03} v_3\,(k_{14} + k_{\text{off}})}{k_{\text{on}}} \\ \psi_2 &= k_{14} R_{\text{tot}}. \end{aligned} \tag{7-39}$$

The equilibrium point for $x_2(t)$ can be similarly simplified; however the equilibrium points for $x_3(t)$ and $x_4(t)$ cannot be reduced in this way. Each of the parameter vectors in table

Table 7-8 Parameter values for monoclonal and polyclonal IgG production for the simulation of relapse in section 7.6.3

Parameter	Units	Value
I_{m1}	$\mu\mathrm{mol\,day^{-1}}$	60
I_{m2}	$\mu\mathrm{mol\,day^{-1}}$	5
k_{kill}	$\mathrm{day^{-1}}$	0.028
k_{growth}	$\mathrm{day^{-1}}$	0.0118
I_{p}	$\mu\mathrm{mol\,day^{-1}}$	15

7-7 was generated in order to give identical values for the identifiable parameters ψ_1 and ψ_2: $\psi_1 = 7.46556\ \mu\mathrm{mol\,day^{-1}}$ and $\psi_2 = 25.729\ \mu\mathrm{mol\,day^{-1}}$. These parameter values were used to simulate the equilibrium point in figure 7-11A. Figure 7-11B shows the plasma IgG equilibrium point for the four-compartment model minus that for the two-compartment model. Figure 7-11B explains why the two-compartment model tends to overestimate quantities of plasma IgG at the beginning of the simulated treatment, when the total IgG production rate is large, and underestimates plasma IgG for the smaller production rates of around 20–40 $\mu\mathrm{mol\,day^{-1}}$ at the end of treatment.

7.6.3 Simulations of responses during relapse

Whilst clinicians are mostly interested in using the monoclonal immunoglobulin (Ig) response as a surrogate marker for tumour response, plasma monoclonal Ig is also used to determine the time at which the disease is considered to have relapsed or progressed. In this section IgG responses in a relapse setting are investigated. Simulations were produced using equations (7-28) for the two-compartment model and equations (7-32) for the four-compartment model. The system was assumed to be in steady state at $t = 0$. The parameter values used to simulate the two-compartment model are given in table 7-6. The values for parameters k_{21}, k_{12}, v_1 and v_3 are assumed to be the same for both models. The remaining parameter values used in simulating the four-compartment model are given by row 'A1' in table 7-7.

The monoclonal IgG production rate, $I_{\mathrm{m}}(t)$, is now given by

$$I_{\mathrm{m}}(t) = I_{\mathrm{m1}} \exp(-k_{\mathrm{kill}} t) + I_{\mathrm{m2}} \exp\big(k_{\mathrm{growth}} t\big). \tag{7-40}$$

This model is introduced in chapter 8. The parameter values for monoclonal and poly-

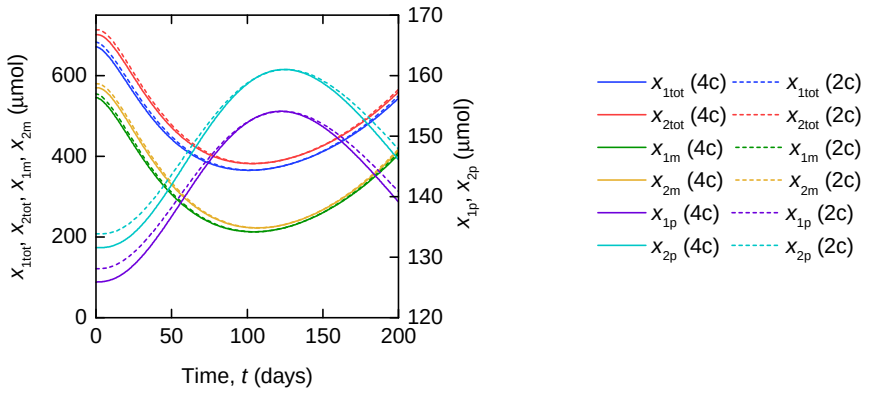

Figure 7-12 Monoclonal, polyclonal and total IgG, in compartments 1 and 2, simulated using the two-compartment model (dashed lines) and the four-compartment model (solid lines). The monoclonal IgG production rate initially falls and then increases during a relapse. Note the different scales for total and monoclonal quantities (left axis) and polyclonal quantities (right axis).

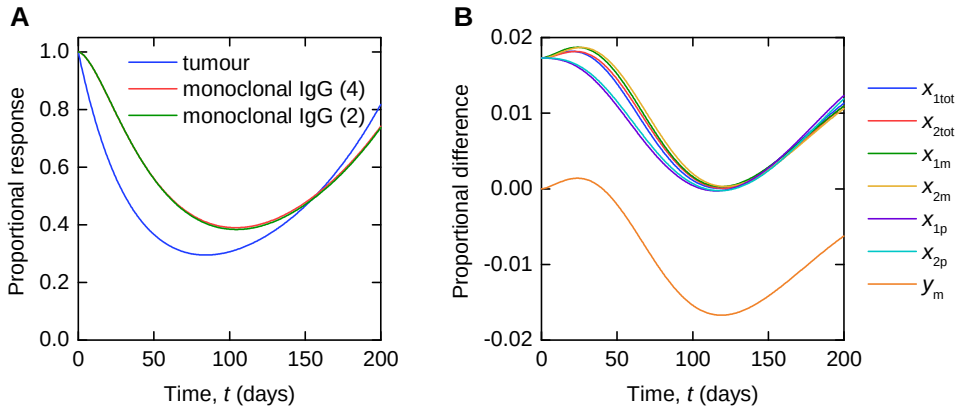

Figure 7-13 (A) The monoclonal IgG response during relapse, simulated for both the two-compartment model and the four-compartment model. (B) Proportional differences between the four-compartment model and the two-compartment model, for monoclonal, polyclonal and total quantities of IgG and the monoclonal IgG response, during relapse.

clonal IgG production are given in table 7-8.

The simulation shown in figure 7-12 shows the responses of monoclonal, polyclonal and total IgG in plasma and the peripheral compartment, respectively, for both the two- and four-compartment models. The two-compartment model now overestimates each quantity, relative to the four-compartment model, throughout the simulation, peaking at around 1.9% overestimation.

Figure 7-13A shows the tumour response, given by equation (7-36), the monoclonal IgG

response for the two-compartment model, given by equation (7-31), and the monoclonal IgG response for the four-compartment model, given by equation (7-35). Figure 7-13B shows the proportional differences between the quantities of IgG and monoclonal IgG responses, for the two models, respectively. The proportional difference between the two models does not approach a steady state at the end of the simulation. The simulation was produced by attempting to replicate the trajectory shown by the monoclonal IgG concentration of a real patient, monitored for approximately 200 days. It is possible that the two models could diverge at a later time, producing very different predictions. This was checked by simulating the model over 800 days and finding that the proportional differences plateau around this time, with none of the proportional differences reaching an absolute value of more than 5%.

7.7 Conclusions

In this chapter the relationship between the two- and four-compartment models analysed in chapters 5 and 6, respectively, has been investigated. The assumptions required to derive the two-compartment model from the four-compartment model were tested using simulations. The simulations revealed that whilst the QSS assumption is more difficult to violate than for the classical enzyme reaction model, the assumption of the equality of the plasma and endosomal concentrations of unbound IgG is not supported by the four-compartment model in its current form. A possible modification to the model was briefly mentioned; however this alternative model would require further validation and is therefore not presented in this thesis.

Whilst the assumption of the equality of the plasma and endosomal concentrations is not necessarily valid with feasible parameter values, the two models nonetheless produce similar predictions, when the parameters $V_{\max}$ and K_{M} are estimated from experimental data rather than being derived from the four-compartment model parameters. The simulated quantities in section 7.6 did not differ by more than 6%; however, when making more complex predictions it is possible that the models may diverge and this is something to be aware of.

References

1. J. G. Hattersley, PhD thesis, University of Warwick, 2009.
2. L. Michaelis, M. L. Menten, *Biochemische Zeitschrift* **49**, 333–369 (1913).
3. J. D. Murray, *Mathematical Biology: I. An Introduction* (Springer, New York, ed. 3, 2002), ISBN: 9786610009367.
4. F. G. Heineken, H. M. Tsuchiya, R. Aris, *Mathematical Biosciences* **1**, 95–113 (1967).
5. J. G. Hattersley et al., *Computer Methods and Programs in Biomedicine* **109**, 126–133 (2013).
6. A. Solomon, T. Waldmann, J. Fahey, *The Journal of Laboratory and Clinical Medicine* **62**, 1–17 (1963).
7. D. K. Shah, A. M. Betts, *Journal of Pharmacokinetics and Pharmacodynamics* **39**, 67–86 (2012).

8

Predicted responses of immunoglobulins A and G in multiple myeloma

In this chapter predictions are made of the responses of immunoglobulin A (IgA) and immunoglobulin G (IgG), in IgA multiple myeloma and IgG multiple myeloma, respectively. The predictions are based on a two-compartment model of IgG metabolism, which was analysed in chapter 5, and a two-compartment model of IgA metabolism from the literature, described in section 8.1.1. These models describe the quantities of IgA or IgG in plasma and in a peripheral compartment. An important component of these models is the monoclonal immunoglobulin (Ig) production rate, which in multiple myeloma is time-dependent [1], requiring additional parameters for its description. By coupling the parameterised metabolic models with parameterised input functions, the models can be used to predict how plasma monoclonal Igs evolve over time, in response to a changing tumour burden.

There are a number of hypotheses that can be made relating to the behaviour of monoclonal Igs (particularly IgG) in multiple myeloma patients. In this chapter we investigate whether these hypotheses are supported by the mathematical models of IgA and IgG metabolism. This thesis is in large part motivated by the concentration-dependent metabolism of IgG and how this affects the response of monoclonal IgG to a decreas-

ing tumour burden during therapy. In particular, does monoclonal IgG respond faster in patients presenting with large plasma concentrations, due to saturation of recycling receptors? Another potential issue that may be caused by the long metabolic half-life of IgG is the persistence of monoclonal IgG in the patient's system after treatment, when a maximal proportion of the tumour has been eradicated. At normal concentrations, IgG is recirculated by the neonatal Fc receptor (FcRn), which may give a falsely high indication of the proportion of cancerous cells remaining in the bone marrow.

The majority of multiple myeloma patients have IgG- or IgA-producing clones [2]. It is known that the two proteins are eliminated at very different rates, which implies that monoclonal IgG responds more slowly than IgA, for a similar tumour response. Yet, patient responses are assigned in the same way for both IgA and IgG patients. In this chapter the difference between monoclonal IgA and monoclonal IgG responses is investigated. Similarly, when a clone of plasma cells is proliferating, the response of the monoclonal Ig (this time an increase) is likely to be different for IgA and IgG tumours. However, the recommended criteria for relapse, given in section 2.2 of chapter 2, are currently the same for all patients regardless of the isotype of the monoclonal Ig.

It must be noted that the number of malignant plasma cells in the body cannot be measured in practice; it is therefore not possible to validate the predictions made in this chapter using longitudinal measurements of both the myeloma cell population and the monoclonal Ig concentration. However, from the outset, the purpose of this work has been to investigate whether the metabolism of Igs influences their role as prognostic markers. If we assume that the survival outcomes of patients are driven by the response of their cancer, that is the proportion of malignant cells that are successfully killed at a clinically relevant time, then it is possible to qualitatively predict how the effects of Ig metabolism may influence the association between the monoclonal Ig response and survival. In particular we wish to ask the question: is it appropriate to interpret monoclonal IgA and monoclonal IgG responses in the same way, knowing that IgA and IgG are eliminated from the body at very different rates? This will be the subject of chapter 9, in which survival analysis is performed using data from the IFM (Intergroupe Francophone du Myélome) 2009/01 clinical trial [3; 4] of newly diagnosed multiple myeloma patients.

In this chapter, serum protein electophoresis (SPEP) data from the IFM 2009/02 clinical

trial [5] of relapsed and refractory multiple myeloma patients, with IgA or IgG myeloma, are referred to in order to produce simulations that represent realistic responses. The IFM 2009/02 dataset is appropriate for this purpose as monoclonal Ig concentrations were sampled frequently during the initial months following treatment, with measurements taken at 28-day intervals. The two-compartment model of IgA metabolism described in section 8.1.1 is based on the description of systemic IgA metabolism provided by Waldmann et al. [6]; an equivalent model has also been presented by Hattersley et al. [7]. The simulations in this chapter were produced in Mathematica [8] and Berkeley Madonna [9].

In this chapter tumour responses and monoclonal Ig responses are discussed. Responses are calculated and plotted as the proportion of the value at the start of treatment, so for example a patient might have a monoclonal IgA response of 0.25 after 30 days of treatment and the response at the start of treatment is by definition equal to 1. In practice however physicians and medical researchers usually talk about responses in terms of the depth of response, for example the IgA response of 0.25 is referred to as a 75% response. This chapter is largely about underestimation of the tumour response by the monoclonal Ig response; in this sense a monoclonal IgA response of 75% underestimates a tumour response of 80%, for example. Throughout this chapter discussions pertaining to sizes of responses and under- and overestimations of tumour responses are with regard to the depth of response; thus a response of 75% (0.25) is considered greater than a response of 60% (0.4). Both definitions of response are used in this chapter but the one being used should be clear from the context of the discussion.

8.1 Models for the dynamics of IgA and IgG in multiple myeloma

With the assays currently available (see chapter 2, section 2.4) clinicians are, in theory, able to monitor total Ig', monoclonal Ig', Ig'κ and Ig'λ, where the apostrophe (') is used to indicate either A or G, depending on the Ig isotype produced by the clonal plasma cells of the patient. Model-based predictions need to consider how these quantities interact. The polyclonal IgG in particular must be accounted for, as the elimination rate of monoclonal

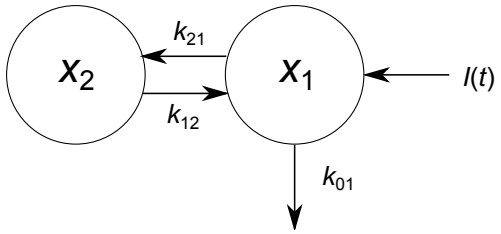

Figure 8-1 Schematic of compartmental model of IgA metabolism described in section 8.1.1

Table 8-1 States and parameters of model of IgA metabolism

Name	Units	Value	Physiological interpretation
x_1	µmol	–	Quantity of IgA in the central (plasma) compartment
x_2	µmol	–	Quantity of IgA in the peripheral compartment
k_{01}	day^{-1}	0.25*	Fraction of IgA in plasma that is catabolised per day
k_{21}	day^{-1}	0.441†	Rate constant of flow of IgA from plasma to peripheral compartment
k_{12}	day^{-1}	0.422†	Rate constant of flow of IgA from peripheral compartment to plasma

*Strober et al. [10]; †values assumed comparable to values for IgG estimated in chapter 5

IgG depends on the total IgG concentration.

8.1.1 Two-compartment model of IgA metabolism

The metabolism of systemic IgA is not as complex as that of IgG as its catabolic rate is independent of its concentration in plasma. Like IgG, IgA is known to be distributed among a central (plasma) compartment and a peripheral compartment. The following model of IgA metabolism has been presented by Hattersley et al. [7]. The metabolism of IgA is described by

$$\begin{aligned} \dot{x}_1(t) &= -\left(k_{21} + k_{01}\right) x_1(t) + k_{12} x_2(t) + I(t) \\ \dot{x}_2(t) &= k_{21} x_1(t) - k_{12} x_2(t), \end{aligned} \tag{8-1}$$

where $x_1(t)$ and $x_2(t)$ represent the quantities in µmol of IgA in plasma and the peripheral compartment, respectively. $I(t)$ represents the synthesis of IgA in plasma in $\mu\text{mol}\,\text{day}^{-1}$. The rate constants, k_{ij}, represent material flow from compartment j to compartment i. A schematic of the model is shown in figure 8-1. Table 8-1 summarises the model states and parameters.

Systemic IgA metabolism has been studied using tracer experiments, although less exten-

sively than IgG metabolism [6]. The type of data for IgG that were utilised in chapters 5 and 6 have not been found in the literature for IgA; therefore, for the model of IgA metabolism, parameters are not estimated from experimental data in this thesis, but are taken from the literature.

Given the similar size of the proteins IgA and IgG (150 kDa), the rate constants of distribution between the central and peripheral compartments, k_{12} and k_{21}, can be assumed to be approximately equal for IgA and IgG [7]. This can be additionally justified by considering the relative quantities in the two compartments at steady state. The intravascular proportion in steady state is given by $\frac{k_{12}}{k_{12}+k_{21}}$ and is comparable between IgA and IgG at approximately 50% [10; 11]. Metabolic studies of IgA have found that the fraction of plasma IgA catabolised per day (k_{01} in equations 8-1) is 0.25 day^{-1} [10]. This is markedly greater than that of IgG in normal subjects (0.063 day^{-1} [6]) and explains the approximately five-fold greater plasma concentration of IgG compared to IgA in healthy subjects.

The normal production rate of endogenous IgA, I_{E} (µmol day^{-1}), is given by $I_{\mathrm{E}} = k_{01}x_{1,\mathrm{E}}$, where $x_{1,\mathrm{E}}$ is the quantity of endogenous IgA in plasma in steady state. The IgA production rate and the quantity of IgA in plasma were found to be 11 µmol day^{-1} and 44 µmol, respectively, for a 70 kg individual [10].

8.1.1.1 Stability analysis

When the production rate is constant, $I(t) = I_0$, the system given by equations (8-1) has a single equilibrium point given by

$$\hat{x}_1 = \frac{I_0}{k_{01}}, \qquad \hat{x}_2 = \frac{k_{21}}{k_{12}}\hat{x}_1. \tag{8-2}$$

Linearising the system about the equilibrium point gives

$$\begin{bmatrix} \dot{x}_1(t) \\ \dot{x}_1(t) \end{bmatrix} = \begin{bmatrix} -(k_{21}+k_{01}) & k_{12} \\ k_{21} & -k_{12} \end{bmatrix} \begin{bmatrix} x_1(t) \\ x_2(t) \end{bmatrix}. \tag{8-3}$$

The eigenvalues of the matrix in equation 8-3 are given by

$$\begin{aligned}\lambda_1 =&\frac{1}{2}\left(-k_{01}-k_{12}-k_{21}-\sqrt{-4k_{01}k_{12}+\left(k_{01}+k_{12}+k_{21}\right)^2}\right)\\ \lambda_2 =&\frac{1}{2}\left(-k_{01}-k_{12}-k_{21}+\sqrt{-4k_{01}k_{12}+\left(k_{01}+k_{12}+k_{21}\right)^2}\right).\end{aligned} \tag{8-4}$$

For a stable equilibrium point, the eigenvalues of the system must have negative real parts for all permitted parameter values. Firstly it can be shown that the eigenvalues λ_1 and λ_2 are always real. The expression within the square root in equation 8-4 can be rearranged to give

$$-4k_{01}k_{12}+\left(k_{01}+k_{12}+k_{21}\right)^2=\left(-k_{01}+k_{12}+k_{21}\right)^2+4k_{01}k_{12}. \tag{8-5}$$

The parameters k_{01}, k_{12} and k_{21} are all real and positive; therefore the right hand side of 8-5 is always positive and the eigenvalues in equation 8-4 are always real.

All terms in the expression for λ_1 are preceded by minus signs, therefore λ_1 is always negative. λ_2 is negative provided that the value of the principal square root in equation 8-4 is less than the value of $(k_{01}+k_{12}+k_{21})$. Since

$$-4k_{01}k_{12}+\left(k_{01}+k_{12}+k_{21}\right)^2>0 \tag{8-6}$$

and

$$-4k_{01}k_{12}+\left(k_{01}+k_{12}+k_{21}\right)^2<\left(k_{01}+k_{12}+k_{21}\right)^2, \tag{8-7}$$

then

$$\sqrt{-4k_{01}k_{12}+\left(k_{01}+k_{12}+k_{21}\right)^2}<\sqrt{\left(k_{01}+k_{12}+k_{21}\right)^2}=k_{01}+k_{12}+k_{21}. \tag{8-8}$$

Therefore λ_2 is negative. Both eigenvalues are real and negative for all permitted parameter values and therefore the equilibrium point is stable.

8.1.2 Extension of model of IgA dynamics for multiple myeloma

A model is required that describes the dynamics of monoclonal IgA (either IgAκ or IgAλ, depending on the patient), polyclonal IgAκ and polyclonal IgAλ. The equations for this model are given by

$$\begin{aligned}\dot{x}_{1\mathrm{A}j}(t)&=-\left(k_{21}+k_{01}\right)x_{1\mathrm{A}j}(t)+k_{12}x_{2\mathrm{A}j}(t)+I_{\mathrm{A}j}(t)\\ \dot{x}_{2\mathrm{A}j}(t)&=k_{21}x_{1\mathrm{A}j}(t)-k_{12}x_{2\mathrm{A},j}(t),\end{aligned} \tag{8-9}$$

for $j = \mathrm{m}, \kappa\mathrm{p}, \lambda\mathrm{p}$.

Here $x_{1\mathrm{A}j}$ is the quantity in µmol in plasma of monoclonal IgA ($j = \mathrm{m}$), polyclonal IgAκ ($j = \kappa\mathrm{p}$) or polyclonal IgAλ ($j = \lambda\mathrm{p}$). Likewise $x_{2\mathrm{A}j}$ is the quantity in µmol in the peripheral compartment of monoclonal IgA ($j = \mathrm{m}$), polyclonal IgAκ ($j = \kappa\mathrm{p}$) or polyclonal IgAλ ($j = \lambda\mathrm{p}$). $I_{\mathrm{A}j}(t)$ represents the production rate of each type of IgA in plasma. The parameter values used are given in table 8-1.

When the production rates are constant ($I_{\mathrm{A}j}(t) = I_{\mathrm{A}j0}$) the system has a stable equilibrium point given by

$$\hat{x}_{1\mathrm{A}j} = \frac{I_{\mathrm{A}j0}}{k_{01}}, \qquad \hat{x}_{2\mathrm{A}j} = \frac{k_{21}}{k_{12}}\hat{x}_{1\mathrm{A}j}, \tag{8-10}$$

for $j = \mathrm{m}, \kappa\mathrm{p}, \lambda\mathrm{p}$.

Clinicians are most interested in the quantity of monoclonal IgA as a proportion of its initial value at the start of treatment. This is referred to as the monoclonal IgA response and is given by

$$y_{\mathrm{A}}(t) = \frac{x_{1\mathrm{Am}}(t)}{x_{1\mathrm{Am}}(T_0)}, \tag{8-11}$$

for $t > T_0$, where $x_{1\mathrm{Am}}(t)$ is given by equations (8-9) and treatment is assumed to begin at time $t = T_0$.

8.1.3 Extension of the two-compartment model of IgG dynamics for multiple myeloma

The model presented here is an extension of the two-compartment model of IgG metabolism studied in chapter 5, now explicitly differentiating between different IgG types. The equations describing the rates of change of monoclonal IgG, polyclonal IgGκ and polyclonal IgGλ are given by

$$\begin{aligned}
\dot{x}_{1\mathrm{G}j}(t) &= -\left(k_{21} + k_{31} - \frac{V_{\max}}{K_{\mathrm{M}} + x_{1\mathrm{Gtot}}(t)}\right) x_{1\mathrm{G}j}(t) + k_{12}x_{2\mathrm{G}j}(t) + I_{\mathrm{G}j}(t) \\
\dot{x}_{2\mathrm{G}j}(t) &= k_{21}x_{1\mathrm{G}j}(t) - k_{12}x_{2\mathrm{G}j}(t),
\end{aligned} \tag{8-12}$$

for $j = \mathrm{m}, \kappa\mathrm{p}, \lambda\mathrm{p}$, with $x_{1\mathrm{Gtot}}(t) = x_{1\mathrm{Gm}}(t) + x_{1\mathrm{G}\kappa\mathrm{p}}(t) + x_{1\mathrm{G}\lambda\mathrm{p}}(t)$.

Here $x_{1\mathrm{G}j}$ is the quantity in µmol in plasma of monoclonal IgG ($j = \mathrm{m}$), polyclonal IgGκ ($j = \kappa\mathrm{p}$) or polyclonal IgGλ ($j = \lambda\mathrm{p}$). Likewise $x_{2\mathrm{G}j}$ is the quantity in µmol in

Table 8-2 Parameters values for model of IgG dynamics in multiple myeloma, estimated in chapter 5

Name	Units	Value
k_{21}	day^{-1}	0.441
k_{31}	day^{-1}	0.159
$V_{\max}$	$\mu\text{mol}\,\text{day}^{-1}$	40.0
K_{M}	μmol	272
k_{12}	day^{-1}	0.422

a peripheral compartment of monoclonal IgG ($j = \text{m}$), polyclonal IgGκ ($j = \kappa\text{p}$) or polyclonal IgGλ ($j = \lambda\text{p}$). $I_{\text{G}j}(t)$ represents the production rate of each type of IgG in plasma. The parameter values used are given in table 8-2.

When the Ig production rates are constant ($I_{\text{G}j}(t) = I_{\text{G}j0}$) the system has a stable equilibrium point (for feasible parameter values; see chapter 5, section 5.2.1) given by

$$\begin{aligned}\hat{x}_{1\text{Gtot}} &= \frac{-k_{31}K_{\text{M}} + I_{\text{Gtot0}} + V_{\max} + \sqrt{4k_{31}K_{\text{M}}I_{\text{Gtot0}} + (-k_{31}K_{\text{M}} + I_{\text{Gtot0}} + V_{\max})^2}}{2k_{31}} \\ \hat{x}_{2\text{Gtot}} &= \frac{k_{21}}{k_{12}}\hat{x}_{1\text{Gtot}},\end{aligned} \tag{8-13}$$

where $x_{1\text{Gtot}}$ and $x_{2\text{Gtot}}$ are the total quantities of IgG in plasma and the peripheral compartment, respectively, and the total production rate of IgG is given by

$$I_{\text{Gtot0}} = I_{\text{Gm0}} + I_{\text{G}\kappa\text{p0}} + I_{\text{G}\lambda\text{p0}}. \tag{8-14}$$

The equilibrium points for the different IgG types are given by

$$\hat{x}_{1\text{G}j} = \frac{I_{\text{G}j0}}{I_{\text{Gtot0}}}\hat{x}_{1\text{Gtot}}, \qquad \hat{x}_{2\text{G}j} = \frac{I_{\text{G}j0}}{I_{\text{Gtot0}}}\hat{x}_{2\text{Gtot}}, \tag{8-15}$$

for $j = \text{m}, \kappa\text{p}, \lambda\text{p}$.

The monoclonal IgG response is given by

$$y_{\text{G}}(t) = \frac{x_{1\text{Gm}}(t)}{x_{1\text{Gm}}(T_0)}, \tag{8-16}$$

for $t > T_0$, where $x_{1\text{Gm}}(t)$ is given by equations (8-12) and treatment is assumed to begin at time $t = T_0$.

8.2 Models for Ig production rates

The models given in section 8.1 can be used to simulate the dynamics of IgA and IgG in multiple myeloma when coupled with parameterised input functions. When assumptions are made about the relationship between the clonal plasma cell population and the monoclonal Ig production rate, these models can be used to investigate the relationship between a growing or shrinking plasma cell clone and the monoclonal Ig that it produces. It is then possible to predict the monoclonal Ig response to a given tumour trajectory under various conditions including tumour growth, response to therapy and relapse.

The average monoclonal Ig synthesis rate per plasma cell has been reported in the literature as 1.45×10^{-11} g day^{-1} (9.7×10^{-11} µmol day^{-1}) [1] and 1.21×10^{-11} g day^{-1} (8.1×10^{-11} µmol day^{-1}) [12]. Sullivan et al. [1] have found that for individual patients this rate remains constant during the course of the disease. Thus the monoclonal Ig production rate at time t, denoted by $I_{\mathrm{m}}(t)$, can be assumed to be proportional to the myeloma cell population at time t, denoted by $N_{\mathrm{m}}(t)$. In this section models for the Ig production rates are provided, assuming proportionality between the plasma cell population and the rate of Ig synthesis.

8.2.1 Mono-exponential response to therapy

The simplest approach to modelling the tumour burden in response to therapy is to assume mono-exponential decay of the myeloma cell population [13; 14]. The evolution of the myeloma cell population is thus given by

$$N_{\mathrm{m}}(t) = N_0 \exp(-k_{\mathrm{kill}} t), \qquad N_{\mathrm{m}}(0) = N_0, \tag{8-17}$$

where $N_{\mathrm{m}}(t)$ is the myeloma cell population, N_0 is the myeloma cell population at time $T_0 = 0$ days, when treatment is assumed to begin, and k_{kill} (day^{-1}) is the (positive) rate constant of tumour kill.

In practice there are a multitude of therapeutic agents and regimens that are used in the treatment of multiple myeloma. The mono-exponential model is a highly simplistic representation of the more complex evolution of the tumour burden that is the resultant

product of the pharmacokinetics, pharmacodynamics and dosing regimen of the therapeutic agent(s) used. Cancer drugs are heterogenous and may operate by killing the existing cancer cells, inhibiting proliferation or both, often through a number of mechanisms that are not always clear. Considering a therapy that kills cancer cells and assuming first order kinetics, the rate at which cancer cells are killed is proportional to the number (or quantity or concentration) of cells and the concentration of drug; this is known as the linear log-kill hypothesis [15, p. 21]. Letting $c(t)$ denote the concentration of drug in $\mu\text{mol}\,\text{l}^{-1}$, the rate of cell death under this hypothesis is given by

$$\phi c(t) N_{\text{m}}(t), \tag{8-18}$$

where ϕ ($\text{l}\,\mu\text{mol}^{-1}\,\text{day}^{-1}$) is a constant representing the effectiveness of the drug.

The unforced proliferation rate of the cancer cells has previously been modelled by exponential, Gompertz or logistic growth curves [15, ch. 1]. Taking the simplest of these, exponential growth, the evolution of the myeloma cell population is now given by

$$\dot{N}_{\text{m}}(t) = r_{\text{m}} N_{\text{m}}(t) - \phi c(t) N_{\text{m}}(t), \tag{8-19}$$

where r_{m} (day^{-1}) represents the proliferation rate of the cells in the absence of intervention.

The drug concentration at the site of action, $c(t)$, is the realisation of the dosing regimen and the pharmacokinetic profile of the agent. The simplest approach is to assume that the drug concentration is constant, $c(t) = c_0$. In reality the concentration is likely to change in a periodic fashion, increasing with dose administration and decaying in the interim period. For simplicity, c_0 can be considered as the average concentration of drug over time; then the rate of change of the myeloma cell population is given by

$$\dot{N}_{\text{m}}(t) = (r_{\text{m}} - \phi c_0) N_{\text{m}}(t). \tag{8-20}$$

The tumour cell population now follows mono-exponential decay when the drug has a high enough concentration and efficacy relative to the proliferation rate of the cells: $\phi c_0 > r_{\text{m}}$.

Assuming a constant Ig production rate per plasma cell, the monoclonal Ig production rate $I_{\text{m}}(t)$ can thus be described by

$$I_{\text{m}}(t) = I_{\text{m0}} \exp(-k_{\text{kill}} t), \tag{8-21}$$

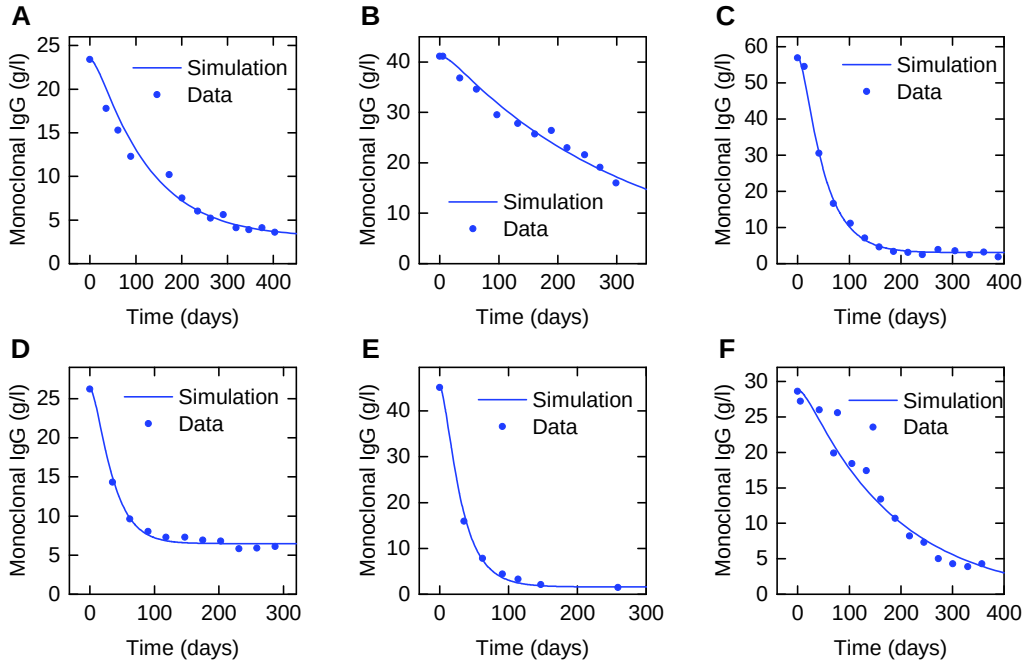

Figure 8-2 Symbol: monoclonal IgG concentration (SPEP) in IgG myeloma patients undergoing treatment. Line: simulation of monoclonal IgG concentration in response to a shrinking tumour burden.

Table 8-3 Parameter values used to produce the simulations in figure 8-2

Parameter	Units	A	B	C	D	E	F
$I_{\mathrm{m}0}$	$\mu\mathrm{mol\,day}^{-1}$	53	104	152	61	116	68
$I_{\mathrm{m}\infty}$	$\mu\mathrm{mol\,day}^{-1}$	5	0	5	11.5	2.5	0
k_{kill}	day^{-1}	0.01	0.0037	0.03	0.055	0.07	0.007

with $I_{\mathrm{m}}(0) = I_{\mathrm{m}0}$.

The therapy may fail to kill 100% of the clonal cells. In this scenario the myeloma cell population can be described by

$$N_{\mathrm{m}}(t) = (N_0 - N_\infty)\exp(-k_{\mathrm{kill}}t) + N_\infty, \tag{8-22}$$

where $N_{\mathrm{m}}(t)$ tends to N_∞ for large t. The monoclonal Ig production rate is then given by

$$I_{\mathrm{m}}(t) = (I_{\mathrm{m}0} - I_{\mathrm{m}\infty})\exp(-k_{\mathrm{kill}}t) + I_{\mathrm{m}\infty}, \tag{8-23}$$

with $I_{\mathrm{m}}(0) = I_{\mathrm{m}0}$ $\mu\mathrm{mol\,day}^{-1}$ and the quantity $I_{\mathrm{m}}(t)$ tending to $I_{\mathrm{m}\infty}$ $\mu\mathrm{mol\,day}^{-1}$ for large t. Examples of monoclonal IgG concentrations, measured by SPEP, are shown in figure 8-2. Superimposed on the data are simulations of the monoclonal IgG concentration when

the monoclonal IgG production rate is described by equation (8-23). The parameter values used to produce these simulations are given in table 8-3 and are used to represent 'reasonable' parameter values for the simulations in this chapter.

When the goal of therapy is to kill as great a proportion of the cancer cells as possible, physicians are most interested in the proportion of cancer cells remaining. This is referred to in this thesis as the tumour response, $y_{\mathrm{m}}(t)$, and is given by

$$y_{\mathrm{m}}(t) = \frac{N_{\mathrm{m}}(t)}{N_{\mathrm{m}}(T_0)}, \qquad y_{\mathrm{m}}(T_0) = 1, \tag{8-24}$$

for $t > T_0$, where therapy is assumed to begin at T_0 days (often with $T_0 = 0$). When the monoclonal Ig production rate is assumed to be directly proportional to the clonal plasma cell population, then the tumour response is given by

$$y_{\mathrm{m}}(t) = \frac{I_{\mathrm{m}}(t)}{I_{\mathrm{m}}(T_0)}, \qquad y_{\mathrm{m}}(T_0) = 1, \tag{8-25}$$

for $t > T_0$, again where therapy is assumed to begin at T_0 days. Throughout this chapter it is assumed that Ig synthesis rates are directly proportional to plasma cell populations; therefore equation (8-25) applies to each of the models presented in this section.

8.2.2 Tumour growth

Growth of myeloma cell populations can be approximated by the Gompertz function [1], given by

$$\dot{N}_{\mathrm{m}}(t) = r_{\mathrm{m}} N_{\mathrm{m}}(t) \log\left(\frac{K_{\mathrm{m}}}{N_{\mathrm{m}}(t)}\right), \tag{8-26}$$

where N_{m} is the population of monoclonal plasma cells, K_{m} is the so-called carrying capacity, representing the maximal population that can be reached, and r_{m} (day^{-1}) is a constant related to the rate of tumour growth. The Gompertz equation has been used to model multiple myeloma cell population growth in several publications [1; 12; 16–18]. Mechanistically, the Gompertz model represents the effect of competition for resources in the bone marrow limiting the growth of the clonal cell population.

Sullivan et al. [1] provide parameter values for an alternative parameterisation of the Gompertz equation for a sample of 11 patients with IgG multiple myeloma, from which r_{m} and K_{m} can be derived. The calculated values of K_{m} agree with those in Swan et al.

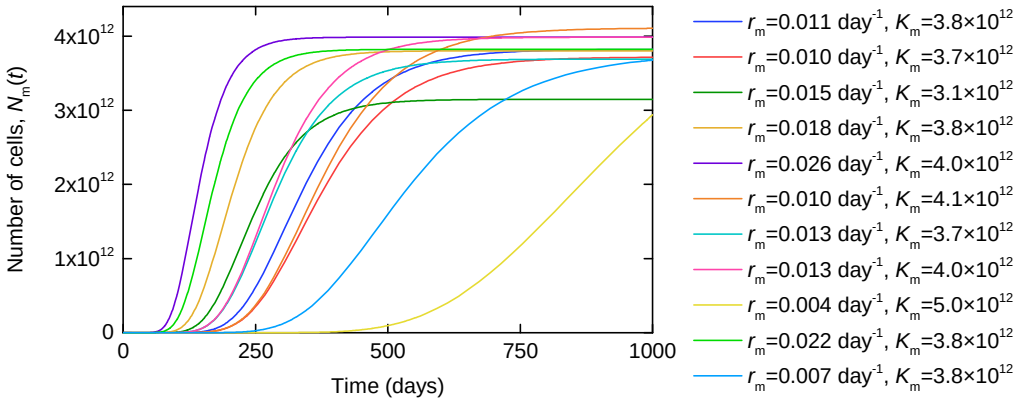

Figure 8-3 Multiple myeloma growth curves, simulated using equation (8-26) with parameter values calculated from data in [1]

[18] and Dingli et al. [12]. The predicted growth curves using these parameter values are shown in figure 8-3. The plot shows the evolution of the myeloma cell population if left untreated.

Considering a scenario in which the tumour cell population is growing up to the commencement of therapy, which is modelled according to the log-kill hypothesis, the growth and subsequent decline of the myeloma cell population is given by

$$\begin{aligned} \dot{N}_{\mathrm{m}}(t) &= r_{\mathrm{m}} N_{\mathrm{m}}(t) \log\left(\frac{K_{\mathrm{m}}}{N_{\mathrm{m}}(t)}\right) - \phi c \left(N_{\mathrm{m}}(t) - N_{\mathrm{m1}}\right) \\ N_{\mathrm{m}}(0) &= N_{\mathrm{m0}} \\ \phi c &= \begin{cases} 0, & t < T_0 \\ \Phi, & t \geq T_0 \end{cases}, \end{aligned} \tag{8-27}$$

where c (µmol l^{-1}) is the average concentration of drug at the site of action, assumed constant, ϕ (l µmol^{-1} day^{-1}) is a constant expressing the effectiveness of the drug, N_{m1} is a constant, representing a population of plasma cells against which the therapy is ineffective, and T_0 (days) is the time at which therapy commences. Since the parameters ϕ and c only appear as the product ϕc, the parameter $\Phi = \phi c$ (day^{-1}) is defined.

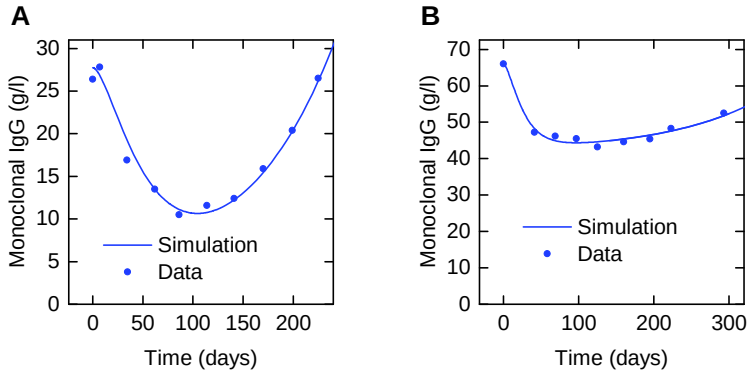

Figure 8-4 Symbol: monoclonal Ig concentration (SPEP) in (A) an IgG myeloma patient and (B) an IgA myeloma patient. Line: simulation of monoclonal Ig concentration, responding to a tumour burden that is initially shrinking and then growing.

8.2.3 Relapse

A simple way to model relapse is to introduce another exponential term in equations (8-22), this time with a positive exponent, as follows,

$$N_{\mathrm{m}}(t) = N_1 \exp\left(-k_{\mathrm{kill}}t\right) + N_2 \exp\left(k_{\mathrm{growth}}t\right) + N_\infty, \qquad N_{\mathrm{m}}(0) = N_1 + N_2 + N_\infty, \quad (8\text{-}28)$$

where k_{growth} is a positive constant. This model is not derived mechanistically, but theoretically represents a scenario in which a proportion of the clone is killed (N_1), a proportion continues to grow (N_2) and a proportion remains stable (N_∞).

The monoclonal Ig production rate, $I_{\mathrm{m}}(t)$, is then given by

$$I_{\mathrm{m}}(t) = I_{\mathrm{m1}} \exp(-k_{\mathrm{kill}}t) + I_{\mathrm{m2}} \exp\left(k_{\mathrm{growth}}t\right) + I_{\mathrm{m}\infty}, \qquad I_{\mathrm{m}}(0) = I_{\mathrm{m1}} + I_{\mathrm{m2}} + I_{\mathrm{m}\infty}. \quad (8\text{-}29)$$

Each of the models given by equations (8-21), (8-23) and (8-29) are constrained cases of a model based on two exponentials and a constant. Examples of monoclonal IgG concentrations, measured by SPEP, are shown in figure 8-4. Superimposed on the data are simulations of the monoclonal IgG concentration when the monoclonal IgG production rate is described by equation (8-29).

The following, more detailed, model of relapse incorporates tumour growth, tumour kill during therapy, and relapse due to decreasing effectiveness of therapy. The myeloma cell

population is described by

$$\begin{aligned} \dot{N}_{\mathrm{m}}(t) &= r_{\mathrm{m}} N_{\mathrm{m}}(t) \log\left(\frac{K_{\mathrm{m}}}{N_{\mathrm{m}}(t)}\right) - \Phi(t) N_{\mathrm{m}}(t) \\ N_{\mathrm{m}}(0) &= N_{\mathrm{m0}}, \end{aligned} \tag{8-30}$$

where the effectiveness of therapy, $\Phi(t)$, is now assumed to decrease over time and is given by

$$\Phi(t) = \begin{cases} 0, & t < T_0 \\ \phi_0 \exp\bigl(-k_\phi (t - T_0)\bigr) & t \geq T_0, \end{cases} \tag{8-31}$$

where ϕ_0 day^{-1} is the initial effectiveness of therapy at time $t = T_0$ and k_ϕ day^{-1} is a rate constant describing the rate of loss of effectiveness.

8.2.4 Polyclonal Ig production rate

The simplest approach to modelling the polyclonal Ig production rates is to assume that they remain at a normal level. The average IgG production rate in normal subjects is 15 µmol day^{-1} [6]. On average, the proportion of serum IgG that is IgGκ is 64% and IgGλ 36% [19]. Thus the average normal production rates are $I_{\mathrm{G}\kappa\mathrm{p}} = 9.6$ µmol day^{-1} and $I_{\mathrm{G}\lambda\mathrm{p}} = 5.4$ µmol day^{-1}, of IgGκ and IgGλ, respectively. Likewise the average IgA production rate in normal subjects is 11 µmol day^{-1} [10], with IgAκ representing 55% of serum IgA [19]. Thus the average normal production rates are $I_{\mathrm{A}\kappa\mathrm{p}} = 6.0$ µmol day^{-1} and $I_{\mathrm{A}\lambda\mathrm{p}} = 5.0$ µmol day^{-1}, of IgAκ and IgAλ, respectively.

Polyclonal plasma cells in the bone marrow are frequently depleted in multiple myeloma, causing a corresponding decrease in the overall synthesis rate of normal polyclonal Ig. There are several complex mechanisms involved, but fundamentally the suppression of polyclonal cells is believed to be due to competition between monoclonal and polyclonal cells for survival niches in the bone marrow microenvironment [20–23].

The mechanisms behind the suppression of polyclonal plasma cells in the bone marrow are not entirely clear; however mechanistic models of competition can frequently be reduced to commonly applied descriptive models [24, ch. 2]. The most well-known model of

competition is the Lotka-Volterra competition model [25; 26], given by

$$\begin{aligned}\dot{N}_1(t) &= r_1 N_1(t)\left(K_1 - N_1(t) - \alpha_{12}N_2(t)\right)/K_1 \\ \dot{N}_2(t) &= r_2 N_2(t)\left(K_2 - N_2(t) - \alpha_{21}N_1(t)\right)/K_2,\end{aligned} \tag{8-32}$$

where N_1 and N_2 are two competing populations, r_i is the growth rate of N_i, K_i is the carrying capacity of N_i and α_{ij} is the competition coefficient, representing the negative action that N_j has on N_i $(i = 1, 2)$. The carrying capacity, K_i, is the maximum population size of N_i, representing the effect of intra-species competition for finite resources. When only one species is present, the dynamics are of logistic growth form, given by

$$\dot{N}_1(t) = r_1 N_1(t)\left(K_1 - N_1(t)\right)/K_1. \tag{8-33}$$

In an alternative model the individual populations are assumed to observe Gompertzian growth in the absence of competition [27]. The model equations are given by

$$\begin{aligned}\dot{N}_1(t) &= r_1 N_1(t)\log\left(\frac{K_1}{N_1(t) + \alpha_{12}N_2(t)}\right) \\ \dot{N}_2(t) &= r_2 N_2(t)\log\left(\frac{K_2}{N_2(t) + \alpha_{21}N_1(t)}\right),\end{aligned} \tag{8-34}$$

where all variables and parameters are interpreted in the same way as in equation (8-32). Now the growth of an individual population in the absence of competition is Gompertzian, given by equation (8-26).

Assuming that growth of the myeloma cell population follows the Gompertz curve, a model for the populations of malignant and normal polyclonal plasma cells is given by

$$\begin{aligned}\dot{N}_{\mathrm{m}}(t) &= r_{\mathrm{m}} N_{\mathrm{m}}(t)\log\left(\frac{K_{\mathrm{m}}}{N_{\mathrm{m}}(t) + \alpha_{\mathrm{mp}}N_{\mathrm{p}}(t)}\right) \\ \dot{N}_{\mathrm{p}}(t) &= r_{\mathrm{p}} N_{\mathrm{p}}(t)\log\left(\frac{K_{\mathrm{p}}}{N_{\mathrm{p}}(t) + \alpha_{\mathrm{pm}}N_{\mathrm{m}}(t)}\right),\end{aligned} \tag{8-35}$$

where N_{m} and N_{p} are the numbers of monoclonal and polyclonal plasma cells in the bone marrow, r_{m} and r_{p} are the proliferation rates of monoclonal and polyclonal plasma cells, K_{m} and K_{p} are the carrying capacities of the monoclonal and polyclonal cells, α_{mp} is the negative effect of competition from N_{p} on N_{m}, and α_{pm} is the negative effect of competition from N_{m} on N_{p}.

Due to the lack of availability of known parameter values, the model can be simplified by assuming that the polyclonal cells do not have a negative effect on the malignant

cells, such that $\alpha_{\mathrm{mp}} = 0$. Given the proliferative ability of clonal plasma cells and the suppression of polyclonal plasma cells seen in myeloma patients, the clonal cells clearly have a competitive advantage. Then the myeloma cell growth follows the Gompertz function, as described in section 8.2.2. Now the populations of monoclonal and polyclonal plasma cells are described by

$$\begin{aligned} \dot{N}_{\mathrm{m}}(t) &= r_{\mathrm{m}} N_{\mathrm{m}}(t) \log\left(\frac{K_{\mathrm{m}}}{N_{\mathrm{m}}(t)}\right) \\ \dot{N}_{\mathrm{p}}(t) &= r_{\mathrm{p}} N_{\mathrm{p}}(t) \log\left(\frac{K_{\mathrm{p}}}{N_{\mathrm{p}}(t) + \alpha_{\mathrm{pm}} N_{\mathrm{m}}(t)}\right). \end{aligned} \tag{8-36}$$

The parameter values for the monoclonal cell population can be found in the literature, as shown in section 8.2.2. The parameters describing the polyclonal plasma cells are r_{p}, K_{p} and α_{pm}. At the time of writing the author is unable to find a mathematical model of long-lived plasma cell homeostasis in the literature; indeed the mechanisms of homeostasis are still not clear [23; 28]. For the sake of simplicity the parameter r_{p} can be assumed to be equal to r_{m}. K_{p} corresponds to the normal population of bone marrow plasma cells. Again it is difficult to find values for this parameter in the literature, however typical steady state immunoglobulin production rates in healthy humans are known. Assuming that long-lived plasma cells in the bone marrow are responsible for the majority of long-term antibody generation, the polyclonal plasma cell population can be calculated from the polyclonal immunoglobulin production rate and the synthesis rate per plasma cell. Taking the average values of normal polyclonal immunoglobulin production of 11 and 15 $\mu\mathrm{mol\,day}^{-1}$ for IgA and IgG, respectively, and an average immunoglobulin synthesis rate per cell of 8×10^{-11} $\mu\mathrm{mol\,day}^{-1}$ gives $K_{\mathrm{p}} = 1.375 \times 10^{11}$ for IgA and $K_{\mathrm{p}} = 1.875 \times 10^{11}$ for IgG. The phenomenon of polyclonal plasma cell suppression has not been incorporated into the simulations presented in this chapter; however, this could be the subject of future research.

8.3 Comparison of IgA and IgG responses to a decreasing tumour burden

In this section, the effect of the different elimination rates of IgA and IgG on their responses to a shrinking plasma cell clone is investigated. The monoclonal Ig responses

Table 8-4 Parameters values used in the simulation in section 8.3. Certain parameter values were adjusted in order that the monoclonal IgG concentration approximately replicates the patient data shown in figure 8-2D.

Name	Units	Value	Source
I_{m0}	$\mu\mathrm{mol\,day^{-1}}$	61	Adjusted to replicate patient data
$I_{\mathrm{m}\infty}$	$\mu\mathrm{mol\,day^{-1}}$	11.5	Adjusted to replicate patient data
k_{kill}	$\mathrm{day^{-1}}$	0.055	Adjusted to replicate patient data
$I_{\mathrm{G}\kappa\mathrm{p}}$	$\mu\mathrm{mol\,day^{-1}}$	9.6	Waldmann et al. [6], Bradwell et al. [19]
$I_{\mathrm{G}\lambda\mathrm{p}}$	$\mu\mathrm{mol\,day^{-1}}$	5.4	Waldmann et al. [6], Bradwell et al. [19]

of IgA and IgG myeloma patients are compared, assuming that the responses of their respective tumours to treatment are identical.

A scenario is considered in which two patients, with IgA- and IgG-producing plasma cell clones, respectively, undergo a course of therapy beginning at time $T_0 = 0$ days. The monoclonal IgA production rate, $I_{\mathrm{Am}}(t)$, and the monoclonal IgG production rate, $I_{\mathrm{Gm}}(t)$, are each set equal to $I_{\mathrm{m}}(t)$ given by equation (8-23). The parameter values for the monoclonal Ig production rate are given in table 8-4. The parameter values for the monoclonal Ig production rate were chosen so that the monoclonal IgG concentration during treatment approximates the patient data shown in figure 8-2D. The polyclonal IgG production rates are assumed to be constant and take the average values in normal subjects, given in table 8-4. It is not necessary to include polyclonal IgA as the system equations for monoclonal and polyclonal IgA are not coupled.

The dynamics of IgA and IgG are described by equations (8-9) and equations (8-12), respectively. The parameter values are given in tables 8-1 and table 8-2. At time $T_0 = 0$ days the system is assumed to be in steady state. The initial conditions for the quantities of IgG and IgA are therefore set to the steady state values given by equations (8-13) and (8-10), respectively.

Clinicians are most interested in two quantities: the population of myeloma cells as a proportion of its initial value (tumour response) and the quantity of plasma monoclonal Ig as a proportion of its initial value (monoclonal Ig response). The tumour response is given by equation (8-25). The monoclonal Ig responses are given by equations (8-11) and (8-16), for the IgA myeloma and IgG myeloma patients, respectively, with $T_0 = 0$ days.

Figure 8-5A shows a simulation of the two patients' monoclonal Ig responses, respectively,

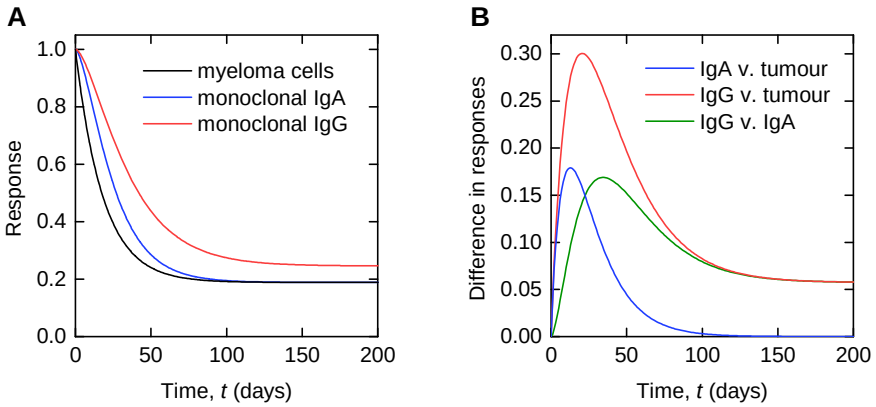

Figure 8-5 (A) Monoclonal IgA and monoclonal IgG responses for identical tumour responses. (B) Differences between monoclonal IgA and tumour responses, monoclonal IgG and tumour responses, and monoclonal IgG and monoclonal IgA responses. The model used to produce the simulation is described in section 8.3.

with both patients assumed to have an identical tumour response, as described above. It can be seen that for the given tumour response, both monoclonal IgA and monoclonal IgG underestimate the depth of the tumour response, that is, they overestimate the proportion of cancer cells remaining at time t. Due to its slower rate of catabolism, monoclonal IgG underestimates the tumour response by a greater margin than monoclonal IgA. Due to the nonlinear relationship between the steady state of IgG and its production rate (see equation (8-13)), the monoclonal IgG response does not tend towards the same value as the tumour response at the end of the simulation.

The degree of underestimation of response is clearly dependent on the time at which the monoclonal Ig is measured. For these particular conditions, the maximal difference between the myeloma cell population response and monoclonal IgA response is 0.18 at $t = 13$ days. The maximal difference between myeloma response and monoclonal IgG response is 0.30 at $t = 21$ days. The differences between the monoclonal IgA response and the myeloma cell response, the monoclonal IgG response and the myeloma cell response, and the monoclonal IgG response and the monoclonal IgA response are depicted in figure 8-5B. There is a difference of 0.058 between the monoclonal IgA and IgG responses at time $t = 200$ days. If responses were assessed at this time, the IgA patient would be considered to have had an 81.1% response, whereas the IgG patient would be assigned a response of 75.3%. The true tumour response is 81.1%. In the clinical setting, 200

days represents the approximate time at which induction therapy is completed and the patient is assumed to have achieved a maximal response to treatment. This is therefore considered the most critical time at which to assess the response. The underestimation of the tumour response by the monoclonal IgG response at this time suggests that IgG patients may be given falsely poor prognoses.

8.3.1 Sensitivity of responses to model parameter values

In this section the sensitivity of the responses of monoclonal IgA and monoclonal IgG to the parameters of the metabolic models is investigated. The sensitivity function of a variable with respect to a parameter is given by the partial derivative of the variable with respect to the parameter. For example, the sensitivity function of the monoclonal IgA response with respect to the parameter k_{21} is given by

$$s_{y_{\mathrm{A}},k_{21}}(t) = \frac{\partial y_{\mathrm{A}}}{\partial k_{21}}(t). \tag{8-37}$$

Due to the range in size of the parameter values, the sensitivity functions are each scaled by the size of the respective parameter values. The scaled sensitivity functions are plotted in figure 8-6, evaluated for the parameter values given in tables 8-1 and 8-2. For example, the scaled sensitivity function of $y_{\mathrm{A}}(t)$ with respect to the parameter k_{21} is given by

$$\tilde{s}_{y_{\mathrm{A}},k_{21}}(t) = k_{21}\frac{\partial y_{\mathrm{A}}}{\partial k_{21}}(t). \tag{8-38}$$

The scaled sensitivity functions have the same units as $y_{\mathrm{A}}(t)$ and are therefore unitless.

The scaled sensitivity functions show the importance of each parameter in determining the response, relative to the parameter's size. Figure 8-6A shows that the parameter k_{01} is the most important parameter in determining the monoclonal IgA response. Figure 8-6B shows that the parameter k_{31} is the most important parameter during the transient phase of the monoclonal IgG response. The parameter $V_{\max}$ is the most important parameter determining the final monoclonal IgG response, with changes in k_{21} and k_{12} having no impact upon the final response.

The simulation shown in figure 8-5 was produced using parameter values that represent the average parameter values within the population; however there is uncertainty associated with these parameter values. The standard error as a percentage of the parameter

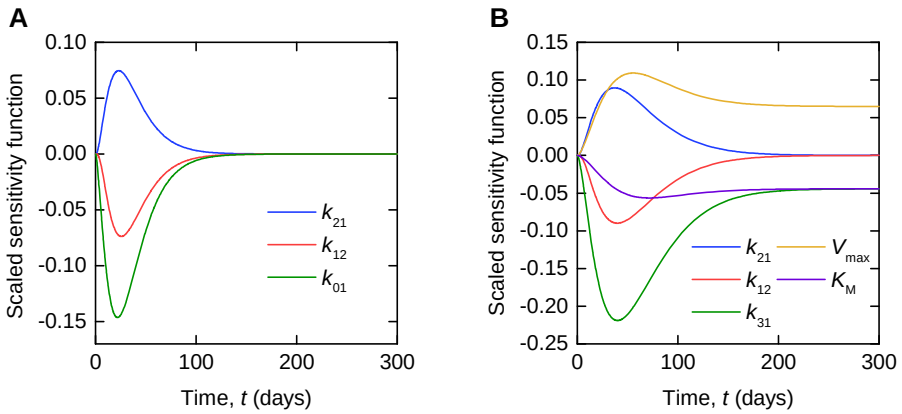

Figure 8-6 Scaled sensitivity functions of (A) monoclonal IgA response and (B) monoclonal IgG response, with respect to the parameters of the metabolic models

Table 8-5 Relative standard error (RSE %) and 95% confidence intervals for the parameter values of the metabolic models

Parameter	RSE (%)	95% confidence interval
k_{31}	7.0	$(0.137, 0.181)$
$V_{\max}$	26	$(19.1, 60.9)$
K_{m}	20	$(162, 382)$
k_{21}	19	$(0.278, 0.604)$
k_{12}	27	$(0.187, 0.657)$
k_{01}	–	$(0.217, 0.288)$

estimate, for each parameter of the two-compartment model of IgG metabolism, is given in table 8-5, along with 95% confidence intervals. The parameter k_{01} has not been estimated in this thesis, but is taken from the literature [10]. Strober et al. [10] provide estimates for k_{01} from twelve subjects, with a sample mean of 0.252 day^{-1} and sample standard deviation of 0.0559 day^{-1}. A confidence interval for the population mean was calculated using

$$CI = \left(0.252 - 2.20 \times \frac{0.0559}{\sqrt{12}}, 0.252 + 2.20 \times \frac{0.0559}{\sqrt{12}}\right), \tag{8-39}$$

where 2.20 is the critical value for the Student's T distribution with $12 - 1 = 11$ degrees of freedom. This confidence interval is also provided in table 8-5.

In order to take into account the uncertainty in the parameter values, the maximum and minimum responses of monoclonal IgA and IgG are considered, for the parameter confidence intervals given in table 8-5. According to the local sensitivity functions plotted in

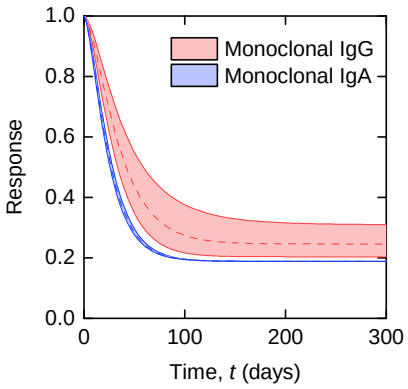

Figure 8-7 Maximal and minimal monoclonal IgA and IgG responses, when the parameters k_{01}, k_{31}, $V_{\max}$ and K_{m} are allowed to vary within their 95% confidence intervals. The region within the maximal and minimal responses is shaded, for each of monoclonal IgA and monoclonal IgG.

figure 8-6, an increase in each parameter has the effect of either increasing or decreasing the value of the monoclonal Ig response over the whole simulated time interval. Whilst the sensitivity functions are local, the general pattern is the same when the parameters are varied within the confidence intervals given. It is thus possible to consider a maximal/minimal response in monoclonal IgG by maximising/minimising parameters $V_{\max}$ and k_{21} and minimising/maximising parameters k_{31}, K_{M} and k_{12}. Similarly for monoclonal IgA, maximising/minimising k_{21} and minimising/maximising k_{01} and k_{12} results in a maximal/minimal response.

Maximal and minimal monoclonal Ig responses, when the parameters are allowed to vary within their 95% confidence intervals, are plotted in figure 8-7. Given that the parameters k_{21} and k_{12} are considered equivalent for both models, only the parameters k_{31}, $V_{\max}$, K_{M} and k_{01} are allowed to vary, whilst k_{21} and k_{12} are fixed to the values given in table 8-2. The region between the minimal and maximal predicted responses is shaded, for both the monoclonal IgA response and the monoclonal IgG response. The shaded region for the monoclonal IgG response is significantly larger than that for monoclonal IgA; this is because there are three parameters allowed to vary for IgG, compared to only one for IgA. The shaded region for IgG is particularly large because correlations between the parameter estimates have not been taken into account. For example, the minimal response is simulated using the lower limit of $V_{\max} = 19.1\ \mu\mathrm{mol\,day}^{-1}$ and the upper limit of $K_{\mathrm{m}} = 382\ \mu\mathrm{mol}$; however these parameter are strongly positively correlated, with a correlation coefficient of 0.976. The shaded region for monoclonal IgG responses in figure

Table 8-6 Parameters values used in the simulation in section 8.3.2. The parameter values were chosen in order that the monoclonal IgG concentration approximately replicates the patient data shown in figure 8-2D.

Name	Units	Value	Source
r_{m}	day^{-1}	0.01	Sullivan et al. [1]
K_{m}	n/a	4×10^{12}	Sullivan et al. [1]
N_{m1}	n/a	8.625×10^{10}	Adjusted to replicate patient data
N_{m0}	n/a	1	
Φ	day^{-1}	0.085	Adjusted to replicate patient data
T_0	days	300	Adjusted to replicate patient data
k_{syn}	$\mu\mathrm{mol\,day}^{-1}$	8×10^{-11}	Dingli et al. [12]
$I_{\mathrm{G}\kappa\mathrm{p}}$	$\mu\mathrm{mol\,day}^{-1}$	9.6	Waldmann et al. [6], Bradwell et al. [19]
$I_{\mathrm{G}\lambda\mathrm{p}}$	$\mu\mathrm{mol\,day}^{-1}$	5.4	Waldmann et al. [6], Bradwell et al. [19]

8-7 is therefore a conservative representation of the confidence we have in the prediction. A more accurate prediction interval could be made by considering a confidence region for the parameters k_{31}, V_{max} and K_{M}, that takes into account parameter correlations. Nevertheless, the value of the minimal monoclonal IgG response is greater than the value of the maximal monoclonal IgA response, for the entire simulated time interval.

8.3.2 Tumour growth prior to the commencement of therapy

To produce the simulations shown in figure 8-5, it was assumed that the system is in steady state at time $T_0 = 0$, that is, all production rates including the monoclonal Ig production rate are constant up to time $T_0 = 0$. It is more realistic to assume that the myeloma cells are actively proliferating and the monoclonal Ig production rate is increasing when therapy commences. In this section Gompertzian growth of the myeloma cell population is assumed prior to the commencement of therapy, at time $T_0 = 300$ days, which is then modelled according to the log-kill hypothesis. The myeloma cell population is therefore described by equation (8-27). The parameter values for the myeloma cell population model and monoclonal Ig production rates are given in table 8-6. The values of the parameters T_0, Φ and N_{m1} were adjusted so that the monoclonal IgG concentration during treatment approximates that shown in figure 8-2D.

Again, two patients are considered – one with an IgA-producing clone and one with an IgG-producing clone. For both patients, the monoclonal Ig production rate is assumed

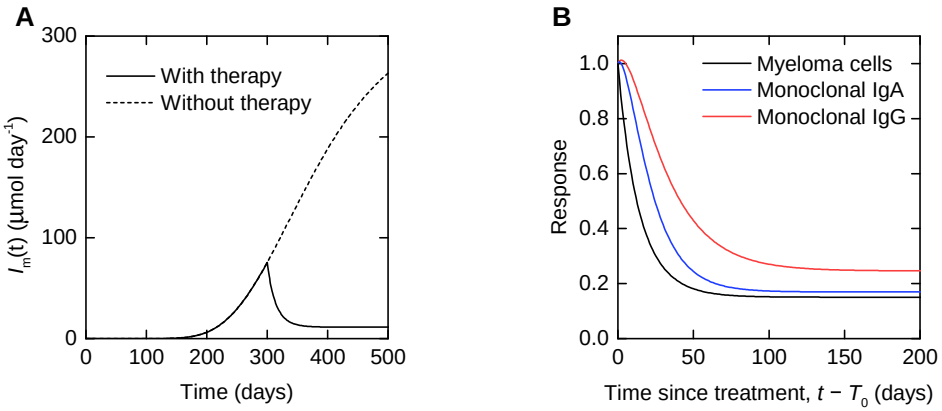

Figure 8-8 (A) Monoclonal Ig production rate up to and during therapy, as described in section 8.3.2. (B) IgA and IgG response for the same tumour response, as described in section 8.3.2.

to be directly proportional to the population of malignant cells, with the proportionality constant k_{syn} μmol per cell, that is $I_{\text{Am}}(t) = P_{\text{Gm}}(t) = k_{\text{syn}} N_{\text{m}}(t)$. As before, normal polyclonal Ig production rates are assumed, given in table 8-6.

The quantities of IgA and IgG are described by equations (8-9) and equations (8-12), respectively, with the parameter values given in tables 8-1 and 8-2. The purpose of this simulation is to investigate the responses of monoclonal Igs when the production rate is increasing at the start of treatment, such that the system is not in steady state when treatment begins; rather, the system is assumed to be in steady state in the very early stages of tumour growth, when the growth rate is very slow. Therefore the tumour growth is simulated with a starting population of $N_{\text{m0}} = 1$ at time 0 days. At time 0 days, the initial conditions of IgA and IgG are given by the steady states in equations (8-10) and (8-13), respectively. Assuming an average plasma volume of 3 l, the concentrations of monoclonal IgA and monoclonal IgG at the start of treatment, $T_0 = 300$ days, are given by 26.0 g l^{-1} and 14.3 g l^{-1}, respectively.

Figure 8-8A shows a simulation of the monoclonal Ig production rate during clonal cell population growth and then decay. The dashed line shows the trajectory that would have been followed if the clone were left untreated. The plot in figure 8-8B shows the response of the clonal cell population and the monoclonal Ig, for the IgA myeloma patient and the IgG myeloma patient. As expected, the response in the tumour is underestimated by the monoclonal Ig, and to a greater extent by monoclonal IgG than monoclonal IgA. For

Table 8-7 Parameters values used in the simulation in section 8.4

Name	Units	Value	Source
k_{kill}	day^{-1}	0.05	Chosen for reasonable response rate
I_{m0} (A)	$\mu\text{mol}\,\text{day}^{-1}$	300	Chosen for a large initial monoclonal IgG concentration
$I_{\text{m}\infty}$ (A)	$\mu\text{mol}\,\text{day}^{-1}$	50	Chosen for a reasonable final response
I_{m0} (B)	$\mu\text{mol}\,\text{day}^{-1}$	15	Chosen for a small initial monoclonal IgG concentration
$I_{\text{m}\infty}$ (B)	$\mu\text{mol}\,\text{day}^{-1}$	2.5	Chosen for a reasonable final response
$I_{\text{G}\kappa\text{p}}$	$\mu\text{mol}\,\text{day}^{-1}$	9.6	Waldmann et al. [6], Bradwell et al. [19]
$I_{\text{G}\lambda\text{p}}$	$\mu\text{mol}\,\text{day}^{-1}$	5.4	Waldmann et al. [6], Bradwell et al. [19]

the parameter values used, the maximal difference between the monoclonal IgA response and the tumour is 0.273, 11 days after therapy begins. For the IgG myeloma patient, a maximal difference of 0.425 occurs 18 days after the start of treatment.

Now that the assumption of steady state at the beginning of treatment has been removed, the differences between the two monoclonal Ig responses and the tumour response are greater. The final tumour response, at $t = 500$ days, of 84.9% is now slightly underestimated by the monoclonal IgA response of 83.0%. The final tumour response is underestimated by almost 10% by the final monoclonal IgG response.

8.4 The effect of concentration-dependent elimination on IgG response

The purpose of this section is to investigate how the concentration-dependent elimination of IgG, due to recycling by saturable FcRn receptors, influences the response of monoclonal IgG in IgG multiple myeloma. Patients with IgG-producing plasma cell clones are considered. The concentration-dependency of IgG elimination suggests that patients with larger initial tumour burdens would have faster monoclonal IgG responses than those with smaller initial tumour burdens, when the tumour response is the same, due to saturation of FcRn receptors. The size of this effect is investigated in this section.

Two patients (A and B) with IgG-producing clones are considered. It is assumed that the two patients have identical tumour responses, however the initial monoclonal IgG production rates are different. The monoclonal IgG production rate for both patients is

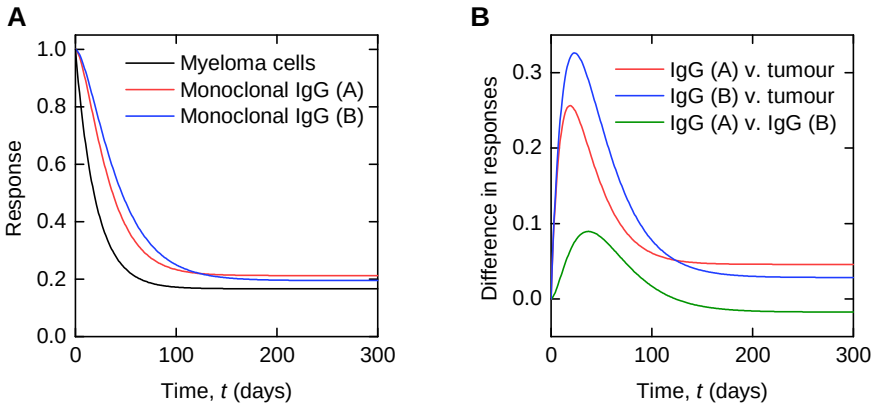

Figure 8-9 (A) Monoclonal IgG responses for identical tumour responses, with different initial monoclonal IgG production rates. (B) Differences between monoclonal IgG and tumour responses and the difference between the two monoclonal IgG responses. The simulation is described in section 8.4.

assumed to be described by equation (8-23). The parameter values for the monoclonal IgG production rate are given in table 8-7. The initial monoclonal IgG production rate is much larger for patient A; it is therefore expected that this patient will have a faster monoclonal IgG response.

The dynamics of IgG are described by equations (8-12), with the parameter values given in table 8-2. The polyclonal IgG production rates are assumed to be constant and take the normal values in table 8-7. Assuming that immediately prior to $t = 0$ days the system is in steady state, this also means that the initial conditions of IgG are different for the two patients. The initial conditions for the quantities of IgG are set to the steady state values given by equation (8-13). Patient A, with an initial monoclonal IgG production rate of $I_{\mathrm{m}0} = 300\ \mu\mathrm{mol\,day^{-1}}$, has an initial quantity of plasma monoclonal IgG of $x_{1,\mathrm{m}}(0) = 2100\ \mu\mathrm{mol}$. Patient B, with $I_{\mathrm{m}0} = 15\ \mu\mathrm{mol\,day^{-1}}$, has $x_{1,\mathrm{m}}(0) = 163\ \mu\mathrm{mol}$. Assuming a plasma volume of 3 l, these initial conditions can be converted to 105 $\mathrm{g\,l^{-1}}$ and 8.14 $\mathrm{g\,l^{-1}}$, respectively, which represent the extremes of the range of baseline monoclonal IgG concentrations seen in actual patient data (a range of 1.8 to 66.9 $\mathrm{g\,l^{-1}}$ is seen in the IFM 2009/02 dataset).

The tumour response and two monoclonal IgG responses are plotted in figure 8-9A. The simulation illustrates the effect of the concentration dependence of IgG metabolism. A patient who is observed, via the monoclonal IgG marker, to initially respond faster to

therapy (patient A in the simulation) may in fact have a faster monoclonal IgG response because recycling receptors are saturated, and not because the tumour is responding faster to treatment. Interestingly, by the end of the simulated timecourse, the monoclonal IgG response for patient B has 'overtaken' that of patient A. The patient with the smaller initial tumour burden has the greater final depth of response; this is because of the nonlinear relationship between the steady state of plasma IgG and its production rate. The differences between the two monoclonal IgG responses, respectively, and the tumour response, are plotted in figure 8-9B, along with the difference between the two monoclonal IgG responses. The maximal difference between the monoclonal IgG responses of the two patients is 9% after 37 days of treatment.

8.4.1 Therapy initiated at different stages in the tumour growth curve

In section 8.4 the effect of the initial monoclonal IgG production rate on the response rate of monoclonal IgG was considered, with the system assumed to be in steady state at the start of treatment. Now a more complex, but more realistic, scenario is considered, in which two IgG-producing clones are treated at different stages in their growth. As in the simulation at the beginning of section 8.4, the concentration of plasma monoclonal IgG when treatment begins is 105 $\mathrm{g\,l^{-1}}$ for the large tumour burden (patient A) and 8.14 $\mathrm{g\,l^{-1}}$ for the small tumour burden (patient B).

The trajectory of the myeloma cell population, for each of the patients A and B, is described by equation (8-27). In the current simulation the growth parameters for the myeloma cell populations, r_{m} and K_{m}, are the same for each tumour, taking the values in table 8-8. Treatment starts at $T_0 = 625$ days for patient A and $T_0 = 241.75$ days for patient B, in order to give the same initial plasma concentrations of IgG as in the previous simulation. The parameters Φ and N_{m1} were adjusted to produce a tumour response that approximates the one in the previous simulation, at the beginning of section 8.4. The monoclonal IgG production rates are assumed to be directly proportional to the populations of malignant cells, with the proportionality constant k_{syn} µmol per cell, for both patients A and B. The polyclonal IgG production rates are assumed to be constant. All parameter values describing IgG production rates are given in table 8-8.

Table 8-8 Parameter values used in the simulation in section 8.4.1. Certain parameter values were adjusted in order that the tumour response approximately replicates the tumour response simulated in section 8.4.

Name	Units	Value	Source
r_{m}	day^{-1}	0.01	Sullivan et al. [1]
K_{m}	n/a	4×10^{12}	Sullivan et al. [1]
N_{m1} (A)	n/a	4.125×10^{11}	Adjusted to approximate the tumour response in section 8.4
N_{m1} (B)	n/a	2.25×10^{10}	Adjusted to approximate the tumour response in section 8.4
N_{m0}	n/a	1	
Φ (A)	day^{-1}	0.054	Adjusted to approximate the tumour response in section 8.4
Φ (B)	day^{-1}	0.08	Adjusted to approximate the tumour response in section 8.4
T_0 (A)	days	625	Chosen for a large initial monoclonal IgG concentration
T_0 (B)	days	241.75	Chosen for a small initial monoclonal IgG concentration
k_{syn}	$\mu\mathrm{mol\,day}^{-1}$	8×10^{-11}	Dingli et al. [12]
$I_{\mathrm{G\kappa p}}$	$\mu\mathrm{mol\,day}^{-1}$	9.6	Waldmann et al. [6], Bradwell et al. [19]
$I_{\mathrm{G\lambda p}}$	$\mu\mathrm{mol\,day}^{-1}$	5.4	Waldmann et al. [6], Bradwell et al. [19]

The dynamics of IgG for both patients A and B are described by equations (8-12), with the parameter values given in table 8-2. At $t = 0$ the system is assumed to be in steady state; the initial conditions of IgG for each IgG patient are thus calculated from equations (8-13).

Figure 8-10A illustrates the scenario in which two tumours, with the same growth parameters, are treated at different stages of their growth. The blue curve shows a tumour that is treated at an earlier stage of growth (patient B) and the red curve shows a tumour that is treated 383.25 days later (patient A), in order to account for the large difference in the initial monoclonal IgG concentrations. In figure 8-10A the monoclonal IgG production rate is plotted, which is proportional to the number of malignant cells. The curves are plotted on two vertical scales in order to illustrate that the proportional response to treatment is the same in both cases.

Figure 8-10B shows the effect of beginning treatment at different growth stages on the monoclonal Ig response. As expected, patient A (large clone) shows a faster monoclonal IgG response than patient B (small clone). Comparing this result with the simulation

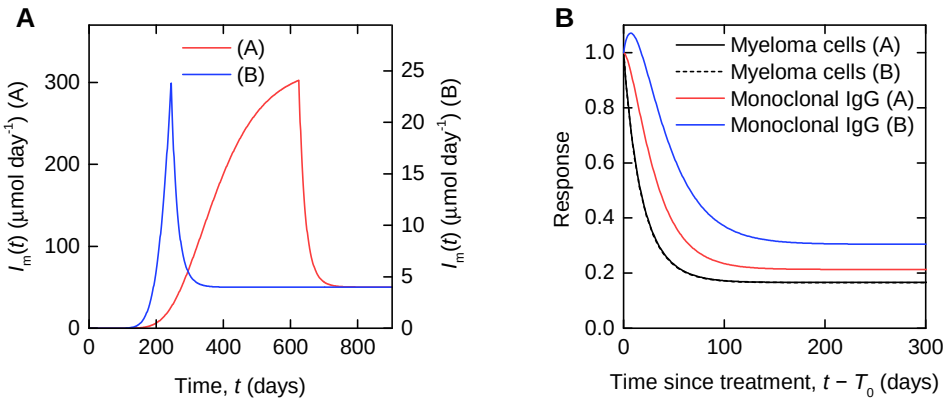

Figure 8-10 (A) Monoclonal IgG production rates and (B) comparison of monoclonal IgG responses, for two patients with different plasma monoclonal IgG concentrations at the beginning of treatment, due to starting treatment at different stages in the tumour growth curve. Note the two vertical axes with different scales in panel (A). The simulation is described in section 8.4.1.

shown in figure 8-9, there is now a considerably larger difference between the two monoclonal IgG responses and the monoclonal IgG response of patient B no longer 'overtakes' that of patient A. The greatest difference between the two monoclonal IgG responses occurs 30.5 days after the beginning of treatment, around the first monitoring point for patients who are followed up monthly. At this time the difference between the two responses is 0.276.

8.5 Tumour responses giving similar monoclonal Ig responses

Having considered in sections 8.3 and 8.4 scenarios in which two patients having the same tumour response show different monoclonal Ig responses, it is natural to consider the reverse problem, in which multiple patients show similar monoclonal Ig responses resulting from different tumour responses.

8.5.1 Identical monoclonal Ig responses at the end of treatment

In section 8.3, the IgA patient had a final monoclonal IgA response of 81.1% whereas the IgG patient had a final monoclonal IgG response of 75.3%, despite both patients having

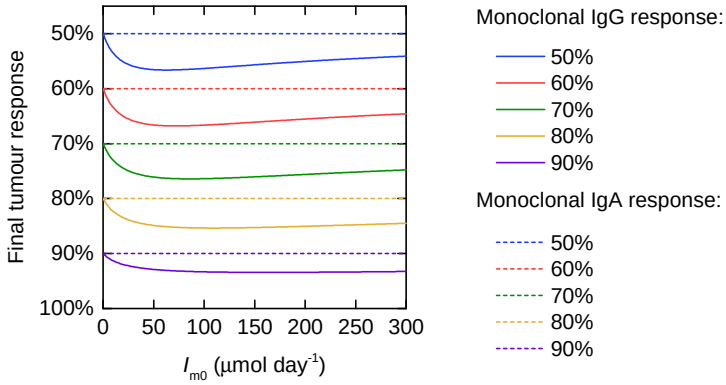

Figure 8-11 Final tumour response plotted against the initial monoclonal Ig production rate, for different final monoclonal Ig responses

a final tumour response of 81.1%. In this section we ask, given the final monoclonal Ig response and the monoclonal Ig isotype (A or G), what is the final tumour response for the patient? As in sections 8.3 and 8.4, the monoclonal Ig production rate is assumed to be given by equation (8-23). The final tumour response is calculated from equation (8-23). The final monoclonal Ig responses are calculated using the steady state values given by equations (8-10) and (8-13).

Figure 8-11 shows the final tumour response plotted against the initial monoclonal Ig production rate, for different final monoclonal Ig responses. Each solid line represents the same final monoclonal IgG response, which may be the result of a range of tumour responses, depending on the initial monoclonal IgG production rate and hence the saturation level of the recycling receptors. For IgA, there is a linear relationship between the production rate and the quantity of IgA in plasma; therefore the final monoclonal IgA response always equals the final tumour response, as represented by the constant dashed lines in figure 8-11. Figure 8-11 shows that a 50% monoclonal IgG response can represent a tumour response of up to 57% when the initial monoclonal IgG production rate is 63 µmol day^{-1}. A 90% monoclonal IgG response can represent a tumour response of up to 93%, when the initial monoclonal IgG production rate is 163 µmol day^{-1}. The simulation shown in this figure imply that the underestimation of the tumour response by the monoclonal IgG response is more important for modest monoclonal IgG responses between 50% (Partial Response; PR) and 80%. For very good partial response (VGPR; 90%) the underestimation of tumour response is less dramatic. This trend continues as

even deeper monoclonal Ig responses are considered, such as 95% and 99%. This is to be expected as the tumour response must be deeper than the monoclonal IgG response; when the monoclonal IgG response is 99% the tumour response cannot be underestimated by more than 1%.

8.5.2 Tumour responses resulting in similar transient monoclonal IgG responses

As shown in section 8.4, the rate of the monoclonal IgG response depends on the monoclonal IgG concentration at the start of treatment as well as the tumour response. In that section, a patient with an initial monoclonal IgG production rate of $I_{\mathrm{m0}} = 15$ µmol day^{-1} was shown to have a slower monoclonal IgG response (initially) than the patient with an initial monoclonal IgG production rate of $I_{\mathrm{m0}} = 300$ µmol day^{-1}, despite having identical tumour responses. However, if the patient with the smaller initial tumour burden were to have a faster tumour response, then the monoclonal IgG of the two patients may respond at a similar rate. The question then is: at what rate must the smaller tumour respond, in order for that to be the case?

In this section tumour responses modelled by equation (8-22) are considered. The monoclonal IgG production rates are given by equation (8-23). To simplify the scenario, the parameter $I_{\mathrm{m}\infty}$ is assumed to be zero and different values of the parameters I_{m0} and k_{kill} are considered, with the aim of finding contours of I_{m0} and k_{kill} which produce similar monoclonal IgG responses. All other features of the simulations are as in section 8.4.

As an example, a patient is considered whose tumour response is parameterised by $I_{\mathrm{m0}} = 300$ µmol day^{-1} and $k_{\mathrm{kill}} = 0.05$ day^{-1} (identical to patient A in section 8.4 but with $I_{\mathrm{m}\infty} = 0$ µmol day^{-1}). A second patient is considered with a much smaller monoclonal IgG production rate at the start of treatment, given by $I_{\mathrm{m0}} = 5$ µmol day^{-1}, and we ask what value of k_{kill} is required for this patient in order that the two responses are closely similar. The 'most similar' response is defined here as the response with the smallest maximal difference, over time, to the response of the first patient. For clarity, we now refer to the parameters for the first patient (A) as I_{m01} and k_{kill1} and those for the second patient (B) as I_{m02} and k_{kill2}; therefore $I_{\mathrm{m01}} = 300$ µmol day^{-1}, $k_{\mathrm{kill1}} = 0.05$

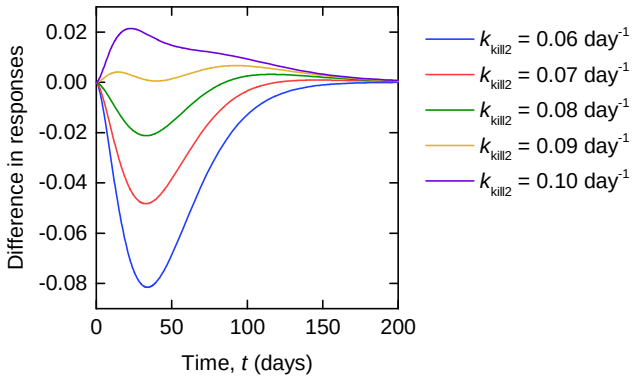

Figure 8-12 The difference between the monoclonal IgG responses of patients A and B, as described in section 8.5.2

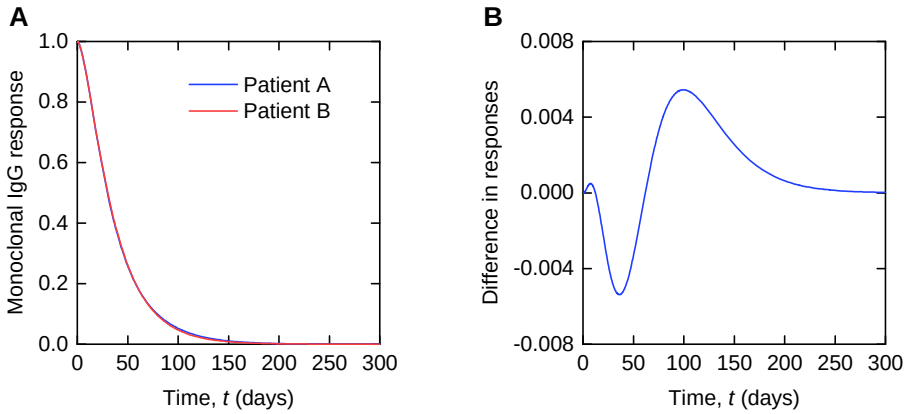

Figure 8-13 (A) Monoclonal IgG responses for patient A with $I_{m01} = 300$ µmol day^{-1} and $k_{kill1} = 0.05$ day^{-1} and patient B with $I_{m02} = 5$ µmol day^{-1} and $k_{kill2} = 0.087$ day^{-1}. (B) The difference between the monoclonal IgG responses of patient A and patient B.

day^{-1}, $I_{m02} = 5$ µmol day^{-1} and we are interested in finding values for k_{kill2}.

Figure 8-12 shows the differences between the two patients' monoclonal IgG responses for different values of the parameter k_{kill2}, between $k_{kkill2} = 0.06$ day^{-1} and $k_{kill2} = 0.1$ day^{-1}, as the optimal value of k_{kkill2} is within this range. The difference is given by the monoclonal IgG response of patient A minus the monoclonal IgG response of patient B, where the monoclonal IgG response is given by $y_G(t)$ in equation (8-16). A negative value of the difference means that the monoclonal IgG response of patient A is faster. When $k_{kill2} = 0.06$ day^{-1}, the monoclonal IgG response is much faster for patient A than patient B; however as the value of k_{kill2} increases, the difference between the responses becomes smaller, until eventually patient B has a faster monoclonal IgG response than

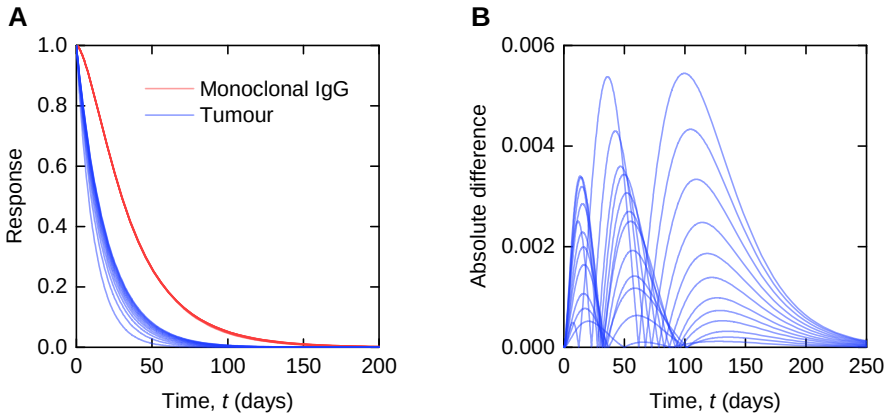

Figure 8-14 (A) A range of tumour responses (blue) yielding very similar monoclonal IgG responses (red). (B) The difference between each monoclonal IgG response plotted in panel (A) and the monoclonal IgG response of patient A with $I_{\mathrm{m01}} = 300$ µmol day^{-1} and $k_{\mathrm{kill1}} = 0.05$ day^{-1}.

patient A, when $k_{\mathrm{kill2}} = 0.1$ day^{-1}. The difference with the smallest maximum, for the parameter values shown, is given by $k_{\mathrm{kill2}} = 0.09$ day^{-1}. By defining a function that finds the maximal absolute difference between the two responses, over a range of $t = 0$ to $t = 500$ days, and minimising that function over a range of values of k_{kill2}, the maximal absolute difference is found to be 5.45×10^{-3} when $k_{\mathrm{kill2}} = 0.087$ day^{-1}. The monoclonal IgG responses of patients A and B are plotted in figure 8-13A, where $k_{\mathrm{kill2}} = 0.087$ day^{-1}. The difference between the two responses is plotted in figure 8-13B. The two monoclonal IgG responses are extremely similar, despite the different tumour response rates.

The same approach can then be taken for alternative values of I_{m02}, which will yield many pairs of values of I_{m02} and k_{kill2} which give similar monoclonal IgG responses. The generated pairs of I_{m02} and k_{kill2}, along with the original parameters I_{m01} and k_{kill1}, give a set of tumour response parameters that yield similar transient monoclonal IgG responses. Values of k_{kill2} that minimise the maximal difference between the monoclonal IgG responses of patients A and B were found for values of I_{m02} between 5 and 300 µmol day^{-1}. Examples of these monoclonal IgG responses are plotted in figure 8-14A, along with the corresponding tumour responses, showing a range of tumour responses that yield very similar monoclonal IgG responses. The differences between each of these monoclonal IgG responses and the monoclonal IgG response of patient A are plotted in figure 8-14B.

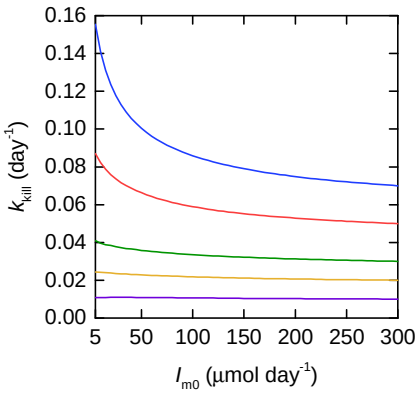

Figure 8-15 Parameter contours for tumour responses corresponding to very similar monoclonal IgG responses. The red line corresponds to the simulations shown in figure 8-14.

The process can be repeated for different values of k_{kill1} in order to find similar monoclonal IgG responses for a range of response rates. This approach was taken in order to find multiple contours of tumour response parameters which correspond to similar monoclonal IgG responses; these parameter contours are plotted in figure 8-15. The plot illustrates that faster monoclonal IgG responses (larger values of k_{kill}) may result from a broader range of tumour response rates, whereas very slow monoclonal IgG responses only result from very slow tumour responses. This suggests that clinicians may need to be aware that very fast monoclonal IgG responses in patients with large initial monoclonal IgG concentrations may be due to metabolic effects rather than a particularly fast tumour response. However, the plot suggests that there is little need to be concerned about fast tumour responses producing particularly slow monoclonal IgG responses in patients presenting with small monoclonal IgG concentrations. However, this may be of concern in a trial where particularly fast responses are to be expected. Furthermore, in this section it has been assumed that the system is in steady state at the beginning of treatment. Other simulations in this chapter have shown that when a more realistic assumption of tumour growth at T_0 is applied, the effects of Ig metabolism on monoclonal Ig responses are generally amplified.

Table 8-9 Parameter values used in the simulation in section 8.6.1. Certain parameter values were adjusted in order that the monoclonal IgG concentration approximately replicates the patient data shown in figure 8-4A.

Name	Units	Value	Source
k_{kill}	day^{-1}	0.028	Adjusted to replicate patient data
k_{growth}	day^{-1}	0.0118	Adjusted to replicate patient data
I_{m1}	$\mu\text{mol}\,\text{day}^{-1}$	60	Adjusted to replicate patient data
I_{m2}	$\mu\text{mol}\,\text{day}^{-1}$	5	Adjusted to replicate patient data
$I_{\text{G}\kappa\text{p}}$	$\mu\text{mol}\,\text{day}^{-1}$	9.6	Waldmann et al. [6], Bradwell et al. [19]
$I_{\text{G}\lambda\text{p}}$	$\mu\text{mol}\,\text{day}^{-1}$	5.4	Waldmann et al. [6], Bradwell et al. [19]

8.6 Comparison of IgA and IgG responses during relapse

Another scenario in which the effects of metabolism may be relevant is relapse. In this section two models of relapse and their corresponding monoclonal Ig responses are considered. Based on the results of previous simulations, the difference between the monoclonal IgA and monoclonal IgG responses is investigated. In each example, two patients are considered, one with an IgA- and one with an IgG-producing clone.

8.6.1 Two-exponential model of relapse

In the following simulation, the myeloma cell population is described by equation (8-28), with the monoclonal Ig production rate, $I_{\text{m}}(t)$, described by equation (8-29). The tumour response is given by equation (8-25). Whilst the model may seem simplistic and lacking in mechanistic basis, it adequately reproduces the behaviour seen in patient data, shown in figure 8-4. Normal polyclonal Ig production rates are assumed. The parameter values for the Ig production rates are provided in table 8-9. The parameter values were selected so that the plasma concentration of monoclonal IgG approximately replicates the SPEP concentration data of a real patient, assuming an average plasma volume of 3 l.

The dynamics of IgA and IgG are described by equations (8-9) and (8-12), respectively, with the parameter values given in tables 8-1 and 8-2. At time $T_0 = 0$ days the system is assumed to be in steady state, with the initial conditions of the quantities of IgG and

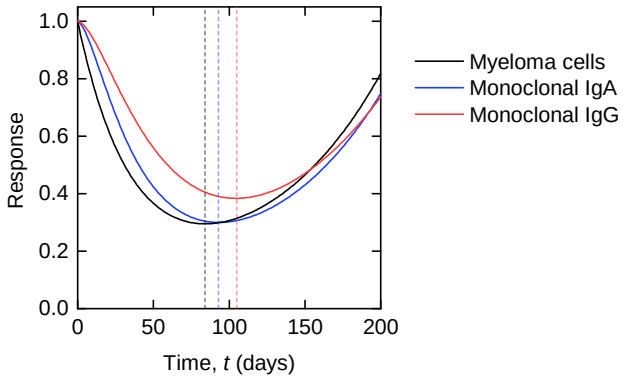

Figure 8-16 Monoclonal IgG and IgA responses during tumour kill and subsequent relapse. Vertical dashed lines are used to indicate the minima of the curves, at 84, 93 and 105 days, respectively.

IgA set to the steady states given by equations (8-13) and (8-10), respectively.

This scenario is plotted in figure 8-16. The simulation shows the response and subsequent regrowth of the tumour, as a proportion of its initial size. It also shows the corresponding responses in plasma monoclonal IgA and IgG, for IgA- and IgG-producing clones, respectively. In each case the proportion of the quantity at time $T_0 = 0$ days is plotted. The simulation illustrates the delay between the turning point in the cancer cell population and the turning point in the monoclonal Ig response, for each patient. For the particular parameter values used in this simulation, there is a delay of 9 days between the turning point in the myeloma cell response and that in the monoclonal Ig response, for the IgA-producing clone, and 21 days for the IgG-producing clone.

Figure 8-17 shows how the time delay between the minimal myeloma cell population and the minimal monoclonal Ig concentration changes, for both IgA and IgG patients, as selected model parameters vary. The bold portion of each line in figure 8-17 indicates the 95% confidence interval for that parameter. Figure 8-17A shows that, for an IgA patient, varying the parameter k_{01} between 0.4 and 1.6 times its value results in the greatest change in the relapse delay. However, the relative standard error of the parameter k_{12} is the largest, such that within the 95% confidence intervals of the parameters, varying the parameter k_{12} gives the largest range in the relapse delay, between 7.14 and 16.0 days. For the IgG patient, the delay between tumour relapse and monoclonal IgG relapse appears to be most sensitive to the parameter k_{31}, followed by k_{12}, k_{21}, $V_{\max}$ and K_{M}. This suggests that experimental design should focus on improving the precision of

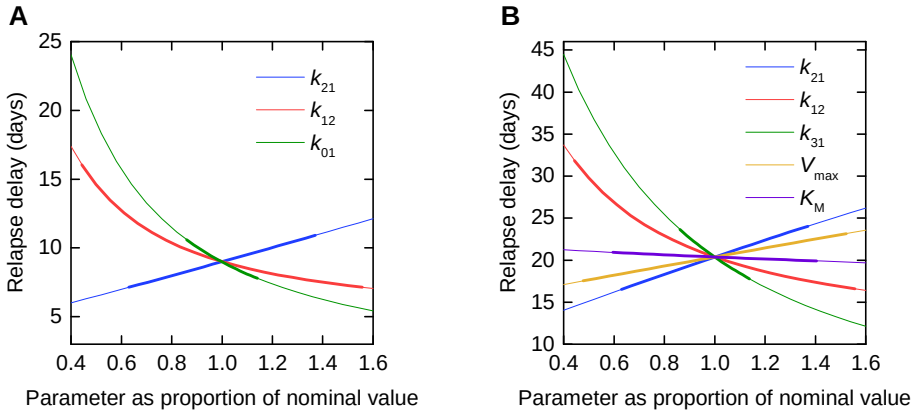

Figure 8-17 The time delay between the minimal myeloma cell population and (A) the minimal monoclonal IgA concentration or (B) the minimal monoclonal IgG concentration, plotted against the metabolic model parameters. Each parameter is varied between 0.4 and 1.6 times its value. The bold portion of each line indicates the 95% confidence interval for that parameter.

the parameters with this order of importance. The large relative standard error in the parameter k_{12} corresponds to a range of 16.6 to 31.8 days delay between tumour and monoclonal IgG relapses. In contrast, the parameter K_{M} has relatively little effect on the relapse delay, with a difference of only one day over the entire range shown.

A significant event is the increase by 25% (or 5 $\mathrm{g\,l^{-1}}$, whichever is greater) in monoclonal protein, a criterion for the assignment of progressive disease (PD). The maximal tumour response is given by 70.5%. The monoclonal IgA reaches approximately the same maximal response as the myeloma cell population, a decrease of 70%. From this maximal response, monoclonal IgA increases by 25% on day 136. However, assuming a typical plasma volume of 3 l, monoclonal IgA does not increase by 5 $\mathrm{g\,l^{-1}}$ until day 193, an increase of 130% from its minimal concentration. At the same time, the myeloma cell population has seen an increase of 156% from its minimum. Due to the slower metabolism of IgG, the monoclonal protein does not achieve as deep a response as the tumour – 61.6% maximal response versus 70.5%. From its maximal response, monoclonal IgG increases by 25% on day 153, but does not see an increase 5 $\mathrm{g\,l^{-1}}$ until day 172. At this time the myeloma cells have increased by 101%.

Whilst the two hypothetical patients have the same tumour response, PD can be assigned to the IgG patient 21 days before the IgA patient. However, with different parameter values describing the tumour response, a 25% increase in IgA and IgG may be sufficient

Table 8-10 Results of the simulations in section 8.6.1

	IgA	IgG
Maximal response in monoclonal protein	−70%	−61.6%
PD days since $t = 0$	193	172
Ig increase from maximal response to PD	+130%	+47%
Myeloma cell increase from maximal response to PD	+156%	+101%

Table 8-11 Parameters values used in the simulation in section 8.6.2. Certain parameter values were adjusted in order that the monoclonal IgG concentration approximately replicates the patient data shown in figure 8-4A.

Name	Units	Value	Source
r_{m}	day^{-1}	0.01	Sullivan et al. [1]
K_{m}	n/a	4×10^{12}	Sullivan et al. [1]
N_{m0}	n/a	1	Adjusted to replicate patient data
ϕ_0	day^{-1}	0.0661	Adjusted to replicate patient data
k_ϕ	day^{-1}	0.0114	Adjusted to replicate patient data
T_0	days	303	Adjusted to replicate patient data
k_{syn}	$\mu\mathrm{mol\,day}^{-1}$	8×10^{-11}	Dingli et al. [12]
$I_{\mathrm{G}\kappa\mathrm{p}}$	$\mu\mathrm{mol\,day}^{-1}$	9.6	Waldmann et al. [6], Bradwell et al. [19]
$I_{\mathrm{G}\lambda\mathrm{p}}$	$\mu\mathrm{mol\,day}^{-1}$	5.4	Waldmann et al. [6], Bradwell et al. [19]

for the assignment of PD. In this case PD would occur in the IgA patient before the IgG patient. Monoclonal IgA responds faster to a relapse in myeloma cells than IgG because of its faster elimination.

8.6.2 Relapse with Gompertzian growth

The simulation in section 8.6.1 is produced from a highly simplified model that is capable of describing the behaviour observed in patient data, plotted in figure 8-4. In this section a more detailed model is considered, which incorporates tumour growth, tumour kill during therapy, and relapse due to decreasing effectiveness of therapy. Again two patients are simulated, with IgA- and IgG-producing clones, respectively. The trajectories followed by their clones are identical; their monoclonal IgA and IgG responses differ due to their different metabolic properties.

The trajectory of the myeloma cells is described by equation (8-30), with the parameter values given in table (8-11). The values of all parameters describing therapeutic interven-

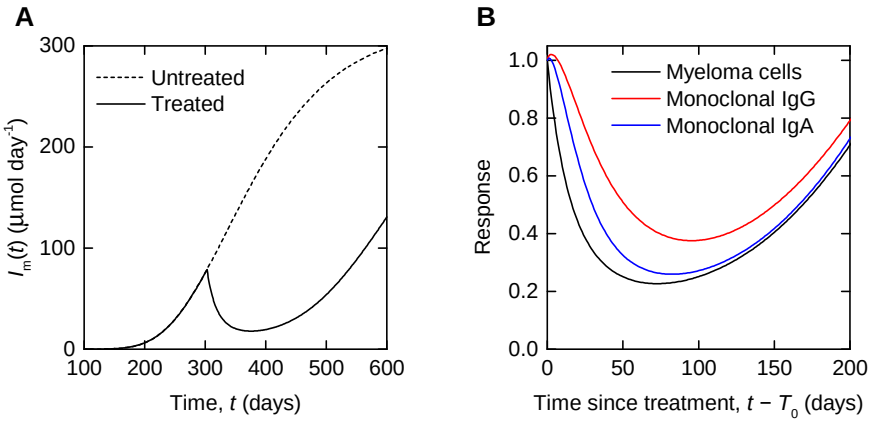

Figure 8-18 (A) Monoclonal Ig production rate for a plasma cell clone that is initially growing, then shrinks due to treatment, and finally grows due to decreasing treatment effectiveness. (B) Monoclonal IgG and IgA responses during tumour kill and subsequent relapse.

tion were chosen so that the trajectory of plasma monoclonal IgG approximately resembles that of a real patient, the data for whom are plotted in figure 8-4A. The monoclonal Ig production rate is assumed to be directly proportional to the population of malignant cells, with the proportionality constant k_{syn} µmol per cell, that is $I_{\text{m}}(t) = k_{\text{syn}}N_{\text{m}}(t)$. The polyclonal IgG production rates are assumed constant and take the normal values in table 8-11.

The quantities of IgA and IgG are described by equations (8-9) and (8-12), respectively, with the parameter values given in tables 8-1 and 8-2. At time 0 days the system is assumed to be in steady state. The initial conditions for IgA and IgG are thus given by the steady states in equations (8-10) and (8-13), respectively.

Figure 8-18A shows the monoclonal Ig production rate (directly proportional to the myeloma cell population) over the course of the disease. The dashed line shows the trajectory that would be taken without intervention. Figure 8-18B shows the responses to therapy of the myeloma cell population and monoclonal IgA and IgG, for the IgA- and IgG-producing clones, respectively. The simulation shows a similar result to the first relapse simulation in section 8.6.1; the delay between tumour relapse and monoclonal Ig relapse is 9 days for the IgA patient and 22 days for the IgG patient (cf. 9 and 21 days when steady state at the start of treatment is assumed).

8.7 Conclusions

In this chapter a number of simulations were performed in order to investigate whether mathematical models of IgA and IgG metabolism, based on the known biology of IgA and IgG, support a number of hypthotheses regarding monoclonal Ig responses to a changing clonal plasma cell population.

Models for the monoclonal Ig production rates were derived using tumour growth models from the literature and comparing the resulting trajectories of monoclonal Ig concentration with SPEP data from a clinical trial. The derived models provide good agreement with the patient data. Future work could involve deriving more complex models of tumour growth that incorporate the pharmacodynamical effects of therapeutic agents in a mechanistic way.

In section 8.3 monoclonal Ig responses for an average IgA myeloma patient and an average IgG myeloma patient were compared for an identical tumour response. Simulations showed that, with certain assumptions in place, monoclonal IgG underestimates the tumour response significantly more than monoclonal IgA. In addition, the tumour response is underestimated by monoclonal IgG when the maximal response has been reached, which in a clinical setting can represent an important assessment point. Whilst the hypothesis that monoclonal IgG underestimates response more than monoclonal IgA has been shown to have merit, variation within the population in terms of metabolic model parameters and tumour model parameters has not been incorporated in this study. Population parameters have been estimated in chapter 5 for the parameters k_{21} and k_{12}; with further work in order to estimate the other population parameters, or with additional assumptions, it would be possible to produce simulations of a cohort of patients, incorporating population-level variability. Whilst in 'average' patients, IgG may underestimate response more than IgA, the effect may lose importance when population-level variability is taken into account. Furthermore, noise on measurements of plasma concentrations may reduce the significance of metabolic effects.

In section 8.4 the effect of the initial size of the plasma cell clone on response rates in IgG myeloma was considered. When the system was assumed to be in steady state at the beginning of treatment, a patient with a smaller clone showed an initially slower

response, but a greater maximal response. The parameter values for the monoclonal IgG production models were chosen in order that the simulation showed the smallest and largest initial monoclonal IgG concentrations that may be expected in real patients; even in this extreme scenario, the difference between the monoclonal Ig responses in the two IgG patients is less significant than the difference between the IgA and IgG patients compared in section 8.3. However, when more realistic assumptions are made regarding the tumour growth trajectory at the beginning of therapy, the monoclonal IgG response for the smaller clone changes significantly, giving a large difference of up to 27.6% between the two monoclonal IgG responses. Again, variability in the population has not been taken into account; this may be the subject of future research. Variability in terms of the cellular synthetic rate has also been neglected: it is possible that two patients may have very different initial monoclonal IgG concentrations due to different cellular synthesis rates, rather than different clone sizes. In this case the difference between the two monoclonal IgG responses may be reduced. Future studies must incorporate these sources of variability in order to assess the magnitude of the metabolic effects at a population or cohort level.

Simulations of the monoclonal Ig response in an IgA patient and an IgG patient whose myeloma cell clone initially shrinks and then grows were investigated, showing a difference between IgA and IgG patients in the time delay between tumour relapse and the monoclonal Ig relapse. The sensitivity of the time delay to the metabolic model parameters was investigated, showing certain parameters to be much more important than others; this information could be fed back into experiment design in order to improve the precision of estimates of the more important parameters. The relapse scenario was initially considered with the system assumed to be in steady state and then with the tumour assumed to be growing, at the beginning of treatment. The two assumptions yielded similar results in terms of the delay between the tumour relapse and the monoclonal Ig relapse; however, as for the previous simulations, the difference between the depth of the monoclonal IgA and monoclonal IgG responses is increased. In general, relaxing the assumption of steady state at the beginning of treatment tends to produce larger differences between monoclonal IgA and monoclonal IgG responses.

Unfortunately validating the predictions made in this chapter is difficult. The instan-

taneous production rate of monoclonal Ig and the total number of myeloma cells in the body are not directly measurable. It is therefore not possible to obtain longitudinal measurements of the tumour burden in order to validate the predictions; however, efforts have been made to ensure that the simulated models show good qualitative agreement with the available patient data. This chapter has shown through model simulations the behaviour that may arise in monoclonal IgA and IgG responses in multiple myeloma based on their respective metabolic properties, findings which may have important implications for patient monitoring and response assessment.

References

1. P. W. Sullivan, S. E. Salmon, *The Journal of Clinical Investigation* **51**, 1697–1708 (1972).
2. K. Anderson, *Mayo Clinic Proceedings* **78**, 15–17 (2003).
3. U.S. National Library of Medicine, *Study comparing conventional dose combination RVD to high-dose treatment with ASCT in the initial myeloma up to 65 years (IFM/DFCI2009)*, 2010, (2018; https://clinicaltrials.gov/ct2/show/study/NCT01191060).
4. M. Attal et al., *New England Journal of Medicine* **376**, 1311–1320 (2017).
5. X. Leleu et al., *Blood* **125**, 1411–1417 (2015).
6. T. A. Waldmann, W. Strober, *Progress in Allergy* **13**, 1–110 (1969).
7. J. G. Hattersley et al., *Computer Methods and Programs in Biomedicine* **109**, 126–133 (2013).
8. Wolfram Research Inc., *Mathematica Version 11.1*, Champaign, IL, 2017.
9. R. I. Macey, G. F. Oster, *Berkeley Madonna 8.3.18*, Berkeley, CA, 2009.
10. W. Strober et al., *The Journal of Clinical Investigation* **47**, 1905–1915 (1968).
11. J. M. Woof, J. Mestecky, in *Mucosal Immunology*, ed. by J. Mestecky et al. (Academic Press (Elsevier), Amsterdam, ed. 4, 2015), chap. 17, ISBN: 9780124159754.
12. D. Dingli et al., *Cancer Science* **98**, 734–739 (2007).
13. A. R. Bradwell, *Serum Free Light Chain Analysis* (The Binding Site Ltd., Birmingham, ed. 6, 2010), ISBN: 9780704427969.
14. J. G. Hattersley, PhD thesis, University of Warwick, 2009.
15. H. Schättler, U. Ledzewicz, *Optimal Control for Mathematical Models of Cancer Therapies* (Springer, New York, ed. 1, 2010), ISBN: 9781493929726.
16. D. Dingli et al., *Cancer Science* **98**, 1035–1040 (2007).
17. D. Dingli et al., *Cancer Gene Therapy* **16**, 873–882 (2009).
18. G. W. Swan, T. L. Vincent, *Bulletin of Mathematical Biology* **39**, 317–337 (1977).
19. A. Bradwell et al., *Leukemia* **27**, 202–207 (2013).
20. B. Paiva et al., *Leukemia* **25**, 697–706 (2011).
21. M.-C. Kyrtsonis, A. Mouzaki, A. Maniatis, *Medical Oncology* **16**, 73–77 (1999).
22. S. M. Tete, M. Bijl, S. S. Sahota, N. A. Bos, *Frontiers in Immunology* **5** (2014).

23. A. Radbruch et al., *Nature Reviews Immunology* **6**, 741–750 (2006).

24. P. J. Morin, *Community Ecology* (Wiley-Blackwell, Oxford, ed. 2, 2011), ISBN: 9781444341966.

25. A. J. Lotka, *Elements of Physical Biology* (Williams & Wilkins Company, Philadelphia, ed. 1, 1925).

26. V. Volterra, *Nature* **118**, 558–560 (1926).

27. Y. Yu, W. Wang, Z. Lu, *Journal of Mathematical Analysis and Applications* **334**, 333–348 (2007).

28. T. Slocombe et al., *Journal of Immunology* **191** (2013).

9

Response assessment in multiple myeloma

In chapter 8 the behaviour of monoclonal immunoglobulin A (IgA) and monoclonal immunoglobulin G (IgG) was investigated in the context of their application as response markers in multiple myeloma. In that chapter, predictions were performed using simulations of compartmental models. One of the main findings of chapter 8 was that the monoclonal immunoglobulin (Ig) response, that is the percentage reduction in blood monoclonal Ig during treatment, may underestimate the tumour response in IgG patients compared to IgA patients, due to the different metabolic half-lives of IgA and IgG. This could have important implications for tumour response assessment in multiple myeloma using measured responses in monoclonal IgA and IgG.

It is not possible to truly ascertain whether the monoclonal IgG response underestimates the tumour response; whilst patients' monoclonal IgA or IgG responses are reported, the response of the tumour is not measurable in practice. However, the purpose of this work is to investigate whether the metabolic properties of IgA and IgG are relevant to the use of monoclonal Ig as a response marker. The drive for improved complete response (CR) rates in multiple myeloma is based on the fundamental assumption that deeper tumour responses are correlated with improved survival outcomes [1]. It is suggested here that, if monoclonal Ig response underestimates tumour response in IgG patients compared to IgA patients, then monoclonal Ig response will also underestimate survival outcomes in

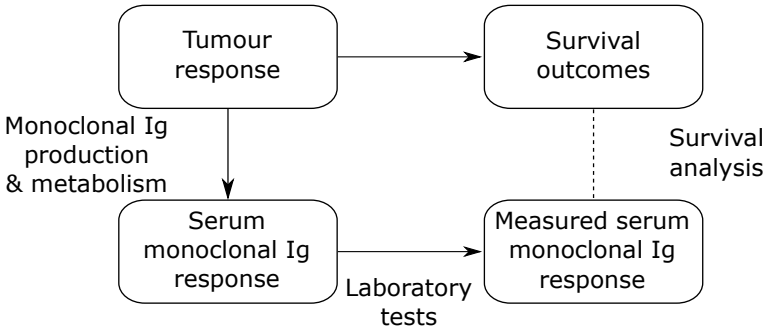

Figure 9-1 Illustration of how survival analysis based on monoclonal Ig responses and Ig metabolism are related

IgG patients, when compared to IgA patients. Equivalently, monoclonal Ig response may overestimate survival outcomes in IgA patients, when compared to IgG patients.

The aim of the present chapter is to investigate whether IgA and IgG metabolism is relevant to response assessment in multiple myeloma, by ascertaining whether monoclonal IgG response underestimates survival outcomes compared to monoclonal IgA response. In this chapter a dataset from a large-scale clinical trial of newly diagnosed multiple myeloma patients, including 526 patients with IgA- or IgG-producing clones, is analysed. The dataset is introduced in section 9.1.

In chapter 8 the relationship between a changing tumour burden and blood monoclonal Igs was considered. In this chapter the relationship between survival outcomes and measured serum monoclonal Ig responses, represented by survival models, is analysed. The relationship between Ig metabolism and the application of the monoclonal Ig response as a survival marker is depicted simply in figure 9-1. All survival analyses were performed using the R language and environment for statistical computing version 3.0.1 [2] with the Survival package version 2.37-4 [3].

9.1 IFM 2009/01 clinical trial data

Data from the IFM (Intergroupe Francophone du Myélome) 2009/01 clinical trial [4; 5] are analysed in this chapter. The data analysed in this chapter were collected in the first five years of the trial, which is ongoing. The analysed dataset consists of data for 687 newly diagnosed patients under 66 years of age, who were randomised into two protocol

arms. Patients in both trial arms were treated with induction therapy of lenalidomide, bortezomib, and dexamethasone (RVD). The patients in one arm were treated with consolidation therapy consisting of high-dose melphalan plus autologous stem cell transplantation, whereas those in the other arm were treated with additional cycles of RVD. The cohort includes patients with intact Ig multiple myeloma (IIMM), light chain multiple myeloma and oligosecretory disease. Since the investigations in this thesis are centred on intact Ig behaviour, only the 526 patients with IIMM are eligible to be analysed in this chapter. These patients' plasma cell clones produce either monoclonal IgA or IgG.

Baseline, longitudinal, and event time information are reported in the dataset. The analysis in this chapter is based on the association between monoclonal Ig responses and survival times; therefore the data that are most important here are longitudinal measurements of blood Ig concentrations and survival times. Key time points are recorded for each patient, signifying important phases of monitoring. These are screening, pre-maintenance and post-maintenance. Screening is the first time point for each patient. After screening, patients were given induction and consolidation therapy according to their randomly assigned protocol arm. After consolidation therapy all patients then received maintenance therapy for one year; the time point labelled 'pre-maintenance' marks the beginning of maintenance therapy and 'post-maintenance' signifies its end. After maintenance therapy patients were followed up every two months until the end of the trial period recorded in the dataset, or until an event occurrence.

9.1.1 Event times

The event times recorded in the dataset are progression-free survival (PFS) and overall survival (OS) along with associated event indicators, signifying whether an event has occurred or is right-censored at the given time. Event times are calculated as the time between two dates: the date at which the event (progression or death) occurred and another clinically relevant date at which the response to treatment can be evaluated – here pre-maintenance is used. Thus PFS and OS from pre-maintenance are available to be analysed. The Kaplan-Meier estimator of the survival function for IIMM patients is plotted in figure 9-2A for PFS from pre-maintenance and in figure 9-2B for OS from pre-maintenance. The latest event times recorded in the dataset pertain to events or censoring

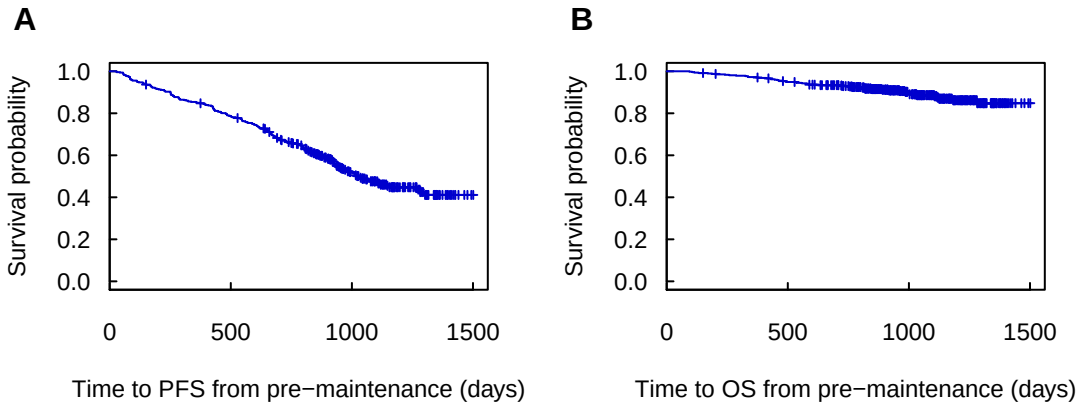

Figure 9-2 (A) Progression-free survival (PFS) and (B) overall survival (OS) from pre-maintenance in intact immunoglobulin multiple myeloma (IIMM) patients. Right-censored events are indicated by symbols (+).

in September 2015. PFS was the primary end point for the trial. In the dataset relatively few deaths are recorded and there is little association between the monoclonal Ig response and the hazard of death; therefore OS is not considered in the following analyses.

9.1.2 Monoclonal Ig concentrations

Heavy/light chain measurements

In this dataset, patients are primarily monitored using blood Igs measured by the heavy/light chain (HLC) assay (see section 2.4 in chapter 2). HLC measurements are, in theory, recorded at every monitoring point: at screening, at pre-maintenance, and then at frequent intervals until the end of patient follow-up, possibly due to a progression or death. Some HLC data are missing for various reasons – these are outlined in section 9.4.1. Some patients also have HLC measurements taken between screening and pre-maintenance. In IgA patients, IgAκ and IgAλ concentrations are reported; in IgG patients, IgGκ and IgGλ concentrations are reported.

Patient monitoring times are illustrated in figure 9-3. The time at which blood samples were taken, measured in days since screening, is plotted on the horizontal axis, against patient number on the vertical axis. All patients in the trial are represented in the plot, some of whom have light chain or oligosecretory disease. The density of points at 0 days shows that all patients had blood samples taken at screening. The band of points

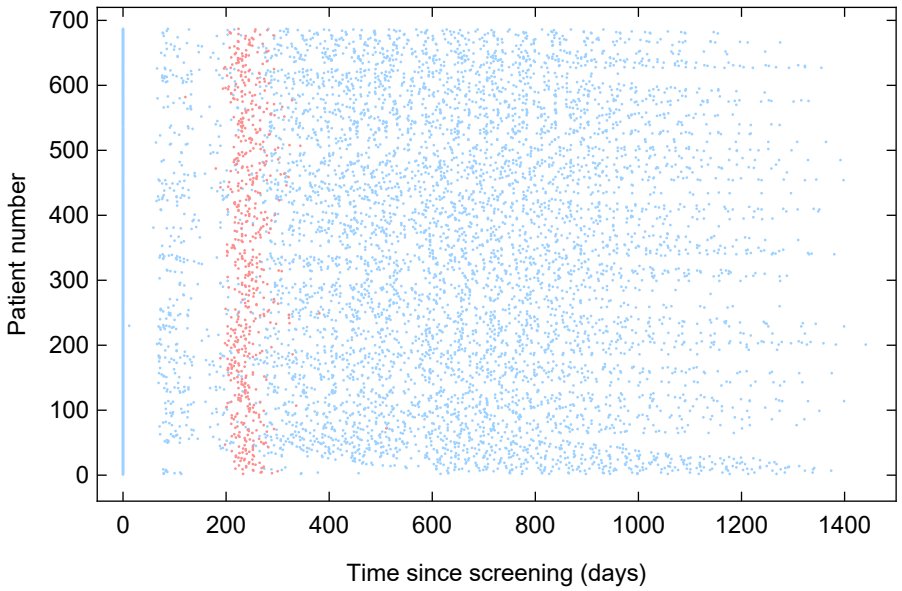

Figure 9-3 Monitoring times of all patients in the IFM 2009/01 study. Each point represents the time in days since screening at which relevant samples were collected. The points highlighted in pink represent the pre-maintenance time point.

Table 9-1 The Igs considered as involved and uninvolved for different monoclonal Ig isotypes. The involved and uninvolved Igs are measured by the HLC assay.

Monoclonal Ig	Involved HLC	Uninvolved HLC
IgAκ	Monoclonal IgAκ + polyclonal IgAκ	Polyclonal IgAλ
IgAλ	Monoclonal IgAλ + polyclonal IgAλ	Polyclonal IgAκ
IgGκ	Monoclonal IgGκ + polyclonal IgGκ	Polyclonal IgGλ
IgGλ	Monoclonal IgGλ + polyclonal IgGλ	Polyclonal IgGκ

highlighted in pink shows the clinically relevant pre-maintenance time point, between around 200 and 300 days since screening.

For IIMM patients, the most important marker is the Ig of the same heavy and light chain types as the monoclonal Ig. In an IgAλ patient, for example, the IgAλ concentration is the most important as this is the protein that is produced by their plasma cell clone. This is referred to as the involved Ig or involved HLC. The HLC measurement of the same heavy chain type, but alternative light chain type, for example IgAκ in an IgAλ patient, is referred to as the uninvolved HLC [6]. The uninvolved HLC provides a useful indicator of the level of polyclonal Ig. The involved and uninvolved HLC quantities for different monoclonal Ig isotypes are summarised in table 9-1.

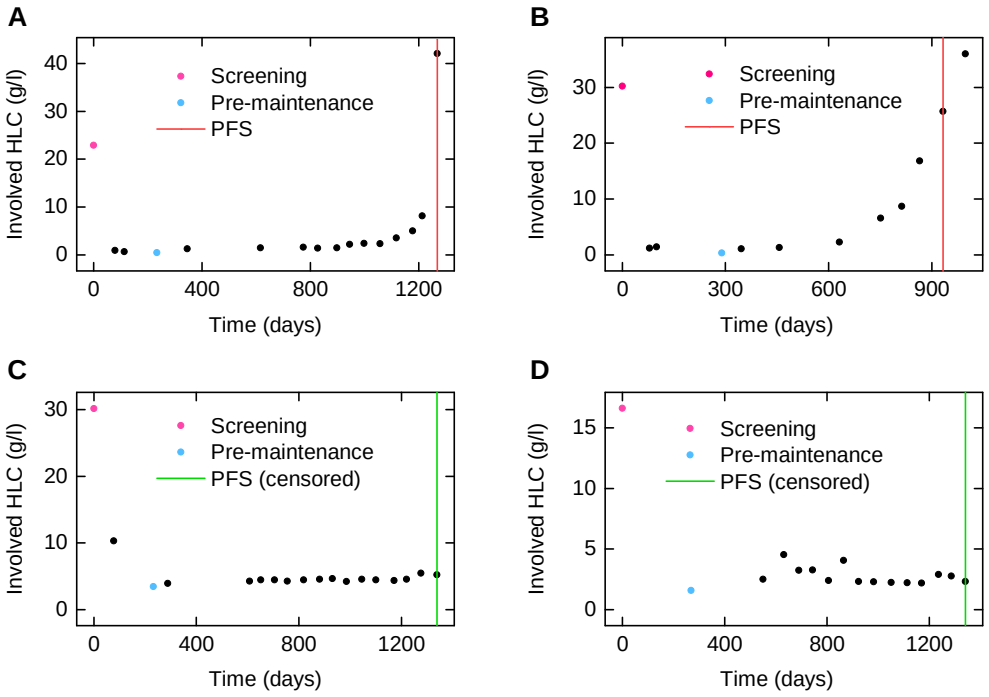

Figure 9-4 Examples of patient data collected in the IFM 2009/01 trial. Involved HLC is plotted over time for four patients. Screening and pre-maintenance samples are highlighted. PFS is shown in red where progression occurs and green where it is censored.

Plots of the involved HLC over time are shown for four patients in figure 9-4. The involved Ig concentration is elevated at screening and then falls as the clonal plasma cells are killed by therapy and the production rate of monoclonal protein decreases. PFS is indicated by a vertical line at the event time, with a red line indicating an event occurrence and a green line indicating a right-censored event.

Whilst the HLC assay does not discriminate between monoclonal and polyclonal Ig, at presentation the involved HLC is usually dominated by the monoclonal Ig. However, when deep responses are achieved following treatment, the monoclonal Ig is greatly reduced and now the polyclonal component may represent a significant proportion of the involved HLC. The importance of the polyclonal Ig can be seen by looking at the uninvolved HLC at pre-maintenance. A histogram of the uninvolved HLC of the same heavy chain type as the involved HLC (e.g. IgGκ in an IgGλ patient) at pre-maintenance is shown in figure 9-5. Patients with missing data for HLC at screening or pre-maintenance, missing PFS data or errors in the HLC data (see section 9.4.1) are omitted, leaving 97 IgA patients and 336 IgG patients. The number of IgA patients in each bin is divided by the total

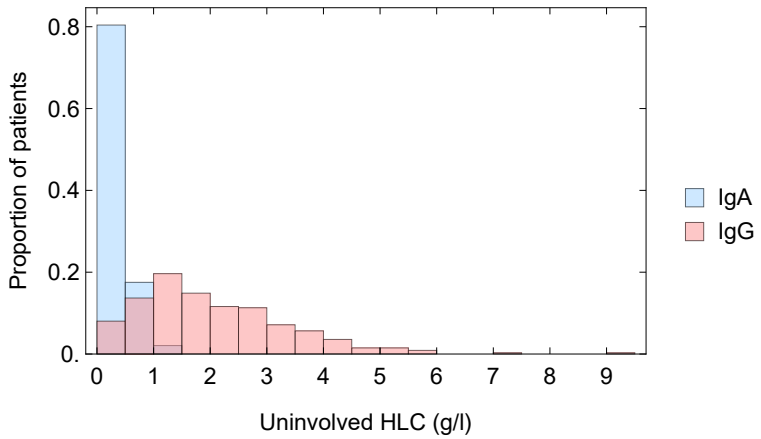

Figure 9-5 Histogram of uninvolved HLC at pre-maintenance. Frequencies are normalised by the total number of IgA patients or IgG patients, respectively.

number of IgA patients, and similarly for IgG, for ease of comparison. The histogram illustrates the difference in polyclonal IgG and IgA concentration. In normal subjects the concentration of IgG is five times that of IgA; it is therefore expected that at pre-maintenance the polyclonal IgG concentration will be greater than the polyclonal IgA concentration.

The difference between polyclonal IgA and IgG concentrations has implications for the interpretation of the involved HLC concentration at pre-maintenance and subsequent monitoring points when the monoclonal Ig concentration is low. Now the polyclonal part of the involved HLC is significant and, importantly, greater in IgG patients than in IgA patients. Ideally physicians wish to only monitor the monoclonal Ig that is produced by the cancer. Whilst the monoclonal and polyclonal parts of the involved HLC are not truly separable, fortunately the uninvolved HLC concentration provides an indicator of the polyclonal Ig concentration of the same heavy chain type as the monoclonal Ig.

It is reasonable to assume that the polyclonal part of the involved HLC and polyclonal uninvolved HLC are strongly correlated. Polyclonal serum IgA and IgG are produced primarily by long-lived plasma cells in the bone marrow [7; 8]. There is no reason to believe that κ polyclonal Ig would be any more or less suppressed than λ polyclonal Ig, and vice versa. If the true ratio of polyclonal IgAκ/IgAλ or IgGκ/IgGλ were known for each patient, the unknown polyclonal part of the involved HLC could be calculated using the known concentration of the uninvolved HLC. The true Ig'κ/Ig'λ ratio for each

individual patient is not known; however since there is no reason to believe that polyclonal Ig of one light chain type would be more or less suppressed than the other, the median values of the ratios IgAκ/IgAλ and IgGκ/IgGλ found in normal subject sera are used here. These values are provided by Bradwell et al. [9]. The median values in normal subjects of the ratios of IgAκ/IgAλ and IgGκ/IgGλ are denoted by $r_{\mathrm{A}\kappa/\mathrm{A}\lambda}$ and $r_{\mathrm{G}\kappa/\mathrm{G}\lambda}$, respectively.

The monoclonal Ig concentration is estimated by multiplying the uninvolved Ig concentration by the appropriate normal ratio and subtracting this quantity from the involved Ig concentration. This quantity is denoted here by mHLC and is calculated it as follows:

$$\begin{aligned}
\mathrm{mHLC}_{\mathrm{IgA}\kappa} &= \mathrm{iHLC}_{\mathrm{IgA}\kappa} - r_{\mathrm{A}\kappa/\mathrm{A}\lambda}\mathrm{uHLC}_{\mathrm{IgA}\lambda} \\
\mathrm{mHLC}_{\mathrm{IgA}\lambda} &= \mathrm{iHLC}_{\mathrm{IgA}\lambda} - \frac{1}{r_{\mathrm{A}\kappa/\mathrm{A}\lambda}}\mathrm{uHLC}_{\mathrm{IgA}\kappa} \\
\mathrm{mHLC}_{\mathrm{IgG}\kappa} &= \mathrm{iHLC}_{\mathrm{IgG}\kappa} - r_{\mathrm{G}\kappa/\mathrm{G}\lambda}\mathrm{uHLC}_{\mathrm{IgG}\lambda} \\
\mathrm{mHLC}_{\mathrm{IgG}\lambda} &= \mathrm{iHLC}_{\mathrm{IgG}\lambda} - \frac{1}{r_{\mathrm{G}\kappa/\mathrm{G}\lambda}}\mathrm{uHLC}_{\mathrm{IgG}\kappa}.
\end{aligned} \tag{9-1}$$

As the true polyclonal Ig'κ/Ig'λ ratio for each individual patient is not known, in some cases where the involved HLC is very small, subtracting the estimated involved polyclonal Ig can result in negative values for the mHLC. Clearly this is not possible and where negative values occur they are replaced with zero. Where negative values occur this means that the patient's polyclonal Ig favours the uninvolved light chain type, compared with the average normal subject. With no further information available, the only option is to assume that the monoclonal Ig is in these cases zero.

Serum protein electrophoresis and immunofixation

Also provided in the dataset is the monoclonal Ig concentration measured by serum protein electrophoresis (SPEP), but only at important monitoring points, including screening and pre-maintenance. The SPEP assay is less sensitive than the HLC assay (see section 2.4 in chapter 2) and therefore at pre-maintenance the monoclonal Ig is in many patients not detectable by SPEP. Also provided at key monitoring points is a binary indicator variable, indicating whether there is a detectable M-spike that can be quantified.

The heavy and light chain types of the monoclonal Ig are provided in the dataset for all

patients with an intact Ig paraprotein, as confirmed by immunofixation. As with SPEP, it is also indicated at key monitoring points whether the monoclonal Ig is detectable by immunofixation.

9.1.3 Monoclonal Ig responses

The monoclonal Ig response at any time t_j days, during or after treatment, is defined as the monoclonal Ig concentration at time t_j divided by the the monoclonal Ig concentration at screening, $t_0 = 0$ days. Alternatively the response may refer to the percentage reduction in monoclonal Ig, between times $t_0 = 0$ and t_j. In this sense, larger reductions in monoclonal Ig represent 'deeper' responses. Both definitions of response are used in this chapter; it should be clear from the context of the discussion which particular definition is being used.

Responses need to be compared at the same time between patients. This can be a clinically relevant time point, such as pre-maintenance, or, if patients are followed up at regular intervals, responses could be evaluated six months from screening, for example. In this particular dataset, the most clinically relevant time point at which to assess response is pre-maintenance. At pre-maintenance, induction and consolidation therapy is complete and subsequent therapy has the aim of maintaining the previously achieved response [10]. In this chapter therefore we focus on responses evaluated at pre-maintenance.

mHLC responses

The mHLC response at pre-maintenance can be calculated as the mHLC at pre-maintenance divided by the mHLC at screening. A histogram of mHLC responses is shown for IgA and IgG patients in figure 9-6. The frequency in each bin is divided by the total number of IgA or IgG patients, respectively, for ease of comparison, since there are many more IgG patients than IgA patients. Those patients with missing PFS data or missing or erroneous data for mHLC at screening or pre-maintenance are excluded, leaving 97 IgA patients and 336 IgG patients. The histogram shows that, on average, monoclonal IgA responses are deeper than monoclonal IgG responses.

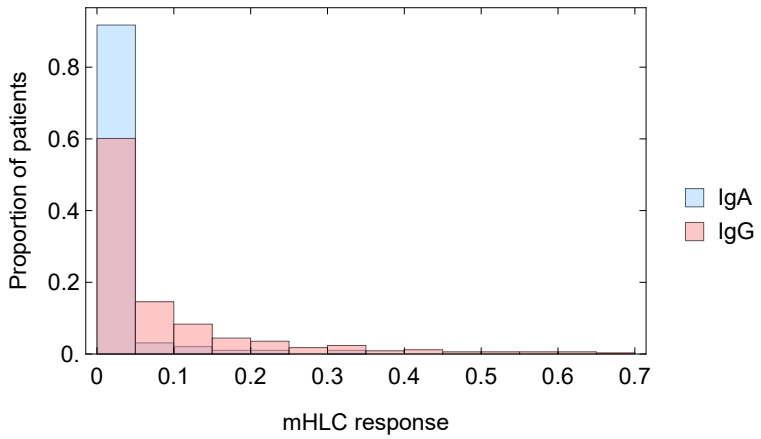

Figure 9-6 Histogram of mHLC responses at pre-maintenance. Frequencies are normalised by the total number of IgA patients or IgG patients, respectively. Details are provided in section 9.1.3.

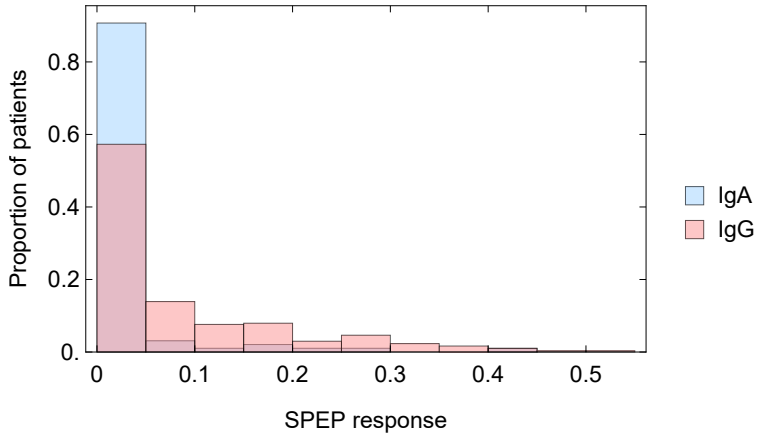

Figure 9-7 Histogram of SPEP responses at pre-maintenance. Frequencies are normalised by the total number of IgA patients or IgG patients, respectively. Details are provided in section 9.1.3.

SPEP responses

Similarly, the SPEP response at pre-maintenance can be calculated as SPEP at pre-maintenance divided by SPEP at screening. A histogram of SPEP responses is shown for IgA and IgG patients in figure 9-7. The frequency in each bin is divided by the total number of IgA or IgG patients, respectively, for ease of comparison, since there are many more IgG patients than IgA patients. Those patients for whom PFS or SPEP concentration at screening is missing are excluded. Those patients for whom SPEP concentration is not provided at pre-maintenance, due to a lack of quantifiable M-spike, are considered as having zero SPEP at pre-maintenance, or a 100% SPEP response.

Patients for whom SPEP concentration at pre-maintenance is missing for any other reason are excluded. In total there are 97 IgA patients and 302 IgG patients represented in the histogram. The histogram shows that, on average, monoclonal IgA responses are deeper than monoclonal IgG responses.

9.2 Relevant simulations of monoclonal Ig responses during treatment

In chapter 8, section 8.3, responses of monoclonal IgA and IgG to a decreasing tumour burden were compared using simulations. It was predicted that, due to the long metabolic half-life of IgG, monoclonal IgG falls at a slower rate than monoclonal IgA for the same response in the myeloma cell population. It was predicted that when the monoclonal Ig settles at a new steady state after treatment, the proportional reduction in monoclonal IgG underestimates the proportional reduction in myeloma cells, whereas the proportional reduction in monoclonal IgA does not (assuming that the system is in steady state at the beginning of treatment).

Figure 9-4 shows the first two IIMM patients, as ordered by patient ID, that have a progression and the first two for whom the progression event is censored (not including patients with missing data who were not eligible to be analysed). These plots of the involved Ig concentration over time show the typical pattern that is seen in the data for all patients. Samples are taken at infrequent intervals before pre-maintenance. At pre-maintenance the involved Ig appears to have settled around a low concentration where it remains until either it increases during relapse, or the study reaches an end. It therefore appears that a maximal proportion of the cancer cells has been killed and that the system of Igs is approaching a steady state at pre-maintenance. From conversations with research collaborators this coincides with their clinical understanding. In some patients, it appears that at pre-maintenance the involved HLC is still falling, however even for these cases it is approaching the steady level at which it will eventually settle.

Referring back to the simulations in section 8.3 of chapter 8, the difference between monoclonal IgA and IgG responses narrows as the cancer cells and Igs approach a steady

state. The aim of this chapter is to determine whether the difference between measured monoclonal IgA and monoclonal IgG responses seen in the data is significant enough to influence their association with survival outcomes.

9.3 Methodology for survival analyses

The aim of this chapter is to ascertain whether the monoclonal Ig response underestimates survival outcomes in IgG patients compared with IgA patients. Having inspected the available data, a more specific version of this aim is to ascertain whether monoclonal IgG response at pre-maintenance underestimates PFS from pre-maintenance, compared to the monoclonal IgA response.

If the monoclonal IgG response underestimates PFS compared to the monoclonal IgA response, then when patients are grouped by whether they have achieved a certain monoclonal Ig response, or not, the group of 'responders' is missing certain IgG patients whose tumour response was underestimated by their IgG response. Therefore the IgG patients who were classed as responders, will, on average, have improved survival compared to IgA responders. Those IgG patients who were wrongly classed as non-responders similarly will improve the PFS of IgG patients, compared to IgA patients, in the non-responder category. Ignoring the different metabolic properties of the respective proteins, patients achieving the same monoclonal Ig response would be expected to have a similar outlook.

In order to analyse the data, patients are grouped according to having achieved, or not, a certain percentage reduction in their monoclonal Ig at pre-maintenance. As illustrated in figures 9-6 and 9-7, at pre-maintenance the patients have achieved very deep monoclonal Ig responses, whether measured by mHLC or SPEP. Therefore we are restricted in the monoclonal Ig response threshold values that can be used to group the patients. The response threshold values used in this section are therefore between 90% and 99.5%.

In order to investigate whether the monoclonal IgG response at pre-maintenance underestimates PFS compared to the monoclonal IgA response, proportional hazards models with monoclonal Ig response and monoclonal Ig isotype (IgA or IgG) as explanatory variables are compared. The monoclonal Ig response is treated as a factor with two levels, determined by a chosen threshold value, for example a 95% reduction in monoclonal Ig.

In this way there is an effect associated with having achieved a certain level of response; let α_1 denote this effect. The isotype of the monoclonal Ig, IgA or IgG, can also be incorporated as a factor in the model. Let β_{IgG} denote the effect associated with having an IgG paraprotein.

With two explanatory variables there are five possible models to describe the data, which are here denoted by $\text{M1}, \ldots, \text{M5}$ as follows:

$$\begin{aligned}
&\text{M1} : h_i(t) = h_0(t) \\
&\text{M2} : h_i(t) = \exp\big(\alpha_1 x_{\text{response},i}\big) h_0(t) \\
&\text{M3} : h_i(t) = \exp\big(\beta_{\text{IgG}} x_{\text{isotype},i}\big) h_0(t) \\
&\text{M4} : h_i(t) = \exp\big(\alpha_1 x_{\text{response},i} + \beta_{\text{IgG}} x_{\text{isotype},i}\big) h_0(t) \\
&\text{M5} : h_i(t) = \exp\big(\alpha_1 x_{\text{response},i} + \beta_{\text{IgG}} x_{\text{isotype},i} + \gamma_{1,\text{IgG}} x_{\text{response},i} x_{\text{isotype},i}\big) h_0(t).
\end{aligned} \tag{9-2}$$

In equations (9-2),

- $h_i(t)$ is the hazard function of individual i in the study;
- $h_0(t)$ is the baseline hazard function;
- α_1 is the effect associated with having achieved the specified response;
- β_{IgG} is the effect associated with having an IgG paraprotein;
- $x_{\text{response},i}$ is the value for patient i of an indicator variable X_{response} that takes the value 1 for patients who have achieved the specified response and 0 for those who have not;
- $x_{\text{isotype},i}$ is the value for patient i of an indicator variable X_{isotype} that takes the value 1 for IgG patients and 0 for IgA patients;
- the coefficient $\gamma_{1,\text{IgG}}$ represents the effect of an interaction between the response status and monoclonal Ig isotype.

The models are defined such that the baseline hazard function $h_0(t)$ corresponds to the hazard function of an IgA patient who has not achieved the specified reduction in monoclonal IgA.

M1 is the null model, in which the hazard function depends on neither the monoclonal Ig response nor the isotype of the monoclonal Ig. In M2 and M3, the hazard of pro-

gression depends on either the monoclonal Ig response or the isotype of the monoclonal Ig, respectively. In M4, the hazard function is dependent on both the response and the isotype. In M5 the hazard function is dependent on both the response and the isotype, with an interaction term between the two factors. The interaction allows for a difference in the effect of one factor dependent on the level of the other factor. For example, the interaction would allow for IgG patients to have improved survival compared to IgA patients among those who had achieved the specified response, but for IgA patients to have improved survival among those patients who had not achieved the response.

9.4 Analysis of mHLC response and progression-free survival from pre-maintenance

In the IFM 2009/01 clinical trial, monoclonal Igs were primarily monitored using the HLC assay. In this section, the association between the mHLC response at pre-maintenance and PFS from pre-maintenance is analysed. Proportional hazards models describing PFS are estimated over a range of mHLC response threshold values. The models, $\mathrm{M1}, \ldots, \mathrm{M5}$, are given by equations (9-2) in section 9.3.

9.4.1 Missing data

PFS from pre-maintenance is missing for 53 IIMM patients, 50 of whom have no recorded pre-maintenance monitoring point. These patients were omitted from subsequent analyses. A further 29 patients had to be excluded who had missing data for involved or uninvolved HLC at either screening or pre-maintenance. IgA and IgG patients were affected equally by missing data, with 5% of IgA patients and 7% of IgG patients affected, respectively. Three IgG patients had to be omitted from analyses because of suspected antigen excess, or data entry error, in their involved HLC concentration at screening, giving a falsely low concentration [11]. This issue affected IgA and IgG patients equally; however some of the affected patients had already been removed due to missing data in other samples. Seven IgA patients had to be excluded because the involved or uninvolved HLC concentrations in their pre-maintenance samples were below the sensitivity of the

assay. One further patient was excluded due to a possible data entry error resulting in an exceptionally high uninvolved HLC concentration at screening, such that mHLC could not be accurately calculated. In total, 93 patients were excluded, leaving 433 patients eligible for analysis – 97 with IgA-producing clones and 336 with IgG-producing clones.

9.4.2 Example: 95% mHLC response threshold

Firstly the models based on a response threshold of a 95% reduction in mHLC are explained, as an example. Here, patients who have achieved at least a 95% reduction in mHLC are compared with those who have not, in the models where the variable X_{response} is included, that is models M2, M4 and M5. The models were fitted using the `coxph()` function in the R Survival package [3]. The proportional hazards assumption was tested for all fitted models using the `cox.zph()` function. There was no statistically significant evidence at the 5% level to reject the proportional hazards assumptions for any of the explanatory variables in any of the fitted models, unless otherwise stated.

For model M2 the maximum likelihood (ML) estimate of the coefficient α_1 is given by $\hat{\alpha}_1 = -0.696$, such that the estimate of the hazard ratio is given by $\exp(\hat{\alpha}_1) = 0.499$. The 95% confidence interval estimate of the hazard ratio is given by $(0.380, 0.655)$, which does not include the value 1. This result shows that patients who achieve at least a 95% reduction in mHLC have a significantly improved PFS compared to those who do not.

Fitting model M3 gives the ML estimate $\hat{\beta}_{\text{IgG}} = -0.0582$, such that the point estimate of the hazard ratio is given by $\exp\left(\hat{\beta}_{\text{IgG}}\right) = 0.9434$. The 95% confidence interval estimate of the hazard ratio is given by $(0.6857, 1.298)$. The 95% confidence interval is centred around the value 1, showing that there is little difference in PFS between IgA and IgG patients.

In model M4 the hazard of progression depends on both the response status and the monoclonal Ig isotype. Now the coefficient estimates are given by $\hat{\alpha}_1 = -0.7806$ and $\hat{\beta}_{\text{IgG}} = -0.3227$. The 95% confidence interval estimate of $\exp(\alpha_1)$ is given by $(0.3430, 0.6119)$. The same interval for the coefficient $\exp\left(\beta_{\text{IgG}}\right)$ is given by $(0.5158, 1.0168)$. This confidence interval only just includes the value 1, suggesting that in the presence of the term $\alpha_1 x_{\text{response},i}$, the term $\beta_{\text{IgG}} x_{\text{isotype},i}$ has an effect on PFS, with IgG patients surviving

Table 9-2 $-2\log\hat{L}$ and AIC for proportional hazards models fitted in section 9.4.2

Model	$-2\log\hat{L}$	AIC
M1	2392.689	2392.689
M2	2368.806	2370.806
M3	2392.563	2394.563
M4	2365.483	2369.483
M5	2365.323	2371.323

longer without progression than IgA patients. Likewise in the presence of $\beta_{\text{IgG}}x_{\text{isotype},i}$, the inclusion of $\alpha_1 x_{\text{response},i}$ has a statistically significant effect on PFS, with responders surviving longer.

Model M5 contains the response status and the monoclonal Ig isotype as explanatory variables, along with an interaction between the two. The interaction term is not statistically significant ($p = 0.688$) and so M5 can be discarded in favour of M4.

Model comparison

Proportional hazards models can be compared formally using the likelihood ratio test for nested models and the Akaike Information Criterion (AIC) for both nested and non-nested models, as described in chapter 4 [12]. For the models fitted in this section, the values of $-2\log\hat{L}$ and the AIC are given in table 9-2.

Using a likelihood ratio test it is first checked whether there is strong evidence for an interaction between the response status and the monoclonal Ig isotype of the patient, that is, whether the term $\gamma_{1,\text{IgG}}x_{\text{response},i}x_{\text{isotype},i}$ should be included in the model in the presence of the terms $\alpha_1 x_{\text{response},i}$ and $\beta_{\text{IgG}}x_{\text{isotype},i}$. The test statistic is given by the difference between the values of $-2\log\hat{L}$ for M4 and for M5: $-2\log\hat{L}_4 + 2\log\hat{L}_5 = 0.16$. A chi-squared test on one degree of freedom is not significant ($p = 0.688$) and it can therefore be concluded that there is insufficient evidence to include the interaction term in the model.

Now Models M2 and M3 are each compared with the null model M1. The comparison between M1 and M2 is to determine whether there is a significant difference in PFS between responders and non-responders. The difference in the values of $-2\log\hat{L}$ for M1

and M2 is given by $-2\log\hat{L}_1 + 2\log\hat{L}_2 = 23.88$, which on 1 d.f. is statistically significant (p<0.001). Thus there is strong evidence that the response status is required in the model, in the absence of other explanatory variables. This is in line with expectation.

Comparing models M3 and M1 gives a test statistic of $-2\log\hat{L}_1 + 2\log\hat{L}_3 = 0.127$ on 1 d.f. which is not statistically significant ($p = 0.72$), suggesting that there is not strong evidence to include the monoclonal Ig isotype in the model, in the absence of any other explanatory variables. This implies that there is no significant difference in PFS between IgA and IgG patients.

The inclusion of the isotype of the monoclonal Ig does not offer a statistically significant improvement over the null model, in which there are no explanatory variables. However, if it is supposed that monoclonal Ig response underestimates PFS in IgG patients compared to IgA patients, then in a model associating PFS with response, i.e. M2, the isotype of the monoclonal Ig now becomes important. This can be evaluated by comparing the models M4, including both the response status and isotype, and M2, including only the response status. The difference in $-2\log\hat{L}$ between the two models is given by $-2\log\hat{L}_2 + 2\log\hat{L}_4 = 3.32$. A chi-squared test on 1 d.f. yields $p = 0.068$; whilst this is not significant at the 5% level, there is some evidence that now the inclusion of the monoclonal Ig isotype improves the fit of the model to the data. Importantly, including the monoclonal Ig isotype only improves a model in which response status is an explanatory variable. This is consistent with the hypothesis that the monoclonal IgG response underestimates PFS compared to the monoclonal IgA response.

9.4.3 Further response thresholds

It is possible that the response in monoclonal IgG underestimates PFS at any chosen response level. In section 9.4.2 the explanatory variable X_{response} takes the value 1 for patients whose monoclonal Ig falls by at least 95% and 0 for patients whose monoclonal Ig falls by less than 95%, between screening and pre-maintenance, with the coefficient α_1 representing the effect on the hazard function of achieving this particular level of response. The choice of a 95% reduction in monoclonal Ig is arbitrary, however.

The models containing the explanatory variable X_{response} – M2, M4 and M5 – were fitted

Table 9-3 95% confidence interval estimates for the parameters in models M2 and M4, for mHLC response at pre-maintenance. Details are provided in section 9.4.3.

Response threshold %	M2: $\exp(\hat{\alpha}_1)$ 95% C.I.	M4: $\exp(\hat{\alpha}_1)$ 95% C.I.	M4: $\exp\left(\hat{\beta}_{\text{IgG}}\right)$ 95% C.I.
90	(0.3979, 0.724)	(0.3782, 0.7006)	(0.5908, 1.1403)
91	(0.3649, 0.6482)	(0.3408, 0.6192)	(0.5588, 1.0853)
92	(0.3604, 0.6333)	(0.3336, 0.6014)	(0.5450, 1.0620)
93	(0.377, 0.6561)	(0.3454, 0.6192)	(0.5342, 1.0466)
94	(0.3685, 0.6366)	(0.3317, 0.5935)	(0.5118, 1.0099)
95	(0.3799, 0.6549)	(0.3430, 0.6119)	(0.5158, 1.0168)
96	(0.3791, 0.6508)	(0.3354, 0.6001)	(0.4949, 0.9840)
97	(0.392, 0.6718)	(0.3399, 0.6123)	(0.4795, 0.9632)
98	(0.4032, 0.6917)	(0.3546, 0.6358)	(0.4921, 0.9818)
99	(0.3943, 0.6922)	(0.3384, 0.6247)	(0.4728, 0.9476)
99.5	(0.3556, 0.6409)	(0.3188, 0.5926)	(0.5021, 0.9831)

to the data over a range of different threshold values for the reduction in mHLC. The thresholds for response are between 90% reduction and 99.5% reduction in mHLC between screening and pre-maintenance. For each response threshold, the explanatory variable X_{response} takes the value 1 for patients achieving at least the specified response, and 0 for those who do not. For each explanatory variable within each model, the proportional hazards assumption was tested and found not to be violated.

The 95% confidence interval estimates for the parameters in models M2 and M4 are given in table 9-3. For both M2 and M4, the confidence interval estimate of $\exp(\alpha_1)$ has its upper bound less than 1 for all values of the response threshold used. This allows us to conclude that, for the particular threshold values used, achieving at least the specified response at pre-maintenance is associated with an improved PFS. Model M4 also includes the coefficient β_{IgG}, representing the effect of having an IgG paraprotein. Now the interval estimates of $\exp\left(\hat{\beta}_{\text{IgG}}\right)$ have their upper bound less than, or very close to 1, for response thresholds between 94% and 99.5%, implying that an IgG paraprotein is associated with an improved PFS, having accounted for the response status of the patient.

For lesser response thresholds, between 90% and 93%, the 95% confidence interval estimate of the hazard ratio $\exp\left(\hat{\beta}_{\text{IgG}}\right)$ now includes the value 1. This suggests that the difference in PFS between IgA and IgG patients in not statistically significant, having taken into account the response status of the patients. The trend however is the same as

Table 9-4 Comparison of models M2 and M4, for mHLC response at pre-maintenance. Details are given in section 9.4.3.

Response threshold %	$-2\log\hat{L}$		AIC		M4 vs. M2 p-value
	M2	M4	M2	M4	
90	2377.642	2376.299	2379.642	2380.299	0.246
91	2370.698	2368.599	2372.698	2372.599	0.147
92	2368.481	2366.003	2370.481	2370.003	0.115
93	2369.891	2367.136	2371.891	2371.136	0.097
94	2367.192	2363.728	2369.192	2367.728	0.063
95	2368.806	2365.483	2370.806	2369.483	0.068
96	2367.8	2363.781	2369.8	2367.781	0.045
97	2369.561	2365.061	2371.561	2369.061	0.034
98	2371.22	2367.153	2373.22	2371.153	0.044
99	2371.24	2366.383	2373.24	2370.383	0.028
99.5	2366.42	2362.406	2368.42	2366.406	0.045

for the other response thresholds used, with IgG patients having improved PFS to IgA patients.

Table 9-4 gives the values of $-2\log\hat{L}$ and the AIC for models M2 and M4, estimated for each response threshold. For each response threshold value the interaction between the response status and the monoclonal Ig isotype did not significantly improve the model fit and so the values of $-2\log\hat{L}$ and the AIC for M5 are not provided. Also provided in the table is the p-value of the likelihood ratio test comparing models M2 and M4. The test evaluates the strength of the evidence for including the term $\beta_{\text{IgG}}x_{\text{isotype},i}$ in the model, in the presence of the term $\alpha_1 x_{\text{response},i}$.

The small p-values in table 9-4 suggest that, for values of the response threshold between 94% and 99.5%, there is evidence to support the inclusion of the monoclonal Ig isotype in the model along with the response status of the patient. This suggests that, having accounted for the response achieved by the patient, patients with IgG paraproteins have improved PFS compared to IgA patients.

For smaller values of the mHLC response threshold, between 90% and 93%, the evidence for including the isotype term weakens. This may be because there are very few IgA patients who do not achieve the specified response thresholds in these models, such that grouping patients by a 90% mHLC response, for example, is less meaningful for IgA patients. Fitting model M2 for IgA patients only shows that IgA responders do not have

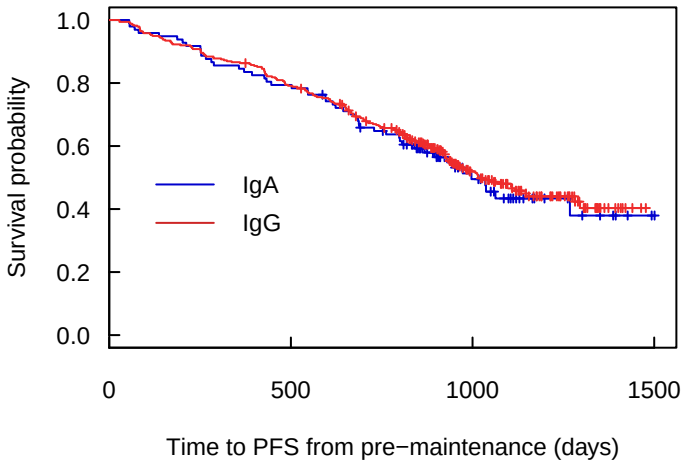

Figure 9-8 Survival plot of PFS stratified by monoclonal immunoglobulin isotype for the patients analysed in section 9.4. Details are given in section 9.4.3.

significantly improved PFS over non-responders, at the 5% significance level, for response thresholds between 90% and 92%.

The results can be illustrated with plots of the Kaplan-Meier estimator of the survival function of PFS, shown in figures 9-8 and 9-9. Figure 9-8 shows a plot of PFS stratified by the monoclonal Ig isotype, i.e. IgA or IgG. This plot represents model M3 and illustrates the lack of difference in PFS between IgA and IgG patients.

Figure 9-9 shows plots of PFS now stratified by the mHLC response and the monoclonal Ig isotype, with different mHLC threshold values defining the response status in each plot. These plots represent model M4 and illustrate that IgG patients have improved PFS compared to IgA patients when grouped by mHLC response.

These plots may also help to explain why the difference in PFS between IgA and IgG patients is less significant for lesser response thresholds, in particular 90% and 92%, shown in figures 9-9A and 9-9B. At pre-maintenance very deep mHLC responses are achieved across the cohort, particularly by IgA patients (see figure 9-6), with only five IgA patients achieving less than a 90% reduction in mHLC, and only eight achieving less than a 95% reduction, out of a total of 97 IgA patients. Inspecting figure 9-9A, for example, there is a clear difference in the PFS of IgG responders and IgG non-responders, shown in red and light red, respectively ($p < 0.001$). However for IgA patients, very few patients have not achieved a 90% response. There is not a clear difference in PFS between IgA responders

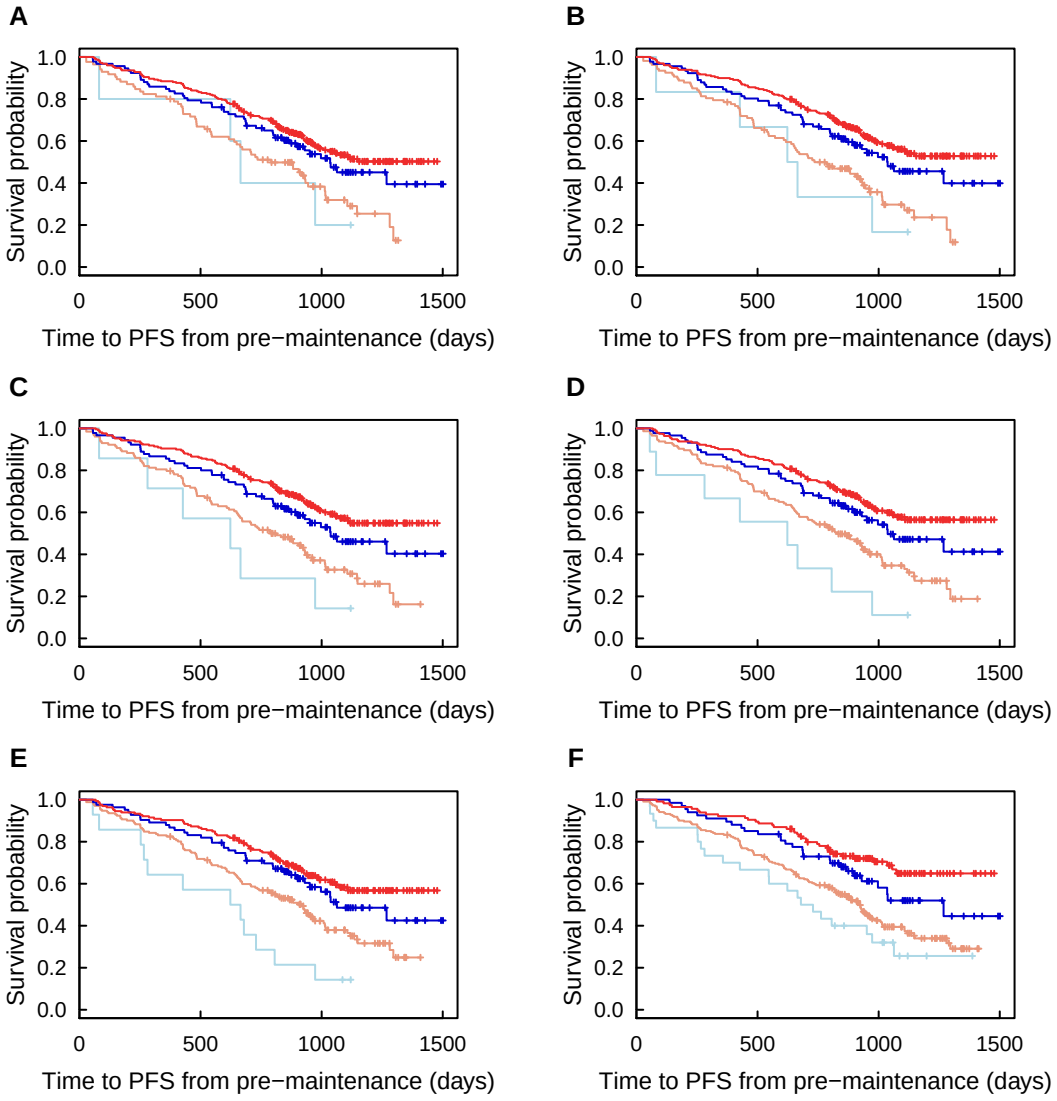

Figure 9-9 Survival plots of PFS by mHLC response and monoclonal Ig isotype, for six of the response threshold values used: (A) 90%, (B) 92%, (C) 94%, (D) 96%, (E) 98% and (F) 99.5%. Dark red – IgG responders; light red – IgG non-responders; dark blue – IgA responders; light blue – IgA non-responders. Details of the survival models are provided in section 9.4.3.

and IgA non-responders ($p = 0.22$). In order to show a clear difference between the PFS of all four groups, a sufficient number of patients need to be represented in each group. This is why the analyses were not performed for response thresholds of 50%, for example, as such a response is not meaningful in this particular sample.

9.5 Analysis based on mHLC response quantiles

The results in section 9.4.3 show that mHLC response significantly underestimates PFS in IgG patients compared to IgA patients, for mHLC response thresholds between 94% and 99.5%, with the same trend observed for thresholds between 90% and 93%. Considering the plots in figure 9-9, it can be seen that too few IgG patients have been classed as responders, or equivalently, too many IgA patients have been classed as responders, for each of the response thresholds used. It is therefore desirable to move some of the IgG patients from the non-responders group to the responders group, by using a lesser response threshold for IgG patients, or alternatively, move some of the IgA patients from the responders group to the non-responders group, by using a deeper response threshold for IgA patients. Given the relatively few IgA patients in the non-response category, for each threshold used, in this section a deeper mHLC response threshold is used for IgA patients, keeping the same threshold values as before for IgG patients.

The question then is, for an IgG mHLC response threshold of, say, 90%, what is an appropriate IgA mHLC response threshold, that will result in the same PFS for IgA patients and IgG patients, having accounted for their response status? A simple approach is to consider the quantiles of the distributions of mHLC response. Given that there is no overall difference between the PFS of IgA and IgG patients, it is assumed that the median mHLC response for IgA patients and the median mHLC response for IgG patients represent an equivalent tumour response, and so on for other quantiles.

The q^{th} response quantile is defined here as the mHLC response below which q% of mHLC responses lie, for IgA patients and for IgG patients, respectively. Figure 9-10 shows a Q-Q plot of the distributions of IgG mHLC response and IgA mHLC response, along with the line of equality, from 0 to 0.6, that is 100% reduction to 40% reduction in mHLC. In this plot the mHLC response is defined as mHLC at pre-maintenance divided

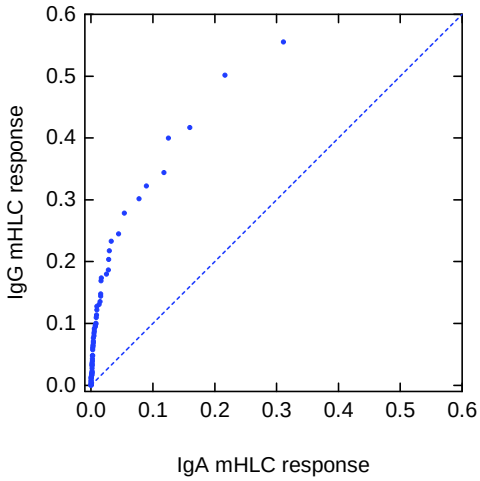

Figure 9-10 IgG mHLC response quantiles plotted against IgA mHLC response quantiles. Details are provided in section 9.5.

Table 9-5 mHLC response quantiles. The mHLC response is given by the value of the mHLC at pre-maintenance divided by the value of the mHLC at screening. Details are provided in section 9.5.

	mHLC response quantile	
q (%)	IgG	IgA
74.7	0.1	0.0083
70.5	0.09	0.0056
68.1	0.08	0.005
65.1	0.07	0.004
61.9	0.06	0.0031
60.1	0.05	0.00292
57.2	0.04	0.0022
52.6	0.03	0.002
49.1	0.02	0.0017
37.2	0.01	0.00055
34.2	0.005	0.0004

by mHLC at screening. The plot illustrates the difference between the distributions of mHLC responses in IgA and IgG patients, respectively.

The mHLC response quantiles were found for both IgA and IgG patients, for values of q between 35.2 and 74.7. These values were chosen because 35.2% of IgG patients achieved mHLC responses below 0.005 (greater than 99.5% reduction) and 74.7% achieved mHLC responses below 0.1 (greater than 90% reduction). These response thresholds correspond to the minimum and maximum thresholds used for the analysis in section 9.4.3. The mHLC response quantiles are provided in table 9-5.

Table 9-6 95% confidence interval estimates for the parameters in models M2 and M4, with different mHLC response thresholds for IgA and IgG. Details in section 9.5.

Response threshold IgG %	Response threshold IgA %	M2: $\exp(\hat{\alpha}_1)$ 95% C.I.	M4: $\exp(\hat{\alpha}_1)$ 95% C.I.	M4: $\exp\left(\hat{\beta}_{\text{IgG}}\right)$ 95% C.I.
90	99.17	$(0.3866, 0.6816)$	$(0.3867, 0.6817)$	$(0.6880, 1.3026)$
91	99.44	$(0.3454, 0.5987)$	$(0.3455, 0.5989)$	$(0.6907, 1.3078)$
92	99.50	$(0.3431, 0.5918)$	$(0.3431, 0.5919)$	$(0.6869, 1.3005)$
93	99.60	$(0.3622, 0.6221)$	$(0.3621, 0.6219)$	$(0.6811, 1.2895)$
94	99.69	$(0.3578, 0.6136)$	$(0.3579, 0.6138)$	$(0.6880, 1.3025)$
95	99.71	$(0.3626, 0.6221)$	$(0.3627, 0.6222)$	$(0.6890, 1.3046)$
96	99.78	$(0.3587, 0.6168)$	$(0.3587, 0.6168)$	$(0.6852, 1.2973)$
97	99.8	$(0.3744, 0.6475)$	$(0.3746, 0.6477)$	$(0.6905, 1.3074)$
98	99.83	$(0.3844, 0.67)$	$(0.3845, 0.6701)$	$(0.6870, 1.3007)$
99	99.95	$(0.3267, 0.6107)$	$(0.3266, 0.6106)$	$(0.6828, 1.2927)$
99.5	99.96	$(0.299, 0.5777)$	$(0.2990, 0.5775)$	$(0.6828, 1.2928)$

The analyses in section 9.4.3 were then repeated using the mHLC response thresholds given in table 9-5. The methodology is the same as in section 9.4.3, with the same group of patients analysed. Models M1 and M3 do not contain the variable X_{response} and therefore remain unchanged. The results of fitting models M1 (the null model) and M3 are given in section 9.4.2.

The models containing the explanatory variable X_{response} – M2, M4 and M5 – were fitted to the data with each of the mHLC response quantiles in table 9-5 used for the mHLC response thresholds. For each response threshold, the explanatory variable X_{response} takes the value 1 for patients achieving at least the specified mHLC response, now different for IgA patients and IgG patients, and 0 for those who do not. For each explanatory variable within each model, the proportional hazards assumption was tested and found not to be violated.

The 95% confidence interval estimates for the parameters in models M2 and M4 are given in table 9-6. For both M2 and M4, the confidence interval estimate of $\exp(\alpha_1)$ has its upper bound less than 1 for all values of the response thresholds used; therefore it can be concluded that, for the particular threshold values used, achieving at least the specified response at pre-maintenance is associated with an improved PFS. Model M4 also includes the coefficient β_{IgG}, representing the effect of having an IgG paraprotein.

Table 9-7 Comparison of models M2 and M4, with different mHLC response thresholds for IgA and IgG. Details are provided in section 9.5.

Response %		$-2\log\hat{L}$		AIC		M4 vs. M2 p-value
IgG	IgA	M2	M4	M2	M4	
90	99.17	2373.128	2373.016	2375.128	2377.016	0.738
91	99.44	2363.311	2363.214	2365.311	2367.214	0.756
92	99.50	2361.693	2361.574	2363.693	2365.574	0.730
93	99.60	2364.7	2364.543	2366.7	2368.543	0.692
94	99.69	2363.049	2362.937	2365.049	2366.937	0.738
95	99.71	2363.854	2363.748	2365.854	2367.748	0.745
96	99.78	2362.835	2362.706	2364.835	2366.706	0.719
97	99.8	2366.386	2366.289	2368.386	2370.289	0.755
98	99.83	2368.898	2368.78	2370.898	2372.78	0.731
99	99.95	2363.991	2363.846	2365.991	2367.846	0.703
99.5	99.96	2360.97	2360.825	2362.97	2364.825	0.703

Now the interval estimates of $\exp\left(\hat{\beta}_{\text{IgG}}\right)$ are centred around the value 1, for all response thresholds used, implying that there is no significant difference in PFS between IgA and IgG patients, having accounted for the response status of the patients.

Table 9-7 gives the values of $-2\log\hat{L}$ and the AIC for models M2 and M4, estimated for each pair of IgA and IgG response thresholds. Also provided in the table is the p-value of the likelihood ratio test comparing models M2 and M4, evaluating the evidence for including the term $\beta_{\text{IgG}}x_{\text{isotype},i}$ in the model, in the presence of the term $\alpha_1 x_{\text{response},i}$. The p-values in table 9-7 suggest that there is very little evidence to support the inclusion of the monoclonal Ig isotype in the model along with the response status of the patient. This suggests that, having accounted for the mHLC response achieved by the patient, using the thresholds in table 9-5, there is no significant difference between the PFS of IgA patients and IgG patients.

Figure 9-11 shows plots of PFS stratified by the response status and the monoclonal Ig isotype, with the threshold for response indicated for each plot, for IgA and IgG patients respectively. These plots represent model M4 and illustrate that there is no significant difference in PFS between IgA and IgG patients when grouped by the response thresholds indicated.

Now that the assignment of response is based on different thresholds for IgA and IgG patients, the assignment of response no longer overestimates PFS in IgA patients and

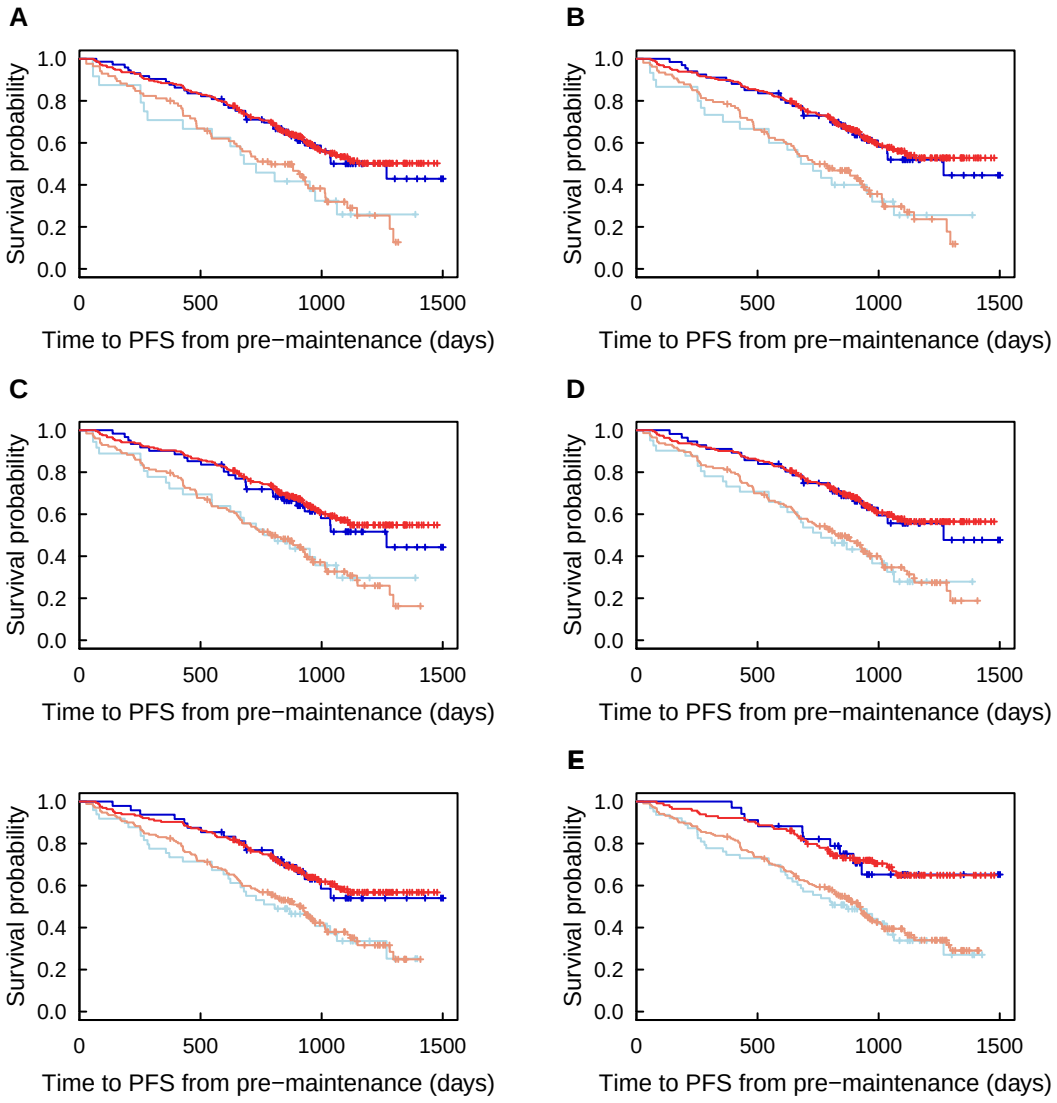

Figure 9-11 Survival plots of PFS by mHLC response and monoclonal Ig isotype. Separate mHLC response thresholds are used for IgA and IgG patients: (A) IgG 90%, IgA 99.17%; (B) IgG 92%, IgA 99.50%; (C) 94%, IgA 99.69%; (D) IgG 96%, IgA 99.78%; (E) IgG 98%, IgA 99.83%; and (F) 99.5%, IgA 99.96%. Dark red – IgG responders; light red – IgG non-responders; dark blue – IgA responders; light blue – IgA non-responders. Details of the survival models are provided in section 9.5.

Table 9-8 Comparison of model M2 when the same mHLC response threshold is used for all patients, and when a deeper mHLC response threshold is used for IgA patients. Details are provided in section 9.5.

Same threshold			Different thresholds			
Response %			Response %			
IgG	IgA	AIC M2	IgG	IgA	AIC M2	ΔAIC
90	90	2379.642	90	99.17	2375.128	4.514
91	91	2372.698	91	99.44	2365.311	7.387
92	92	2370.481	92	99.50	2363.693	6.788
93	93	2371.891	93	99.60	2366.7	5.191
94	94	2369.192	94	99.69	2365.049	4.143
95	95	2370.806	95	99.71	2365.854	4.952
96	96	2369.8	96	99.78	2364.835	4.965
97	97	2371.561	97	99.8	2368.386	3.175
98	98	2373.22	98	99.83	2370.898	2.322
99	99	2373.24	99	99.95	2365.991	7.249
99.5	99.5	2368.42	99.96	99.98	2362.97	5.45

the ability of model M2 to describe the data is improved. Recall that M2 is the model that includes the response status of the patient, but not the monoclonal Ig isotype, as an explanatory variable. In table 9-8, values of the AIC are compared for model M2 before and after adjusting the mHLC response threshold of IgA patients, according to the quantiles given in table 9-5. The AIC is always smaller using the deeper IgA mHLC response threshold, with the size of the difference, ΔAIC, provided in the table. This result provides further support for the hypothesis that the mHLC response at pre-maintenance underestimates/overestimates PFS in IgG/IgA patients. It has been shown that by using a deeper response threshold for IgA patients, there is a stronger association between the achievement of a response and PFS.

Notably, the improvement is seen for IgG response thresholds between 90% and 93%, even though the difference in PFS between IgA and IgG patients was not significant for these thresholds in the analysis in section 9.4.3. This result suggests that in fact mHLC response does overestimate response in IgA patients for response thresholds between 90% and 93%, however there were too few IgA patients in the non-response groups to draw this conclusion from the analysis in section 9.4.3.

9.5.1 Errors in the data

The mHLC response thresholds used for IgA patients, given in table 9-5, are confined to a very small range of 0.0004 (99.96%) to 0.0083 (99.17%). All of the response thresholds used for IgA patients are thus greater than 99% and it seems unlikely that a response of 99.96% represents an improved survival compared to a response of 99.17%.

Measurements of IgAκ and IgAλ concentration using the HLC assay have a coefficient of variation (CV) of up to 5% [13]. Using standard propagation of error formulas [14], and assuming that the involved HLC and uninvolved HLC are statistically independent, the variance of the mHLC can be approximated by

$$\sigma^2_{\text{mHLC}} \approx \sigma^2_{\text{iHLC}} + r^2\sigma^2_{\text{uHLC}}, \tag{9-3}$$

where r is a constant, representing the ratio of the median concentration of IgAκ to the median concentration of IgAλ or vice versa, depending upon the light chain type of the monoclonal IgA, σ^2_{iHLC} is the variance of the involved HLC measurement, and σ^2_{uHLC} is the variance of the uninvolved HLC measurement.

Again using propagation of error formulas, the variance of the mHLC response can be approximated by

$$\sigma^2_{\text{response}} \approx \left(\frac{\text{mHLC}_{\text{preM}}}{\text{mHLC}_{\text{screen}}}\right)^2 \left(\frac{\sigma^2_{\text{mHLCpreM}}}{\text{mHLC}^2_{\text{preM}}} + \frac{\sigma^2_{\text{mHLCscreen}}}{\text{mHLC}^2_{\text{screen}}}\right), \tag{9-4}$$

where $\text{mHLC}_{\text{preM}}$ is the mHLC at pre-maintenance, $\text{mHLC}_{\text{screen}}$ is the mHLC at screening, $\sigma^2_{\text{mHLCpreM}}$ is the variance of the mHLC at pre-maintenance, and $\sigma^2_{\text{mHLCscreen}}$ is the variance of the mHLC at screening.

The CV of the mHLC response is, by definition, given by

$$\text{CV}_{\text{response}} = \frac{\sqrt{\sigma^2_{\text{response}}}}{\text{mHLC}_{\text{preM}}/\text{mHLC}_{\text{screen}}}. \tag{9-5}$$

The CV of measured HLC concentrations tends to decrease for larger concentrations; however, for simplicity, it is assumed that the CV is the same for each measurement, denoted by CV_{HLC}. In this way, the CV of the mHLC response can be approximated by

$$\text{CV}_{\text{response}} \approx \sqrt{\frac{\text{CV}^2_{\text{HLC}}\left(\text{iHLC}_{\text{preM}} + r^2\text{uHLC}_{\text{preM}}\right)}{\left(\text{iHLC}_{\text{preM}} - r\text{uHLC}_{\text{preM}}\right)^2} + \frac{\text{CV}^2_{\text{HLC}}\left(\text{iHLC}_{\text{screen}} + r^2\text{uHLC}_{\text{screen}}\right)}{\left(\text{iHLC}_{\text{screen}} - r\text{uHLC}_{\text{screen}}\right)^2}}, \tag{9-6}$$

where $\text{iHLC}_{\text{preM}}$ is the involved HLC at pre-maintenance, $\text{uHLC}_{\text{preM}}$ is the uninvolved HLC at pre-maintenance, $\text{iHLC}_{\text{screen}}$ is the involved HLC at screening, and $\text{uHLC}_{\text{screen}}$ is the uninvolved HLC at screening.

Substituting into equation (9-6) the average values from the data of $\text{iHLC}_{\text{preM}}$, $\text{uHLC}_{\text{preM}}$, $\text{iHLC}_{\text{screen}}$ and $\text{uHLC}_{\text{screen}}$ for IgA patients gives

$$\text{CV}_{\text{response}} \approx 2.84\text{CV}_{\text{HLC}}, \tag{9-7}$$

for IgAκ, where $r = 1.87$, and

$$\text{CV}_{\text{response}} \approx 1.57\text{CV}_{\text{HLC}}, \tag{9-8}$$

for IgAλ, where $r = 1/1.87$. There is thus an error of up to 15% on calculated values of the mHLC response in IgA patients. The error in the value of the mHLC response due to measurement errors alone is relatively small at only 15%; however, that does not necessarily imply that a measured mHLC response of 0.0004 (99.96%) represents a better prognosis than a measured mHLC response of 0.0083 (99.17%). There are other sources of error to account for, apart from measurement errors, such as day-to-day biological variation.

In figure 9-12A, PFS from pre-maintenance is compared for IgG patients who had an mHLC response of greater than 99.5%, between 90% and 99.5%, and less than 90%. There is a large difference between the survival curves for those patients achieving a response of greater than 99.5% and those achieving a response of between 90% and 99.5%. A similar plot is shown in figure 9-12B for IgA patients. In figure 9-12, IgA patients are compared who achieved mHLC responses of greater than 99.96%, between 99.17% and 99.96%, and less than 99.17%. Perhaps surprisingly, the IgA patients who had an mHLC response of greater than or equal to 99.96% have significantly fewer events than those achieving responses of between 99.17% and 99.96%.

Whilst it is not recommended that the mHLC response thresholds given in table 9-5 for IgA patients are used in practice, the analysis in this section shows that the mHLC response marker has a strong association with PFS, even when very deep responses are considered. Current guidelines only discriminate between responses of less than 50%, between 50% and 90%, and greater than 90% [15]. In patients treated with high dose melphalan and autologous stem cell transplantation, these cut-off values for response

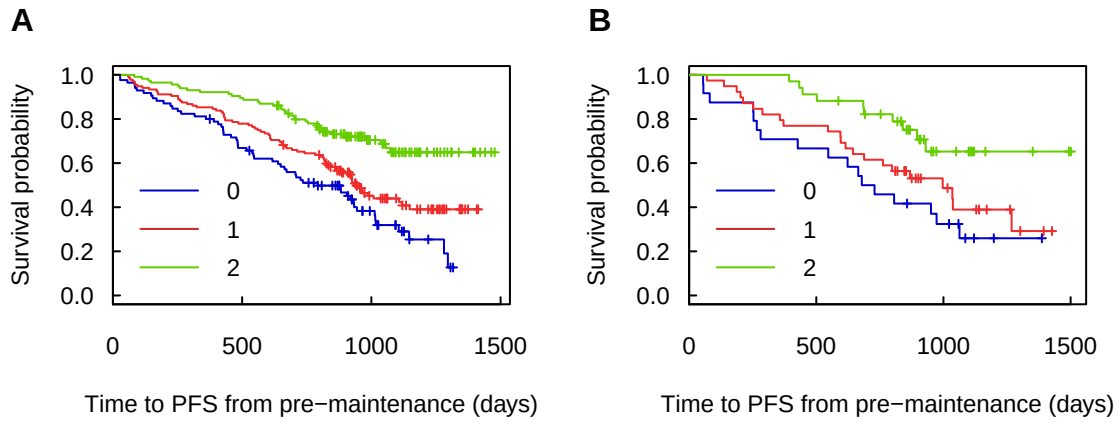

Figure 9-12 (A) PFS from pre-maintenance in IgG patients; 2 signifies a response of greater than or equal to 99.5%, 1 signifies a response of greater than or equal to 90% but less than 99.5%, and 0 signifies a response of less than 90%. (B) PFS from pre-maintenance in IgA patients; 2 signifies a response of greater than or equal to 99.96%, 1 signifies a response of greater than or equal to 99.17% but less than 99.96%, and 0 signifies a response of less than 99.17%.

become less relevant, particularly for IgA patients. The analysis in this section suggests that there is potential for deeper cut-off values to be considered.

9.6 Analysis of SPEP response and progression-free survival from pre-maintenance

In this section, the association between the SPEP response at pre-maintenance and PFS from pre-maintenance is analysed. The analyses performed are the same as the analyses of mHLC response and PFS in section 9.4.3, but now using the SPEP response rather than the mHLC response.

9.6.1 Missing data

As in section 9.4, the 53 IIMM patients with missing PFS from pre-maintenance were excluded from the analysis. Seven patients with no SPEP concentration recorded at

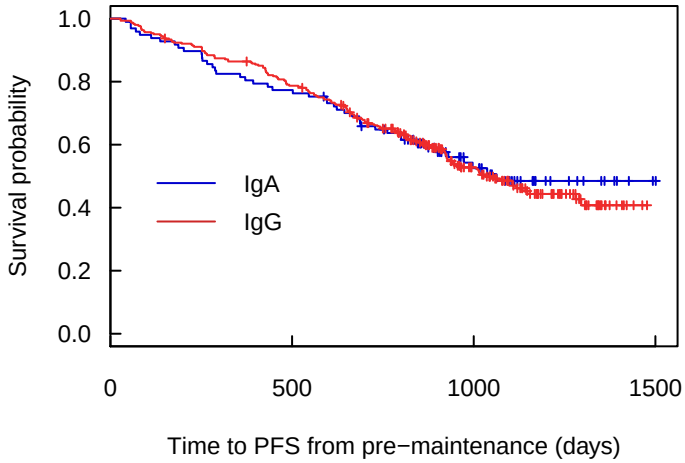

Figure 9-13 Survival plot of PFS from pre-maintenance stratified by monoclonal immunoglobulin isotype, for the patients analysed in section 9.6.2

screening were also omitted. Patients with no SPEP concentration recorded at pre-maintenance, due to a lack of quantifiable M-spike, were considered as having zero SPEP concentration at pre-maintenance, or a 100% SPEP response. 67 patients for whom SPEP concentration at pre-maintenance was missing for any other reason were excluded. In total 127 patients were excluded, leaving 399 patients to be analysed – 97 with IgA-producing clones and 302 with IgG-producing clones.

9.6.2 Survival analysis

The proportional hazards models estimated in this section are described in section 9.3. The proportional hazards assumption was tested for all fitted models and found not to be violated, at the 5% significance level, for any of the explanatory variables in any of the fitted models.

In this section, a different sample of patients is analysed than in section 9.4, due to patients having different missing data for SPEP and HLC. Therefore it is first checked that there is no difference in PFS from pre-maintenance between the IgA and IgG patients, respectively, who are analysed in this section. Recall that model M3 includes the monoclonal Ig isotype, but not the response status of the patient, as an explanatory variable. Fitting model M3 gives the ML estimate of the coefficient $\hat{\beta}_{\text{IgG}} = 0.03662$ and the hazard

Table 9-9 95% confidence interval estimates for the parameters in models M2 and M4, for monoclonal Ig responses measured by SPEP. Details are given in section 9.6.2.

Response threshold %	M2: $\exp(\hat{\alpha}_1)$ 95% C.I.	M4: $\exp(\hat{\alpha}_1)$ 95% C.I.	M4: $\exp\left(\hat{\beta}_{\text{IgG}}\right)$ 95% C.I.
90	$(0.3397, 0.6193)$	$(0.3226, 0.6027)$	$(0.5981, 1.1988)$
91	$(0.3325, 0.6013)$	$(0.3130, 0.5817)$	$(0.5829, 1.1726)$
92	$(0.3325, 0.6013)$	$(0.3130, 0.5817)$	$(0.5829, 1.1726)$
93	$(0.3755, 0.6676)$	$(0.3440, 0.6375)$	$(0.5551, 1.1358)$
94	$(0.3755, 0.6676)$	$(0.3440, 0.6375)$	$(0.5551, 1.1358)$
95	$(0.375, 0.6622)$	$(0.3411, 0.6288)$	$(0.5432, 1.1141)$
96	$(0.3808, 0.6718)$	$(0.3419, 0.6334)$	$(0.5305, 1.0960)$
97	$(0.3451, 0.6095)$	$(0.3046, 0.5656)$	$(0.5029, 1.0404)$
98	$(0.349, 0.6166)$	$(0.3067, 0.5709)$	$(0.4999, 1.0369)$
99	$(0.3404, 0.602)$	$(0.2964, 0.5537)$	$(0.4894, 1.0176)$
99.5	$(0.3404, 0.602)$	$(0.2964, 0.5537)$	$(0.4894, 1.0176)$

ratio $\exp\left(\hat{\beta}_{\text{IgG}}\right) = 1.037$. The 95% confidence interval estimate of the hazard ratio is given by $(0.7428, 1.449)$, which contains the value 1; it can be concluded that there is no statistically significant difference in PFS between IgA and IgG patients, as illustrated by the survival plot in figure 9-13.

The 95% confidence interval estimates for the parameters in models M2 and M4 are given in table 9-9. For both M2 and M4, the confidence interval estimate of $\exp(\alpha_1)$ has its upper bound less than 1 for all values of the response threshold used. It can therefore be concluded that, for the particular threshold values used, achieving at least the specified response at pre-maintenance is associated with an improved PFS. Model M4 also includes the coefficient β_{IgG}, representing the effect of having an IgG paraprotein. The interval estimates of $\exp\left(\hat{\beta}_{\text{IgG}}\right)$ include the value 1 for all of the SPEP response thresholds used. For SPEP response threshold values between 97% and 99.5%, the interval estimates of $\exp\left(\hat{\beta}_{\text{IgG}}\right)$ have their upper bounds close to 1. Note that grouping the patients by SPEP response thresholds of 99% and 99.5% results in the same groups of patients and therefore models M2 and M4 for both of these thresholds, respectively, are equivalent.

Table 9-10 gives the values of $-2\log\hat{L}$ and the AIC for models M2 and M4, estimated for each SPEP response threshold. Also provided in the table is the p-value of the likelihood ratio test comparing models M2 and M4, evaluating the evidence in favour of including

Table 9-10 Comparison of models M2 and M4, for SPEP responses. Details are provided in section 9.6.2.

Response threshold %	$-2\log\hat{L}$		AIC		M4 vs. M2 p-value
	M2	M4	M2	M4	
90	2110.544	2109.685	2112.544	2113.685	0.354
91	2108.152	2107.044	2110.152	2111.044	0.293
92	2110.066	2108.681	2112.066	2112.681	0.239
93	2112.965	2111.415	2114.965	2115.415	0.213
94	2114.277	2112.737	2116.277	2116.737	0.215
95	2111.726	2109.906	2113.726	2113.906	0.177
96	2112.37	2110.293	2114.37	2114.293	0.150
97	2105.34	2102.407	2107.34	2106.407	0.087
98	2106.123	2103.127	2108.123	2107.127	0.083
99	2104.306	2100.962	2106.306	2104.962	0.067
99.5	2104.306	2100.962	2106.306	2104.962	0.067

the term $\beta_{\text{IgG}}x_{\text{isotype},i}$ in the model, in the presence of the term $\alpha_1 x_{\text{response},i}$.

The p-values in table 9-10, for the analysis based on SPEP responses, are notably larger than the p-values in table 9-4, for the analysis based on mHLC responses. When SPEP responses are used, there is not sufficient evidence to support the inclusion of the monoclonal Ig isotype in the model along with the response status of the patient. The same general trend as before however is observed and can be demonstrated by Kaplan-Meier survival plots.

Figure 9-14 shows Kaplan-Meier survival plots of PFS stratified by the SPEP response and the monoclonal Ig isotype, with different response threshold values defining the SPEP response in each plot. These plots represent model M4. Whilst the results of fitting proportional hazards models do not support the inclusion of the monoclonal Ig isotype in a model describing PFS, the survival plots show the same general trend as the same plots produced for mHLC responses, depicted in figure 9-9.

The less significant improvement of M4 compared with M2, for SPEP rather than mHLC, may be partially explained by the larger proportion of data that were missing for SPEP, compared to HLC. The SPEP responses of only 399 patients were analysed, whereas the mHLC responses of 433 patients were analysed. This could contribute to the larger p-values seen in table 9-10.

Another problem with the SPEP responses is that 87 out of the 97 IgA patients analysed

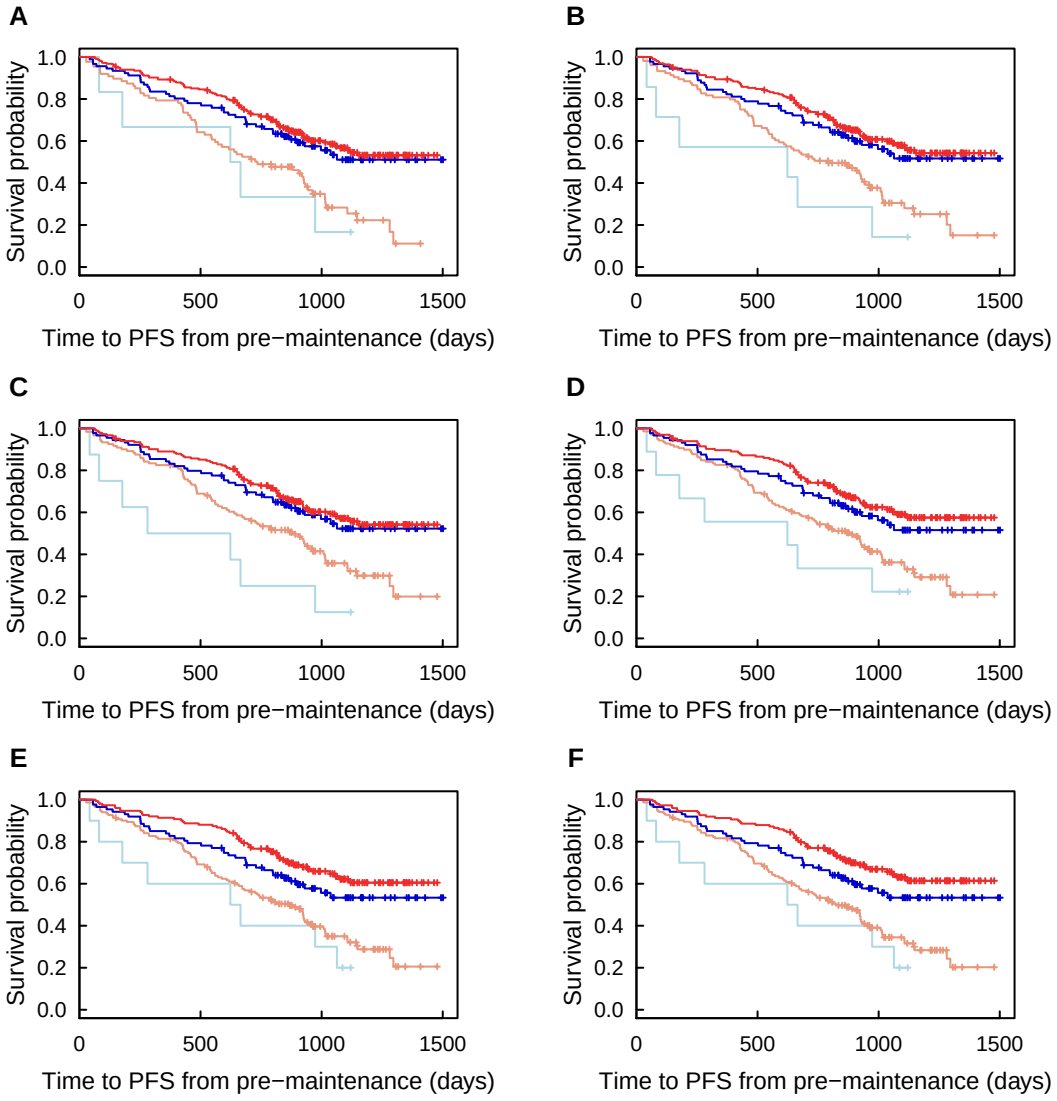

Figure 9-14 Survival plots of PFS by SPEP response and monoclonal Ig isotype, for six of the response threshold values used: (A) 90%, (B) 92%, (C) 94%, (D) 96%, (E) 98% and (F) 99.5%. Dark red – IgG responders; light red – IgG non-responders; dark blue – IgA responders; light blue – IgA non-responders. Details of the survival models are provided in section 9.6.2.

have no quantifiable M-spike. Only 10 of the IgA patients analysed therefore have an SPEP response less than 100%. Therefore, there is little difference between the response thresholds used, where IgA patients are concerned. In fact, six, seven, eight, nine and ten IgA patients have SPEP responses less than 90%, 93%, 94%, 96% and 97%, respectively. Therefore the groupings of IgA patients by SPEP response are largely the same for each of the response thresholds used. This can be seen by inspecting the survival curves of IgA patients (in blue) in figure 9-14. In contrast to IgA patients, 87, 116, 120, 138, and 147 IgG patients have SPEP responses less than 90%, 93%, 94%, 96% and 97%, respectively. Therefore the groupings of IgG patients by SPEP response result in quite different groups when different response thresholds are used.

9.7 Discussion

The analyses in this chapter suggest that mHLC and SPEP responses underestimate/overestimate PFS in IgG/IgA patients; however it is not possible to attribute this effect entirely to the metabolic properties of the respective Igs. Figure 9-1, in the introduction to this chapter, illustrates how monoclonal Ig metabolism may influence the association between the monoclonal Ig response and survival. However, it is not possible, based on the analyses here, to isolate the effect of Ig metabolism from the effect of the laboratory tests used to measure the monoclonal Ig response in practice. For example, measurements of the involved HLC at pre-maintenance include a significant proportion of polyclonal Ig. In this chapter efforts have been made to subtract the polyclonal part of the involved HLC by calculating the mHLC, as described in section 9.1.2; however, this method only results in an estimate of the monoclonal Ig concentration.

SPEP responses are also on average deeper in IgA patients than in IgG patients, as illustrated in figure 9-7. 87 out of 97, or 90%, of IgA patients have no SPEP concentration recorded at pre-maintenance due to an unquantifiable M-spike. By comparison, only 49% of IgG patients have an unquantifiable M-spike at pre-maintenance. This may be due to the recirculation of monoclonal IgG by neonatal Fc receptors, resulting in larger monoclonal Ig concentrations at pre-maintenance in IgG patients. However, it is also known that IgA migrates in the β-region of the gel (see section 2.4 in chapter 2), which could also

offer an explanation for the high proportion of IgA patients with unquantifiable M-spikes at pre-maintenance, and hence the deeper responses seen in IgA patients compared to IgG patients.

In section 8.3 of chapter 8, it was shown that, for the parameter values estimated in chapter 5, monoclonal IgG responds more slowly than monoclonal IgA when tumour responses are comparable. However, the difference between monoclonal IgA and IgG responses depends upon the rate and depth of the tumour response, whether the system is assumed to be in steady state at the beginning of treatment, and the values of the parameters of the metabolism models. In chapter 8, hypotheses pertaining to monoclonal Ig responses were investigated assuming fixed parameter values for the metabolism models, in order to represent average or typical responses. However, in reality, patients will have a range of different parameter values. In order to investigate the importance of the parameter values to the analyses in this chapter, it is necessary to perform the simulations from section 8.3 for a sample of patients, incorporating variability in their parameter values and tumour response rates. This is recommended for future work.

The Ig data analysed in this chapter have been confined to the monoclonal Ig response at pre-maintenance, as pre-maintenance is considered the most clinically relevant time point at which to assess the success of the treatment in killing the cancer. In future work it may be possible to take additional Ig measurements into account by fitting dynamic models to the patient data. Parameterised models for the plasma cell population may be assumed, such as the model used to produce the simulations in sections 8.3 and 8.4 in chapter 8. This approach would also require analysis of the structural and practical identifiability of the parameters to be estimated. Fitting models to the data could provide a more accurate estimate of the 'true' unobserved monoclonal Ig response, not contaminated with measurement errors. It would also be possible to obtain a fitted tumour response, which is assumed to drive patient survival, rather than the monoclonal Ig response. It would then be possible to compare proportional hazards models using monoclonal Ig responses and using tumour responses. In theory the tumour response should have a stronger association with PFS and there should be no difference in PFS between IgA and IgG patients, within responder and non-responder groups, respectively.

Multiple data points could also be used to fit joint models for longitudinal and time-to-

event data. This approach involves estimating the joint distribution of the event time outcomes, such as PFS, and longitudinal outcomes, such as the monoclonal Ig response at multiple monitoring points. In joint models, a time-varying hazard function at time t is assumed to be associated with the level of a time-varying covariate at time t. For the dataset analysed in this chapter, a joint model would be based upon the assumption that the hazard of a disease progression occurring at time t is associated with the monoclonal Ig response at time t.

Using standard proportional hazards models, it is assumed that the hazard function is constant and the same for all patients who have or have not achieved a certain response by pre-maintenance. All subjects who have had a disease progression or died before pre-maintenance are excluded. Using joint models, it would be possible to analyse PFS since screening and include patients in the analysis who did not respond well to induction therapy. Similarly, in the analyses in this chapter, information about response markers acquired after pre-maintenance is not considered. If joint models were used, it would be possible to analyse the association between the hazard of progression after pre-maintenance and the level of the response at any time after pre-maintenance. Such a model could be used to make individualised predictions of PFS, that could be updated at each monitoring point [16, p. 11]. Other information could be included, such as the stage of the disease at screening and the age of the patient; all of this information including accumulated biomarker levels could be used for prediction and decision making on an individual basis [17].

Joint modelling has seen many developments in recent years; however most joint models still tend to be based upon linear sub-models for the longitudinal data, i.e. marker responses [17–19]. When longitudinal data are markedly nonlinear, such as the mHLC and SPEP responses seen in multiple myeloma, their trajectories are usually modelled using splines. In the widely used R package for joint modelling, JM, linear and spline models are available [20]. Estimating the joint distribution of the longitudinal biomarker and event time outcomes whilst simultaneously fitting an underlying dynamic model would require some significant software development. However, even without accounting for differences between monoclonal IgA and IgG responses, joint models are likely to provide much more predictive power and flexibility than classifying patients into response groups

at a single time point.

9.8 Conclusions

In this chapter it has been shown that deeper monoclonal Ig responses are achieved by IgA patients compared to IgG patients at pre-maintenance, however this does not translate into an improvement in PFS for IgA patients. This suggests that monoclonal Ig responses overestimate PFS in IgA patients, or equivalently underestimate PFS in IgG patients. It was found that when patients are grouped by their monoclonal Ig response, IgG responders have improved PFS over IgA responders; similarly IgG non-responders have improved PFS over IgA non-responders. For mHLC responses and certain response thresholds, this finding was statistically significant at the 5% level.

Further support for the hypothesis that the monoclonal IgA response overestimates PFS was provided by repeating survival analyses using a deeper response threshold for IgA patients, compared to IgG patients. The response thresholds used were based on the quantiles of the distributions of mHLC responses. With this approach, there was no longer any difference in PFS between IgA and IgG patients, after they had been grouped by having achieved or having not achieved the specified mHLC response. The ability of a proportional hazards model, based only on the response status of the patient, to describe the variation in PFS was significantly improved.

The aim of this chapter was to investigate whether the monoclonal Ig response underestimates survival outcomes in IgG patients compared to IgA patients, based on the simulations of monoclonal Ig responses in chapter 8. It has been shown that the monoclonal Ig response at pre-maintenance, quantified by mHLC, underestimates PFS in IgG patients. However, it is not known whether the difference in mHLC and SPEP responses between IgA and IgG patients is solely due to the metabolic differences between the Igs; there are also possible differences between measured monoclonal IgA and IgG responses related to the particular laboratory assay used.

References

1. A. A. Chanan-Khan, S. Giralt, *Journal of Clinical Oncology* **28**, 2612–2624 (2010).
2. R Development Core Team, *R: A Language and Environment for Statistical Computing*, Vienna, Austria, 2013, (http://www.r-project.org).
3. T. M. Therneau, *A Package for Survival Analysis in S Version 2.3.8*, 2013, (http://cran.r-project.org/package=survival).
4. U.S. National Library of Medicine, *Study comparing conventional dose combination RVD to high-dose treatment with ASCT in the initial myeloma up to 65 years (IFM/DFCI2009)*, 2010, (2018; https://clinicaltrials.gov/ct2/show/study/NCT01191060).
5. M. Attal et al., *New England Journal of Medicine* **376**, 1311–1320 (2017).
6. E. Koulieris et al., *Experimental Hematology and Oncology* **1** (2012).
7. J. M. Woof, J. Mestecky, in *Mucosal Immunology*, ed. by J. Mestecky et al. (Academic Press (Elsevier), Amsterdam, ed. 4, 2015), chap. 17, ISBN: 9780124159754.
8. R. Benner, W. Hijmans, J. J. Haaijman, *Clinical and Experimental Immunology* **46**, 1–8 (1981).
9. A. Bradwell et al., *Leukemia* **27**, 202–207 (2013).
10. M. Mohty, J.-L. Harousseau, Eds., *Handbook of Multiple Myeloma* (ADIS (Springer), Cham, ed. 1, 2015), ISBN: 9783319182186.
11. J. F. Jacobs, R. G. van der Molen, X. Bossuyt, J. Damoiseaux, *Autoimmunity Reviews* **14**, 160–167 (2015).
12. D. Collett, *Modelling Survival Data in Medical Research* (CRC Press (Taylor & Francis), Boca Raton, ed. 3, 2015), ISBN: 1584883251.
13. The Binding Site Group Ltd., *Hevylite immunoassay instrumentation*, 2018, (2018; http://www.wikilite.com/hevylite-immunoassay-instrumentation).
14. H. Ku, *Journal of Research of the National Bureau of Standards, Section C: Engineering and Instrumentation* **70C**, 263–273 (1966).
15. S. Kumar et al., *The Lancet Oncology* **17**, 328–346 (2016).
16. D. Rizopoulos, *Joint Models for Longitudinal and Time-to-Event Data: With Applications in R* (CRC Press (Taylor & Francis), Boca Raton, ed. 1, 2012), ISBN: 9781439872871.

17. D. Rizopoulos, G. Molenberghs, E. M. Lesaffre, *Biometrical Journal* **59**, 1261–1276 (2017).

18. A. Lawrence Gould et al., *Statistics in Medicine* **34**, 2181–2195 (2015).

19. G. L. Hickey, P. Philipson, A. Jorgensen, R. Kolamunnage-Dona, *BMC Medical Research Methodology* **16** (2016).

20. D. Rizopoulos, *Journal of Statistical Software* **35**, 1–33 (2010).

10

Conclusions

The aim of this project was to investigate the possible effects of immunoglobulin (Ig) metabolism on plasma monoclonal Ig responses in immunoglobulin A (IgA) and immunoglobulin G (IgG) myeloma and to determine which, if any, of these effects are likely to influence the prognostic utility of monoclonal Igs as response markers. Simple models of IgG metabolism, which were deemed suitable for parameter estimation using data from human studies, were selected from the literature. The two models were compared under the conditions of multiple myeloma and were shown to produce very similar, although not identical, responses. Two-compartment models of IgG and IgA metabolism were then used to produce simulations showing the effects of Ig metabolism on monoclonal Ig responses in multiple myeloma. Based on these simulations it was determined that the difference between IgA and IgG responses could mean that IgG patients are assigned falsely modest responses. This effect was studied using proportional hazards survival models in a large dataset of newly diagnosed IgA and IgG myeloma patients. Evidence for an underestimation of progression-free survival using the monoclonal IgG marker was found in this dataset.

10.1 A two-compartment model describing IgG metabolism

In chapter 5, population parameters were estimated for a two-compartment model of IgG metabolism, using timecourse data from tracer studies found in the literature. Two model outputs were considered: the proportion of the tracer dose remaining in plasma ($y_1(t)$) and the proportion of the tracer dose remaining in the body ($y_2(t)$). The errors resulting from the data generating process were considered and expressions for the relationship between the variance and mean of each model output were derived. The second output, $y_2(t)$, was found to have a non-standard relationship between its error variance and its mean, which is not amenable to standard error models available in mixed effects modelling software packages, such as Monolix. Given other issues identified, including systematic errors in both outputs and autocorrelation in measurements of $y_2(t)$, parameter estimation methods assuming two simple error models were compared using synthetic data. The variability of the parameter estimates was similar for both methods but showed large differences between samples of subjects, suggesting that the small sample size largely contributed to the variability.

A recommendation for future work is to perform an additional simulation study using (i) additional subjects and (ii) the raw radioactivity measurements (rather than quantities calculated from radioactivity measurements) in order to determine which strategy for experiment design would offer the most improvement in parameter accuracy or precision. It is presumed by the author that increasing the number of subjects would offer the greater improvement. The estimated population parameters tend to be close to the medians of the true individual parameters, rather than the true population parameter, when these values are compared for synthetic data. For the data simulated in chapter 5, the sample medians of the individual parameters can be significantly different from the true population parameters, since the sample size is small. It has been verified by the author that the raw radioactivity measurements (the plasma radioactivity concentration, the radioactivity of the tracer dose and the radioactivity in urine collections) can be fitted in Monolix using the models described in section 5.5 of chapter 5. If it were possible to take repeated samples and measurements, it may be possible to verify the assumed

error models. If systematic errors in the data were found to have a large effect on the parameter estimates, then this would be a simple way in which to improve parameter accuracy and/or precision without increasing the number of subjects involved and the associated costs.

The source of systematic error in the timecourse data is the division by a measurement at time zero in order to obtain all observations in terms of the proportion of the radioactivity dose. The model outputs fitted to the data ($y_1(t)$ and $y_2(t)$) are therefore by definition equal to 1 at time 0 days. This may cause bias in the parameter estimates, similar to fitting a linear regression model without an intercept. Adding an additional intercept term may improve the accuracy of the parameter estimates. This has not been analysed in this thesis but could form a part of additional simulation studies in any future work.

Another recommendation for future work is to perform a sensitivity analysis with respect to the parameter identification problem, using the generalised sensitivity functions (GSFs) of Thomaseth et al. [1], recently adapted for multiple observations by Kappel et al. [2]. Such analyses can reveal time subintervals on which measurements have the most influence over the parameter estimates. This information can be used to design future experiments in which measurements are taken at certain times in order to maximise the information obtained on the parameters, minimise the number of measurements taken, or minimise the duration of sampling, to improve the comfort of subjects and reduce costs.

Methods for analysing the structural identifiability of mixed effects models, recently developed by Janzén et al. [3], were applied. The application of a population approach in chapter 5 could also benefit from techniques to analyse the sensitivity of population parameter estimates, akin to the GSFs. To the author's knowledge, such a methodology does not yet exist; however it could be used to determine whether the number of individual subjects is sufficient, in a similar way to how GSFs can be used to determine whether the sampling rate is sufficient, in order to accurately estimate the parameter values.

The remaining two-compartment model parameters were estimated from fractional catabolic rate (FCR) and half-life data, using a naive pooled approach. A recommendation for future work is to calculate the FCR and half-life from simulated radioactivity measurements and consider the form taken by the resulting errors. The parameters could then be estimated from the synthetic FCR and half-life data using different assumed error models

and the variability of the parameter estimates compared.

A final recommendation for analysing the two-compartment model is to consider whether an alternative radioactivity dosing schedule could be used to expose the nonlinear behaviour in the timecourse responses, such that all model parameters could be estimated from the same dataset, rather than using separate observations. It might then be possible to obtain population parameter estimates for all model parameters; however, the ethical implications of the effect of the dosing schedule on the subject might not permit this approach.

10.2 A four-compartment model describing IgG metabolism

In chapter 6 a four-compartment model of IgG metabolism was studied. Individual (not population) parameter values were estimated for linearised timecourse outputs using differential evolution. Differential evolution is a stochastic global minimisation algorithm; however, despite trying many different values for the crossover probability and scaling factor, the algorithm yielded many different parameter estimates whose fits to the data were similarly excellent. The structural identifiability of the parameters of the linearised model had been verified; it appeared however that the parameter estimates were insufficiently sensitive to the true parameter values. For four of the subjects, several runs of the differential evolution algorithm gave estimates of zero for one of the model parameters, suggesting that the model is over-parameterised with respect to the available data. A population approach to parameter estimation was not considered due to the ability of the model to produce very similar outputs for very different parameter vectors. The parameters were estimated by unweighted least squares. Alternative, more appropriate error models were not considered; however it is likely that the same problems regarding sensitivity would emerge, were the correct error model used. In chapter 5 errors in the timecourse data were considered and found to be complex.

From the point of view of experiment design, the model could be further studied using sensitivity analysis, by looking at GSFs and the Fisher information matrix, whilst

assuming the true parameter vectors are known. Some preliminary results using GSFs for some of the estimated parameter vectors suggest that refining the sampling grid to every 0.1 days may decrease the correlations between certain parameters, but still the Fisher information matrix has a large condition number for many parameter vectors. This analysis also assumes that the true parameter vectors are known, whereas we have little confidence that the true global minimum has been found for our data.

An expression was derived for the FCR of the endogenous IgG, which is denoted by $\mathrm{FCR_E}$. A re-parameterisation of this expression was used in order to estimate the parameters k_{31}, ψ_1 and ψ_2 from the $\mathrm{FCR_T}$ (FCR of the tracer) data. The parameters k_{31} and ψ_2 are physiologically meaningful and their estimates are close to previously published parameter values. Parameter vectors for the four-compartment model were generated using the constraints provided by fixing k_{31}, ψ_1 and ψ_2 to their estimated values, with certain parameters randomly generated. The $\mathrm{FCR_T}$ and $\mathrm{FCR_E}$ were then compared for these parameter vectors and in some cases large differences were seen. It would be interesting, in future work, to produce simulations of the timecourses of tracer in all four model compartments and compare them for each of the generated parameter vectors. Preliminary simulations not included in this thesis show that parameter vectors estimated from the $\mathrm{FCR_T}$ data result in similar behaviour in plasma and peripheral radiolabelled IgG but different behaviour in the endosomal compartments. The actions of parameters determining recycling, degradation, association and dissociation can approximately balance each other out with respect to the dynamics in the plasma compartment, even though the endosome compartments may be greatly affected by different individual parameter values. It would also be interesting to see which dynamical responses in the model correspond to large differences between $\mathrm{FCR_T}$ and $\mathrm{FCR_E}$. Future work could involve investigating the possibility of a model reduction using the parameters k_{31}, ψ_1 and ψ_2.

10.3 Comparison of models of IgG metabolism

The two models of IgG metabolism from the literature were compared using simulations in chapter 7. A derivation of the two-compartment model from the four-compartment model by Hattersley [4] was investigated using simulations. The equivalence of the two models

depends upon two assumptions: a quasi-steady state assumption for the bound IgG in endosomes and equal concentrations of unbound IgG in plasma and endosomes. It was found that the quasi-steady state assumption was valid for all simulations of IgG responses in multiple myeloma, when parameter vectors which give reasonable responses were used and steady state initial conditions were assumed. In order to find conditions in which this assumption was violated, the model was compared with the classical Michaelis-Menten enzyme reaction. The assumption could be violated by reducing the amount of IgG available to bind to neonatal Fc receptors, either by decreasing the value of the parameter k_{31}, decreasing the initial condition $x_1(0)$, or increasing the value of the parameter k_{03} (in addition to setting the synthesis rate of IgG to zero). These extreme conditions however result in extreme behaviour in plasma IgG, for example maintenance of a large quantity of plasma IgG over a period of tens of years, in spite of zero IgG synthesis.

The second assumption, namely that the concentrations of unbound IgG in endosomes and plasma are equal, is based on knowledge of the process of pinocytosis, whereby IgG is internalised into endosomes at random (i.e. not surface-receptor mediated) within pockets of the extracellular fluid. However, this assumption has not previously been linked with conditions on certain parameter values and it is found that with feasible parameter values the two concentrations are not equal. It is possible to modify the four-compartment model such that the concentrations of unbound IgG in plasma and endosomes are equal, by changing the volume of the endosomes containing IgG into a variable. This model indeed produces equivalent responses to the reduced two-compartment model; however it is not included in this thesis as justification for the changing volume of endosomes would require further analysis, perhaps requiring individual endosomes to be considered as separate entities.

The responses of the four-compartment and two-compartment models were compared for the parameter values estimated in chapters 5 and 6, that is, the two-compartment model parameter values were not derived from the four-compartment model parameter values. IgG responses during multiple myeloma treatment and relapse were compared. The responses were shown to be very similar; however the final monoclonal IgG response could be underestimated by up to 6% by the four-compartment model. However, the larger differences of up to 6% were seen when the absolute final response is very large, up

to 100%. This simulation study also showed the remakarbly similar responses given by randomly generated parameter vectors obeying the constraints provided by setting the parameters k_{31}, ψ_1 and ψ_2 to the values estimated in chapter 6.

Comparing the four-compartment and two-compartment models of IgG metabolism from the literature showed that the two-compartment model is not a valid reduction of the four-compartment model, for feasible parameter values. However, it is possible to derive alternative two-compartment models from the four-compartment model. Future work may involve investigating alternative two-compartment models derived from the four-compartment model.

10.4 Predicted responses in multiple myeloma

In chapter 8 the effects of Ig metabolism on blood monoclonal Ig responses in multiple myeloma were investigated. Three main scenarios were investigated: the difference between monoclonal IgA and IgG responses during treatment, the difference in the rate of monoclonal IgG response between patients with different initial plasma IgG concentrations, and the difference between monoclonal IgA and IgG responses during relapse. The simulations produced in this chapter map extremely well onto the available real data. These detailed simulations allow for investigation of monoclonal Ig responses under various clinical conditions, including response to treatment and relapse. They also allow for investigation of hypotheses regarding Ig metabolism which may have real impact in a practical sense.

Sensitivity analysis was performed with respect to the difference between the average monoclonal IgA and monoclonal IgG responses, showing that certain parameters are much more important than others in determining the difference between the two responses. The sensitivity of the delay between tumour relapse and monoclonal Ig relapse to the model parameters was also analysed, again showing certain parameters to be much more relevant than others. This information could be fed back into the design of future experiments for parameter estimation.

The difference between the monoclonal Ig responses of IgA and IgG patients, for identical tumour responses, was investigated with simulations. As well as considering the differ-

ences in responses of patients whose tumour responses are the same, the reverse problem was considered, in which a range of tumour responses result in identical or similar monoclonal Ig responses. This analysis showed that identical final monoclonal Ig responses may correspond to a range of final tumour responses. For modest monoclonal IgG responses of between 50% and 80%, the final tumour response may be underestimated by between 5% and 7%. Such responses are common in patients who are considered to old or frail for regimens incorporating autologous stem cell transplantation. The large underestimation of tumour response by monoclonal IgG for these levels of response may have a significant impact upon the association between the marker response and survival; this could be studied in future work. The analysis also showed that very similar transient monoclonal Ig responses may result from a range of tumour response rates, particularly when the tumour response rate is fast. In general, it was found that assessments of response are more uncertain during the initial, transient part of the response; clinicians may need to consider that early assessments using monoclonal Igs may not reflect the true quality of the response.

The simulation results in chapter 8 are subject to errors in the models of Ig metabolism, errors in the models of tumour growth, errors in the parameter values for the metabolism models, and oversimplified assumptions, for example assuming the system is in steady state at the beginning of treatment. In chapter 7 the two-compartment model of IgG metabolism was shown to over-estimate the depth of the monoclonal IgG response, when compared to the four-compartment model. If the four-compartment model is a more accurate representation of the biological system, then the level of underestimation of the tumour response by the monoclonal IgG response could be underestimated by the two-compartment model. Simulations in which the clonal plasma cell population is assumed to be growing when treatment begins also show a greater difference between the tumour response and the monoclonal Ig response.

All of the simulations in chapter 8 are intended to represent a typical IgA or IgG patient. Future studies should take into account variability in the population, in terms of the tumour responses, the cellular rate of synthesis of Igs, and the parameter values for IgG and IgA metabolism. Measurement errors should also be considered in order to simulate the data of a cohort of patients and compare it with data from a real clinical trial.

10.5 Response assessment and prognosis in multiple myeloma

In chapter 9 evidence was found for the underestimation of progression-free survival (PFS) by the mHLC (defined in chapter 9) response in IgG patients or, equivalently, overestimation of PFS by the mHLC response in IgA patients. However, the deeper mHLC responses and serum protein electrophoresis (SPEP) responses seen in IgA patients could be due to IgA patients achieving deeper tumour responses (although there is no improved survival seen in IgA patients) or systematic differences in how IgA and IgG are quantified by laboratory tests. In order to assess the relative contributions of the effects of metabolism and systematic errors in quantification of monoclonal Ig responses, a population simulation is required. A recommendation for future work is to simulate a cohort of patients, designed to replicate the data from a clinical trial. Using a population simulation it could be shown whether the metabolic differences between IgA and IgG are significant enough to account for the difference seen in mHLC responses between IgA and IgG patients.

The clinical implication of the results presented in chapter 9 is that IgA and IgG patients may be assigned incorrect responses. According to the International Myeloma Working Group (IMWG) response criteria, a reduction of at least 90% in serum monoclonal Ig represents a very good partial response (VGPR). 75% of IgG patients in the IFM (Intergroupe Francophone du Myélome) 2009/01 trial [5; 6] were assigned VGPR at pre-maintenance, compared with 95% of IgA patients. Achieving VGPR is therefore found not to be meaningful for IgA patients, whereas for IgG patients there is a very significant difference in PFS between those patients who were assigned VGPR or better and those who were assigned partial response (PR). IgA patients assigned VGPR on the other hand have a very similar survival curve to patients who were assigned PR. It was shown in section 9.5 that, in terms of PFS, an mHLC response of at least 90% in IgG patients is comparable to a response of approximately 99% in IgA patients. The implication of this is that IgA patients may receive falsely optimistic information about their prognosis whilst IgG patients may receive falsely pessimistic information.

Using a population simulation it would be possible to investigate alternative response

markers such as the heavy/light chain (HLC) ratio, that is the ratio of IgGκ to IgGλ in IgG patients and the ratio of IgAκ to IgAλ in IgA patients, both of which are measured by the HLC assay. The HLC ratio (normal vs. abnormal) has been shown to correlate strongly with survival [7] and has been considered as a criterion for the assignment of complete response (CR), showing a strong association with PFS compared to current methods. At the beginning of treatment, patients typically have an abnormal HLC ratio due to the elevated involved HLC. As treatment progresses the involved HLC concentration decreases and the HLC ratio normalises. Using a population simulation it would be possible to analyse whether there is a discrepancy between IgA and IgG patients in terms of the proportion of patients whose HLC ratio enters the normal range at pre-maintenance.

References

1. K. Thomaseth, C. Cobelli, *Annals of Biomedical Engineering* **27**, 607–616 (1999).
2. F. Kappel, M. Munir, *Journal of Inverse and Ill-posed Problems* **25**, 499–519 (2017).
3. D. L. Janzén, M. Jirstrand, M. J. Chappell, N. D. Evans, *Computer Methods and Programs in Biomedicine*, 329–339 (2016).
4. J. G. Hattersley, PhD thesis, University of Warwick, 2009.
5. U.S. National Library of Medicine, *Study comparing conventional dose combination RVD to high-dose treatment with ASCT in the initial myeloma up to 65 years (IFM/DFCI2009)*, 2010, (2018; https://clinicaltrials.gov/ct2/show/study/NCT01191060).
6. M. Attal et al., *New England Journal of Medicine* **376**, 1311–1320 (2017).
7. H. Ludwig et al., *Leukemia* **27**, 213–219 (2012).

Appendices

A

Example code for survival analysis in R

Survival curves, given by the Kaplan-Meier estimator and stratified by patient response, are plotted using:

```
survivalCurve<-survfit(Surv(PFStime,PFSevent)~response,data=ifmData)
plot(survivalCurve)
```

The corresponding proportional hazards model, with response as an explanatory variable, and the null model are estimated using:

```
modelResponse<-coxph(Surv(PFStime,PFSevent)~response,data=ifmData)
nullModel<-coxph(Surv(PFStime,PFSevent)~1,data=ifmData)
```

The models are compared by calculating $-2 \log \hat{L}$ for each and performing a chi-squared test on the difference:

```
dNull<-nullModel$loglik*-2
dResponse<-modelResponse$loglik[2]*-2
1-pchisq(dNull-dResponse,1)
```

B

Mathematica code for structural identifiability analysis of mixed effects model

The structural identifiability analysis of the mixed effects model is performed in Mathematica using the following script.

Firstly we define the A, B and C matrices of the system. Parameters are prefixed by θ to represent the fixed component of the parameter.

```
(a = {{-\[Theta]k21 - \[Theta]k01, \[Theta]k12}, {\[Theta]k21, -\
\[Theta]k12}}) // MatrixForm
(c = {{1, 0}, {1, 1}}) // MatrixForm
(b = {{1, 0}, {0, 0}}) // MatrixForm
(x = {{x1}, {x2}}) // MatrixForm
```

The following calculates the transfer functions:

```
gmat = Simplify[((c.(Inverse[((s*IdentityMatrix[2]) - a)])).b)]
```

Extract the numerators and denominators of the transfer functions:

```
n1 = Numerator[gmat[[1, 1]]]
n2 = Numerator[gmat[[2, 1]]]
```

```
d1 = Denominator[gmat[[1, 1]]]
d2 = Denominator[gmat[[2, 1]]]
```

Extract the deterministic moment invariants from the transfer functions:

```
\[Phi]s =
DeleteDuplicates[{Coefficient[n1, s, 0], Coefficient[n2, s, 0],
   Coefficient[d1, s, 0], Coefficient[d1, s, 1],
   Coefficient[d2, s, 0], Coefficient[d2, s, 1]}]
```

Compute the random variable moment invariants:

```
zs = \[Phi]s /. {\[Theta]k01 -> \[Theta]k01*
   Exp[\[Eta]k01], \[Theta]k12 -> \[Theta]k12*
   Exp[\[Eta]k12], \[Theta]k21 -> \[Theta]k21*Exp[\[Eta]k21]}
z1 = zs[[1]]; z2 = zs[[2]]; z3 = zs[[3]]; z4 = zs[[4]];
```

Define the variance-covariance matrix of the random effects:

```
(\[CapitalOmega]\[Rho] = {{\[Sigma]k01^2, \[Rho]k01k12*\[Sigma]k01*\
     \[Sigma]k12, \[Rho]k01k21*\[Sigma]k01*\[Sigma]k21}, {\[Rho]k01k12*\
     \[Sigma]k01*\[Sigma]k12, \[Sigma]k12^2, \[Rho]k12k21*\[Sigma]k12*\
     \[Sigma]k21}, {\[Rho]k01k21*\[Sigma]k01*\[Sigma]k21, \[Rho]k12k21*\
     \[Sigma]k12*\[Sigma]k21, \[Sigma]k21^2}}) // MatrixForm
```

Compute the first order statistical moments of the random variable moment invariants:

```
\[Lambda]1 =
Expectation[
z1, {\[Eta]k01, \[Eta]k12, \[Eta]k21} \[Distributed]
MultinormalDistribution[{0, 0, 0}, \[CapitalOmega]\[Rho]]]
\[Lambda]2 =
Expectation[
z2, {\[Eta]k01, \[Eta]k12, \[Eta]k21} \[Distributed]
MultinormalDistribution[{0, 0, 0}, \[CapitalOmega]\[Rho]]]
\[Lambda]3 =
Expectation[
```

```
z3, {\[Eta]k01, \[Eta]k12, \[Eta]k21} \[Distributed]
MultinormalDistribution[{0, 0, 0}, \[CapitalOmega]\[Rho]]]
\[Lambda]4 =
Expectation[
z4, {\[Eta]k01, \[Eta]k12, \[Eta]k21} \[Distributed]
MultinormalDistribution[{0, 0, 0}, \[CapitalOmega]\[Rho]]]
```

Solve simultaneous equations for first order moments (already known that pop parameters are identifiable):

```
Assuming[{ \[Sigma]k12bar > 0},
Simplify[Solve[\[Lambda]1 == (\[Lambda]1 /. {\[Sigma]k12 -> \
  \[Sigma]k12bar}), \[Sigma]k12, Reals]]]
Assuming[{\[Sigma]k21 > 0, \[Sigma]k21bar > 0},
Simplify[Solve[\[Lambda]2 == (\[Lambda]2 /. {\[Sigma]k21 -> \
  \[Sigma]k21bar}), \[Sigma]k21, Reals]]]
Assuming[{\[Sigma]k01 > 0, \[Sigma]k01bar > 0},
Simplify[Solve[\[Lambda]4 == (\[Lambda]4 /. {\[Sigma]k01 -> \
  \[Sigma]k01bar}), \[Sigma]k01, Reals]]]
Solve[\[Lambda]3 == (\[Lambda]3 /. {\[Rho]k01k12 -> \
  \[Rho]k01k12bar}), \[Rho]k01k12, Reals]
```

Generate second order statistical moments:

```
\[Lambda]12 =
Expectation[
z1^2, {\[Eta]k01, \[Eta]k12, \[Eta]k21} \[Distributed]
MultinormalDistribution[{0, 0, 0}, \[CapitalOmega]\[Rho]]]
\[Lambda]22 =
Expectation[
z2^2, {\[Eta]k01, \[Eta]k12, \[Eta]k21} \[Distributed]
MultinormalDistribution[{0, 0, 0}, \[CapitalOmega]\[Rho]]]
\[Lambda]32 =
Expectation[
z3^2, {\[Eta]k01, \[Eta]k12, \[Eta]k21} \[Distributed]
MultinormalDistribution[{0, 0, 0}, \[CapitalOmega]\[Rho]]]
```

```
\[Lambda]42 =
Expectation[
z4^2, {\[Eta]k01, \[Eta]k12, \[Eta]k21} \[Distributed]
MultinormalDistribution[{0, 0, 0}, \[CapitalOmega]\[Rho]]]
```

Solve simultaneous equations in second order moments to find that $\rho_{k_{12}k_{21}}$ and $\rho_{k_{21}k_{01}}$ are identifiable:

```
Solve[\[Lambda]22 == (\[Lambda]22 /. {\[Rho]k12k21 -> \
   \[Rho]k12k21bar}), \[Rho]k12k21, Reals]
Solve[\[Lambda]42 == (\[Lambda]42 /. {\[Rho]k01k21 -> \
   \[Rho]k01k21bar}), \[Rho]k01k21, Reals]
```

C

Simulation of tracer experiment data

```
(*solve system ODEs to get solutions for x1(t) and x2(t) *)
x1exp=DSolveValue[{x1'[t]==-(k01+k21)*x1[t]+k12*x2[t],
x2'[t]==k21*x1[t]-k12*x2[t],x1[0]==d\[Mu]mol,x2[0]==0},x1[t],t];
x2exp=DSolveValue[{x1'[t]==-(k01+k21)*x1[t]+k12*x2[t],
x2'[t]==k21*x1[t]-k12*x2[t],x1[0]==d\[Mu]mol,x2[0]==0},x2[t],t];

(*y1(t) and y2(t) are given by*)
y1=x1exp/d\[Mu]mol;
y2=(x1exp+x2exp)/d\[Mu]mol;

(*Parameters are rate constants k01, k12 and k21, and the dose of labelled
   IgG in \[Mu]mol*)
Variables[x1exp];

(*population parameters*)
\[Theta]mu={k12pop->0.422,k21pop->0.441,k01pop->0.0778};
\[Theta]sd={k12sd->0.713,k21sd->0.498,k01sd->0.685};
\[Theta]corr={\[Rho]k12k21->0.739,\[Rho]k21k01->0.608,
\[Rho]k01k12->0.872};
\[Theta]pop=Join[\[Theta]mu,\[Theta]sd,\[Theta]corr];

(*experimental parameters: dose in micromoles, alpha and plasma volume*)
```

```
\[Theta]experiment={d\[Mu]mol->0.005,\[Alpha]->9000,plasmaVol->3};
Draw individual parameters from lognormal distribution

(*Parameters of lognormal distribution*)
\[Mu]=Log[{k01pop,k12pop,k21pop}];
(\[CapitalSigma]={{k01sd^2,k01sd*k12sd*\[Rho]k01k12,
k01sd*k21sd*\[Rho]k21k01},{k01sd*k12sd*\[Rho]k01k12,
k12sd^2,k12sd*k21sd*\[Rho]k12k21},{k01sd*k21sd*\[Rho]k21k01,
k12sd*k21sd*\[Rho]k12k21,k21sd^2}})//MatrixForm;
\[Theta]dist=LogMultinormalDistribution[\[Mu],\[CapitalSigma]]
/.\[Theta]pop;

(*number of individual parameter vectors*)
n=7;

(*number of times to simulate the data with new errors*)
lmax=100;

(*Draw n individuals from the distribution*)
\[Theta]indsVals=Table[RandomVariate[\[Theta]dist],{j,n}];

(*replacement rules with individual parameter vectors and experimental
   parameters*)
\[Theta]inds=Table[Join[{k01->\[Theta]indsVals[[j,1]],
k12->\[Theta]indsVals[[j,2]],k21->\[Theta]indsVals[[j,3]]},
\[Theta]experiment],{j,n}];

(*Set cv values here----------------------------------------------------*)
(*cv for plasma measurements and dose measurement*)
cv=0.07;

(*cv for urine measurements*)
cvu=0.3;
```

```
(*Simulate y1(t) data-----------------------------------------------*)
(*radioactivity concentration in plasma, i.e. measured variable from which we
    calculate y1(t) *)
plasmaRadConc=x1exp*\[Alpha]/plasmaVol;

(*Plot the true value of the radiation concentration in plasma, for the first
    set of individuals*)
Plot[Evaluate[Table[plasmaRadConc/.\[Theta]inds[[k]],{k,n}]],{t,0,25},
PlotRange->All];

(*plot plasmaRadConc(t)/plasmaRadConc(0)*)
Plot[Evaluate[Table[(plasmaRadConc/(plasmaRadConc/.t->0))
/.\[Theta]inds[[k]],{k,n}]],{t,0,25},PlotRange->All];

(*measurement timepoints. The time over which we measure depends upon how
    fast are the dynamics of the individual. *)
Do[
tmax[k]=Max[Ceiling[-70*\[Theta]indsVals[[k,1]]+24],7]
,{k,n}
]

(*Assume that measurements are taken daily*)
Do[
timepoints[k]=Table[j,{j,0,tmax[k]}]
,{k,n}
]

(*For our 7 parameter vectors, generate lmax datasets for plasmaRadConc
    [uCi/ml], assuming that this measurement has constant cv *)
Do[
plasmaRadConcTable[l]=Table[Table[(plasmaRadConc/.\[Theta]inds[[j]])
+RandomVariate[NormalDistribution[0,(cv*plasmaRadConc)
/.\[Theta]inds[[j]]]],{t,timepoints[j]}],{j,n}]
,
```

```
{l,lmax}]

(*plot one example of noisy measurements of plasmaRadConc(t)*)
Show[ListPlot[Table[Transpose[{timepoints[k],plasmaRadConcTable[1][[k]]}]
,{k,n}],Joined->False,PlotRange->All],Table[Plot[Evaluate[plasmaRadConc
/.\[Theta]inds[[k]]],{t,0,tmax[k]},PlotRange->All,
PlotStyle->ColorData[97,k]],{k,n}]];

(*calculate y1(t) measurements*)
Do[
y1Table[l]=Table[plasmaRadConcTable[l][[j]]/plasmaRadConcTable[l][[j,1]]
,{j,n}]
,
{l,lmax}
]

(*plot one example of noisy measurements of y1(t)*)
y1plot=Show[ListPlot[Table[Transpose[{timepoints[k],y1Table[1][[k]]}]
,{k,n}],Joined->False,PlotRange->All],Table[Plot[Evaluate[y1
/.\[Theta]inds[[k]]],{t,0,tmax[k]},PlotRange->All,PlotStyle->
ColorData[97,k]],{k,n}]];

(*Simulate y2(t) data----------------------------------------------*)
(*The radiation in urine is given by*)
radUrine=Simplify[\[Alpha]*(d\[Mu]mol-x1exp-x2exp)];
Plot[Evaluate[Table[radUrine/.\[Theta]inds[[k]],{k,n}]],{t,0,25}
,PlotRange->All,AxesLabel->{"time (days)","radUrine (\[Mu]Ci)"}];

(*The amount of radioactivity in the urine collected at each time point*)
dailyRadUrine=Simplify[radUrine-(radUrine/.t->(t-1))];

(*Plot the amount of radioactivity in the urine each day*)
dailyRadUrinePlot=Show[Table[Plot[Evaluate[dailyRadUrine
/.\[Theta]inds[[k]]],{t,1,tmax[k]},PlotRange->All,PlotStyle->
```

```
ColorData[97,k]],{k,n}]];

(*Calculate the radioactivity in urine collections with a constant CV
    (proportional error model)*)
Do[
dailyRadUrineTable[l]=Table[Table[((dailyRadUrine/.\[Theta]inds[[j]])
/.t->Drop[timepoints[j],1])[[k]]+RandomVariate[NormalDistribution[0,
cvu*(((dailyRadUrine/.\[Theta]inds[[j]])/.t->Drop[timepoints[j],1])[[k]])]]
,{k,tmax[j]}],{j,n}]
,
{l,lmax}
]

(*These are the noisy measurements of the radioactivity in each day's urine
    collection*)
Show[dailyRadUrinePlot,ListPlot[Table[dailyRadUrineTable[1][[k]],{k,n}]]];

(*The calculated cumulative urine radioactivity is given by*)
Do[
radUrineTable[l]=Table[Prepend[Accumulate[dailyRadUrineTable[l][[k]]],0]
,{k,n}]
,
{l,lmax}
]

(*plot of the cumulative radioactivity in urine*)
Show[ListPlot[Table[Transpose[{timepoints[k],radUrineTable[1][[k]]}]
,{k,n}]],Table[Plot[Evaluate[radUrine/.\[Theta]inds[[k]]],{t,0,tmax[k]}
,PlotRange->All,PlotStyle->ColorData[97,k]],{k,n}],PlotRange->All];
(*the radioactivity in the dose is given by radDose = alpha*d\[Mu]mol*)
radDose=\[Alpha]*d\[Mu]mol;

(*Simulate measurements of the radioactivity measured in the tracer dose for
    the seven subjects and repeat lmax times*)
```

```
Do[
radDoseTable[l]=Table[(radDose/.\[Theta]experiment)
+RandomVariate[NormalDistribution[0,cv*(radDose/.\[Theta]experiment)]]
,{k,n}]
,
{l,lmax}
]

(*Calculate y2(t) *)
Do[
y2Table [l]=Table[1-(radUrineTable[l][[k]]/radDoseTable[l][[k]]),{k,n}]
,
{l,lmax}
]

(*plot one example of noisy measurements of y2(t)*)
y2plot=Show[ListPlot[Table[Transpose[{timepoints[k],y2Table[1][[k]]}]
,{k,n}]],Table[Plot[Evaluate[y2/.\[Theta]inds[[k]]],{t,0,tmax[k]},
PlotRange->All,PlotStyle->ColorData[97,k]],{k,n}]];

(*y1(t) and y2(t) plotted together*)
Show[y1plot,y2plot];

(*Combine 100 simulated datasets for each parameter vector so they can be
   plotted together*)
Do[y1plotTable[k]=Show[ListPlot[Table[Transpose[{timepoints[k],
y1Table[l][[k]]}],{l,lmax}],Joined->False,PlotStyle->ColorData[97,k],
PlotRange->All],Plot[Evaluate[y1/.\[Theta]inds[[k]]],{t,0,tmax[k]},
PlotRange->All,PlotStyle->ColorData[97,k]]]
,
{k,n}
]
Do[
y2plotTable[k]=Show[ListPlot[Table[Transpose[{timepoints[k],
```

```
y2Table[l][[k]]},{l,lmax}],PlotStyle->ColorData[97,k]],
Plot[Evaluate[y2/.\[Theta]inds[[k]]],{t,0,tmax[k]},PlotRange->All,
PlotStyle->ColorData[97,k]]]
,
{k,n}
]

(*Plot the 100 simulated datasets for each parameter vector*)
Table[Show[y1plotTable[k],y2plotTable[k]],{k,n}];
```

D

Mathematica code for generating expressions for λ_4, A_{14} and A_{34}

```
(*ODEs for the linear model of tracer kinetics*)
dt1 = -(k21 + k31)*t1[t] + k12*t2[t] + k14*t4[t];
dt2 = k21*t1[t] - k12*t2[t];
dt3 = k31*t1[t] - k03*t3[t] - k43*t3[t] + k34*t4[t];
dt4 = -(k14 + k34)*t4[t] + k43*t3[t];

(*ODEs and initial conditions put into one list to be used by DSolve*)
odes = {t1'[t] == dt1, t2'[t] == dt2, t3'[t] == dt3, t4'[t] == dt4};
ics = {t1[0] == d, t2[0] == 0, t3[0] == 0, t4[0] == 0};
eqns = Join[odes, ics];

(*Solve the system of ODEs for t1, t2, t3 and t4*)
odeSol = DSolve[eqns, {t1[t], t2[t], t3[t], t4[t]}, t];

(*We define parameter values from the literature so that we can \
simulate the model and check it looks correct*)
litParams1 = {d -> 1, k21 -> 0.51, k31 -> 0.18, k12 -> 0.41, k14 -> 5,
k03 -> 3, kon -> 1000, v3 -> 0.34, konv3 -> 1000/0.34, Rtot -> 14,
koff -> 100, Ie -> 15, k34 -> 100};
k43value = (k03 (k14 + koff) kon Rtot)/(Ie kon +
```

```
k03 (k14 + koff) v3) /. litParams1;

(*parameter vector from literature*)
litParams = Join[litParams1, {k43 -> k43value}];

(*Simulate the model to check*)
Plot[{Evaluate[t1[t] /. odeSol /. litParams],
Evaluate[t2[t] /. odeSol /. litParams],
Evaluate[t3[t] /. odeSol /. litParams],
Evaluate[t4[t] /. odeSol /. litParams]}, {t, 0, 25}]

(*Calculate the A-matrix of the system*)
(aMat = {{-(k21 + k31), k12, 0, k14}, {k21, -k12, 0, 0}, {k31,
0, -k03 - k43, k34}, {0, 0, k43, -(k14 + k34)}}) // MatrixForm

(*We want A14 and A34, which are the coefficients of \
exp(\[Lambda]4*t) in equation (6-26). \[Lambda]4 is given by: *)
\[Lambda]4 = Eigenvalues[aMat][[4]];

(*expression for t1(t)*)
t1sol = DSolveValue[eqns, {t1[t], t2[t], t3[t], t4[t]}, t][[1]];

(*check with parameter values*)
t1sol /. litParams

(*expression for t3(t)*)
t3sol = DSolveValue[eqns, {t1[t], t2[t], t3[t], t4[t]}, t][[3]];

(*check with parameter values*)t3sol /. litParams

(*Find A14. Evaluate for parameter values and check it's correct \
against t1sol*)
a14 = Coefficient[Normal[t1sol], Exp[t*\[Lambda]4]];
a14 /. litParams
```

```
(*Find A34. Evaluate for parameter values and check it's correct \
against t3sol*)
a34 = Coefficient[Normal[t3sol], Exp[t*\[Lambda]4]];
a34 /. litParams

(*If we want to look at A14 and A34 in full, without Root objects*)
a14Full =
Replace[a14, {Root[x_, y_] :> ToRadicals[Root[x, y]]}, Infinity];
a34Full =
Replace[a34, {Root[x_, y_] :> ToRadicals[Root[x, y]]}, Infinity];

(*lambda4 in full*)
\[Lambda]4Full =
Eigenvalues[aMat, Cubics -> True, Quartics -> True][[4]];

(*Export symbolic expressions to text files*)
SetDirectory[NotebookDirectory[]];
Export["A14.txt", a14Full];
Export["A34.txt", a34Full];
Export["lambda4.txt", \[Lambda]4Full];
```